Whole-body modelling of glucose and lactate dynamics in *Plasmodium falciparum* malaria

By

Johannes P. Meyer

Thesis presented in partial fulfilment of the requirements for the degree of Master of Science in Biochemistry in the Faculty of Science at the University of Stellenbosch

Department of Biochemistry
University of Stellenbosch
Private Bag X1, 7602 Matieland, South Africa

Supervisor: Dr D.D. van Niekerk

Co-supervisor: Prof. J.L. Snoep

March 2020

Declaration

By submitting this thesis electronically, I declare that the entirety of the work contained therein is my own, original work, that I am the sole author thereof (save to the extent explicitly otherwise stated), that the reproduction and republication thereof by Stellenbosch University will not infringe any third party rights and that I have not previously in its entirety or in part submitted it for obtaining any qualification.

Date: March 2020

Abstract

Malaria is the most important parasitic disease affecting man, and continues to threaten public health in developing countries where the disease is endemic. Within the genus *Plasmodium*, *falciparum* is responsible for nearly all deaths from malaria worldwide. Two symptoms that are indicative of severe disease and a high risk of mortality are hypoglycaemia (HG - plasma glucose below 2.2 mM) and hyperlactataemia (HL - plasma lactate in excess of 5.5 mM). Though multiple causes of these metabolic comorbidities have been identified qualitatively, there exists a dearth of quantitative evidence that can give a reliable approximation of which aetiological factors have the highest relative contribution to the appearance of these symptoms. Such a quantitative approach would not only improve our understanding of how malaria progresses to severe disease, but also indicate which mechanisms of host-parasite interaction would be the most amenable to targeting by novel antimalarial chemotherapeutics, since new anti-malarial drugs are required to combat the threat of acquired resistance.

One tool that has proved useful in the process of identifying novel drug targets is mathematical modelling. In this study we present a whole-body model of host and parasite metabolism that can provide a quantitative assessment of glucose and lactate dynamics in both the healthy and infected state. This model, termed *meyer1*, combines independently published models describing separate aspects of host and parasite metabolism to yield an *in silico* platform that is subsequently used to investigate the relative quantitative contribution of the putative causes of HG/HL in the infected state.

Results from model simulations and subsequent metabolic control analysis (MCA) indicated that heterogenous parasite sequestration within the microvasculature of organs important in mediating whole-body glucose and lactate homeostasis has the greatest quantitative impact on the appearance of HG/HL; this finding agrees with qualitative statements previously made in literature. In addition, MCA identified several key enzymatic components of parasite and infected erythrocyte glucose metabolism that, if targeted, would yield the greatest contribution in preventing the appearance of hypoglycaemia in severe disease. These include parasite derived new permeability pathways (NPPs), the parasite glucose transporter (PHT1), and parasite hexokinase and phosphofructokinase.

In addition to these findings, the final *meyer1* model also provides a platform amenable to further development as more clinical data for model parametrisation becomes available. New experimental studies would also assist in providing the data required to supersede the current phenomenological expressions with mechanism-based implementations representing host-parasite interactions mediating microvascular occlusion. This will ultimately lead to more precise identification of novel drug targets at the molecular level that can inhibit the process of parasite sequestration and subsequently help prevent the appearance of HG/HL in severe *P. falciparum* malaria.

Acknowledgements

I would like to extend my gratitude to the following:

My parents, for their love and support.

My supervisors, Dr Dawie van Niekerk and Prof Jacky L Snoep, for their continued patience, understanding, and guidance.

The internet, particularly Stack Exchange, for the seemingly interminable number of technical problems solved through the selfless contributions and assistance of others.

Table of Contents

Chapter 1: Introduction

1.1 Introduction

Malaria is the most prominent parasitic disease that afflicts humans (1). Malaria is an umbrella term that refers to disease caused by protozoans of the genus *Plasmodia*. Belonging to the phylum *Apicomplexa*, these sporozoan parasites are differentiated from other eukaryotes by the possession of an apicoplast, a vestigial plastid that bears evolutionary homology to the chloroplasts found in plant and algal cells. Malaria parasites infect the red blood cells of mammals, birds, and reptiles, and are transmitted between animals via the bites of mosquitos. Within the genus *Plasmodium*, four species are known to infect humans preferentially: *P. falciparum*, *P. vivax*, *P. ovale*, and *P. malariae*. Errant primate malarias, such as those caused by the simian parasite *P. knowlesi*, can constitute a substantial portion of infections in certain regions of South-east Asia (2). Of the four species normally parasitic in humans, *P. falciparum* ranks highest in terms of both lethality and disease severity, responsible for nearly all deaths from malaria while constituting roughly only half of all malaria cases worldwide (3). This high mortality rate is especially prominent in Africa, the region where *P. falciparum* is most widespread (4).

The disease itself is typically characterised by non-specific symptoms resembling influenza, with periodic febrile paroxysms that accompany the renewal of the parasite's lifecycle within the infected host. Over time, the infection is usually controlled by the host's immune system and eventually eliminated (4). However, a fraction of cases do not resolve without treatment, and proceed to severe infection. Progression to severe malaria is particularly likely in young children and those with compromised immune systems. In regions of Africa where the disease is endemic, almost twenty-five percent of childhood mortality has been attributed to severe malaria (4).

Until the disease is completely eradicated there will always be a need for novel antimalarial drugs that can slow or halt the progression of the disease. One of the most notable advancements in the 20th century with regards to malaria research was the formal discovery of artemisinin, achieved through Mao Zedong's directive to have several institutions and hundreds of researchers focus their efforts on finding new medicines to combat this disease (5). Artemisinin, derived from the Asian plant *Artemisia annua*, has since been incorporated into artemisinin combinations therapies (ACTs), a highly effective treatment regimen that has seen widespread deployment. The search for new drugs will continue in order to address the threat of acquired resistance, halt the progression of severe disease and prevent mortality, and eliminate parasite gametocytes to prevent further transmission (4).

Systems biology has emerged as an important tool in the search for new anti-malarial drugs, aiding the pursuit of understanding the mechanisms and efficacy underlying novel candidate drugs. The *in silico*

approach utilised by metabolomics and metabolic modelling grants insights that would otherwise have been prevented by practical or ethical constraints. To date, studies utilising this methodology have yielded identification of the optimal drug dosing intervals to achieve full parasite clearance (6), determination of whether cure rate was improved with use of split drug dosage (7, 8), and a comparison of the relative degrees of resistance induced by two different dosages of mefloquine (9). Another recent study has extended the scope of the modelled organism to include the host, giving a means of predicting the changes in glucose and amino acid metabolism in the human host (10). Use of such theoretical modelling has improved our knowledge of a disease that, despite more than a hundred years of research, still remains incompletely understood (11).

One aspect of the disease that continues to evade full understanding is the appearance of hypoglycaemia and hyperlactataemia (HG/HL) in patients with severe malaria (12). Both of these symptoms are indicative of severe disease and are associated with a high risk of mortality (1, 13). Scientific literature has described HG/HL as having a number of different causes, including parasite metabolism, sequestration resulting in microcirculatory hypoperfusion, kidney and liver failure, or hypovolaemia (1, 14, 15). However, while such qualitative explanations have undoubtedly been useful in guiding the search for novel drugs, they lack the quantitative basis that would provide a more robust understanding of the aetiology underlying the metabolic abnormalities associated with severe malaria, as well as the means with which to improve subsequent clinical outcomes.

It is this gap in understanding that the current research aims to ameliorate. A wealth of studies employing a systems biology approach have already provided many insights regarding metabolism (16–19), including the biological and biochemical networks found in *P. falciparum* and its human host (20, 21). Through the use of kinetic modelling, the overarching goal of the current research is to delineate the aetiology behind the appearance of HG/HL in severe malaria, improve understanding of the disease, and provide a quantitative basis for the pursuit of novel treatments.

In order to obtain such quantitative evidence that can give robust indications of which biochemical targets are most amenable to new antimalarial treatments, an *in silico* platform must first be constructed that can serve as a framework and platform for further development. The whole-body model presented in this thesis is intended to serve as such a framework, whereby the phenomenological implementations of expression describing host-parasite interactions can be accurately parameterised with future clinical data garnered from experimentation specifically suited towards obtaining empirical observations of changes in host metabolism caused by severe *P. falciparum* malaria.

1.2 Research Question, Aims, and Objectives

1.2.1 Research Question

Can a kinetic modelling approach be used to estimate the relative contribution of suggested causes to hypoglycaemia and lactic acidosis in cases of severe *Plasmodium falciparum* malaria?

1.2.2 Aims

The aims of this thesis are:

1. Construction of a whole-body model of glucose and lactate metabolism in the infected human host that allows examination down to and including the enzymatic level

2. Implementation of *in silico* descriptions of aspects of *Plasmodium falciparum* pathophysiology that have been reported in the literature as causal or contributory factors of hypoglycaemia and hyperlactataemia

1.2.3 Objectives

The research objectives are:

1. Identify, reproduce, and test the viability of independently published models giving sufficiently detailed kinetic descriptions of one or more organ compartments relevant to glucose and lactate metabolism.
2. Adapt and merge the selected models into a whole-body model of glucose and lactate metabolism.
3. Validate the whole-body model by comparison of simulation outputs with both the original model's outputs and clinical data of patients with severe *Plasmodium falciparum* malaria.
4. Test whether glycolytic parasite metabolism alone can cause hypoglycaemia and hyperlactataemia in the current model.
5. In the case of model outputs failing to match clinical data; modify and extend the model with features, phenomenological or otherwise, to introduce host-parasite interactions that have a significant effect on plasma glucose and lactate, as reported in literature.
6. Identify which components of the whole-body model have the most significant role in the pathogenesis of lactic acidosis and hypoglycaemia; and determine which of these would be the best targets for existing or novel clinical interventions

1.3 Thesis Structure

This thesis is divided into the following chapters:

i. Chapter 1: Introduction

The general introduction, as presented here.

ii. Chapter 2: Background and Literature Review

This chapter introduces the concepts that are discussed and explored in this thesis. This section includes broad overviews of malaria as a global health burden, the biology and metabolism of the parasite responsible for the disease, and the underpinnings of whole-body glucose and lactate metabolism within the human host. This is followed by more detailed discussions that converge on the proposed pathological mechanisms of hypoglycaemia and hyperlactataemia in cases of severe malaria, and the suitability of systems biology to investigate the underlying aetiology thereof. The chapter ends with a section intended to introduce the reader to the fields of systems biology and kinetic modelling. Discussion of these topics is arranged in an order that guides the reader from a general understanding of malaria to the specific area of research covered by this thesis.

iii. Chapter 3: Methods

The Methods chapter contains descriptions of the methodology employed during the construction of the final model. The rationale for decisions and changes made during the course of research are explained. An additional section is included as an appendix, briefly illustrating the software written as part of this research to expedite the modelling process.

iv. Chapter 4: Results & Discussion

The Results section contains descriptions of results obtained from model simulations as pertaining to the aims and objectives set out in Chapter 1. These include demonstrations of how the model was validated, the results of model simulations satisfying the original research objectives, and other data that support conclusions drawn in this chapter.

v. Chapter 5: Recommendations, Summary & Conclusion

Model shortcomings are discussed, together with recommendations for further development of the model and possible future research. The model concludes with a summary of the thesis and a general conclusion.

Chapter 2: Background and Literature Review

This chapter introduces the concepts that are discussed and explored in this thesis. This section includes broad overviews of malaria as a global health burden, the biology and metabolism of the parasite responsible for the disease, and the underpinnings of whole-body glucose and lactate metabolism within the human host. This is followed by more detailed discussions that converge on the pathological mechanisms leading to hypoglycaemia and hyperlactataemia in cases of severe malaria, and the suitability of systems biology to investigate the underlying aetiology thereof. Discussion of these topics is arranged in an order that guides the reader from a general understanding of malaria to the specific area of research covered by this thesis.

2.1 Epidemiology

The most recent estimates indicate that during 2016, malaria had infected approximately 3% of the world population and claimed the lives of 445 000 people (22). The overwhelming majority of sufferers are young sub-Saharan children, typically those aged five years or younger (1). Additionally, infants born to mothers with malaria have an increased risk of low birth weight, anaemia, and mortality (23). In the genus *Plasmodium*, *P. falciparum* is responsible for nearly all cases of severe disease and subsequent mortality. With regards to transmission, all malaria parasites, including *P. falciparum*, are transmitted via mosquito vectors, specifically female *Anopheline* mosquitos. Of the several hundred *Anopheline* species, more than 70 are capable of transmission (24), with approximately 25 constituting particularly effective vectors (25). *Anopheles gambiae* is thought to constitute the primary vector of *P. falciparum* within Africa (26).

Malaria is found throughout the tropics of Africa, South America, South-east Asia and Oceania, and the Indian subcontinent. *P. falciparum* constitutes virtually all cases of malaria in Africa (27). Though the epidemiology of malaria is relatively easy to discern and interpret on a large geographical scale at low resolution, the situation becomes substantially more complex when considering smaller geographic areas. Even in regions with generally low transmission rates, small geographic regions with a combination of factors favourable to transmission can continue to drive malarial infection and frustrate eradication efforts.

2.2 Parasite Biology & Lifecycle

The process of malaria infection begins with the bite of a female *Anopheline* mosquito, which inoculates the host with plasmodial sporozoites during a blood meal (23). These sporozoites, originating from the mosquito's salivary gland, are injected into the host vascular space as the mosquito aspirates blood. The

number of sporozoites injected is typically small and in the range of 8 to 15, but in some cases may be on the order of a hundred. Post-inoculation, the circulating sporozoites that have not been cleared by splenic filtration rapidly proceed to invade the hepatic parenchyma. Once inside the hepatocyte, the sporozoite undergoes asexual reproduction, a process lasting approximately five and a half days on average in *P. falciparum*. Once this phase is complete, the infected hepatocytes rupture, releasing merozoites into the host circulation. During this pre-erythrocytic phase, many merozoites may be produced, but since only a few hepatocytes were initially invaded, no symptoms are present at this stage (23).

The initiation of the parasite's asexual blood-stage development begins with the invasion of erythrocytes by merozoites. Merozoites are small, motile, ovoid cells which are capable of attaching to the external erythrocytic membrane via an apical complex. The merozoite then proceeds to invade the erythrocyte in a wriggling or boring motion, collecting a vacuole consisting of the invaginated erythrocyte membrane. Once internalised, the parasite lies within the erythrocyte cytosol surrounded by both its plasma membrane and an enveloping parasitophorous vacuolar membrane (PVM)(28). At this point, the intraerythrocytic parasite begins to mature into the next stage, termed the 'ring' stage, due to its eponymous appearance under microscopic examination (21). Further maturation leads to the development of a trophozoite, with a characteristic signet-ring appearance. Later, the parasite further develops and matures into a schizont, a multi-nucleated form of the parasite produced by several cycles of karyokinesis. Each schizont will on average produce around 15 to 30 merozoites, which will subsequently be released into the circulation following rupture and lysis of the infected erythrocyte membrane. The merozoites then proceed to reinvade more erythrocytes, beginning the cycle anew (**Fig. 2.1**).

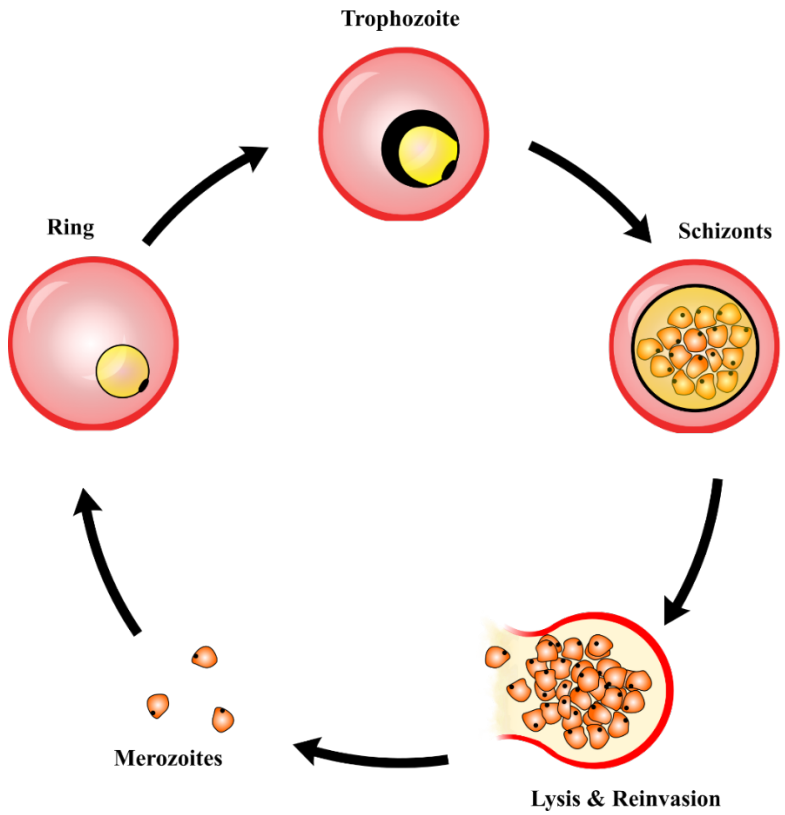

Figure 2.1: The 48-hour lifecycle of asexual blood-stage *Plasmodium falciparum*

The entire cycle lasts approximately 48 hours, a duration specific to *P. falciparum* (23). Over time, these reproductive cycles produce a parasite burden that grows exponentially in volume within a cycle, and in number of parasites over several reproductive cycles (**Fig 2.2**).

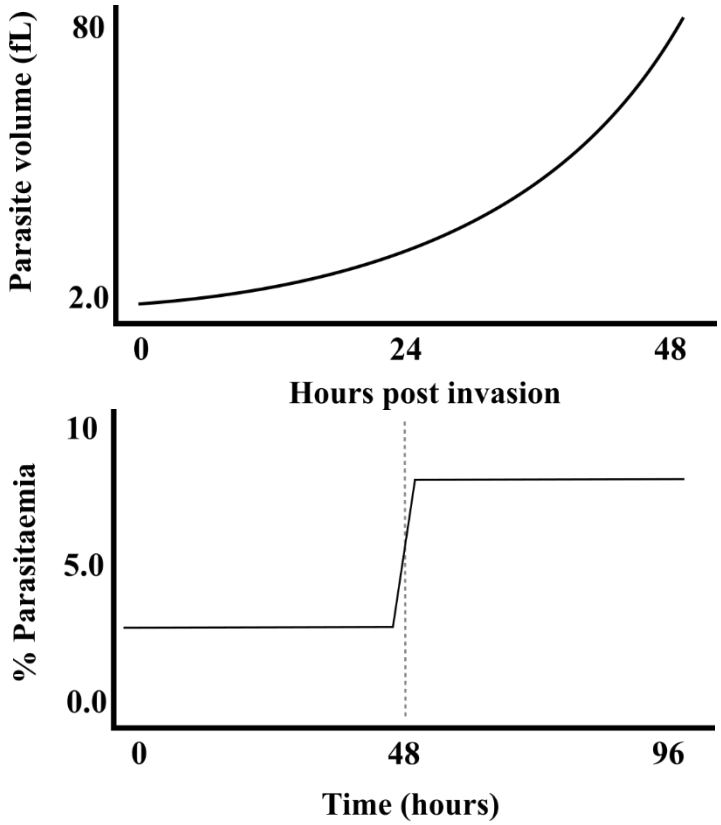

Figure 2.2: Simulations of the change in volume and number of the parasite within and between its 48-hour lifecycle. Simulation parameters obtained from (21)

2.3 Parasite Metabolism

The asexual blood-stage parasite, lying within the infected erythrocyte and enveloped by the PVM, is dependent upon the parasitized red blood cells cytosol and membrane for the trafficking of nutrients. To this end, the parasite exports several hundred proteins to the infected erythrocyte cytosol through the PVM. These parasite-derived proteins proceed to alter the structural properties of the infected erythrocyte membrane, particularly its permeability to low molecular weight solutes (29). The parasite-mediated alteration of the host cell membrane includes the introduction of new permeability pathways, or NPPs. These NPPs are non-specific, integral membrane channel proteins which permit entry of nutrients into the host cell cytosol. Though the host erythrocyte's existing transport functionality is sufficient for the majority of nutrients required by the parasite, the NPPs are necessary for the uptake of glutamate, pantothenate and choline from plasma (21).

The metabolism of protozoans of the genus *Plasmodium*, including *P. falciparum*, is notable in that they are almost completely reliant upon anaerobic glycolysis for the synthesis of ATP during the asexual blood-stage (20, 30). Carbohydrate sources are limited to glucose and fructose, with ribose, mannose or galactose unable

to undergo catabolism by the parasite (31–33). Outside the asexual blood-stage phase of its lifecycle, the parasite is capable of free energy production via TCA cycle activity, with the pyruvate dehydrogenase (PDH) complex being able to produce acetyl-CoA from pyruvate, the penultimate metabolite of anaerobic glycolysis. However, in the asexual phase, the PDH complex is relegated to the apicoplast, thereby leaving flux through lactate dehydrogenase to produce lactate as the only remaining viable pathway for maintaining redox balance within the parasite compartment through pyruvate reduction (20, 34). Complete glycolytic catabolism of glucose by the parasite gives a net yield of approximately two moles of ATP and two moles of lactate per mole glucose utilised (30). Despite this dependence on glycolysis, the maturing intraerythrocytic parasite does not convert all of the imported glucose to lactate, with 30-40% being shuttled to anabolic processes required for growth and differentiation (35).

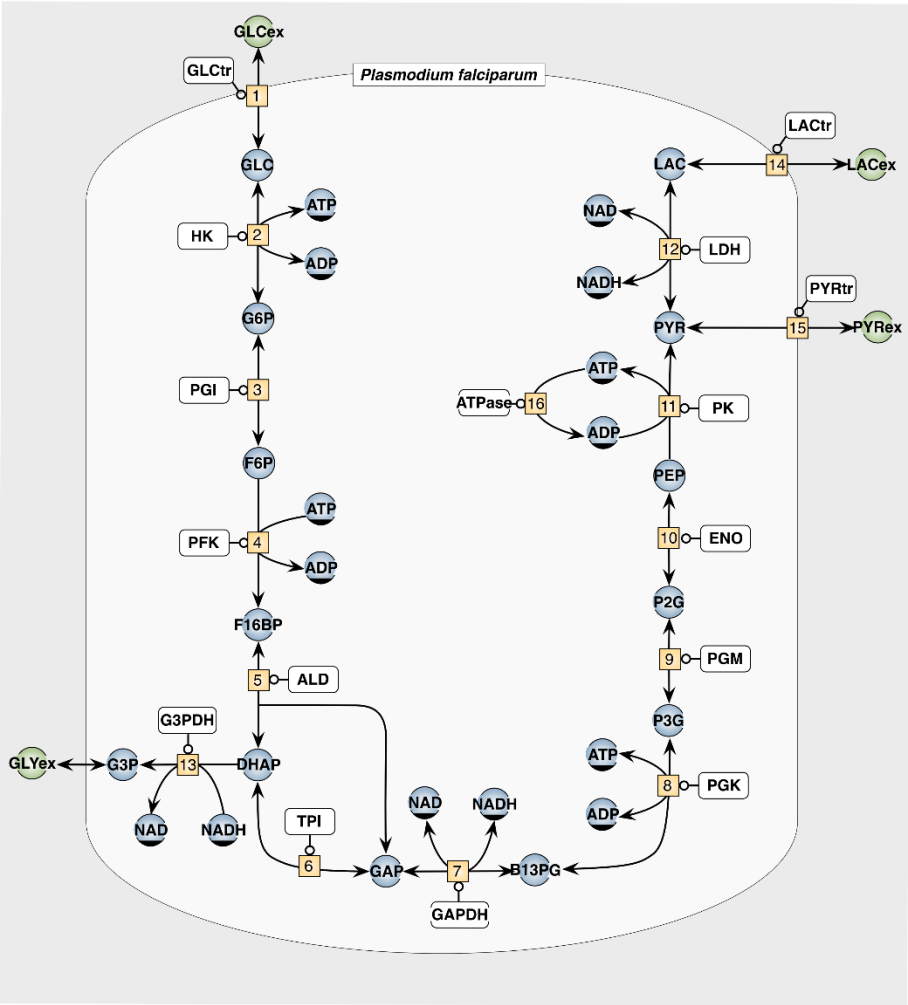

Figure 2.3: Glycolysis in *P. falciparum* as described by Penkler (20)

To satisfy this demand for glucose, and dispose of the lactate produced, the parasite makes use of both existing erythrocytic and novel parasite-derived transport mechanisms. Between the host serum and the parasite cytosol, three membranous barriers are present: the erythrocytic membrane, the PVM, and the parasite cell membrane. Transport of glucose across the host cell membrane is achieved via both endogenous erythrocytic hexose transporters and the NPPs previously described (21, 29). A non-selective, high-capacity channel mediates transport of glucose across the PVM (36), while entry into the parasite cytosol is achieved

through action of parasite hexose transporter 1 (PHT1), a passive, saturable transporter (32, 37). The concerted action of this series of transporters can produce a rate of glucose uptake that can equal up to 100 times that of uninfected erythrocyte (38). Disposal of the end product of anaerobic glycolysis, lactate, is carried out by a lactate-proton cotransporter (39, 40), which mediates the simultaneous efflux of protons and lactate from the parasite cytosol. Subsequent export across the erythrocyte membrane is achieved through existing endogenous mechanisms, including the monocarboxylate transporter 1 (MCT1), band 3 anion transport protein, and diffusion across the lipid bilayer (21).

2.4 General Pathophysiology

The clinical presentation of malaria varies depending on the progression of the disease and the age of the infected individual (41). During the initial infection, a common set of non-specific symptoms appear, such as the appearance of fever, headache, fatigue, abdominal discomfort, muscular aches, and a general feeling of malaise (1). More severe symptoms that also commonly occur include nausea, vomiting, and orthostatic hypotension. The clinical presentation of advanced *P. falciparum* malaria, however, is heterogenous. The set of symptoms accompanying severe infection can be markedly different depending on the age of the infected individual (**Fig. 2.4**). Anaemia, hypoglycaemia, and convulsions are more common in younger patients, while adults are more likely to present with renal failure, jaundice and acute pulmonary oedema. Coma and acidosis, on the other hand, appear to not be significantly affected by age, and occur in approximately half of all patient populations.

The pathophysiology for a particular symptom has been attributed to a number of different aetiologies, e.g. the periodic paroxysms associated with malaria infection are thought to be due to toxins released by the parasite upon erythrocyte rupture (23). While some research has indeed identified substances originating from the parasite that have a stimulatory effect on the immune system, the organ-specific pattern of severe malaria non-periodic pathology lends more credence to the concept of heterogenous parasite sequestration, whereby the particular set of symptoms present is a function of the distribution of sequestered parasites within the infected individual. For example, the presence of kidney or liver failure would indicate that a large proportion of parasites have adhered to the renal and hepatic endothelium. Conversely, the presence of pulmonary oedema has been linked to pathological endothelial activation of the pulmonary microcirculation. The aetiology and significance of parasite sequestration will be discussed in greater detail in **Section 2.6.4**.

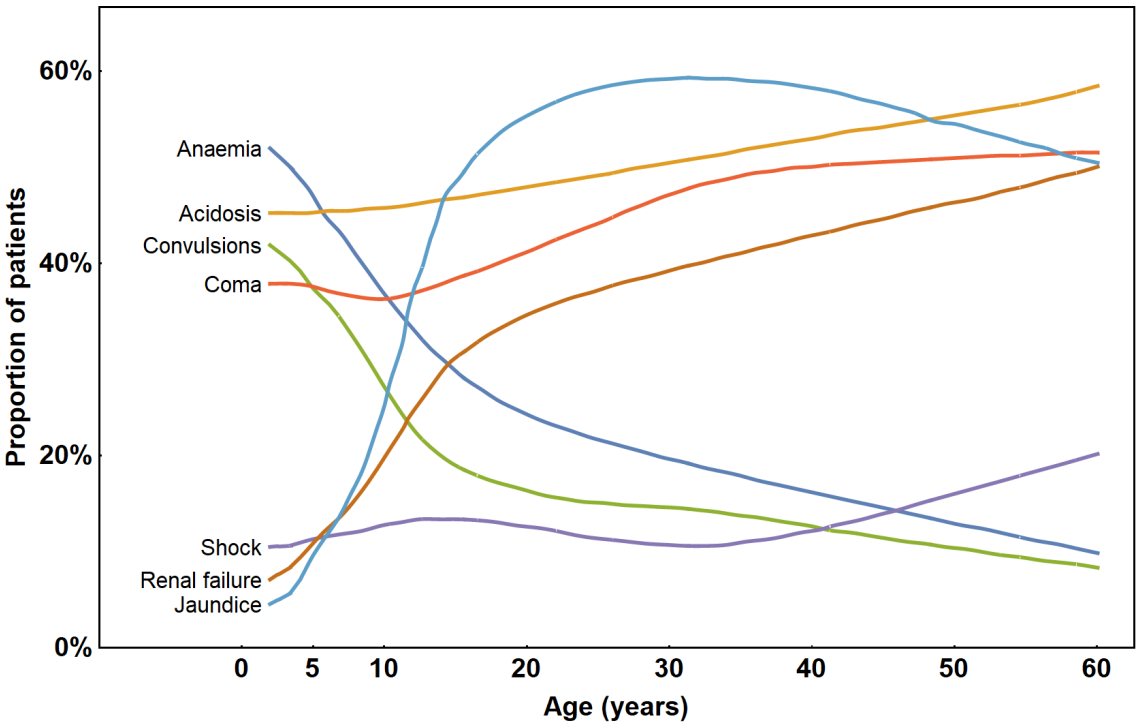

Figure 2.4: Relationship between patient age and clinical presentation in individuals infected with malaria. Adapted from (23)

2.5 Hypoglycaemia

In healthy individuals, blood glucose concentration is typically maintained within the range of 4.0 – 6.0 mM (42). This homeostatic maintenance reflects the balance between glucose provision and utilisation, mediated both exogenously, via dietary intake, and endogenously, via gluconeogenesis and glycogenolysis (43). Whole-body coordination of these processes is achieved through endocrinological means, chiefly through the actions of insulin, glucagon, and catecholamines (44). Hypoglycaemia, defined by the WHO as a blood glucose concentration less than 2.2 mM (45), is relatively common in both children (46) and adults (47) with severe malaria. Hypoglycaemia exhibits particularly high prevalence in children aged three years or less, likely owing to the increased tendency of children to become hypoglycaemic when fasting, especially when accompanied by fever and emesis. Hypoglycaemia is typically associated with worse clinical outcomes and increased mortality. This relationship is especially pronounced in paediatric cases, where hypoglycaemia has been found to be one of the strongest predictors of mortality (13). This association appears to hold less true for adults (48), where its prognostic value is mostly attributed to its co-presentation with acidosis.

Since blood glucose concentration reflects the sum of the opposing homeostatic forces of glucose uptake and release, it follows that hypoglycaemia can be attributed to either a deficient rate of glucose release, an accelerated rate of uptake, or a combination of the two. An insufficient rate of glucose release into the plasma can have a number of causes, such as malnutrition, or derangements of endogenous metabolism, such as impaired gluconeogenesis or glycogenolysis. An abnormally high rate of plasma glucose uptake can possibly be attributed to accelerated carbohydrate metabolism or aberrations of the endocrinological system, such as hyperinsulinaemia. All of these possible causes have been mentioned in the literature as possibly

being responsible for the appearance of hypoglycaemia. The following sections discuss the relative significance of these various aetiologies.

2.5.1 Glucose utilisation

Substantial evidence exists of accelerated glucose turnover in both children (49–52) and adults (47, 53) with severe malaria. The rate of glucose turnover in children is approximately five-fold that found in adults with severe malaria. Increased glucose utilisation is thought to occur due to features of the disease state, such as fever and convulsions, the systemic shift towards anaerobic glycolysis, and, to a lesser degree, glucose uptake by the malaria parasites (12).

Considering the 30 to 100-fold increase in glucose uptake by infected erythrocytes in comparison to healthy red blood cells (38, 54), the manifestation of hypoglycaemia can, at least in part, be ascribed to the metabolic demands imposed by the growing parasite population. However, when compared to the rate of glucose consumption by the host, glucose uptake by infected erythrocytes is relatively minor.

Contemporary literature does not feature definitive statements regarding whether glucose consumption by parasites and infected erythrocytes constitutes the primary cause of hypoglycaemia, or whether it should be considered a contributing factor together with other aetiologies. One review listed several host factors external to parasite metabolism that could cause or contribute to the appearance of hypoglycaemia. These included the Pasteur effect (an increased peripheral glucose uptake due to a shift towards anaerobic glycolysis), upregulated metabolism in the febrile state, and an impairment of hepatic gluconeogenesis and glycogenolysis (23). Some of these factors are thought to be significant in paediatric patients, owing to their substantially higher rates of glucose turnover in response to severe malaria, and their much smaller capacity for glycogen storage.

2.5.2 Gluconeogenesis

Impairment of gluconeogenesis has been frequently cited as one of the chief causes of hypoglycaemia in patients with malaria (55, 56). This consensus was reached after the consideration of two sets of observations from patients with malaria: low rates of gluconeogenesis in hypoglycaemic children (50, 51), and increased plasma concentrations of gluconeogenic precursors (57, 58). Combined with the erstwhile technological limitations and paucity of data, these findings seemed to imply at the time that deficient hepatic synthesis of glucose despite an abundance of gluconeogenic substrates is a major causative factor of hypoglycaemia in patients with malaria. However, there has been some contention regarding this finding as a result of more recent studies examining the role of gluconeogenesis in the pathology of hypoglycaemia in cases of severe malaria.

More recent studies examining glucose dynamics have consistently showed that glucose production is increased in patients with malaria vs. healthy controls (59). Increased gluconeogenesis was found regardless of age, and appeared to correlate with disease severity. Children with severe malaria exhibited dramatically increased rates of glucose production when compared with uncomplicated infections (49, 50). Similarly, in

adults, glucose production was found to be upregulated by approximately 20% in those with uncomplicated infections (56, 60), 35% in pregnant women with uncomplicated malaria (56), and 100% in adults with severe malaria (53). In one notable study of adults with cerebral malaria, gluconeogenesis was found to account for the entirety of endogenous glucose production (61).

Lactate, alanine, and glycerol comprise the bulk of gluconeogenic substrates; the plasma concentrations of these precursors are elevated in both children (62) and adults (63) with severe malaria. To investigate why hypoglycaemia persisted despite the abundance of gluconeogenic precursors, several studies were conducted to determine whether this was due to inhibition of gluconeogenesis. To this end, glucose production was measured after infusion with gluconeogenic substrates. While conversion of glycerol and galactose appeared normal (63), alanine utilisation was found to be impaired (64). These findings suggested selective impairment of gluconeogenesis, whereby pathways 'proximal' to pyruvate were inhibited, while more 'distal' ones were not.

However, contemporary studies have suggested that high plasma concentrations of gluconeogenic precursors in severe malaria are not due to impairment of gluconeogenesis. Instead, emphasis has been placed on factors such as increased anaerobic glycolysis, inhibition of alanine metabolism by hyperlactataemia, reduced hepatic perfusion, or impaired liver function (55, 64). One conclusion that can be drawn from this is that hypoglycaemia due to hepatic impairment is due to a more generalised failure of liver function. However, liver failure is a relatively uncommon complication, even in severe malaria (65, 66).

2.5.3 Glycogen metabolism

Protracted hypoglycaemia gives rise to rapid depletion of glycogen stores, as glycogenolysis is continually upregulated by elevated levels of glucagon. The speed of glycogen depletion is especially pronounced in children, owing to smaller glycogen stores (67). This reduced capacity for glucose provision through glycogenolysis has often been cited as a contributing factor for the sustained presence of hypoglycaemia in children with severe malaria (68). Additionally, endogenous glucose production in response to glucagon infusion is diminished in both children (69) and adults (58), giving further evidence of extensive glycogen depletion in patients with malaria.

However, the hypothesis that hypoglycaemia is exacerbated by impaired glycogenolysis due to diminished glycogen stores has been contradicted. A recent study examined the relative rates of glycogenolysis in fasted adults with or without uncomplicated malaria. Though the rate of glycogenolysis was substantially lower in the malaria patients, the rate of decline of glycogenolysis was slower than that observed in the healthy controls (70). In other words, the rate of glycogenolysis did not appear to be limited to the same degree by reduced substrate availability, implying that glycogen metabolism is altered to guarantee glucose output and maintain euglycaemia. This suggests that glycogen depletion does not contribute to hypoglycaemia in malaria, a notion further supported by the presence of unutilised hepatic glycogen in hypoglycaemic patients with severe malaria (23, 58).

2.5.4 Quinine-Induced Hyperinsulinaemia

Owing to quinine's ability to stimulate insulin secretion by pancreatic beta-cells, hyperinsulinaemia and subsequent hypoglycaemia has been associated with quinine administration (23, 71). While this relationship has been confirmed in adults suffering from severe malaria, a study has concluded that there is no evidence of hypoglycaemia occurring as a result of quinine administration in African children (72).

However, since the effect of antimalarials are beyond the scope of the current research, the utility of this information is relegated to interpretation of clinical data obtained from adults, where measurements of blood glucose concentrations should be given closer scrutiny if quinine administration was present.

2.6 Overview of Lactate Metabolism

2.6.1 Lactate production

Lactate is produced as part of the final step of anaerobic glycolysis in humans, where pyruvate is reduced to form lactate via catalysis by cytosolic lactate dehydrogenase (LDH, **Fig. 2.5**)(73). Under normal physiological conditions, this reversible reaction favours lactate production with an approximate 10:1 lactate-pyruvate ratio (74). Like all preceding steps in glycolysis, this process does not require the presence of oxygen. Lactate production by the LDH catalysed reduction of pyruvate serves as a useful proxy for monitoring anaerobic metabolism.

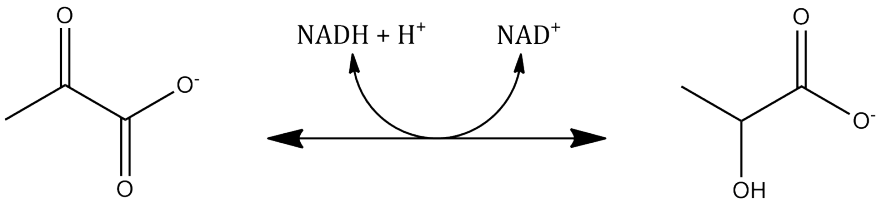

Figure 2.5: The reaction catalysed by lactate dehydrogenase

To produce ATP, glycolysis requires not only glucose, but also a readily available supply of oxidized nicotinamide adenine dinucleotide (NAD^+). Provision of NAD^+ is mediated, in part, by the action of LDH. In a healthy, normoxic individual at rest, approximately 10% of cytosolic pyruvate is reduced to lactate by LDH (75). The reduction of pyruvate is facilitated by NADH, which is oxidized to NAD^+ (76).

$$\frac{[Lactate]}{[Pyruvate]} = K_{Eq} \cdot \frac{[NADH]}{[NAD^+]} \cdot [H^+]$$

Hence, cytosolic lactate concentration is influenced not only by pyruvate concentration, but also by pH and the ratio of $NADH/NAD^+$ (77).

In humans, the bulk of cytosolic pyruvate will be transported into the mitochondria for use by the tricarboxylic acid (TCA) cycle. The TCA cycle, in turn, provides NADH for use by oxidative phosphorylation, a process that requires oxygen. Thus, should an oxygen deficit accrue, LDH activity will rise as pyruvate concentration rises and the $NADH/NAD^+$ ratio increases (78, 79). In this way, the ATP-

generating capacity of glycolysis is preserved by lactate production as NAD^+ is replenished and the concentrations of pyruvate and H^+ are simultaneously decreased (79–81).

Plasma lactate is principally derived from two sources: glucose and alanine (82). Glucose contributes approximately 65% of plasma lactate, following its catabolism via anaerobic glycolysis. Alanine contributes approximately 16-20% of plasma lactate by virtue of its ability to be converted to pyruvate, as catalysed by alanine aminotransferase (83). The remainder is constituted by the catabolism of other amino acids, which include serine, threonine and cysteine (84).

Anaerobic glycolysis produces a maximum of two molecules of ATP per molecule of glucose catabolised; this figure rises to 36 ATP per molecule of glucose in the case of aerobic glycolysis (78, 85). While the shuttling of pyruvate into the mitochondria for the ultimate purpose of oxidative phosphorylation does result in a greater overall net energy yield, the reduction of pyruvate to lactate as part of anaerobic glycolysis is necessitated in some cases. These include insufficient tissue oxygen delivery (DO_2) during intense exercise, or simply the absence of mitochondria, as is the case in erythrocytes. Despite its apparent inefficiency, homolactic fermentation can produce ATP at a rate up to 100 times faster than aerobic glycolysis. (86, 87).

The production of lactate is partitioned amongst various tissues. These include muscle (25%), skin (25%), the brain (20%), intestines (10%) and erythrocytes (20%)(88). Erythrocytes, leukocytes and platelets contribute 80, 13 and 7% of lactate production within the blood, respectively (89, 90). These values are subject to change, especially during illness. In addition to the thermogenic energy expenditure levied by fever, lactate production by leukocytes (particularly neutrophils) increases dramatically as part of the immune response.

Organs that are typically considered net consumers of lactate, such as the liver and kidneys, can become net producers of lactate if microvascular perfusion becomes sufficiently compromised (91–93); this phenomenon becomes especially pertinent in the case of severe malaria, as is discussed in this thesis.

2.6.2 Lactate clearance

Lactate is cleared from the circulation primarily via oxidation to pyruvate, primarily in hepatic, renal, and cardiac tissues. This pyruvate can experience two metabolic fates: oxidative catabolism in the mitochondria, or conversion to glucose as part of gluconeogenesis. Both of these processes begin with the same two steps: oxidation to pyruvate by LDH, and subsequent transport into the mitochondria (94).

2.6.2.1 Oxidative catabolism of pyruvate

The oxidative metabolism of pyruvate within the mitochondria to ultimately yield ATP is a complex process that involves sequential action of the pyruvate dehydrogenase (PDH) complex, the TCA cycle, and the mitochondrial electron transport chain (ETC). The process begins with the oxidative decarboxylation of pyruvate to produce acetyl-CoA, accompanied by the reduction of NAD^+ to NADH (95, 96). This reaction, catalysed by the PDH complex, is irreversible. Acetyl-CoA subsequently proceeds through the TCA cycle, wherein it is metabolised to yield carbon dioxide, NADH and flavin adenine dinucleotide ($FADH_2$)(97, 98).

In the inner mitochondrial membrane, NADH and $FADH_2$ are re-oxidized as part of the ETC, providing reducing equivalents used to reduce molecular oxygen, and protons that give rise to a chemiosmotic gradient. This chemiosmotic gradient is harnessed by ATP synthase to catalyse the oxidative phosphorylation of ADP to finally yield ATP (99, 100).

2.6.2.2 Gluconeogenesis

Gluconeogenesis, an anabolic pathway present primarily in tissues such as the liver and kidney, mediates the endogenous production of glucose, and contributes substantially to lactate clearance (**Fig. 2.6**)(101). Mitochondrial pyruvate carboxylase (PC) catalyses the carboxylation of mitochondrial pyruvate to form oxaloacetate (102).

$$Pyruvate + ATP \overset{PC}{\rightarrow} Oxaloacetate + ADP + P_i$$

Mitochondrial oxaloacetate can then be converted to phosphoenolpyruvate (PEP) via catalysis by phosphoenolpyruvate carboxykinase (PEPCK).

$$Oxaloacetate + GTP \overset{PEPCK}{\longrightarrow} PEP + GDP$$

Alternatively, mitochondrial oxaloacetate can be converted to malate, as catalysed by malate dehydrogenase (MDH) and transported to the cytosol.

$$Oxaloacetate + NAD^+ \overset{MDH}{\longleftrightarrow} Malate + NADH + H^+$$

Cytosolic malate is converted back to oxaloacetate, which can then be converted to PEP by the cytosolic isoenzyme of PEPCK (103). The reactions catalysed by pyruvate carboxylase and PEPCK are irreversible and therefore play a significant role in determining the overall rate of gluconeogenesis (104).

The remainder of gluconeogenesis is effectively glycolysis in reverse, with PEP being sequentially converted through the same set of glycolytic intermediates. Enzymes catalysing the reversible reactions similarly remain unchanged. The two glycolytic enzymes catalysing irreversible reactions, phosphofructokinase-1 and hexokinase, are replaced by fructose-1,6-bisphosphatase 1 and glucose-6-phosphatase, respectively. Like pyruvate carboxylase and PEPCK, they are also irreversible and important in determining overall gluconeogenic activity (87).

Gluconeogenesis, with lactate or pyruvate as the initial substrates, is an endergonic process that results in a loss of free energy. The reactions catalysed by pyruvate carboxylase and 3-phosphoglycerate kinase each involve the hydrolysis of one molecule of ATP; one molecule of GTP is also consumed during the conversion of oxaloacetate to PEP by PEPCK (105). Since two molecules of lactate or pyruvate are required to synthesise one molecule of glucose, a total of six ATP equivalents is consumed. Given that the glycolytic conversion of one molecule of glucose to two molecules of pyruvate yields two molecules of ATP, the net energetic cost of glycolysis followed by gluconeogenesis (i.e. glycolytic conversion of glucose to pyruvate and then back again) is four ATP equivalents (87). Thus, the rate of gluconeogenesis will be impaired should the redox or energy state of the cell be compromised.

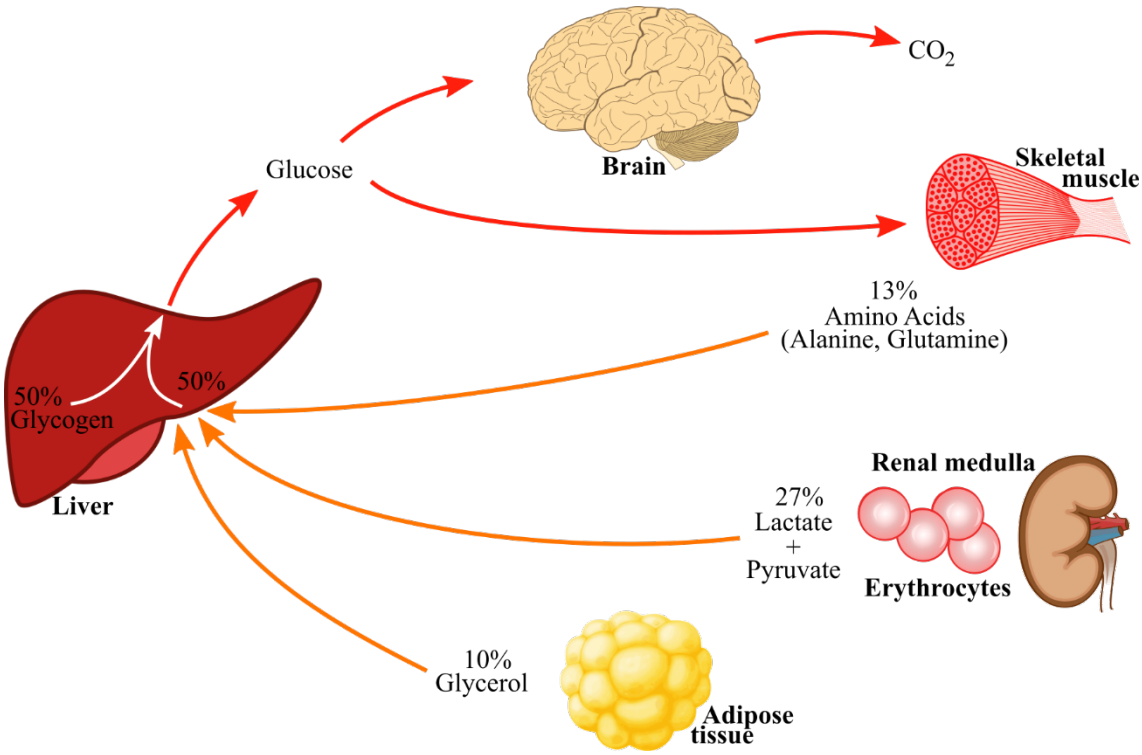

Figure 2.6: Generalised metabolic schema of whole-body glucose metabolism in the fasted state. The liver is responsible for the bulk of glucose provision, with approximately equal fractions originating from glycogenolysis and gluconeogenesis. The approximate percentage contributions of gluconeogenic substrates by other organs are shown adjacent to the orange arrows. The diagram shows a cyclical pattern whereby the catabolic products of glucose metabolism released by peripheral tissues is converted back into glucose by the liver, with the complete oxidation by the brain representing a net loss of glucose and glucose equivalents from the body. Lipid oxidation not shown. Figure adapted from (43)

2.6.2.3 Renal Lactate Excretion

The kidney is capable of the urinary excretion of small organic acids, including lactate (106). Given lactate's metabolic utility, it is typically not excreted by healthy individuals. However, should plasma lactate concentration exceed the renal threshold of approximately 5 mM, the kidney will begin to contribute to lactate clearance via excretion in the urine (88).

2.6.2.4 Organ-specific Lactate Clearance

Exact estimates of the relative contribution of each organ to lactate clearance have been difficult to determine. This has been due to not only technical and methodological limitations (107), but also biological factors, including nutritional status, recent exertion, and the prevailing lactate concentration within the plasma (79, 82).

However, despite these challenges, the literature does contain some approximations of the relative contribution of each organ to lactate removal from circulation. The liver and kidneys, two major sites of gluconeogenesis, account for approximately 60% and 30% of total whole-body lactate clearance respectively (88, 108), with the remainder mediated by the heart and skeletal muscle (109). The predominance of the liver and kidneys is unsurprising considering their role as the two major sites of gluconeogenesis. Lactate is

considered to be the dominant gluconeogenic substrate used by these organs in healthy postprandial humans (110).

Of the lesser gluconeogenic tissues, the myocardium appears to be the most important (111, 112). Isotopic studies have estimated that approximately 5% of systemic lactate uptake is mediated by the heart (113). The majority of lactate taken up by the myocardium is oxidized as a source of energy (114).

The pattern of partitioning of lactate uptake amongst these organs is, however, subject to change, depending on the prevailing physiological conditions. For example, lactate uptake and release by skeletal muscle can vary substantially based on the degree of exertion or the plasma lactate concentration. Resting skeletal muscle exhibits simultaneous uptake and release of lactate, with a net release in healthy humans in the postabsorptive state (115). However, when only considering the absolute rate of lactate uptake, skeletal muscle can account for up to 27% of total removal of lactate from the circulation (116). Additionally, the unidirectional uptake of lactate by skeletal muscle has been found to be closely associated with arterial lactate concentrations (117). Resting skeletal muscle readily oxidizes lactate for the purposes for oxidative metabolism or glycogenesis (118). Taken together, these observations provide an explanation for the phenomenon where skeletal muscle displays a net uptake of lactate under sufficiently high plasma concentrations at rest.

Considering the myriad of different ways lactate clearance is managed by the several different pathways described here, the appearance of HG/HL despite these becomes a point of interest. A number of questions arise when considering the seemingly paradoxical co-presentation of excess plasma lactate and deficient blood glucose when lactate itself is a prime gluconeogenic substrate for the synthesis of glucose. Is the rate of parasite glycolysis so high that it can overcome the entirety of the host's metabolic homeostasis? Does the parasite modify the host's metabolism in a way that prevents it from carrying out gluconeogenesis? Does the parasite perhaps accelerate the host's glycolytic metabolism in such a way that the upregulated conversion of glucose to lactate can account for these symptoms? These questions form part of what initially drove the interest to pursue this research topic, and will form several of the main points discussed in the remainder of the thesis.

2.6.3 Malaria and Hyperlactataemia

2.6.3.1 Clinical significance

Acidosis in severe malaria is associated with a high risk of mortality. Several studies have concluded it to be one of the most powerful, if not the most powerful, prognostic indicator of death in both adults and children (13, 15, 119–121). Acidosis in patients with malaria is determined using measurements of base excess (>8 meq/L), plasma carbonate (<15 mM) or venous plasma lactate (>5 mM)(45). The presence of deep (acidotic) breathing has also gained acceptance as a diagnostic tool for acidosis in settings where laboratory facilities are unavailable (45, 122). Large-scale analyses, combining data obtained from studies in diverse patient populations, have given consistent estimates of the clinical incidence of acidosis in severe malaria to be in

the range of 40-50% (123–126). The prevalence of acidosis appears to be similar in both adults and children (124). Having discussed normal lactate metabolism in the healthy individual, the possible causes of lactic acidosis in severe cases of *P. falciparum* malaria will now be examined.

Lactate plasma concentration is determined by the rate of production versus the rate of removal. Therefore, hyperlactataemia occurs when the rate of lactate production exceeds the rate of removal for an extended period of time. The aetiology of hyperlactataemia within the context of severe *P. falciparum* malaria can thus be divided into increased lactate production, diminished lactate clearance, or a combination of the two.

2.6.3.2 Increased Production by Parasites

During the asexual blood-stage phases of the parasite lifecycle, *P. falciparum* is completely dependent upon glycolysis for free energy production (20). The parasite satisfies this metabolic demand by an up to 100-fold acceleration of glucose uptake by the infected erythrocyte. The intraerythrocytic parasite subsequently converts approximately 60-70% of this glucose to lactate, with the remainder committed to anabolic pathways, such as the synthesis of nucleic acids and the glycosylation of proteins and lipids required for parasite growth (21). The lactate produced by the parasite is exported to the infected erythrocyte's cytosol, from where it is released into the circulation.

The amount of lactate produced by the parasitized erythrocyte population is not insignificant, especially at higher percentage parasitaemias. However, multiple sources have stated that when taking into account the host's capacity for lactate clearance, parasite lactate production alone cannot account for sustained hyperlactataemia (12, 77, 93).

2.6.4 Microvascular Obstruction: A Unifying Aetiology

Though parasite lactate production itself is generally not considered quantitatively sufficient for the presence of hyperlactataemia, the ability of the parasite to adhere to the capillary endothelium has been routinely cited by recent literature as having significant implications for host lactate metabolism. The observed phenomenon whereby *P. falciparum* infected erythrocytes sequester in the peripheral microcirculation, and subsequently compromise capillary perfusion, has been considered to be the central mechanism underlying the development of pathologies associated with severe *P. falciparum* malaria (15, 127–130). Lactic acidosis in particular has been attributed to the changes in host lactate turnover mediated by microvascular obstruction within specific organs. The following sections will first examine the causes of this phenomenon, followed by the changes in host metabolism that subsequently occur.

2.6.4.1 Microvasculature

The term 'microvasculature' refers to the microcirculation within the capillaries and postcapillary venules, which contain erythrocytes, leukocytes and the endothelial lining, as well as the chemical effectors therein, such as cytokines, nitric oxide (NO), and reactive oxygen species (ROS).

Reduced microcirculatory blood flow, within the context of severe *P. falciparum* malaria, has many causes, but the end result is the same: reduced luminal diameter of capillaries and postcapillary venules with subsequently diminished oxygen and nutrient delivery to tissues (4, 15). The causes of disturbed microcirculatory blood flow and their involvement in the pathogenesis of severe malaria are discussed below.

2.6.4.2 Cytoadherence and sequestration

The phenomenon whereby parasitized erythrocytes adhere to and accrue within the blood vessels was first observed over a century ago by Italian pathologists Marchiafava and Bignami (131). Since then, the sequestration of infected red blood cells within the microvasculature of vital organs has been deemed the defining pathological characteristic of severe *falciparum* malaria (127).

Cytoadherence refers to the increased propensity for infected erythrocytes to adhere to the endothelial lining, while sequestration refers to the permanent adherence of parasitized red blood cells to the endothelium in capillaries and postcapillary venules (23), thereby removing them from the circulation and preventing their destruction by the spleen. Among the species of *Plasmodium* known to cause malaria in humans, increased cytoadherence and sequestration is unique to *P. falciparum*. Whereas mature parasites are readily visible on blood smears of other malaria types, they are rarely observed in *P. falciparum* malaria and are considered indicative of serious infection (23).

The process of sequestration begins with the parasite's expression of a family of proteins termed *Plasmodium falciparum* erythrocyte membrane protein 1 (*Pf*EMP1)(127). Subsequent interactions between these parasite-derived molecules and the host cell cytoskeleton lead to the appearance of "knobs": protrusions of the erythrocytic membrane which mediate attachment to vascular endothelial ligands. Intracellular adhesion molecule 1 (ICAM-1) and the cluster of differentiation 36 (CD36) protein are considered the most important endothelial receptors mediating attachment within and outside the cerebral microvasculature, respectively.

The timeline of infected erythrocyte adherence parallels the parasite's progression through its 48-hour asexual life cycle. In the febrile host, cytoadherence manifests approximately 12 hours after merozoite invasion, reaches half-maximal levels between 14-16 hours, and is virtually complete by 24 hours. Accordingly, cytoadherence is relegated to the mature stages of the parasite; ring-form parasites also exhibit adherence, albeit to a lesser degree (132, 133). The parasite thus spends the majority of its 48-hour life cycle sequestered within the peripheral circulation, explaining its absence from blood smears. Parasite adherence is terminated following erythrocyte rupture during merogony (schizogony) at the conclusion of the parasite life cycle, whereupon remnants of the erythrocyte membrane, complete with the attached pigment body, can still be found attached to the vascular endothelium (23).

Parasite sequestration is not distributed uniformly throughout the macro- or microvasculature: the distribution and extent of sequestration can differ both within and between organs. The degree of sequestration is typically highest in the brain (**Fig. 2.7**), followed by lesser, though still substantial, levels in

the liver, kidneys, heart, eyes, intestines, and adipose tissue (134). Within these tissues, the degree of sequestration and subsequent luminal occlusion is distributed heterogeneously, where hypo- and normoperfused regions can be found lying adjacent to one another (127).

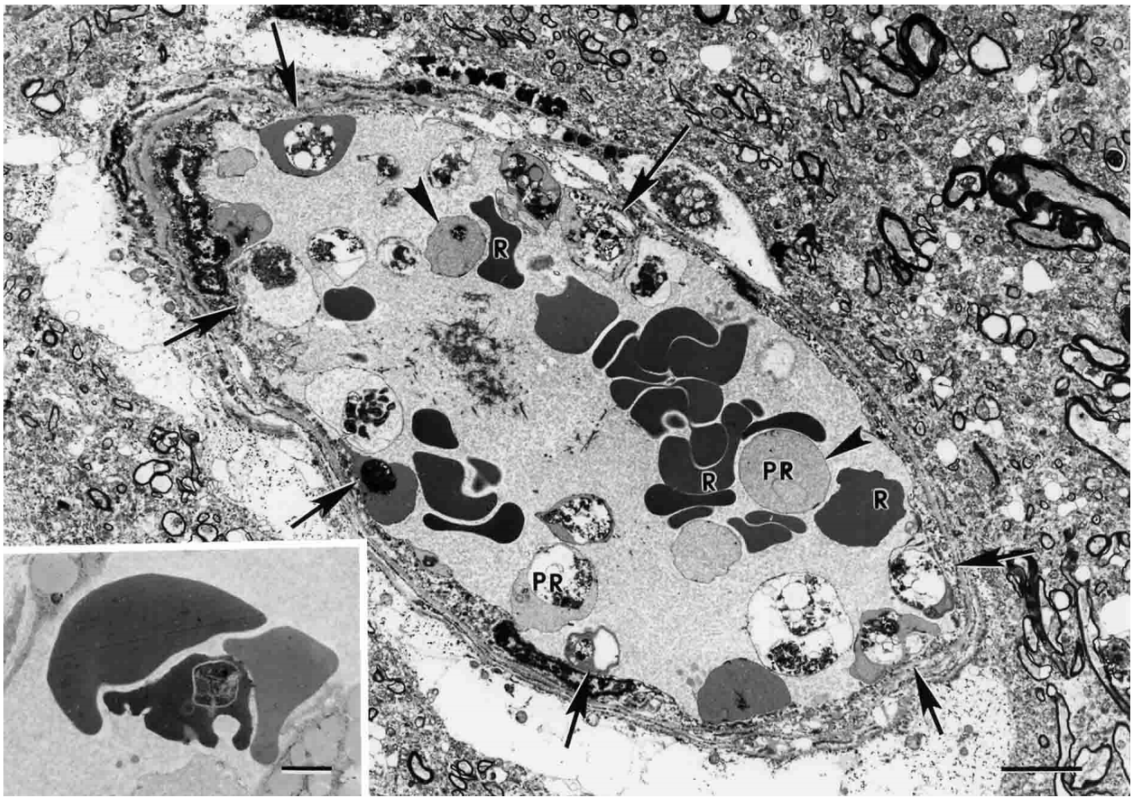

Figure 2.7: Electron microscope image showing cytoadherence and sequestration within a cerebral blood vessel in a case of cerebral malaria. Inset: Possible rosette formation shown by uninfected red blood cells surrounding a parasitized red blood cell. Legend: **PR**, parasitized red blood cell; **R**, uninfected red blood cell; **arrows**, parasitized erythrocyte ghosts; **arrowheads**, parasitized red blood cell surrounded by healthy erythrocytes, representing possible rosette formation. Image adapted from (135)

The study of parasite sequestration has provided not only etiological insights into *P. falciparum* pathophysiology, but also its major role in determining treatment outcome. Strong correlations have been observed between the degree of parasite sequestration and the three major independent predictors of mortality: cerebral malaria, metabolic acidosis, and acute kidney injury (127, 128, 134, 136, 137). General scientific consensus considers parasite sequestration to be the primary cause of microvascular obstruction and endothelial activation (**Section 2.6.4.5**), which lead to tissue hypoperfusion and acidosis. It should be noted, however, that some authors have disputed the order of this cause-and-effect relationship, arguing instead that parasite sequestration lies distal to acidosis and endothelial activation in the causal chain (138, 139).

2.6.4.3 Rosetting, agglutination and aggregation

Following cytoadherence of the parasitized erythrocyte to the endothelial lining, subsequent luminal occlusion can be compounded through rosetting, agglutination and aggregation. These processes encompass phenomena whereby clumps of cells are formed within the capillary or postcapillary venule lumen, as mediated by attachments between infected and uninfected erythrocytes (rosetting); attachments between

platelets and infected red blood cells (aggregation); and attachments between infected red blood cells only (agglutination)(130).

Rosette formation is a phenomenon whereby uninfected erythrocytes adhere to parasitized red blood cells (**Fig. 2.8**). Like cytoadherence, rosette formation begins at approximately the 16-hour mark after merogony. There are, however, several key differences. Rosetting in *P. falciparum* is not a ubiquitous phenomenon: while all fresh isolates of *P. falciparum* exhibit cytoadherence, not all rosette. This could be mediated by the variability in blood group antigens between individuals, as evidenced by the protective effect against rosetting conferred by blood group O (23).

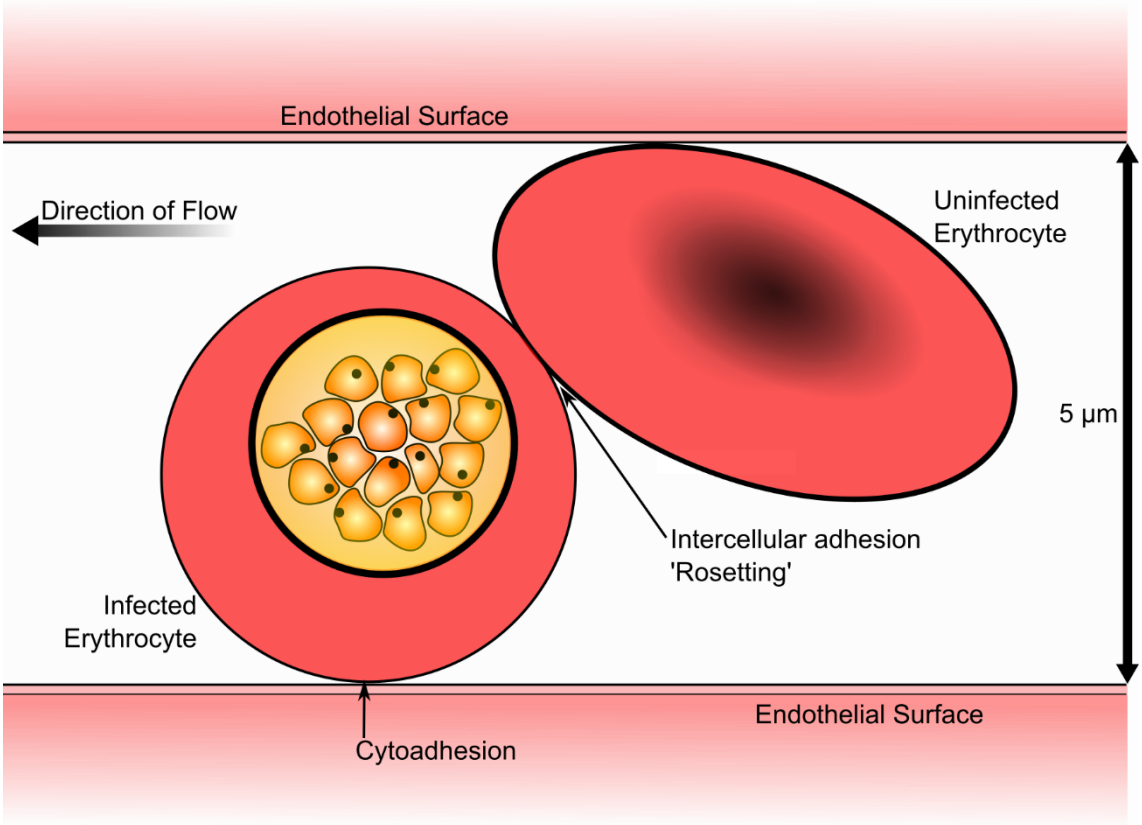

Figure 2.8: Cytoadhesion of infected erythrocytes to the luminal surface of the capillary endothelium impedes microcirculatory blood flow. To maintain blood flow, healthy erythrocytes must squeeze past the immotile parasitized erythrocytes, a process made difficult by the reduced deformability of infected erythrocytes and the propensity for healthy red blood cells to become trapped in nascent rosettes. Diagram adapted from (23)

Approximately five times as much force is required to separate a rosette when compared to the force required to separate a parasitized cytoadherent cell from the endothelium (23). Rosette formation typically occurs in post-capillary venules, likely facilitated by the obstruction of flow in proximal capillaries by cytoadherent infected erythrocytes. This suggests a scenario whereby cumulative luminal occlusion, as mediated by cytoadherence and rosetting, gives rise to ever-increasing degrees of obstruction of microvascular perfusion.

Agglutination (sometimes termed auto-agglutination) describes the formation of crosslinks between infected erythrocytes due to the parasite-induced expression of similar antigens on infected erythrocytic membranes (140). Similarly, aggregation involves adherence between infected erythrocytes, this time mediated by platelets (specifically platelet CD36). These platelet-containing aggregates are associated with disease

severity, and, in addition to rosetting and agglutination, likely contribute to reduced perfusion of the microvasculature (23).

2.6.4.4 Red cell deformability

The diameter of erythrocytes is slightly larger than the luminal diameter of capillaries; this size discrepancy is overcome by the ability of red blood cells to undergo deformation, allowing them to 'squeeze' through the capillaries in single-file. The term red cell deformability (RCD) has thus entered the scientific nomenclature to describe the ability of erythrocytes to pass through the narrow capillaries. The properties of the erythrocyte that determine RCD are its shape, cytoplasmic viscosity, and membrane rigidity (130).

Progression of *P. falciparum* through the trophozoite and schizont stages within the infected erythrocyte is associated with a transition from the normal biconcave disc shape to that more resembling a sphere; this change is accompanied by increased cytoplasmic viscosity and membrane rigidity (130). Thus, all three determinants of RCD are negatively affected by the growing parasite, which itself becomes more spherical and increasingly rigid (23). Additionally, the rigidity of uninfected erythrocytes has also been observed to increase during severe *P. falciparum* infection.

The pathophysiological implications of reduced RCD are readily apparent: rigid erythrocytes, unable to squeeze past parasitized, cytoadherent red blood cells, become trapped in the microvasculature. Loss of motility in close proximity to nascent rosettes likely facilitates the process of rosette formation, thereby further impeding microcirculatory perfusion in a positive-feedback fashion (130).

Diminished RCD is not unique to cases of *P. falciparum* malaria, and can also be observed in sickle cell disease and thalassemia, where elevated plasma lactate is not a typical manifestation (141). This indicates that reduced RCD alone cannot cause sufficient obstruction of the microcirculation to bring about acidosis. However, it remains an important contributing factor when combined with cytoadherent infected erythrocytes and associated phenomena.

2.6.4.5 Endothelial activation

A discussion of the microcirculation is incomplete without a description of the endothelium. Endothelial cells are present in all blood vessels, especially capillaries, where the lumen is enclosed by a layer of endothelium one cell thick. Adjacent endothelial cells are joined by tight junctions, ensuring barrier integrity and maintenance of vascular permeability. Nitric oxide (NO), synthesised by nitric oxide synthase (NOS), is an important signalling molecule within the endothelium; among its many functions are the induction of vasodilation, the prevention of platelet aggregation within the capillary lumen, and averting unnecessary adhesion of leukocytes to the endothelial wall (142). Should leukocytes be required to cross the endothelial barrier to move into the tissues, the binding of the leukocyte to the endothelium is facilitated by ICAM-1, a membranous glycoprotein expressed by both endothelial cells and leukocytes. Parasitized erythrocytes can also bind with ICAM-1 via *Pf*EMP1 (143).

The endothelium can respond to disease states through a process called endothelial activation. Endothelial activation is an immune process that heightens the propensity for inflammation and coagulation (144), and is commonly observed in diseases such as sepsis (145). Within the context of severe *P. falciparum* malaria, alterations in microvascular structure by endothelial activation play an important role in disease pathogenesis.

NF-KB is a protein signalling complex central to the process of inflammation. NF-KB expression is indirectly stimulated by glycosylphosphatidylinositol, a molecule released by lysed infected red blood cells (iRBCs), and by binding of cytoadherent iRBCs to ICAM-1 (4). Furthermore, NF-KB upregulates the expression of adhesion molecules, including ICAM-1, thereby providing additional binding sites for parasitized erythrocytes. An additional downstream effect of upregulated NF-KB is cytoskeletal retraction, whereby cytoskeletal rearrangements within the endothelium disrupt intercellular tight junctions, thereby compromising endothelial barrier integrity and permeability. Parasitized erythrocytes thus induce a positive-feedback cycle, whereby intravascular haemolysis and iRBC adherence, acting through NF-KB, further upregulate the propensity for cytoadherence.

Adherence of infected erythrocytes to the endothelium induces endothelial activation, and endothelial activation is generally inhibited by NO (146). Nitric oxide generally acts to oppose the inflammatory responses inherent to pathological endothelial activation, not least in part due to its inhibitory effects on NF-KB (4, 146, 147). Functional NO signalling can promote survival by slowing the expression of adhesion molecules and preventing the breakdown of the endothelial barrier; these ameliorative effects are complemented by its vasodilatory activity, particularly in post-capillary venules. Conversely, its absence contributes to deterioration of microvascular function. Deficient NO signalling has been correlated with disease severity in both children and adults suffering from malaria (148–150).

When infected erythrocytes burst, intravascular haemolysis releases free haemoglobin and arginase. Haemoglobin can react with NO to form inactive nitrate, while free arginase degrades plasma arginine, one of the substrates utilised by NOS. NOS is further inhibited by Rho kinase, a downstream effector of NF-KB (4), therefore forming a cycle whereby the ameliorative effects of NOS are inhibited by increased NF-KB expression. Disruption of NO signalling by the parasite is thus a multifaceted process, encompassing inactivation, substrate depletion, and inhibition of NO synthesis.

In addition to increased inflammation and impaired NO signalling, parasite-induced endothelial activation also includes increased propensities for thrombosis (4), whereby endothelial cells upregulate the release of procoagulatory substances into the plasma, triggering the formation of blood clots within the lumen of small blood vessels, contributing to further deterioration of microvascular perfusion.

Endothelial activation thus plays a critical role in the pathogenesis of malaria, particularly in the severe disease state. In recognition of the pathological importance of endothelial dysfunction, ongoing research aims to develop adjunctive therapies targeting the endothelium in cases of severe malaria (151).

2.6.4.6 Microvascular Obstruction and Lactate Metabolism

When discussing how microvascular obstruction alters the balance of host lactate turnover, two related but functionally distinct terms warrant explanation: ischemia and hypoxia. Ischemia is defined as inadequate perfusion of tissue, while the insufficient supply of oxygen to respiring tissue is termed hypoxia. While localised microvascular hypoperfusion due to parasite sequestration will likely result in ischemia, there is ambiguity in the literature as to whether the subsequent pathology is due to hypoxia.

Tissues capable of oxidative carbohydrate metabolism that become hypoxic as a result of local microvascular obstruction will display a shift towards anaerobic glycolysis (77). As explained in **Section 2.6.1**, low oxygen tension accelerates anaerobic glycolysis, as pyruvate is unable to complete oxidative catabolism through the TCA-cycle due to impairment of the mitochondrial respiratory chain, likely due to inhibition of pyruvate dehydrogenase. The growing pyruvate and NADH concentrations drive increased flux through LDH, resulting in the intracellular accumulation of lactate, which is subsequently transported into the circulation. The brain, an organ wholly reliant on aerobic glycolysis, is particularly vulnerable to hypoxia caused by parasite sequestration within the cerebral microvasculature.

The liver is one of the major organs mediating uptake of lactate from blood plasma and converting it to useful molecules such as glucose through gluconeogenesis. The host's apparently reduced capacity for lactate clearance has generally been attributed to hepatic ischemia, with multiple studies revealing an inverse relationship between liver blood flow and plasma lactate concentration (12, 93). Reduced hepatic perfusion limits the provision of lactate as a substrate for gluconeogenesis, while concomitantly decreasing the amount of synthesized glucose that can be transported into the general circulation. A smaller body of evidence has pointed towards the possible deleterious effects of hepatic hypoxia on gluconeogenesis. An oxygen deficit within the hepatic microcirculation has been reported to cause inhibition of both pyruvate dehydrogenase and pyruvate carboxylase (108, 152), which catalyse the first step in pyruvate's metabolism through the oxidative and gluconeogenic pathways, respectively.

Renal pathology, resulting from accumulation of infected erythrocytes and immune cells within the glomerular and peritubular capillaries, is also relatively common in adult severe malaria (106). The kidney is an important gluconeogenic organ, and is capable of excreting organic acids during acidosis. Therefore, the appearance of acute kidney injury during malaria carries a worsened prognosis for the sustained presence of hyperlactataemia.

2.6.5 Other Pathologic Factors Related to Lactate Metabolism

Systemic oxygen delivery through the general circulation is determined by the combination of cardiac output, blood haemoglobin content, and arterial oxygen saturation (77). Indices of cardiac function are altered in severe *P. falciparum* malaria, but not to such a degree that it would explain the manifestation of hypoxia; this is reflected by the relatively low incidence of shock (127). Lung abnormalities such as respiratory distress and pulmonary oedema are observed in severe malaria. They can usually be attributed to

metabolic acidosis, severe anaemia, pneumonia coinfection, or clinical use of fluid resuscitation (124, 153). This leaves diminished blood haemoglobin content as a remaining possible cause of systemic hypoxia.

Haemoglobin, found in red blood cells, is responsible for the uptake of oxygen in the lungs and its subsequent release throughout the body. Destruction of erythrocytes thus releases haemoglobin into the blood, which is later excreted in the urine; haemoglobinuria is accordingly used as a diagnostic measure of pathological haemolysis. Severe anaemia (blood haemoglobin <5 g/dL or haematocrit <15%) is commonly observed in severe malaria, though this declines with age (124). Anaemia is caused not only by haemolysis by the proliferating parasite, but also by the spleen, which has been shown to exhibit upregulated removal of both parasitized and uninfected erythrocytes (154). This indiscriminate filtering of both healthy and infected red blood cells is thought to be caused by the changes in red blood cell deformability mediated by asexual blood-stage parasites. Red blood cell count decline in severe malaria is further exacerbated by impaired erythropoiesis after repeat infections (154, 155).

Severe malarial anaemia (SMA) thus seems to provide a reasonable and intuitive explanation for parasite-induced hypoxia: as haematocrit decreases, so too does blood haemoglobin content, and the capacity of the macrovasculature to deliver oxygen to the tissues is compromised, thereby resulting in hypoxia. However, such an explanation is rendered unlikely by a number of observations. SMA, though common (particularly in children), is not associated with an increased risk of mortality, and carries a substantially less severe prognosis when compared with other features of severe malaria (124). Furthermore, SMA does not translate into a comparative incidence of pathologically low (<92%) blood oxygen saturation, thereby casting doubt on a possible cause-and-effect relationship between anaemia and systemic hypoxia. This can be explained by the phenomenon whereby patients are able to tolerate SMA reasonably well, provided that the decline in haematocrit occurs slow enough for a compensatory right-shifted change in the oxygen dissociation curve (proportion of saturated haemoglobin versus prevailing oxygen tension)(23, 77). Thus, while the contribution of SMA to hypoxia should not be considered negligible, it remains an unlikely candidate for the primary cause of hypoxia-induced hyperlactataemia.

Generalized convulsions, a feature of severe malaria and characterised by rapid, repeated contraction and relaxation of skeletal muscle, can also elevate the contribution to blood lactate within clinical settings (23). Mean plasma lactate values of up to 13 mM have been measured in adults following the relatively brief episodes of intense muscular exertion that characterize generalized convulsions (12).

2.7 Modelling of Biochemical Systems

Mathematical modelling is, as the name implies, a means of describing observed phenomena using mathematical equations. Such phenomena can include the motion of planets around the sun, the flow of traffic, or the sound emitted by a plucked string. A model would include one or more functions accompanied by numerical parameters that match the phenomenon under study. Such a model could be defined, in a formal sense, as an abstract representation of one or more variables and the interactions between them (156).

The form and complexity of a mathematical model should match the question it is intended to answer. For example, the rate of a reaction catalysed by an enzyme in solution is the result of a myriad of factors with seemingly interminable complexity. A 'truly realistic' mathematical model would include descriptions for the random motion of substrate molecules within the solution, the intermolecular interactions between the substrate and enzyme, transient changes in enzyme conformation, and so on. However, the Michaelis-Menten equation describing the reaction velocity of an irreversible enzyme-catalysed reaction, shown below, achieves this with only two parameters and a single variable. For a substrate *s* and a product *p*,

$$S \rightarrow P$$

$$v = \frac{V_{MAX} \cdot [S]}{K_M + [S]}$$

This equation allows the rate of an enzyme-catalysed reaction to be predicted based on the substrate concentration, maximum reaction velocity (V_{MAX}), and the substrate's equilibrium dissociation constant to the enzyme (K_M). Since the reaction velocity is expressed as the change in concentration over time, it follows that a set of ordinary differential equations describing the rate of change of each metabolite could be expressed as

$$v = \frac{d[P]}{dt} = -\frac{d[S]}{dt}$$

The parameters governing this reaction can be determined with relative ease using standard enzymatic assay methods. If the objective is to simply describe and predict the concentration of substrate and product over time, then such a compact model can successfully answer this question, despite not including detailed descriptions at the molecular level. Such a minimalist description satisfies the "Minimum Description Length" principle that essentially states that the most accurate and useful model is usually also the smallest (157, 158).

Of course, the biochemical processes present in nature are rarely so straightforward. A biochemical reaction can be reversible, involve a number of substrates or products each with its own associated kinetic parameters, or be catalysed by different enzymes which may be subject to different modes of regulation. Furthermore, while it is certainly useful to examine a single reaction in isolation, this only involves a single component of what is usually a much larger reaction network. The biochemistry of a living organism is characterised by a highly organised set of reactions occurring simultaneously, where one product could be the substrate for many other reactions, and vice versa. These networks can occur in different compartments, whether this be on the level of the organelle, cell, or organ. A single organism could contain millions of reactions and chemical species that are subject to constant change.

However, such considerations do not prevent each reaction being characterised in a manner similar to the one shown above. Once a sufficient number of reactions have been described mathematically and equipped with the suitable parameters, the activity of the pathway as a whole can be described and predicted. For example, if the properties of glycolysis in a microorganism have been characterised experimentally and expressed mathematically, simulation of such a model could predict the rate of glucose consumption and the

concomitant production of molecules such as ATP. This is typically achieved using computational methods, whereby the system is simulated with a given set of conditions and parameters. The answer to broader questions, such as which component of the pathway is most important in determining the rate of glucose consumption, can also be answered by analytical techniques carried out computationally. Such modelling and analytical techniques are the mainstay of systems biology.

The modelling of biochemical systems spans several domains of biology, with applications including the prediction of a protein's function from its structure, the investigation of the constituent parts of signalling networks, or the analysis of gene regulatory networks (156). The work described in this thesis falls under the auspice of molecular systems biology, which involves the modelling of biochemical pathways to examine the emergent properties of a system as a function of its smaller, constituent parts. As described previously, these smaller components could be on the scale of a single compartment, a pathway, an enzyme, or a parameter. The utility of kinetic modelling in this regard is the ability to discern properties and outcomes of a large-scale biochemical system that could otherwise not be derived analytically from first principles. The ability to construct and simulate ever larger and more complex biological phenomena is enabled by the perpetual advancements in sophistication of software platforms and the processing power of the hardware on which they operate.

2.7.1 Metabolic Control Analysis

A skilled biochemical systems biologist could likely make intuitive deductions about the properties of a simple, straightforward biochemical network following cursory inspection. However, once more complicated pathways are considered, such as the complex, branched, and intricately regulated biochemical networks so ubiquitous in cellular metabolism, a more sophisticated and systematic approach is required.

Metabolic control analysis, or MCA, is a powerful tool that can yield both qualitative and quantitative insights concerning biochemical networks that exhibit stationary properties, such as steady-states. It involves the mechanistic examination of enzyme pathways to determine how the kinetic behaviour of the sequence as a whole varies with the properties governing the activity of each individual enzyme. In other words, MCA is used to discern the relationship between the parameter components of a model and its steady-state properties, thereby revealing the *sensitivity* of the system at steady-state to a change in a particular parameter.

Though these relationships are expressed in terms of different coefficients, the fundamental relationship is the same. MCA coefficients are effectively the ratio of fractional changes in a model parameter x, and a steady-state property y, normalised by division of a respective quantity (159).

$$\Delta x = \frac{x - x_{wt}}{x_{wt}} \qquad \Delta y = \frac{y - y_{wt}}{y_{wt}}$$

$$\frac{\Delta y}{\Delta x} = \frac{x_{wt}}{y_{wt}} \cdot \frac{(y - y_{wt})}{(x - x_{wt})}$$

If x is perturbed by a fractional amount and y changes by the same fractional amount, then the coefficient can be said to be 1; in other words, there is a one-to-one ratio in the fractional change in x and the fractional change in y. A more formal definition of this expression is that of the sensitivity coefficient (159):

$$c_x^y = \left(\frac{x}{y}\frac{\Delta y}{\Delta x}\right)_{\Delta x \to 0}$$

An extension of this approach is a double perturbation, whereby x is both increased and decreased by a percentage, and the coefficient is calculated as a gradient **(Fig. 2.9)**.

$$\frac{\Delta y}{\Delta x} = \frac{(y_\uparrow - y_{wt}) - (y_\downarrow - y_{wt})}{2 \cdot \Delta x \cdot x_{wt}}$$

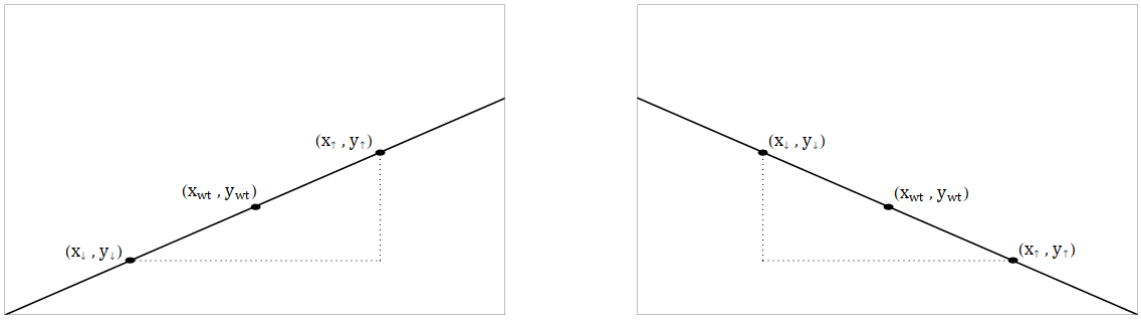

Figure 2.9: Graphical representation of positive (left) and negative (right) sensitivity coefficients.

These coefficients yield two very useful pieces of information: whether the dependent quantity y is directly or inversely proportional to the value of the independent quantity x, and the magnitude (or slope) of this relation. Thus, should a comprehensive sensitivity analysis be conducted on an entire model, one could ascertain not only which components increase or decrease a property of interest, but also which of them influence it the most.

2.7.2 The Coefficients of MCA

When examining the effects of changes within a biochemical system, the level of analysis can lie either *locally* or *globally*. In other words, if we are interested in the changes of a component on the *local* level, such as the rate of a single reaction, then local coefficients would be utilised. If, however, the change in the *global* state is to be determined, such as the change in the system's steady state, then global coefficients would be used.

To illustrate, consider the example of the *elasticity* coefficient, a local coefficient used to quantify the fractional change in a specific rate upon a fractional change in the concentration of a metabolite (substrate elasticity) or the value of a parameter (parameter elasticity), while the concentrations of all other remaining intermediates are kept constant at a value corresponding to a given reference state (**Table 2.2**)(160). This allows the properties of the specific reaction to be analysed *locally* and in isolation.

Mathematically, substrate elasticity, or the sensitivity of a reaction rate v_k to the change in the metabolite concentration S_i can be expressed as

$$\varepsilon_{S_i}^{v_k} = \frac{S_i}{v_k}\frac{\delta v_k}{\delta S_i}$$

Similarly, for parameter elasticity:

$$\varepsilon_{p_i}^{v_k} = \frac{p_i}{v_k}\frac{\delta v_k}{\delta p_i}$$

Global coefficients, as their name implies, pertain to the system as a whole. There are two types of global coefficient: *control* coefficients and *response* coefficients (**Table 2.1**).

Table 2.1: The coefficients of MCA

		Dependent variable: Flux	Dependent variable: Concentration
Independent variable	Reaction rate (v)	Flux control coefficient	Concentration control coefficient
	Parameter (e.g. K_M, K_i, k_a)	Flux response coefficient	Concentration response coefficient

Control and response coefficients differ only in the independent variable used in their calculation: reaction rates or parameters, respectively. This can be illustrated considering the finite perturbation method: in the former case, an entire rate expression is increased or decreased by a fraction, the example below using 1%:

$$v_{\uparrow}^{v} = (1 + 0.01)\left(\frac{V_{MAX} \cdot [S]}{K_M + [S]}\right) \quad ; \quad v_{\downarrow}^{v} = (1 - 0.01)\left(\frac{V_{MAX} \cdot [S]}{K_M + [S]}\right)$$

in the latter case, a fractional change would be introduced to a specific parameter instead, here chosen to be K_M:

$$v_{\uparrow}^{p} = \left(\frac{V_{MAX} \cdot [S]}{(K_M \cdot (1 + 0.01)) + [S]}\right) \quad ; \quad v_{\downarrow}^{p} = \left(\frac{V_{MAX} \cdot [S]}{(K_M \cdot (1 - 0.01)) + [S]}\right)$$

One can thus form distinct definitions for the two types of coefficients, shown here using up and down perturbations. For the flux control coefficient, the control of rate v_i over flux J_k can be given as

$$C_{v_i}^{J_k} = \frac{(J_{\uparrow}^{k} - J_{wt}^{k}) - (J_{\downarrow}^{k} - J_{wt}^{k})}{2 \cdot \Delta v^{i} * v_{wt}^{i}}$$

Similarly, the concentration control coefficient of rate v_i over steady-state concentration S_k can be defined as

$$C_{v_i}^{S_k} = \frac{(S_{\uparrow}^{k} - S_{wt}^{k}) - (S_{\downarrow}^{k} - S_{wt}^{k})}{2 \cdot \Delta v^{i} * v_{wt}^{i}}$$

Flux and concentration response coefficients, quantifying the response to a parameter perturbation, can be expressed similarly

$$R_{p_i}^{J_k} = \frac{(J_{\uparrow}^{k} - J_{wt}^{k}) - (J_{\downarrow}^{k} - J_{wt}^{k})}{2 \cdot \Delta p^{i} * p_{wt}^{i}} \quad ; \quad R_{p_i}^{S_k} = \frac{(S_{\uparrow}^{k} - S_{wt}^{k}) - (S_{\downarrow}^{k} - S_{wt}^{k})}{2 \cdot \Delta p^{i} * p_{wt}^{i}}$$

This section has discussed the meaning and derivation of the coefficients of MCA. Illustrative examples of how these coefficients are used to examine biological networks can be found in **Table 2.2**.

Table 2.2: The coefficients of MCA

Coefficient	Other intermediates fixed?	Example Notation	Schematic Representation
Substrate elasticity	Yes	$\varepsilon_{S_1}^{v_1}$	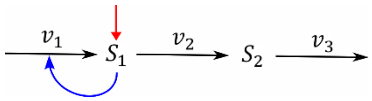
Parameter elasticity	Yes	$\varepsilon_{K_M(v_2)}^{v_2}$	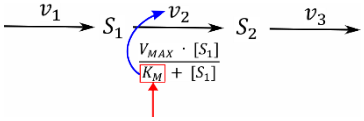
Flux control	No	$C_{v_2}^{J_1}$	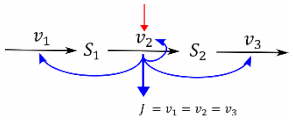
Concentration control	No	$C_{v_2}^{S_1}$	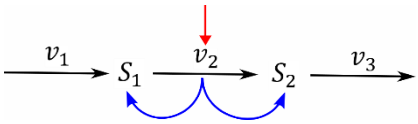
Flux response	No	$R_{K_M(v_2)}^{J_1}$	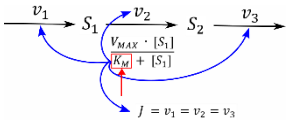
Concentration response	No	$R_{K_M(v_2)}^{S_1}$	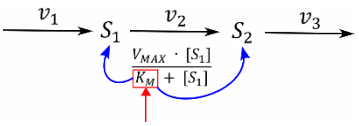
Red arrows indicate the perturbed entity (variable, reaction rate, parameter); blue arrows indicate the entities the change of which are considered.			

Chapter 3: Building the Model

The previous chapter described how severe malaria is a complex disease involving multiple organs and cell types within the blood. Further discussion dealt with the changes in metabolism observed in the host as a result of infection by the malaria parasite, with specific examination of the associated pathophysiology of hypoglycaemia and metabolic acidosis. The chapter was concluded with an introduction to the concepts of kinetic modelling and metabolic control analysis, and how use of these methodologies is suitable in answering the research question of how severe *P. falciparum* malaria can give rise to these metabolic aberrations. This chapter goes on to discuss how these methodologies were applied to satisfy the research aims and objectives.

Section 3.1 details the underlying rationale of constructing a multi-compartment model, explaining the choice of constituent models which were merged to yield the final whole-body model. This section also describes how this merging process was carried out, with particular attention paid to how the original, independently-published models were modified to be compatible and give reasonable descriptions when compared to clinical data.

In **Section 3.2**, we discuss which components were added to the model as part of the current research, and why they were considered suitable for incorporation with regards to answering the research question. **Section 3.2.1** describes additions made at the whole-body level to ensure that the individual compartments functioned congruently and exhibited reasonable behaviour when connected through the common plasma compartment. **Section 3.2.2** goes on to describe the novel components introduced to specifically address the host-parasite interactions that could contribute to the development of hypoglycaemia and metabolic acidosis, as discussed in Chapter 2. A summary of these changes and additions is provided in **Section 3.2.3**.

Finally, **Appendix A** outlines the *in silico* methodologies employed during model construction and analysis. This section gives an overview of how the model was structured in a computational environment, as well as the software written to discern model structure, view simulation outputs, and efficiently conduct metabolic control analysis.

3.1 Model Construction and Validation approach

In the first chapter of this thesis, the aims and objectives of the current research were stated, all of which depended on the construction of a whole-body model of glucose and lactate metabolism, which could subsequently serve as an *in silico* platform for investigating the causes of hypoglycaemia and lactic acidosis in severe *P. falciparum* malaria. To achieve this goal, contemporary scientific literature was reviewed to provide a contextual background and understanding of the metabolic processes that connect glucose and

lactate in both healthy and diseased states. The suitability of mathematical modelling to provide answers to the research question was explained, as well as the practical considerations and limitations of this approach.

Glycolysis is embedded in a network of reactions, which may provide or consume substrates, products, or intermediates, the precise structure of which is dependent on the particular needs of the organ in question. For example, the brain displays a strong preference for glucose, utilising the majority for the free energy production required to sustain neural activity. By contrast, the liver may catabolise glucose for energy, synthesise it through gluconeogenesis, or store it as glycogen, depending on the prevailing metabolic needs of the body. Furthermore, some organs, such as adipose tissue, may only take up glucose from circulation following stimulation by insulin, subsequently converting it to lipids for storage as fat. The relative contribution of each organ to plasma glucose concentration will thus vary depending on the metabolic and endocrinological state of the body at a particular point in time.

Since all tissues are capable of catabolizing glucose (42), a whole-body model of glucose metabolism would ideally include compartments describing each and every organ, tissue, and cell in the human body. Such a 'complete' model would not only describe pathways pertaining to carbohydrate metabolism, but also those of fat and protein, since these possess a plethora of intermediates that can be used by the processes of glycolysis or gluconeogenesis. Of course, such an exhaustive model has yet to be constructed, and is the subject of ongoing research by teams across the world. Furthermore, even if such a model did exist, its interminable size and complexity would undoubtedly be beyond the scope of this thesis, not to mention the computational burden of simulating such a model.

However, the most detailed model is not necessarily the best model to answer a specific research question; the level of detail is dependent upon the answers being sought.

These practical limitations thus necessitate a different approach. Fortunately, there exists a wealth of independently published models describing the metabolism of one or more compartments with varying degrees of detail and complexity. Examples include a whole-body model constructed for the purpose of examining glycogen regulation, with a more detailed hepatic compartment geared towards investigating the role of substrate cycling (161). Conversely, another model investigating skeletal muscle energy metabolism features only a single compartment, but includes detailed and comprehensive kinetic descriptions of both cytosolic and mitochondrial pathways (17). A common feature of these models is the inclusion of a blood or plasma compartment, representing the circulatory system with which all tissues must exchange metabolites.

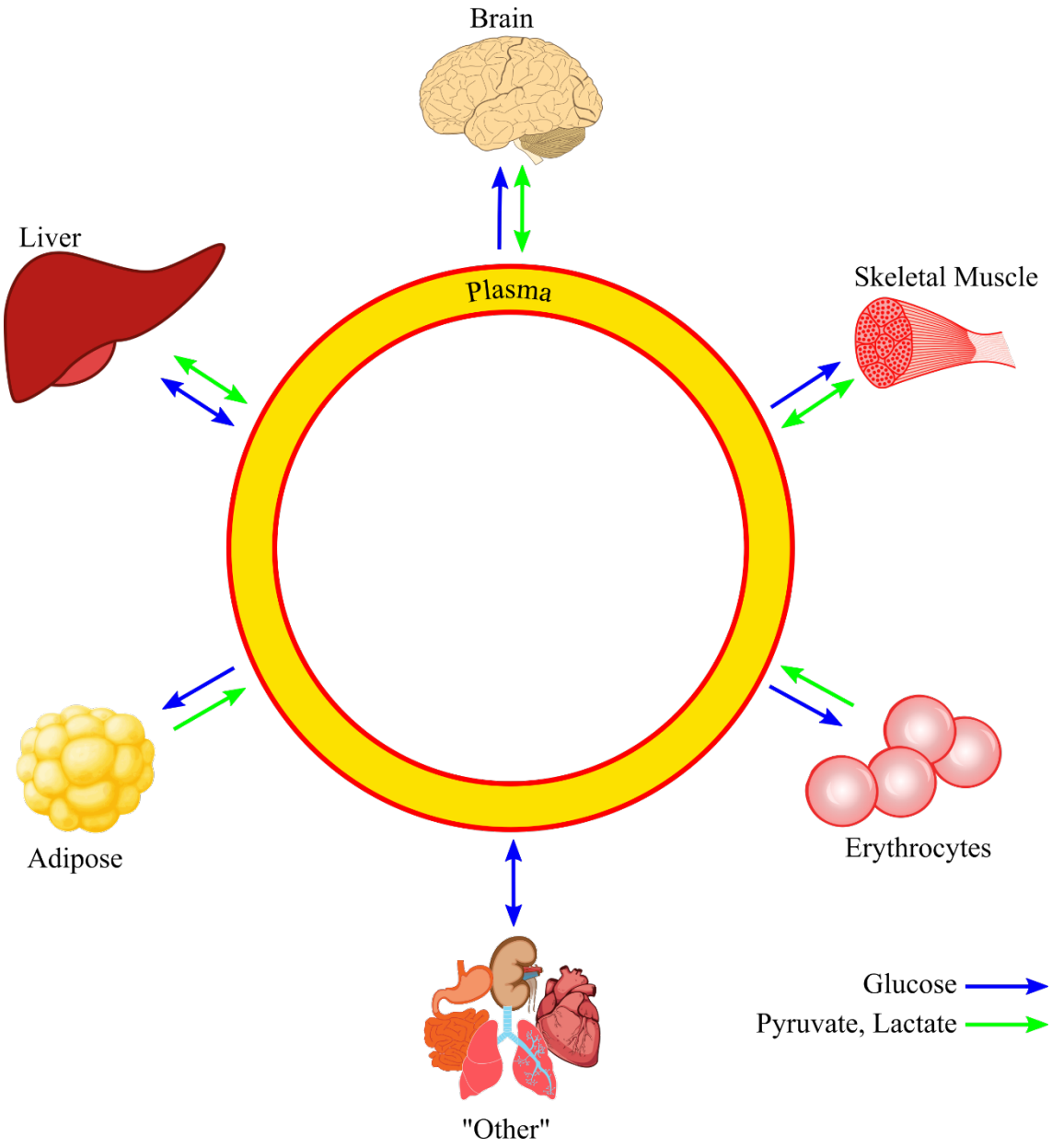

Figure 3.1: Diagram depicting a possible whole-body model limited to dynamic descriptions of glucose, pyruvate, and lactate metabolism. The plasma compartment provides a common framework to which other compartments can be freely connected or removed via their respective transporters. The direction and specificity of metabolite transport can be specified on a per-compartment basis. The level of detail in each compartment can also vary. For example, the liver may feature detailed descriptions of glucose metabolism involving bidirectional exchange of multiple metabolites with plasma, while less significant organs can be relegated to a lumped compartment termed “Other” that mediates only glucose uptake from plasma.

The plasma compartment common to different models can therefore be thought of as a unifying vessel to which other compartments can be ‘plugged’ into in a modular fashion (**Fig. 3.1**). The majority of the research in this thesis was conducted in this manner, whereby each compartment was added sequentially and evaluated to identify any discrepancies that resembled anomalous or unexpected behaviour. These discrepancies could include errors in reproduction, unit incompatibilities, or unforeseen interactions between compartments. If it was determined that a compartment needed to be added or removed, it was a relatively

simple matter of simply 'disconnecting' it from the master plasma compartment by removal of its rate equations from the plasma ODEs. Details of such model development methodology are given in **Section 3.3.1**.

The first step in integrating the independently published models was to confirm that they had been reproduced accurately. This was done after the models had been reconstructed in Wolfram Mathematica, and was achieved by comparing the outputs produced with those shown in the original independent publications. In each case, the model was reproduced and its results compared in isolation i.e. it was not combined with other models prior to comparison of outputs. In cases where the published and reproduced results differed substantially despite exhaustive troubleshooting efforts, reasonable attempts were made to understand why the discrepancies persisted, and to keep their presence in mind when proceeding with further model development. Simulation outputs of the final model were compared to data from clinical studies, specifically the plasma concentrations of glucose and lactate in both the healthy and diseased state. Such comparison is necessary not only to check the veracity and plausibility of model outputs, but ultimately to confirm the model's ability to answer the research question.

The final model, hereafter referred to as ***meyer1***, contains ten compartments adapted from three publications, with additional changes, modifications, and additions from other sources where noted. The models and their respective compartments are detailed in the following sections.

3.1.1 Erythrocyte and Parasite Compartments

The model presented in this thesis has its foundation in *green1*, a model published by Kathleen Green in 2017 as part of her thesis titled 'Whole body modelling of glucose metabolism in malaria patients'(162). The green1 model was based on previous work conducted by Francois du Toit, published in 2015 (21). This latter model (*dutoit3*) describes glucose metabolism in infected erythrocytes. The model constructed by du Toit was, in turn, based on pioneering work by Gerald Penkler, who published a kinetic model of glucose catabolism in *Plasmodium falciparum* (*penkler1*) in 2013 (20). The parasite glycolytic pathway in *penkler1* is comprised of detailed kinetic descriptions with parameters obtained from experiments characterising each enzyme within the Embden-Meyerhof-Parnas pathway, yielding a system of eighteen coupled ODEs.

Following this, du Toit proceeded to construct a multi-compartmental model that could simulate the metabolic behaviour of an infected erythrocyte (**Fig. 3.2**); this was done by adapting a previous model of erythrocyte metabolism published by Mulquiney and Kuchel (163–165). The work published by du Toit described not only the process of adapting and merging these models, but also the results of experimental validation, whereby the volume of the growing intraerythrocytic parasite, as well as extracellular substrate concentrations, was measured over the course of the parasite's 48-hour lifecycle.

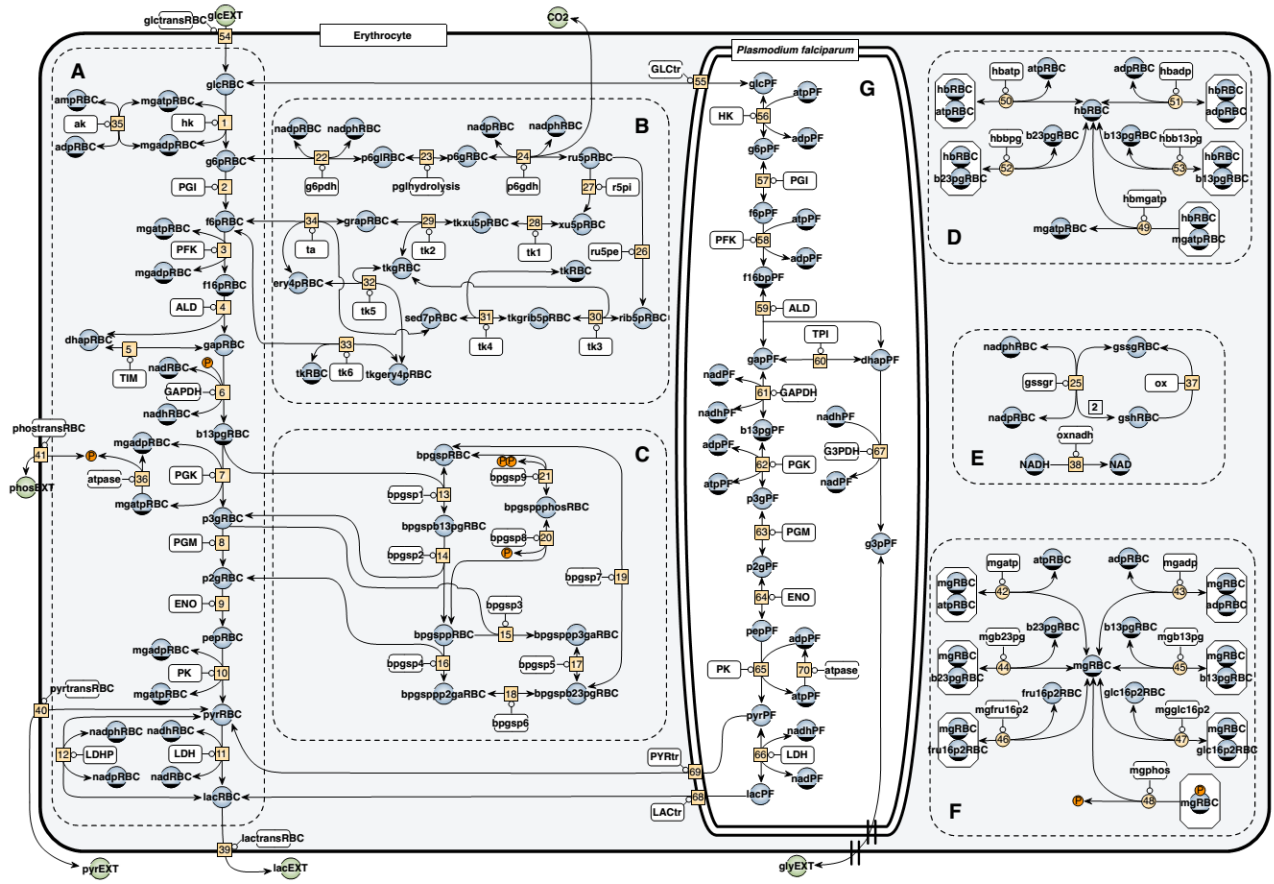

Figure 3.2: Compartments and pathways present in the combined *P. falciparum*-infected red blood cell model. Reactions are grouped in a modular fashion: **A**, Glycolysis; **B**, pentose phosphate pathway; **C**, Rapoport-Leubering shunt; **D**, haemoglobin complexes; **E**, glutathione metabolism; **F**, magnesium complexes; **G**, parasite compartment. Reproduced from (21)

Green (162) built upon this model to investigate how the accelerated glycolytic flux of infected erythrocytes contributed to the pathogenesis of hypoglycaemia and lactic acidosis, two of the metabolic comorbidities characterising severe malaria that are associated with a high risk of mortality. This research yielded a whole-body model of glucose metabolism that utilised the model published by du Toit and combined it with another independently published whole-body model by Xu *et al.* (161). This latter model, originally used for the purpose of examining substrate cycling within the context of glycogen turnover and whole-body glucose homeostasis, was merged with the infected erythrocyte model of du Toit. This process required extensive modification and adaption to ensure the compatibility of the different units of mass and concentration between the femtomole amounts present in the infected erythrocyte model and the millimolar concentrations present in the model published by Xu *et al*. Addition of both an infected and uninfected erythrocyte compartment to the Xu model necessitated numerous changes to accommodate the introduction of a sophisticated red blood cell compartment to an otherwise generalised, coarse-grained model. Further changes and replacements were also made to glucose and lactate transporters in the erythrocyte and liver compartments, respectively. Finally, the model was validated with simulation outputs from both the existing models, as well as clinical data obtained from studies measuring blood glucose and lactate concentrations in patients with severe malaria.

Four compartments were obtained from this model and subsequently incorporated into *meyer1*, namely that of the uninfected erythrocyte, infected erythrocyte, and blood plasma. The remaining hepatic, skeletal muscle, and adipose compartments from the original Xu model were not utilised in the current study.

3.1.2 Hepatic Compartment - Overview

A model describing hepatic glucose metabolism (hereafter referred to as H1) was published by 2012 by Matthias König, Sascha Bulik, and Hermann-Georg Holzhütter (18). The authors set out to construct a detailed mathematical model describing the metabolism of glucose by the liver. Additional features included descriptions of hormonal control by insulin, glucagon, and epinephrine, as well as incorporation of allosteric regulation (**Fig. 3.3**). The model was subsequently used to simulate experimental data corresponding to four physiological phenomena: (i) the relative quantitative contributions levied by hepatic glycolysis, gluconeogenesis and glycogen metabolism under varying concentrations of external plasma glucose; (ii) the timecourses of hepatic glycogen concentration under fed and fasting states; (iii) the switching between net hepatic glucose production and utilization as a function of hypo- and hyperglycaemia, and (iv) the effect of varying hormone concentrations on liver glucose metabolism. Procurement of model parameters in the original study was done either through literature review, or fitting to multiple experimental data sets.

Several features of H1 made it particularly attractive for incorporation into the current model. The model features a detailed description of both glycolysis and gluconeogenesis. Additionally, glycogen turnover is comprehensively described, with expressions denoting not only the activity of glycogen synthase and glycogen phosphorylase, but also glucose-1-phosphate 1,6-phosphomutase (G1PI) and UTP-glucose-1-phosphate uridylyltransferase (UGT). A rudimentary description of mitochondrial metabolism is included to account for initial gluconeogenic flux of pyruvate through pyruvate carboxylase and phosphoenolpyruvate carboxykinase. Finally, hormonal regulation is incorporated throughout the model, supplementing descriptions of allosteric regulation.

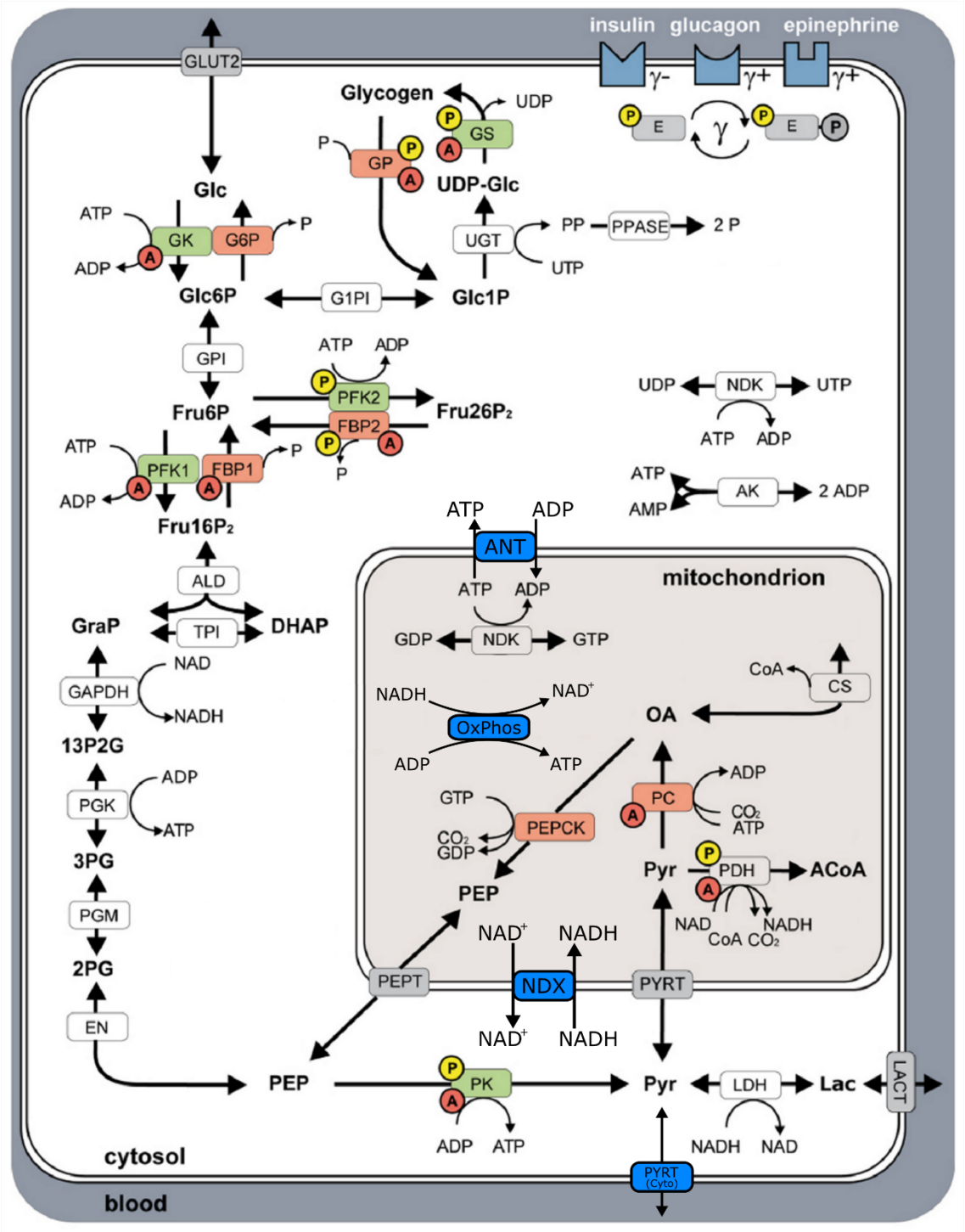

Figure 3.3: Structure of the reaction networks in H1. Reactions unique to hepatic glucose utilisation are shown in green, and those unique to glucose production indicated in red. Enzymes regulation by hormonal or allosteric mechanisms are marked with a yellow P and red A, respectively. Reactions that have been added to the original model in this work are indicated in blue. Reactions and species that were disabled or absent in the original model have been removed. Abbreviations: ANT: ADP/ATP translocase; NDX: NAD^+/NADH exchanger; OxPhos: oxidative phosphorylation; PYRT: pyruvate transporter. Figure adapted from (18)

H1 also features descriptions of hepatic exchange of glucose and lactate with the plasma compartment, which were considered highly valuable after taking into account the primary role these two metabolites play within the scope of this thesis. With these descriptions in place, the model could provide a platform for

simulating the dynamics of hepatic glucose metabolism under varying plasma concentrations of glucose and lactate, thereby making it wholly suitable for incorporation into a model investigating the metabolic underpinnings of hypoglycaemia and hyperlactataemia associated with severe malaria.

However, as with all *in silico* descriptions of biological phenomena, the model was limited by the need to make assumptions and simplifications. While not all of these were necessarily prohibitive for use within the current model, those that were significantly problematic did need to be addressed, and are thus mentioned here. First, H1 does not allow for changing concentrations of energy carriers and reducing equivalents, in particular the concentrations of NAD^+/NADH and ATP/ADP. To quote the original paper, "[t]he model is limited to physiological states where changes in the energy- and redox state can be neglected, […] consequently, the model is not able to simulate conditions where this assumption of energy decoupling is not valid, for example, **under hypoxic or ischemic conditions**" (emphasis added)(18). Thus, while including a basic description of mitochondrial metabolism, the model does not include descriptions of oxidative phosphorylation or translocation and exchange of energy carriers and reducing equivalents between the cytosol and mitochondrion. Given the substantial role that parasite-mediated microvascular occlusion and the resulting ischemia plays in malaria pathogenesis, the lack of detailed mitochondrial oxidative metabolism was considered to be an important issue.

Second, while transport of glucose and lactate between the hepatic and plasma compartments is described, that of pyruvate is not. Within the context of the current model this constitutes a significant issue, because the erythrocyte model previously described exhibits significant levels of pyruvate export (in addition to lactate), and there will thus be an interminable accumulation of pyruvate within the plasma compartment if an accompanying method of uptake from the plasma is not included. Physiologically, the liver would constitute the chief organ responsible for removal of plasma pyruvate via monocarboxylate transporters. However, a description of hepatic pyruvate transport between the cytosol and plasma compartments was not originally present.

Third, the model is limited to glycolytic metabolism with lactate constituting the only metabolic terminus free to leave the hepatic compartment. Other metabolic fates of glycolytic intermediates, such as conversion to alanine, entry into lipogenic pathways, or metabolism by the tricarboxylic acid cycle are not considered. However, this limitation only becomes pertinent if the model is to be expanded to encompass the entirety of gluconeogenesis with the inclusion of amino acid and glycerol pathways, an endeavour that was beyond the scope of this research. It should be noted, however, that the authors have recently released an updated, expanded version of the model, named HEPATOKIN1 (166), that addressed most, if not all, of the issues and limitations described above. The authors have graciously made a copy of the model available through personal correspondence, though it was regrettably unable to be utilised due to time constraints.

In *meyer1*, one compartment was incorporated from this model to represent the liver, consisting of the hepatic mitochondrial and the hepatic cytosolic subcompartments.

3.1.3 Hepatic Compartment - Modifications

3.1.3.1 Reducing equivalents

In König's original model (18), the cellular redox and energy states were kept constant. This meant that the concentrations of NAD^+, NADH, ATP and ADP remained unchanged in both the cytosolic and mitochondrial compartments. Additionally, since the concentrations were kept fixed, no transport equations were included that described the movement of these molecules across the mitochondrial membrane.

The decision to omit this additional complexity was likely made due to both its minimal relevance to the research objectives, and the lack of impact on the model's predictive power. However, within the context of the current model, the lack of a dynamic system of reducing equivalents and energy carriers severely limits the ability to produce plausible simulations of hepatic metabolism under conditions of cellular hypoxia, hypoglycaemia, and high extracellular concentrations of lactate.

To address these issues, a number of changes were made. First, the concentrations of the hepatic metabolites ATP, ADP, AMP, NAD^+ and NADH were unclamped, thereby allowing them to vary as a function of their respective fluxes. For ATP, ADP, NAD^+ and NADH, this included the introduction of separate variables for their respective cytosolic and mitochondrial concentrations. These variables were defined with initial values identical to the original clamped concentrations used for reproduction of the published results.

Next, two rate equations were introduced that allowed the movement of ATP, ADP, NAD^+ and NADH between the cytosol and mitochondria. First, the activity of adenine nucleotide translocase, an antiporter mediating the exchange of free ATP and ADP across the inner mitochondrial membrane, was modelled using a facilitated transport flux expression based on one previously described by Li *et al*. (17) for skeletal muscle. Note the use of the compartmental phosphorylation state (PS) in lieu of a substrate concentration variable.

$$ATP_{cyto} + ADP_{mito} \leftrightarrow ADP_{cyto} + ATP_{mito}$$

$$v\_HEPATIC\_ATP\_TRANSLOCASE \rightarrow T_{max} \cdot (PS\_M\_CYTO - PS\_M\_MITO)$$

Where

$$PS\_M\_CYTO \rightarrow \frac{PS\_CYTO}{M\_CYTO + PS\_CYTO}$$

$$PS\_M\_MITO \rightarrow \frac{PS\_MITO}{M\_MITO + PS\_MITO}$$

Where M_CYTO and M_MITO are constants. Furthermore:

$$PS\_CYTO \rightarrow \frac{HEPATIC\_VAR\_atp}{HEPATIC\_VAR\_adp}$$

$$PS\_MITO \rightarrow \frac{HEPATIC\_VAR\_atp\_mito}{HEPATIC\_VAR\_adp\_mito}$$

Since the original H1 model lacked the required metabolites and kinetic descriptions, the incorporation of expressions modelling the malate-aspartate and glycerophosphate shuttle systems for NADH were not

deemed practically viable. In the current model, using the same approach of Li *et al*. (17), the effective exchange of NADH and NAD^+ between the cytosol and mitochondria was modelled using an expression similar to that described above, again with compartmental redox state supplanting substrate concentration variables.

$$NADH_{cyto} + NAD^+_{mito} \leftrightarrow NAD^+_{cyto} + NADH_{mito}$$

$$v\_HEPATIC\_EXCHANGER\_NADH \rightarrow T_{max} \cdot (RS\_CYTO - RS\_MITO)$$

Where

$$RS\_CYTO \rightarrow \frac{REDOX\_STATE\_NADH\_CYTO}{M\_CYTO + REDOX\_STATE\_NADH\_CYTO}$$

$$RS\_MITO \rightarrow \frac{REDOX\_STATE\_NADH\_MITO}{M\_MITO + REDOX\_STATE\_NADH\_MITO}$$

And

$$REDOX\_STATE\_NADH\_CYTO \rightarrow \frac{HEPATIC\_VAR\_nadh}{HEPATIC\_VAR\_nad}$$

$$REDOX\_STATE\_NADH\_MITO \rightarrow \frac{HEPATIC\_VAR\_nadh\_mito}{HEPATIC\_VAR\_nad\_mito}$$

While these transporters operate only across the inner mitochondrial membrane in a physiological setting (exchanging metabolites between the mitochondrial intermembrane space and matrix), for the purposes of this model, movement of these molecules across the outer mitochondrial membrane was considered to be instantaneous, effectively making these transporters operate between the cytosolic and lumped mitochondrial compartments.

Following the implementation of these changes, an additional rate equation was introduced to model the process of oxygen utilisation and oxidative phosphorylation within the mitochondria, whereby ADP and NADH could be recycled into ATP and NAD^+. To maintain consistency and compatibility, this expression was incorporated verbatim from an earlier paper published by Dash *et al*. (167) where it was employed in their model for muscle cell metabolism . In the current model, the concentrations of oxygen and phosphate are kept fixed, and the values of the remaining parameters are left unchanged.

$$6\,ADP_{mito} + 2\,NADH_{mito} \leftrightarrow 2\,NAD^+_{mito} + 6\,ATP_{mito}$$

$$v\_HEPATIC\_O2\_H2O \rightarrow V_{max} \cdot \left(\frac{\frac{ADP_{mito}}{ATP_{mito}}}{K^{PS} + \frac{ADP_{mito}}{ATP_{mito}}}\right) \cdot \left(\frac{\frac{NADH_{mito}}{NAD^+_{mito}}}{K^{RS} + \frac{NADH_{mito}}{NAD^+_{mito}}}\right) \cdot \left(\frac{Oxygen \cdot Phosphate}{K_M + Oxygen \cdot Phosphate}\right)$$

Finally, the kinetic expression of adenylate kinase, present but disabled in the original model, was enabled in H1. Adenylate kinase itself is important in mediating cellular energy homeostasis via ongoing interconversion of the adenine nucleotides ATP, ADP, and AMP, a role that was judged to be significant enough as to warrant inclusion in the current model.

3.1.3.2 Pyruvate transporter

The liver contains multiple isoforms of monocarboxylate transporters (MCTs), several of which are capable of transporting lactate and pyruvate (168). H1 did not originally contain a description of pyruvate transport to and from the plasma compartment. The decision to add such a description was made based on both its physiological plausibility, and the tendency of infected erythrocytes to export pyruvate into plasma (20), which would subsequently be taken up by the liver. Thus, without a means for the pyruvate to be cleared from the plasma, such as through hepatic uptake, the model would show an unrealistic accumulation of pyruvate within the plasma compartment. The option of keeping the plasma pyruvate concentration fixed and not introducing a pyruvate transporter term into the hepatic compartment was not pursued for several reasons. First, the ratio of lactate to pyruvate in the plasma is often used as a diagnostic measure in clinical studies when determining the degree of metabolic acidosis (93, 130). This was interpreted as a indicating that both the levels of plasma lactate and pyruvate were important when modelling lactic acidosis. Second, a constant pyruvate concentration would have 'upstream' effects with regards to (infected) erythrocyte metabolism, whereby pyruvate export from red blood cells would not be subject to dynamic equilibrium with the plasma compartment. Third, with the exception of glycerol, pyruvate constitutes the immediate product of gluconeogenic conversion of alanine and lactate, and as such stands as a focal point of gluconeogenic metabolism. To abstain from introducing a dynamic relationship between this focal point of hepatic gluconeogenesis and the plasma compartment therefore seemed unreasonable. This decision was further encouraged by the fact that both lactate and pyruvate are transported by the same MCTs, and that a lactate transporter equation was already present in H1. The dynamic relationship could thus be easily implemented by using the existing rate equation with different parameters obtained from literature (168–171).

The kinetic rate expression for the pyruvate transporter was adapted from H1's existing description of lactate transport; this approach was substantiated by the knowledge that pyruvate and lactate are both transported by the same MCT isoforms, albeit with different affinities. The rate expression is as follows:

$$Pyruvate_{Plasma} \xleftrightarrow{Pyruvate\ Transporter} Pyruvate_{Hepatic\ Cytosol}$$

$$v_{PT} = \frac{V_{max} \cdot \left(Pyruvate_{Plasma} - \frac{Pyruvate_{Hepatic\ Cytosol}}{K_{eq}}\right)}{K_M \cdot \left(1 + \frac{Pyruvate_{Plasma}}{K_M} + \frac{Pyruvate_{Hepatic\ Cytosol}}{K_M}\right)}$$

3.1.3.3 Sub-compartment volume scaling

Hepatocytes contain mitochondria, which mediate several metabolic pathways relevant to the scope of the overall model. Thus, during the process of integrating H1 with the rest of the model, particular attention was paid to ensure that the hepatocyte's cytosolic and mitochondrial compartments functioned in a manner congruent to the rest of the model. The primary aspect of this congruency was ensuring that the mitochondrial subcompartment was effectively defined as its own entity within the hepatic cytosol, similar to how the parasite compartment was defined as a subcompartment within the infected erythrocyte cytosol. Such an implementation was further indicated by the aforementioned conversion of hepatic cytosolic and mitochondrial ATP/ADP and NAD^+/NADH to dynamic variables. To distinguish between the concentrations of these metabolites, separate volume denominators would have to be implemented with their molar amounts. Such an approach would also allow the transport of absolute molar amounts between the cytosolic and mitochondrial compartments to satisfy stoichiometric constraints and mass conservation.

Subsequent changes were made with the purpose of (i) defining two separate compartments with distinct volumes, metabolites, and reactions, and (ii) scaling these compartments according to the existing H1 parameters, while still keeping their relative magnitudes physiologically plausible. Using this approach, the liver would be represented by two separate compartments, with one comprising the entirety of hepatic cytosol, and the other all of hepatic mitochondria. This methodology parallels that used by other independent authors for the remaining compartments featured in the current model, where the metabolism of a single cell is scaled up to represent an organ (162).

Changes began with determining the overall dimensions of the hepatic compartment. First, the total volume of the liver was estimated to be approximately the same as its weight, assuming unitary density (172). For a normal adult male, this would be approximately 1.5 litres. Estimation of total liver volume was made due to discovery of an existing parameter in the original H1 model defining the hepatic parenchymal volume fraction. Thus, the value for total liver volume was multiplied by the H1 parameter defining the hepatic parenchymal volume fraction.

$$Volume_{Parenchymal}^{Hepatic} = Volume_{Total}^{Hepatic} \cdot HEPATIC\_VOLUME\_PARENCHYMAL\_FRACTION$$

$$\text{Where } HEPATIC\_VOLUME\_PARENCHYMAL\_FRACTION = \frac{7}{12}$$

This process was repeated with two other existing parameters, which were interpreted to indicate the respective cytosolic and mitochondrial volume fractions (also found in the original H1 model) of the parenchymal volume:

$$Volume_{Cytosol}^{Hepatic} = Volume_{Parenchymal}^{Hepatic} \cdot HEPATIC\_VOLUME\_CYTOSOLIC\_FRACTION$$

$$\text{Where } HEPATIC\_VOLUME\_CYTOSOLIC\_FRACTION = \frac{5}{6}$$

$$Volume_{Mitochondrial}^{Hepatic} = Volume_{Parenchymal}^{Hepatic} \cdot HEPATIC\_VOLUME\_MITOCHONDRIAL\_FRACTION$$

Where $HEPATIC\_VOLUME\_MITOCHONDRIAL\_FRACTION = \frac{1}{6}$

These expressions for hepatic cytosolic and mitochondrial volume were subsequently used both as denominators for the mass-based metabolite variables (redefining them in terms of concentration for use in rate equations), and as coefficients of reactions, to scale the enzymatic activity according to the size of the relevant compartment and transforming the units of the rates from concentration per unit time, to mole per unit time.

$$HEPATIC\_VAR\_atp = \frac{HEPATIC\_atp[t]}{Volume_{Cytosol}^{Hepatic}}$$

$$HEPATIC\_VAR\_atp\_mito = \frac{HEPATIC\_atp\_mito[t]}{Volume_{Mitochondrial}^{Hepatic}}$$

3.1.4 Inclusion of Extra-hepatic Compartments

Having reproduced and validated the parasite, erythrocyte, infected erythrocyte and hepatic compartments (see **Chapter 4**), it was considered whether or not these compartments, in combination with the plasma compartment, would be sufficient to achieve the research aims and objectives. It was decided to extend the model to include several additional compartments involved in glucose and lactate metabolism, with the implementation described in **Section 3.1.5**. The rationale for this decision is outlined below.

i. **Existing descriptions were found to be inadequate.** The original *green1* model did feature rudimentary implementations of skeletal muscle and adipose compartments, but these were found to be lacking in the detail required to allow them to respond in a physiologically plausible manner when subject to the extremes of blood glucose and lactate concentrations that are associated with severe malaria. The skeletal muscle compartment, adapted from Xu *et al*. (161), was effectively a very coarse-grained compartment that converted glucose to lactate through a series of three reactions. The adipose compartment, also adapted from Xu *et al*., simply imported glucose and, through another series of three reactions, converted it to free fatty acids, the latter of which was clamped and had no subsequent interaction with the model. It was decided to adapt a different independently published model entirely, ideally one that could more realistically simulate the metabolic behaviour of these organs under a range of blood glucose and lactate concentrations.

ii. **Malaria affects the metabolism of multiple organs.** As described and explained in **Section 2.6.4**, only the immature forms of the parasite remain motile in the circulation, with the remainder adhering to the microcirculatory capillary endothelium during sequestration prior to schizont rupture. The tissue distribution of sequestered parasite is heterogenous both within affected tissues, and between infected individuals, giving rise to a range of possible clinical presentations affected by multiple factors, including the age of the host (**Fig. 2.4**). The literature presented in Chapter 2 suggests that the metabolic effects of parasite sequestration within different tissues, including but not limited to

the liver, could be an important causative factor in mediating the appearance of HG/HL in severe *P. falciparum* malaria. If the current model is to address this, then the incorporation and inclusion of sufficiently detailed compartments outside of the liver and erythrocytes is a necessity.

iii. **Modular descriptions of whole-body glucose and lactate metabolism are available and could be easily incorporated.** A cursory search for independently published models yielded discovery of one published by Kim et al. that had a particular focus on the dynamics of whole-body lactate metabolism during exercise (16). Examination of this model showed that it did not contain excessive detail, was defined in a modular fashion that would expedite the addition or removal of compartments as necessary, and would be wholly compatible with the existing model under construction. The methodological approach taken when incorporating this model is detailed in the following sections.

3.1.5 Muscle, Brain, Cardiac, Adipose, and GIT Compartments - Overview

A multi-compartmental model of fuel homeostasis during exercise (here referred to as K1) was published in 2007 by Jaeyeon Kim, Gerald Saidel, and Marco Cabrera (16). K1 features seven tissue compartments, namely the brain, heart, liver, gastrointestinal tract, skeletal muscle, adipose tissue, and an umbrella compartment, termed ‘Other’, that denotes the remainder of compartments that collectively have an effect on plasma glucose levels. The kinetic behaviour of each compartment is drawn from a base template of lumped pathways and reactions that encompasses the anabolism and catabolism of the glucogenic substrates glucose, glycogen, lactate, pyruvate, alanine, glycerol, fatty acids, and triglycerides (**Fig. 3.4**). Each compartment has a unique subset of reactions appropriate to its metabolic role (see **Figs. 3.4, B.3 & B.8** for examples of different implementations between compartments). For example, direct glyceraldehyde-3-phosphate reduction to glycerol-3-phosphate (lumping in the dihydroxyacetone intermediate) is only present in the adipose compartment, alanine synthesis from pyruvate is only present and skeletal muscle, and glycogen metabolism is present in all compartments save for the gastrointestinal tract and adipose tissue. All organ compartments include a complete description of glycolysis, that, while lumped, is subject to both hormonal and allosteric regulation, as well as intermediate and terminal branch points that carry flux into glycogenic, lipogenic, and tricarboxylic acid cycle pathways. A summary of the compartments with their accompanying set of reactions is given in **Table 3.1**.

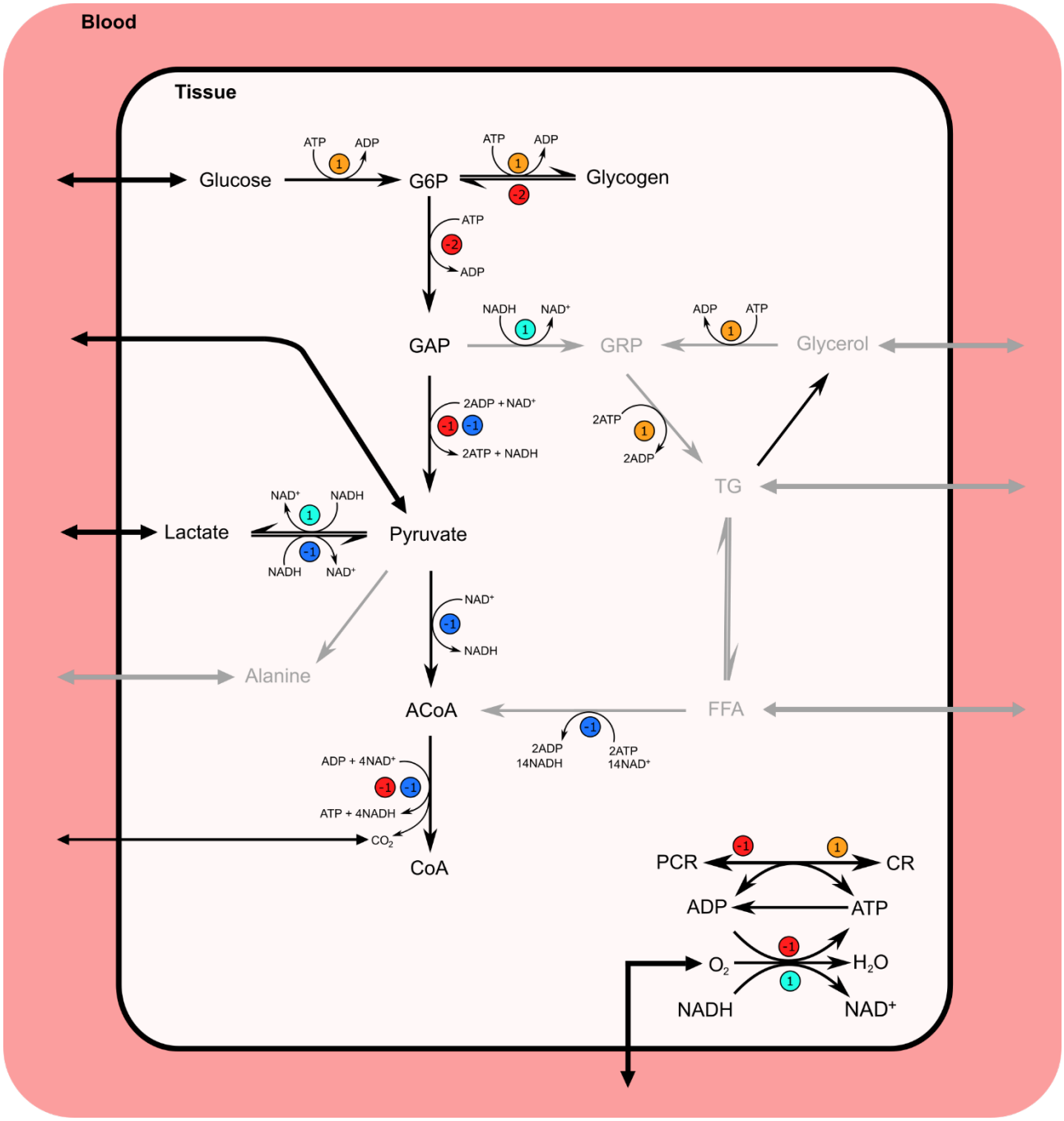

Figure 3.4: Schema illustrating the template of reaction pathways present in the different tissues of K1. Cyan and blue circles represent the exponent of reducing equivalent controllers, while orange and red indicate those of energy carrier controllers (**see text**). Grey arrows and metabolites indicate clamped fluxes and species. Figure adapted from (16)

Reaction parameters are specific to each compartment, in line with its relative contribution to overall fuel homeostasis. Additionally, hormonal regulation of key reactions by insulin, glucagon and epinephrine is incorporated on a per-compartment basis, as a function of an integral-rein controller (see **Section 3.1.8**) simulating plasma hormone concentrations.

With H1 already providing a suitably comprehensive model to describe hepatic glucose metabolism, K1's consistent, modular, multi-compartmental description of whole-body glucose metabolism was found to effectively 'fill in the gaps' of the remaining organs mediating plasma glucose and lactate turnover. Whereas

lumped and simplified reaction networks are not particularly desirable when attempting to model an organ so crucial to whole-body glucose turnover as the liver, they are very expedient when modelling 'lesser' non-gluconeogenic organs that, within the scope of this model, are essentially 'glucose-in-lactate-out' compartments. For this purpose, and for contributing to the ability to answer the research question outside of the hepatic and erythrocyte compartments previously described, the K1 model has several features that make it suitable for addition to the current whole-body model.

Table 3.1: Reactions present in the K1 model that are not common to all compartments

			Brain	Heart	Muscle	GIT	Liver	Adipose
Gluconeogenesis	I	PYR → GAP					■	
	II	GAP → G6P					■	
	III	G6P → GLC					■	
Glycogenesis		G6P → GLY	■	■	■		■	
Glycogenolysis		GLY → G6P	■	■	■		■	
Fatty acid synthesis		ACoA → FFA					■	
Fatty acid oxidation		FFA → ACoA		■	■		■	
Lipolysis		TG → FFA + GLR		■	■	■	■	
Triglyceride synthesis		FFA + GRP → TG		■	■	■	■	
Glycerol phosphorylation		GLR → GRP		■	■		■	
GAP reduction		GAP → GRP						■
GRP oxidation		GRP → GAP					■	
Alanine transamination		ALA → PYR					■	
Alanine synthesis		PYR → ALA			■			
Phosphocreatine hydrolysis		PCR → CR	■	■	■	■		
Phosphocreatine synthesis		CR → PCR	■	■	■	■		

Shaded blocks are reactions that are included; blank blocks are not included in the respective compartment column.

Abbreviations: ACoA, acetyl-CoA; ALA, alanine; CR, creatine; FFA, free fatty acids; G6P, glucose 6-phosphate; GAP, glyceraldehyde 3-phosphate; GLC, glucose; GLR, glycerol; GRP, glycerol phosphate; GLY, glycogen; PCR, phosphocreatine; PYR, pyruvate; TG, triglyceride

K1 also features dynamic descriptions of energy carriers (ATP/ADP) and reducing equivalents (NAD^+/NADH), the respective ratios of which are incorporated into the relevant rates as controllers, which serve as dynamic terms that regulate reaction rate in lieu of more complex substrate binding constant terms:

$$X + Y \xrightarrow{E_1 \rightarrow E_2} A + B$$

$$\phi_{X+Y\rightarrow A+B} = V_{X+Y\rightarrow A+B} \cdot \left(\frac{PS^{\pm}}{\mu^{\pm} + PS^{\pm}}\right) \cdot \left(\frac{RS^{\pm}}{\nu^{\pm} + RS^{\pm}}\right) \cdot \left(\frac{\frac{C_X}{K_X} \cdot \frac{C_Y}{K_Y}}{1 + \frac{C_X}{K_X} + \frac{C_X}{K_X} + \frac{C_X}{K_X} \cdot \frac{C_Y}{K_Y}}\right)$$

$$PS^{+} = \frac{C_{ATP}}{C_{ADP}} \qquad RS^{+} = \frac{C_{NADH}}{C_{NAD^{+}}}$$

$$PS^{-} = (PS^{+})^{-1} \qquad RS^{-} = (RS^{+})^{-1}$$

In accordance with its approach of lumped reactions, K1 does not feature reversible reactions, but rather pairs of irreversible reactions acting in opposition, and coupled with controller energy metabolite pairs (PS/RS) where appropriate. To illustrate, let us use the example of lactate dehydrogenase (LDH), which is implemented differently between H1 and K1. In H1, the rate equation is expressed as follows:

$$pyr + nadh \leftrightarrow lac + nad$$

$$v_{LDH} = \frac{\frac{V_{MAX}}{K_M^{pyr} K_M^{nadh}} \cdot ([pyr][nadh] - \frac{[lac][nad]}{K_{eq}})}{(1 + \frac{[nadh]}{K_M^{nadh}})(1 + \frac{[pyr]}{K_M^{pyr}}) + (1 + \frac{[lac]}{K_M^{lac}})(1 + \frac{[nad]}{K_M^{nad}}) - 1}$$

Whereas in the corresponding metabolic process in K1's hepatic compartment,

$$pyr + nadh \rightarrow lac + nad$$

$$v_{PYR\rightarrow LAC} = V_{MAX} \cdot \left(\frac{RS^{+}_{Hepatic}}{\nu^{+}_{Hepatic} + RS^{+}_{Hepatic}}\right) \cdot \left(\frac{\frac{[pyr]}{K_M^{pyr}}}{1 + \frac{[pyr]}{K_M^{pyr}}}\right)$$

$$lac + nad \rightarrow pyr + nadh$$

$$v_{LAC\rightarrow PYR} = V_{MAX} \cdot \left(\frac{RS^{-}_{Hepatic}}{\nu^{-}_{Hepatic} + RS^{-}_{Hepatic}}\right) \cdot \left(\frac{\frac{[lac]}{K_M^{lac}}}{1 + \frac{[lac]}{K_M^{lac}}}\right)$$

K1 considers nine substrates to be capable of transport between the blood and tissue compartments: glucose, pyruvate, lactate, glycerol, alanine, free fatty acids, triglycerides, oxygen and carbon dioxide. The net uptake or release of substrate mass s_i and concentration C_i in compartment x is expressed in the original paper by Kim *et al*. with the dynamic mass balance

$$\frac{\Delta s_i}{\Delta t} = Q_x \cdot (C_{plasma,i} - \sigma_{x,i}\, C_{x,i})$$

Where Q_x denotes the rate of blood flow through compartment x in litres per minute, $\sigma_{x,i}$ represents the partition coefficient of substrate s_i in compartment x, and $C_{plasma,i}$ and $C_{x,i}$ the plasma and compartmental millimolar concentrations of substrate s_i, respectively (16).

The advantages and disadvantages of K1 generally contrast with those of H1. Where H1 has fewer overall rates and metabolites with more complex and detailed individual descriptions, K1 has an abundance of variables and kinetic expressions that attempt to encompass the entirety of whole-body glucose turnover with generalised, generic descriptions that feature no enzyme mechanistic detail and little to no modification between compartments beyond different values of parameters. While an overabundance of information is

certainly preferable to a dearth thereof, the additional pathways and metabolites not immediately consequent upon the glycolytic/gluconeogenic pathway between glucose and pyruvate/lactate (e.g. alanine, glycerol, free fatty acids and triglycerides) introduces another problem: are they to be included as free, dynamic variables, clamped and kept constant, or removed?

3.1.6 Muscle, Brain, Cardiac, Adipose, and GIT Compartments - Modifications

As stated in the previous section, K1 includes several metabolites that are not present in H1, namely alanine, glycerol, free fatty acids (FFAs) and triglycerides. In the original K1 model, all of these metabolites are present in the hepatic compartment, and undergo exchange with the blood compartment. Thus, since K1's hepatic compartment has effectively been supplanted by H1, these variables pose a problem in that they either require incorporation into H1, or need to be removed from the model.

Initial research for this thesis using different models pursued the former option by attempting to introduce the 'missing' reactions and metabolites into the hepatic compartment using kinetic expressions and parameters from other models or online databases, effectively employing a 'mix-and-match' approach. However, this approach was discontinued for several reasons. First, and perhaps foremost, the introduction of previously unconsidered reactions into a model that was parameterised in their absence invariably produces anomalous and unrealistic results that are difficult to rectify. Second, if one were to add species and reactions for the purpose of comprehensiveness and modelling the physiological reality as closely as possible, it becomes difficult to decide where to set the arbitrary limit of complexity. An illustrative example, encountered in much earlier versions of the multi-compartmental model, is that of amino acid metabolism. Of the amino acids, alanine is the prime gluconeogenic substrate in the liver, but glutamine is a very close second. However, unlike the simple, reversible reaction carried out by alanine transaminase, glutamine must first undergo hydrolysis by glutaminase, followed by conversion to α-ketoglutarate, subsequent flux through the TCA cycle to oxaloacetate, after which it can enter the gluconeogenic pathway by eventual conversion to phosphoenolpyruvate. While the inclusion of such descriptions would indeed increase how 'realistic' the model is, it adds additional complexity, computational burden, and errors or anomalous results that are exceedingly difficult to troubleshoot. Furthermore, the decision to include an additional amino acid, but not the remaining eighteen glucogenic amino acids, can be criticised as unreasonable and arbitrary. Finally, such additions and the resulting model are impossible to validate without the appropriate data.

Following consideration of these issues, it was subsequently decided that the aforementioned variables present in K1, but not H1, would be clamped and kept constant at their original concentrations as published by Kim *et al*. (16), who used values at steady-state that reflected a normal overnight fasted human at rest. These concentrations would serve as an starting point that was validated previously by the original authors. A summary is provided in **Table 3.2**.

Table 3.2: Implementation in *meyer1* of metabolites present in the K1 model that are clamped (kept constant), variable, or are not common to all compartments

	Brain	Cardiac	Muscle	GIT	Adipose
Alanine	N/A	N/A	N/A	N/A	N/A
Glycerol	N/A	Clamped	Clamped	N/A	N/A
FFA	N/A	Clamped	Clamped	Clamped	Clamped
Triglycerides	N/A	N/A	N/A	N/A	N/A
Glycogen	Variable	Variable	Variable	N/A	N/A
GRP	N/A	Clamped	Clamped	Clamped	Clamped
PCR	Variable	Variable	Variable	Variable	N/A
CR	Variable	Variable	Variable	Variable	N/A
Glucose	Variable				
Pyruvate					
Lactate					
Oxygen					
CO_2					
G6P					
GAP					
ACoA					
CoA					
NAD^+					
NADH					
ATP					
ADP					

N/A indicates that the metabolite was either not originally present, or removed due to all relevant reactions being clamped.

Abbreviations as in **Table 3.1**.

While this was relatively straightforward to implement, it then raised the question of how to define the reactions that featured both clamped and unclamped metabolites as substrates and products. While the clamped metabolites are assigned constant concentrations reflecting the healthy, rested state, the unclamped metabolites are free to vary and respond to the metabolic changes associated with malaria infection. If some of the unclamped metabolites are involved in multiple reactions, of which some are fully dynamic, then it

creates the situation where the capacity of the model to give accurate descriptions is impaired, because portions of the model are unresponsive to changes in whole-body metabolism. To illustrate, let us consider the following examples. In both the cardiac and skeletal muscle, glycerol (GLR) undergoes phosphorylation to form glycerol-3-phosphate (GRP), using the hydrolysis of ATP to ADP for the provision of a phosphoryl group.

$$GLR + ATP \rightarrow GRP + ADP$$

While both GLR and GRP are clamped, ATP and ADP are not. Three other reactions had such a combination of clamped and unclamped variables: triglyceride synthesis, present in all compartments except for the brain,

$$GRP + 3\,FFA + 6\,ATP \rightarrow TG + 6\,ADP + 7\,P_i$$

GAP reduction, present only in adipose tissue,

$$GAP + NADH \rightarrow GRP + NAD^+$$

And fatty acid oxidation, present in cardiac, skeletal muscle and adipose tissue:

$$FFA + 8\,ACoA + 2\,ATP + 14\,NAD^+ \rightarrow 8\,ACoA + 2\,ADP + 2\,P_i + 14\,NADH$$

Following metabolic control analysis of the erstwhile iteration of the model, it was discovered that these reactions, particularly cardiac and muscular glycerol phosphorylation and triglyceride synthesis, exhibited very high control over plasma glucose (**Fig. 3.5**) and lactate concentrations (**Fig. 3.6**), which at the time appeared anomalous. Further investigation confirmed these suspicions, as both these reactions involve ATP hydrolysis (**Fig. 3.4**). Since glycerol, glycerol phosphate, and triglyceride concentrations are clamped, this effectively translates to a constant, significant level of ATP hydrolysis that substantially overshadows the remaining, dynamic portions of the model.

Figure 3.5: Rates exhibiting control over plasma glucose concentration, ranked in terms of absolute value in descending order. Green bars indicate positive coefficients, while red bars indicate negative coefficients.

Figure 3.6: Rates exhibiting control over plasma lactate concentration, ranked in terms of absolute value in descending order. Green bars indicate positive coefficients, while red bars indicate negative coefficients.

In other words, this relatively high rate of ATP hydrolysis would overshadow the comparatively low flux through other ATP-consuming reactions under conditions of hypoglycaemia and hyperlactataemia. The high control exhibited by these reactions was not judged as a scientifically meaningful finding or an emergent property of the model, since they display these high degrees of control while some of their constituent variables are kept constant at values reflecting the healthy, uninfected state. As explained at the beginning of

this section, to unclamp them would involve changes to the model that are beyond the scope of the current research.

Further investigation showed that, by decreasing the clamped concentration of GRP in the cardiac compartment by factor of 10 and doubling it within the muscle compartment, the control of these reactions on plasma glucose and lactate levels was drastically reduced, as well as substantially improving the ability of the model to describe clinical data. It is possible that these changes brought the system closer to a state that represented equilibrium during malaria infection. These changes were, however, admittedly biased and made in order to have simulation outputs match clinical data, and not to predict *in vivo* concentrations. However, considering that only two clamped metabolites were changed, and that this measure was much more viable than a more comprehensive reworking of the entire model that would be impractical in terms of time, such modifications were judged to be permissible.

Additionally, the definition of some clamped variables, such as triglyceride, are not present or declared in the current model at all. This is due to a custom optimisation function written to remove any rates, assignments, or parameters that are not present in the final model submitted for numeric solving. Since some of the rates in K1 have only clamped variables as substrates and products, and thus do not affect the fluxes of the model in any meaningful capacity, they were removed, so as to minimise the information submitted for computation (**Table 3.2**).

3.1.7 Hormonal Compatibility Changes

Models H1 and K1 utilised different approaches with regards to describing the concentrations of insulin, glucagon, and epinephrine, the chief hormones regulating glucose metabolism across multiple compartments.

K1 adapted a method previously described by Saunders et al. (173, 174) to describe the dynamic plasma concentrations of insulin and glucagon. This method involves use of an integral rein controller, composed of a system of coupled ODEs that determine hormonal concentration over time. This controller uses as input not only blood glucose concentration, but also the concomitant concentrations of insulin and glucagon, as the level of one hormone inhibits the rate of secretion of the other. Given K1's particular focus on exercise, the level of plasma epinephrine is not dictated by any metabolic inputs, but an empirical relation whereby epinephrine levels rise as a function of the degree of physical exertion.

With hormonal concentration dynamics so described, K1 has further descriptions whereby the maximum rate coefficients of reactions known to be hormonally regulated are stimulated as a function of plasma hormone concentrations. For reactions considered to be affected by glucagon and insulin, the model utilises a hyperbolic function with the plasma glucagon-insulin ratio (GIR) as input.

$$V = V^0 \cdot \left(1 + \frac{\lambda^G \cdot \left(GIR(t) - GIR(0)\right)^2}{\alpha^G + \left(GIR(t) - GIR(0)\right)^2}\right)$$

With initial value GIR(0), maximum effect λ and affinity constant α. Epinephrine-mediated stimulation is described similarly:

$$V = V^0 \cdot \left(1 + \frac{\lambda^E \cdot \left(C_E(t) - C_E(0)\right)^2}{\alpha^E + \left(C_E(t) - C_E(0)\right)^2}\right)$$

Note that these descriptions describe only stimulation of the relevant reactions; no descriptions for inhibition are present. This is understandable when considering the purpose of the original model, which sought to simulate the changes in fuel homeostasis during exercise, and was not intended to be used for description of metabolic changes during the majority of the day when the individual is not subject to exertion.

Conversely, H1 makes use of a different approach, using phenomenological functions termed glucose-hormone responses (GHR). These sigmoid functions describe the plasma concentration of a given hormone between its minimum, basal concentration and maximum concentration. The function for insulin increases monotonically with increasing blood glucose concentration:

$$[Insulin] = Insulin_{base} + (Insulin_{max} - Insulin_{base}) \cdot \frac{[Glucose_{Plasma}]^n}{k_{Insulin}^n + [Glucose_{Plasma}]^n}$$

A similar function is applied in the original H1 model to glucagon (and epinephrine, with its corresponding set of parameters), this time monotonically decreasing with increasing blood glucose concentration:

$$[Glucagon] = Glucagon_{base} + (Glucagon_{max} - Glucagon_{base}) \cdot \left(1 - \frac{[Glucose_{Plasma}]^n}{k_{Glucagon}^n + [Glucose_{Plasma}]^n}\right)$$

$$[Epinephrine] = Epinephrine_{base} + (Epinephrine_{max} - Epinephrine_{base}) \cdot \left(1 - \frac{[Epinephrine_{Plasma}]^n}{k_{Epinephrine}^n + [Glucose_{Plasma}]^n}\right)$$

With these functions in place, their relative contribution to the cell's overall phosphorylation state is calculated by applying a Michaelis-Menten like transformation to each, converting each to a hyperbolic function with a half-saturation value as follows:

$$Hormone_M = \frac{Hormone_{norm}}{K_\gamma^{hormone} + Hormone_{norm}}$$

where

$$Hormone_{norm} = [Hormone] - Hormone_{\ base}$$
$$K_\gamma^{hormone} = k_\gamma \cdot (Hormone_{\ max} - Hormone_{\ base})$$

Note that the expression for epinephrine contains an additional coefficient that scales its effectiveness down by 20%.

The fraction of hepatic enzymes currently phosphorylated (denoted γ) is subsequently expressed as

$$\gamma(Insulin, Glucagon, Epinephrine) = \frac{1}{2} \cdot \left(1 + max\left[Glucagon_M, \alpha_{Epi} \cdot Epinephrine_M\right] - Insulin_M\right)$$

During the combination of these models, the issue of how to incorporate their respective hormonal regulatory components had to be addressed. Had both models given the same hormonal (insulin, glucagon, epinephrine)

concentration outputs, it would simply have been a matter of implementing one model's hormonal controller and having it control all compartments. Unfortunately, this was not the case (**Fig. 3.7**).

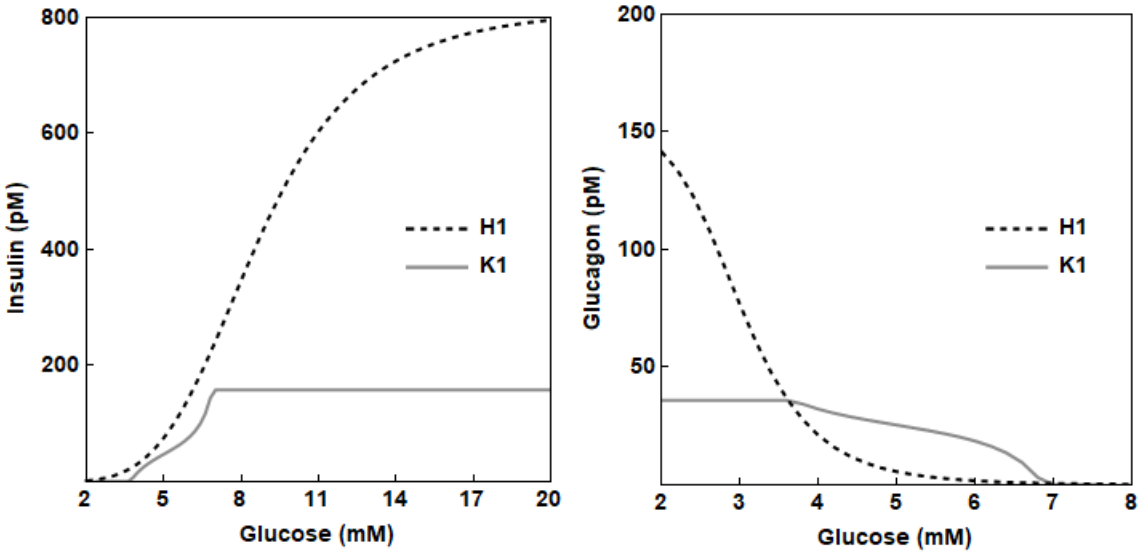

Figure 3.7: Hormone concentration vs glucose concentration plots for the original H1 (**dashed line**) and K1 (**solid line**) models.

A possible solution would have been to include both controllers, and have each govern its respective compartment, as per the original models. However, several drawbacks make this approach impractical. First, inclusion of K1's insulin and glucagon variables, in addition to the variables already present in H1, would have added computational load, model complexity, and hinder troubleshooting. Second, as mentioned before, K1 was not designed to simulate hyperglycaemic states, which have been observed in some malaria patient subpopulations (175). Additionally, it lacks a dynamic description of plasma epinephrine concentration, a limitation absent in H1. Third, attempts to reproduce and validate K1's original descriptions were met with limited success (**Figs. 3.5 & 3.6**), limiting the confidence with which its hormonal controller could be applied to H1. Finally, the bulk of K1's hormonal modifiers occur in its hepatic compartment, which has already been supplanted by H1.

With these considerations in mind, the decision was made to utilize H1's descriptions of hormone concentrations. K1's remaining non-hepatic hormonal modulation terms (located in the cardiac, skeletal muscle, adipose, and GIT compartments) were adapted to accept H1's plasma hormone concentrations as input. In the case of epinephrine-mediated regulation, this was achieved by simply replacing the input to the hyperbolic function with the normalized hormone concentration (concentration above baseline) originally described in H1 (see second equation within **Section 3.1.7**):

$$V = V^0 \cdot \left(1 + \frac{\lambda^E \cdot (Epinephrine_{norm})^2}{\alpha^E + (Epinephrine_{norm})^2}\right)$$

3.2 Model Construction – Novel Additions

One of the research objectives described in **Section 1.2.3** was to modify and extend the model with features, phenomenological or otherwise, to introduce host-parasite interactions that have a significant effect on plasma glucose and lactate, as reported in literature, to prepare for the contingency that, without these changes, the model would fail to describe the clinical data. When this indeed did prove to be the case, multiple modifications and additions were implemented in the interest of improving the descriptive capacity of the model. In an ideal model, these additions would be based on scientific studies, where the novel components are parameterised via processing of numerical sets of input and output data. In this way, the changes, modifications and additions would be able to describe unknown phenomena while still having a quantitative basis in reality.

In the current research, however, such changes and additions were made without the aid of quantitative data to guide the process of deriving and parameterising phenomenological functions governing phenomena such as host-parasite metabolic interactions. At the time of writing, the situation is one where a consensus has been reached by multiple independently published sources stating that a particular cause-and-effect relationship exists between parasite infection and host metabolism, but such statements are wholly limited to the qualitative realm. A good example of this is the causal chain that has been established between parasite sequestration within the hepatic microvasculature, impedance of liver function, and the contribution of this compromised hepatic metabolism to the appearance of hypoglycaemia and hyperlactataemia in severe malaria (12, 49, 63, 93, 108, 176). The few studies that have measured quantitative data demonstrating the positive relationship between the degree of microvascular obstruction and plasma lactate levels have limited applicability in the current research, as the data was collected through orthogonal polarization spectral imaging of capillaries in the rectal mucosa (128). The authors of this paper noted that the changes in microcirculatory blood flow through the rectal mucosa could also be present in other organs, including the liver, where compromised tissue oxygenation could have a deleterious effect on lactate metabolism, citing the heterogeneity in the degree of sequestration between organs observed in autopsy studies (132, 135).

These findings thus necessitated the use of a ‘top-down’ modelling approach, which is typically less preferable than the ‘bottom-up’ method used when deriving other novel additions made to the model. For example, when parameterising features such as scaling organ compartment weight by age or choosing a value for a glucose input function, decisions are made based on numerical data and quantitative observations. In other words, these components are built upon empirical observations, and are extended and adapted ‘up’ towards description of the clinical data of plasma glucose and lactate concentration in severe malaria. Conversely, the ‘top-down’ method is effectively the opposite approach, where in the absence of such empirical data, the values of parameters are chosen based on the quality of the descriptions they yield, irrespective of how closely they resemble physiological values, the latter of which remain to be determined. This ‘top-down’ approach was thus necessitated for the derivation, parameterisation and implementation of several novel components, particularly those relating to renal lactate excretion and parasite-mediated

modulation of host metabolism, due to the relative abundance of published qualitative statements and the paucity of quantitative data.

It could be argued that the model features presented here, particularly those related to modelling microvascular disturbances, are not applicable, since they are not derived from detailed mechanistic interpretations of physiological processes or fitted to quantitative measurements. Since such quantitative data simply is not available at the time of writing, the next course of action would be to base these functions on an in-depth model derived from the biophysics of blood flow in the microcirculation. However, considering that this model is concerned with metabolic phenomena that manifest at the whole-body level, and that the dynamics of luminal capillary blood flow would constitute an entire research project on its own, the work presented below constitutes what was judged to be the most reasonable and practical implementation considering the time and means available. Ample effort has been given to substantiate these changes with references to the existing literature, and the mechanistic basis of novel additions are explained where possible. A summary of these changes with their accompanying rationale is provided at the end of **Section 3.2** in **Tables 3.5 & 3.6**.

3.2.1 Plasma Compartment

3.2.1.1 Compartment Age and Weight Scaling

Recent literature has emphasised the role of age in the presentation and prognosis of severe malaria, highlighting not only differences in disease severity, but also the relative incidence of pathological manifestations (23, 124). While syndromes such as coma and metabolic acidosis do not appear to be associated with age, hypoglycaemia and anaemia are found to be more prevalent in children, with adults typically being more prone to hepatic and renal failure (**Fig. 2.4**).

Thus, the ability to scale the model compartments with the age of the individual being simulated became an appealing prospect, and was subsequently implemented. The decision to add this feature was made for a number of reasons: simple, expedient formulae that estimate body weight from age are already in use in the clinical setting (177, 178); the volume of individual organ compartments can be directly inferred and scaled from total body weight; and the mass-based units of the model mean that the absolute mass of metabolites can be scaled with body weight, while keeping their respective concentration relatively constant (**Fig 3.8**).

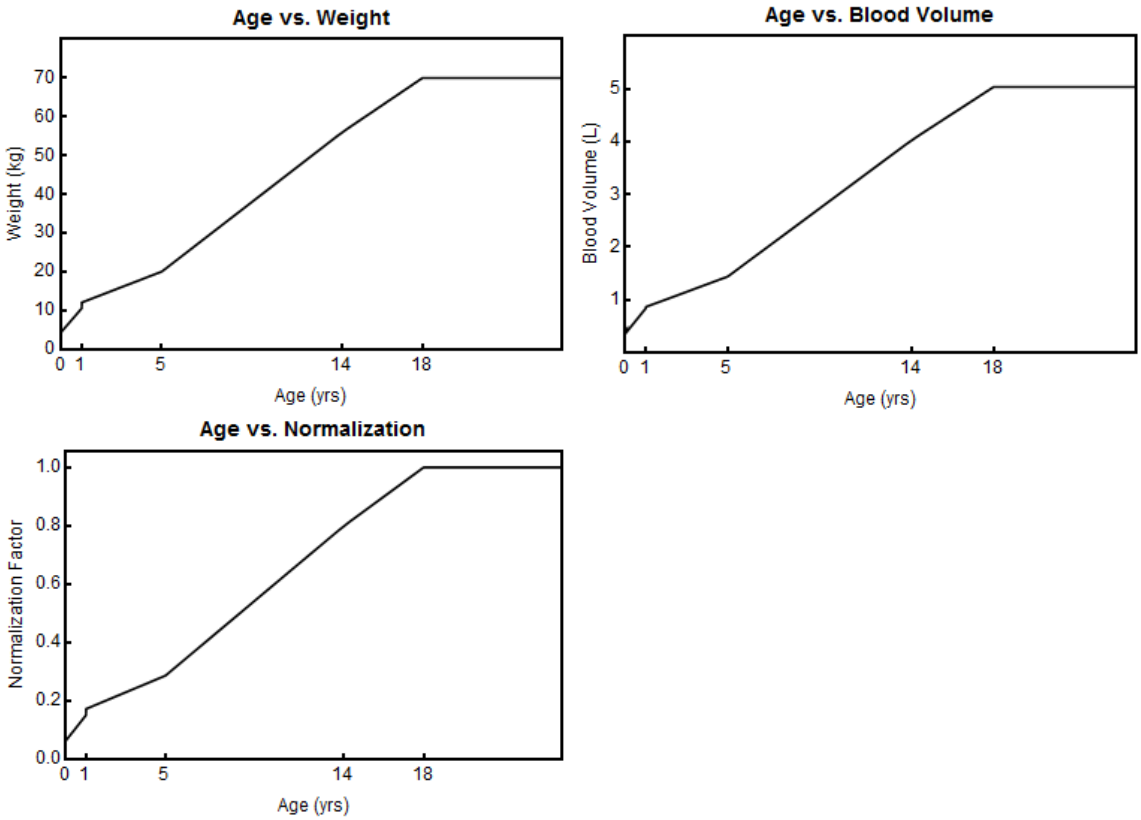

Figure 3.8: Plots of simulated weight, blood volume, and organ compartment volume normalization factors as a function of age. Top-left panel corresponds to formulae shown in Table 3.3, while the top-right panel corresponds to those shown in Table 3.4. Bottom-left panel shows the normalisation factor (bodyweight/bodyweight$_{adult}$) used to potentially scale individual organ volumes

Calculation of weight as a function of age was done using a modified version of a previously established method (177), with additional formulae added for adolescents and adults (**Table 3.3**). An individual aged 18 or older was assumed to have a bodyweight of 70 kilograms.

Table 3.3: Formulae for simulated weight as a function of age

					Weight (kg)
0	≤	Age	<	1	$0.5 \times ((Age \times 12) + 9)$
1	≤	Age	<	5	$2 \times (Age + 5)$
5	≤	Age	<	14	$4 \times Age$
14	≤	Age	<	18	$3.5 \times (Age - 14) + 56$
18	≤	Age			70

Additionally, the total blood volume was estimated using a formula adapted from anaesthesiology (**Table 3.4**)(179). Values were averaged to compensate for the lack of distinction between males and females.

Table 3.4: Formulae for total blood volume as a function of age

						Blood Volume (L)
Neonates (<28 days old)	0	≤	Age	<	$\frac{28}{365}$	$Weight\ (kg) \times 0.09\ L/kg$
Infants	$\frac{28}{365}$	≤	Age	<	1	$Weight\ (kg) \times 0.08\ L/kg$
Adults	1	≤	Age			$Weight\ (kg) \times 0.072\ L/kg$

Finally, since the H1 and K1 models were originally designed to simulate adults weighing 70 kg, compartment volumes and other scalable components are multiplied by the normalised ratio of age-determined bodyweight to adult bodyweight.

$$(ORGAN)\_COMPARTMENT\_VOLUME \rightarrow (ORGAN)\_COMPARTMENT\_WEIGHT\_DEFAULT \times \frac{PLASMA\_MISC\_BODYWEIGHT}{PLASMA\_MISC\_BODYWEIGHT\_DEFAULT}$$

Where (ORGAN)_COMPARTMENT_WEIGHT_DEFAULT is the typical weight of the given tissue in a 70 kg adult male.

It should be noted that, while this scaling was implemented successfully and produced reasonable simulation outputs, this functionality was not utilised in a meaningful capacity during further research. Instead, all simulations were conducted at a constant simulated age of 18 and body weight of 70 kg. While the investigation of how simulation outputs with regards to steady-state plasma glucose and lactate concentrations would differ as a function of age could possibly yield useful insight into malaria pathophysiology (**Section 2.4**), development of this feature was discontinued due to the time required to both collect data with which to parameterise the relative growth of individual compartment volumes through various stages of life, and to implement and test such functionality. Furthermore, the greater relevance of other novel model components (such as host-parasite interactions, **Section 3.2.2**) also placed further development of age and weight scaling at a lower priority. This functionality has, however, been incorporated into the model for future investigations.

3.2.1.2 Volume scaling

The volume of the 'blood' compartment was defined as consisting of several distinct sub-compartments, namely the plasma, uninfected erythrocyte cytosol, infected erythrocyte cytosol, and the parasite cytosol. The volume of each of these compartments is a fraction of the total blood volume, which, in turn, is defined by a function estimating total blood volume from age.

$$PLASMA\_COMPARTMENT\_VOLUME\_LITERS \rightarrow fAgeWeightBV[PLASMA\_AUX\_AGE]$$

The subsequent total erythrocytic cytosolic volume is derived as a subfraction of the total blood compartment volume ('plasma' indicating the volume of the blood not taken up by cells):

$$RBC\_CYTOSOL \rightarrow RBCu\_MISC\_AlphaCellWaterFraction \cdot BLOOD\_HAEMATOCRIT \cdot BLOOD\_TotVolmL$$

Where RBCu_MISC_AlphaCellWaterFraction indicates the free liquid cytosolic volume portion of the erythrocyte, BLOOD_HAEMATOCRIT indicates the volumetric fraction of the blood taken up by erythrocytes, and BLOOD_TotVolmL the volume of the blood compartment in millilitres.

This erythrocyte cytosol compartment is then further divided into infected and uninfected sub-compartments:

$$RBCu\_VOLUME \rightarrow (1 - PF\_AUX\_PS) \cdot RBC\_CYTOSOL$$

$$RBCi\_VOLUME \rightarrow PF\_AUX\_PS \cdot RBC\_CYTOSOL$$

Where PF_AUX_PS indicates percentage parasitaemia. Finally, the infected erythrocyte compartment is again separated into the infected erythrocyte cytosol, and the parasite cytosol:

$$RBCi\_CELL\_VOLUME\_FRACTION \rightarrow 1 - \frac{PF\_MISC\_volPFTroph}{RBCu\_MISC\_volRBCDefault}$$

Where the fraction PF_MISC_volPFTroph/RBCu_MISC_volRBCDefault indicates the fraction of the erythrocytic volume taken up by the parasite. The parameter volPFTroph represents an averaged volume of the parasite across all intraerythrocytic lifecycle stages. Thus, the total infected erythrocyte volume can be calculated by multiplying the infected erythrocytic volume portion by the *total* volume of infected erythrocytes, parasites included:

$$RBCi\_CELL\_VOLUME \rightarrow RBCi\_CELL\_VOLUME\_FRACTION \cdot RBCi\_VOLUME\_FRACTION$$

A similar approach is used to calculate the volume of the parasite compartment, by multiplying the percentage parasitaemia by the total infected and uninfected erythrocyte volume to obtain the fraction of erythrocytes that are infected, and subsequently multiplying this again by the volume fraction of the erythrocytic volume taken up by the parasite:

$$PF\_VOLUME \rightarrow (PF\_AUX\_PS \cdot RBC\_CYTOSOL) \cdot \frac{PF\_MISC\_volPFTroph}{RBCu\_MISC\_volRBCDefault}$$

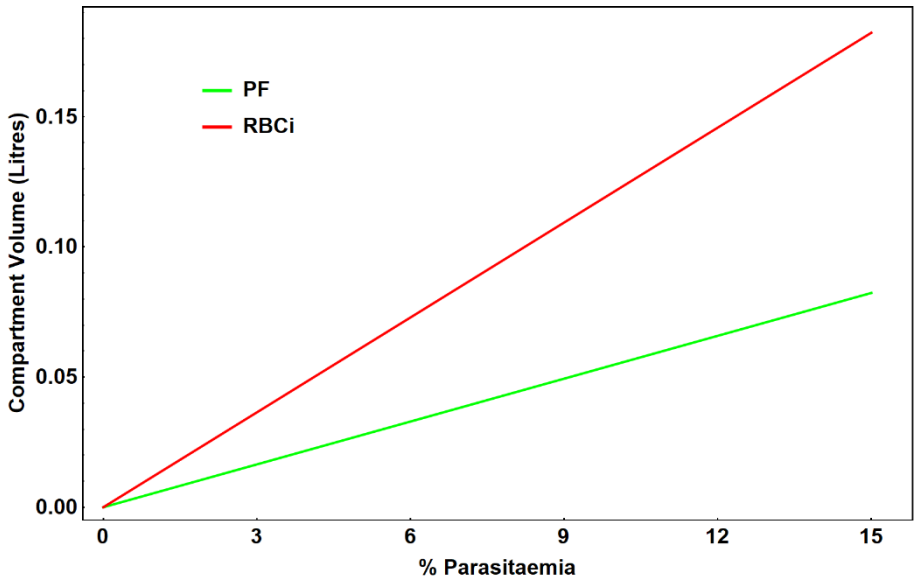

Figure 3.9: Parasite and infected erythrocyte compartments volumes as a function of percentage parasitaemia obtained from the equations for PF_VOLUME and RBCi_CELL_VOLUME, respectively (see text above)

3.2.1.3 Renal lactate excretion

Implementation of renal lactate excretion (clinically observed above 5 mM plasma concentration)(88) was done using an extended hyperbolic tangent function. This function bears close resemblance to the activation or "squashing" function used in neural networks to clip for large quantities and to maintain a bounded response (158).

$$y = \frac{1}{2} \cdot (1 + \tanh[a \cdot (x - c)])$$

With gradient proportional to a and inflection point at c (**Fig 3.10**).

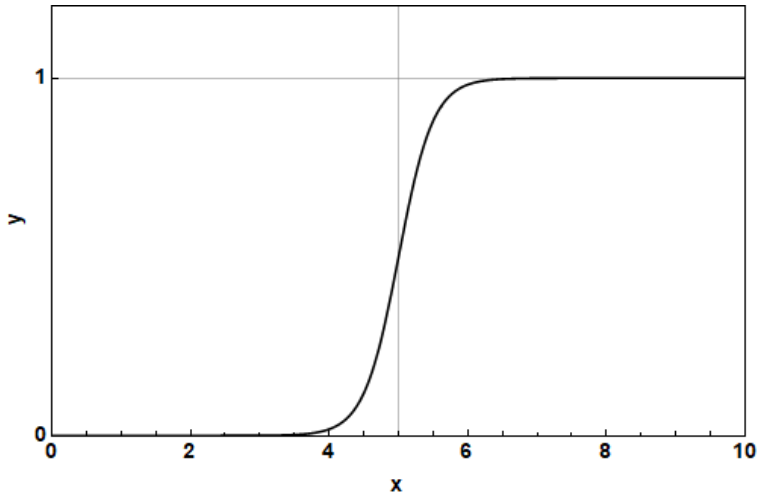

Figure 3.10: The tanh 'switch' function

This function was defined following difficulties using a piecewise function. Within the context of computing numerical differential solutions for the model, the piecewise function introduces numerical and computational instability, likely owing to its Boolean processing of model variables which leads to problematic stiff equations. Usage of a piecewise function as part of a controller function can become problematic if the input variable continually oscillates around the piecewise threshold. To illustrate, let us consider a possible piecewise implementation of a renal excretion function, which is only active at or above a plasma lactate concentration of 5 mM:

$$f(x) = \begin{cases} 0, & [Lactate_{Plasma}] < 5.0 \\ k_{deg} \cdot [Lactate_{Plasma}], & [Lactate_{Plasma}] \geq 5.0 \end{cases}$$

While such a straightforward function can be readily implemented using Mathematica's built-in functionality, it poses several problems. First, it is not physiologically plausible; the kidney does not completely halt all excretory function when the plasma lactate concentration falls below 5 mM. Second, if the plasma lactate concentration happened to reach a steady-state at 5 mM, computation would be slowed by the task of having to switch between two mathematical definitions at each time step.

Having encountered these problems, a 'switch function' was implemented in the trigonometric form described above. Like the piecewise function, this function can still give near-absolute outputs of 'true' and 'false' (1 and 0, respectively), but can also accommodate a 'grey-scale' transition between the two (**Fig**

3.10). This switch function was used to rapidly ramp up ('switch on') renal lactate excretion as it neared and exceeded a threshold value of plasma lactate concentration.

This function was subsequently implemented in the rate equation denoting renal lactate excretion from the plasma compartment. Parameters were determined according to the values which gave descriptions that best agreed with the clinical data (**Section 4.1.3**) based on visual inspection (see **Section 4.3.4** and **Fig. 4.12** for an example of how parameter values were chosen according to congruence with clinical data upon visual inspection).

3.2.1.4 Glucose feed function

Since the model is an open system, where species such as lactate are removed from the plasma compartment through means such as renal excretion, a corresponding function had to be implemented for glucose entry into the plasma. Implementation of such a glucose 'feed' function was necessitated for steady-state analysis, since, without a constant input of glucose, the model would eventually evolve to equilibrium as all glucogenic stores, such as glycogen, became depleted.

The most realistic way to model the intake of nutrients (specifically glucose) in an individual would likely be the introduction of a stomach and/or gastrointestinal compartment(s), which would receive a predefined influx of nutrients at times of the day that correspond to meals. While this approach was successfully implemented, the nature of a steady-state model precludes any kinetics that do not equilibrate with time.

This therefore leaves the introduction of a constant, zero-order rate of glucose influx into the plasma compartment as the most practical option. This method is also representative for the clinical setting where a constant intravenous infusion of glucose is provided, to prevent hypoglycaemia in children with severe malaria who are incapable of ingesting meals (49, 180).

Therefore, a relatively straightforward function was introduced, comprised simply of a constant rate of glucose influx, defined in units of milligrams per kilogram bodyweight per minute. This input parameter is subsequently converted to millimoles per minute via division by the molar mass of glucose and multiplication with bodyweight.

The magnitude of the glucose influx rate was chosen to be approximately 2 mg/kg/min, to align with the intravenous infusion given to unconscious, hypoglycaemic children with severe malaria (62). This could potentially be increased to 5 mg/kg/min, as is the case in emergency settings (65), although this would likely not be sustained for longer than two hours.

$$PLASMA\_GLUCOSE\_FEED\_MM \rightarrow \frac{PLASMA\_GLUCOSE\_FEED\_MGKGMIN}{PLASMA\_MISC\_MR\_GLC}$$

$$v\_ENZ\_PLASMA\_GLUCOSE\_FEED \rightarrow PLASMA\_GLUCOSE\_FEED\_MM \cdot BODYWEIGHT\_KG$$

Here, *PLASMA_GLUCOSE_FEED_MM* represents the rate of glucose infusion, expressed in millimoles per kilogram of bodyweight per minute, and *PLASMA_MISC_MR_GLC* the molar mass of glucose.

3.2.1.5 Glucose utilization function

To account for the remainder of glucose utilisation not specified by other compartments, two phenomenological functions were implemented to account for glucose uptake by the renal and splanchnic organs. These functions were parameterised in the current research, based on previous literature describing glucose usage on a per-compartment basis (181–184). They were further adapted to increase glucose consumption at a rate proportional to the plasma glucose concentration as an indirect, phenomenological inclusion of the effect of insulin release. The phenomenological rate equation for renal glucose utilisation is shown below.

$$v\_PLASMA\_GLUCOSE\_UTIL\_RENAL = PLASMA\_GLUCOSE\_UTIL\_RENAL\_k \cdot PLASMA\_VAR\_glucose^{PLASMA\_GLUCOSE\_UTIL\_RENAL\_N}$$

Where PLASMA_GLUCOSE_UTIL_RENAL_k represents a first-order rate coefficient, PLASMA_VAR_glucose represents the millimolar concentration of plasma glucose, and PLASMA_GLUCOSE_UTIL_RENAL_N represents an exponential modifier. This rate equation is of the exponential form $y = a \cdot x^2$ to accommodate a higher rate of glucose uptake by 'other' tissues (i.e. those not explicitly assigned a compartment) at higher plasma concentrations of glucose, thereby giving a proxy, phenomenological description of insulin's effect on glucose uptake as blood glucose concentration increases. Parameter values were chosen based on how well the corresponding simulation outputs of glucose utilisation of the whole model in the healthy state resembled the results published in the references (181–184).

3.2.2 Parasite-Mediated Modulation of Host Metabolism

3.2.2.1 Uninfected Erythrocytes

One of the most striking examples of parasite-mediated changes in host metabolism was illustrated by a series of experiments performed by Mehta *et al*. (185). Exposure of healthy, uninfected erythrocytes to culture medium (CM) conditioned by *P. falciparum*-infected erythrocytes showed an almost complete inhibition of key glycolytic enzymes in the healthy red blood cells. The enzymes in question were phosphofructokinase (PFK) and pyruvate kinase (PK). The activity of glucose 6-phosphate dehydrogenase (G6PDH), a component of the pentose phosphate pathway, remained relatively unaffected.

To incorporate this inhibitory effect into the model, a phenomenological function was implemented using a hyperbolic inhibitory function (**Fig. 3.11**), defined as follows:

$$RBCu\_PF\_INHIB\_TERM = 1 - \frac{\%\ Parasitaemia}{RBCu\_PF\_INHIB\_TERM\_K + \%\ Parasitaemia}$$

In the absence of data describing how the degree of inhibition varies with parasitaemia, both the hyperbolic form of the function and the accompanying inhibition constant were initially chosen arbitrarily and subsequently varied according to the results of later analysis.

This inhibition component was introduced as a coefficient to the rate expressions of PFK and PK in uninfected erythrocytes. This marked the first phenomenological implementation of host-parasite metabolic interaction in the combined *meyer1* model.

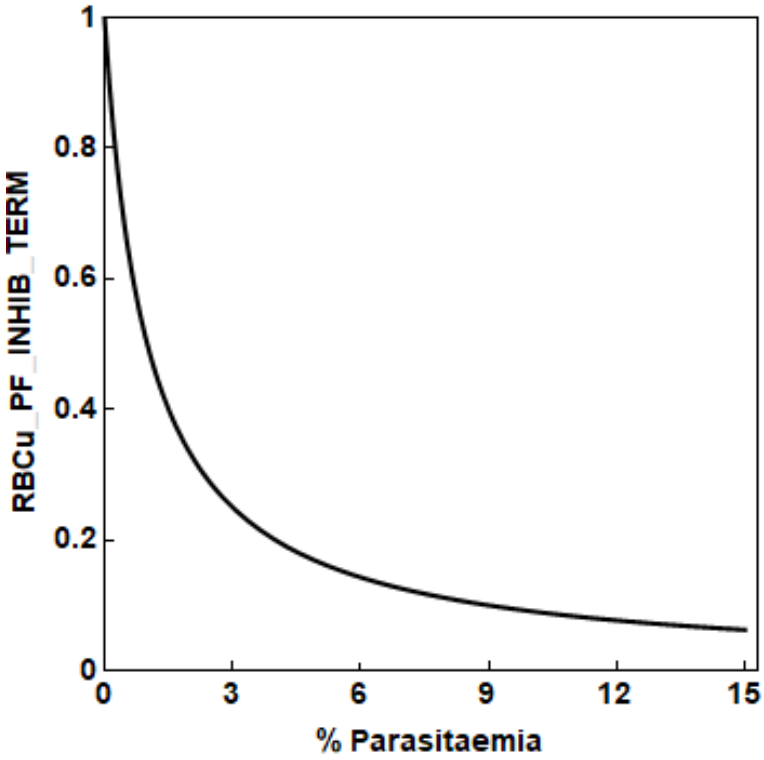

Figure 3.11: Plot of the numerical inhibition value vs percentage parasitaemia

3.2.2.2 Hepatic microvascular occlusion

To model the effects of heterogenous microvascular occlusion on whole-body glucose and lactate metabolism, phenomenological functions and modifiers were introduced to various compartments, which altered the properties of specific rates as a function of percentage parasitaemia (similar to the PK and PFK inhibition discussed in **Section 3.2.1**). Due to the lack existing mathematical descriptions in literature, these functions and modifiers were novel additions derived phenomenologically as part of the current research. The hepatic perfusion and hypoxia modulation parameters were the third and fourth to be introduced, respectively.

3.2.2.2.1 Perfusion

Obstruction of microvascular flow has been observed in blood vessels supplying and draining the liver; based on the results examined in **Section 2.6.4**, it is assumed that this is due at least in part to the presence of infected erythrocyte aggregates and membrane remnants. Additionally, disruption of endothelial barrier integrity would also be a likely confounding factor.

The existing mathematical framework describing the rates of transporters of glucose, lactate, and pyruvate was used to implement the effect of increasing parasitaemia on the ability of the hepatic compartment to

exchange chemical species with plasma. First, a phenomenological hyperbolic function was used to transform parasitaemia input into a saturable output:

$$HEPATIC\_PF\_INHIB\_PERFUSION = \frac{HEPATIC\_PF\_INHIB\_PERFUSION\_MAX \cdot \%\,Parasitaemia}{HEPATIC\_PF\_INHIB\_PERFUSION\_KM + \%\,Parasitaemia}$$

Initial implementations used this function to decrease the maximal velocities of transporters. However, this method was discarded following the reasoning that the parasite altered the endothelial milieu and not the hepatocyte membranes; in other words, the maximal velocity of the transporter enzymes would not be affected, since neither the conformation of the enzymes themselves nor their effective concentration is altered. Instead, the sequestered parasites that adhere to the luminal surface of the endothelial capillary surface impede diffusion of metabolites to and through the endothelial wall. Attached to the inside of the capillary, they take up the volume of plasma available for metabolites to diffuse to the adjacent capillary wall. In the current study this effect was implemented as an increased affinity binding constant, or K_M. Furthermore, since the sequestered erythrocytes adhere to the luminal side and do not penetrate to the hepatocyte parenchyma, this inhibition would be limited to the affinity binding constant of the plasma metabolites only. Finally, the function was defined as hyperbolic and saturable both to match the general trend of the clinical data, and the reasoning that there exists a limited luminal capillary surface for the parasites to adhere to, and a finite intraluminal capillary volume for the parasitized and infected erythrocytes to rosette and agglutinate within.

Thus, another approach was employed, which involved an increase in the dissociation constant of the hepatic transporters for the *extracellular* species (**Fig. 3.12**). This was implemented as shown below, with the form of the rate equation being the same as that published in the original paper by König et al.:

$$K_M^{Mod} = K_M \cdot (1 + HEPATIC\_PF\_INHIB\_PERFUSION)$$

$$v_T = \frac{V_{max} \cdot \left(S_{Plasma} - \frac{S_{Hepatic\ Cytosol}}{K_{eq}}\right)}{K_M^{Mod} \cdot \left(1 + \frac{S_{Plasma}}{K_M^{Mod}} + \frac{S_{Hepatic\ Cytosol}}{K_M}\right)}$$

Parameter values optimised on the basis of how closely the corresponding simulation outputs resembled clinical data (see **Appendix C.1.2**).

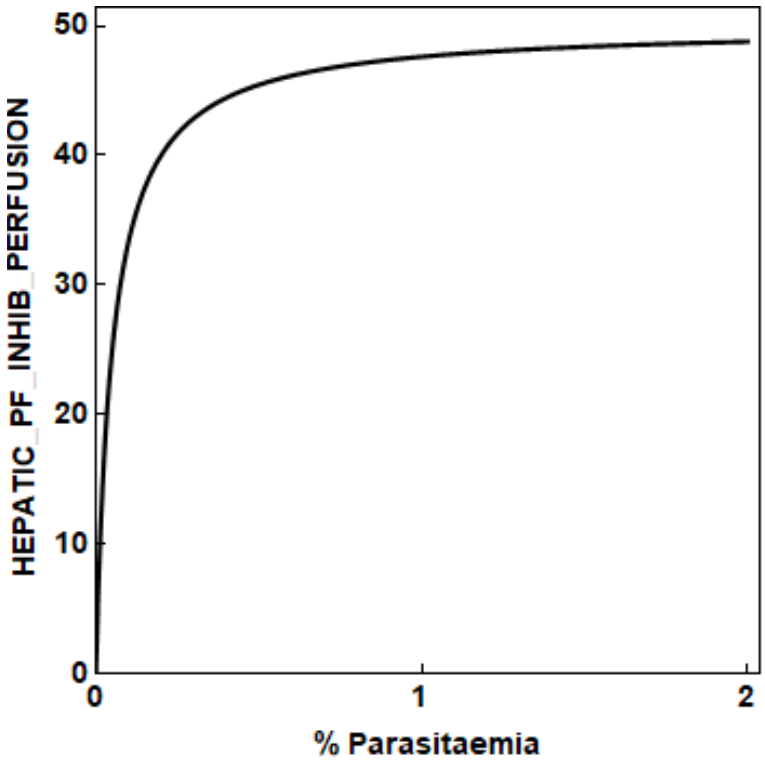

Figure 3.12: Plot of increase in the plasma-side affinity binding constants for the hepatic glucose, lactate, and pyruvate transporters.

3.2.2.2.2 Hypoxia

Among the varied sequelae consequent upon microvascular obstruction, lack of tissue oxygenation is the most readily apparent and often the most cited. Though blood oxygenation has consistently been found to not be reduced by malaria infection, it stands to reason that, if a tissue becomes ischemic due to parasite-blocked capillaries, localised hypoxia would be an almost certain outcome. Furthermore, much of the literature reflects a consensus that the appearance of glycaemia with concomitant hyperlactataemia is due to accelerated generalised anaerobic glycolysis, of which the cause is usually insufficient oxygen supply.

Incorporation of this phenomenon into the hepatic compartment of the model was implemented using separate descriptions from those utilised to model perfusion. This was done based on the reasoning that (i) oxygen diffuses between the blood and the tissues, and is not actively transported, (ii) H1 does not include any description of oxygen transport or turnover, and (iii) hypoxia affects the functions of enzymes mediating metabolic turnover, not transport.

The function relating plasma percentage parasitaemia to tissue hypoxia was of the hyperbolic type (**Fig 3.13**). Inhibition was limited to approximately 60% of normal, based on how well the model described steady-state plasma glucose and lactate concentrations when compared with clinical observations (**Section 4.1.3**) of these metabolites.

$$HEPATIC\_PF\_INHIB\_HYPOXIA = 1 - \frac{HEPATIC\_PF\_INHIB\_HYPOXIA\_MAX \cdot \%\,Parasitaemia}{HEPATIC\_PF\_INHIB\_HYPOXIA\_KM + \%\,Parasitaemia}$$

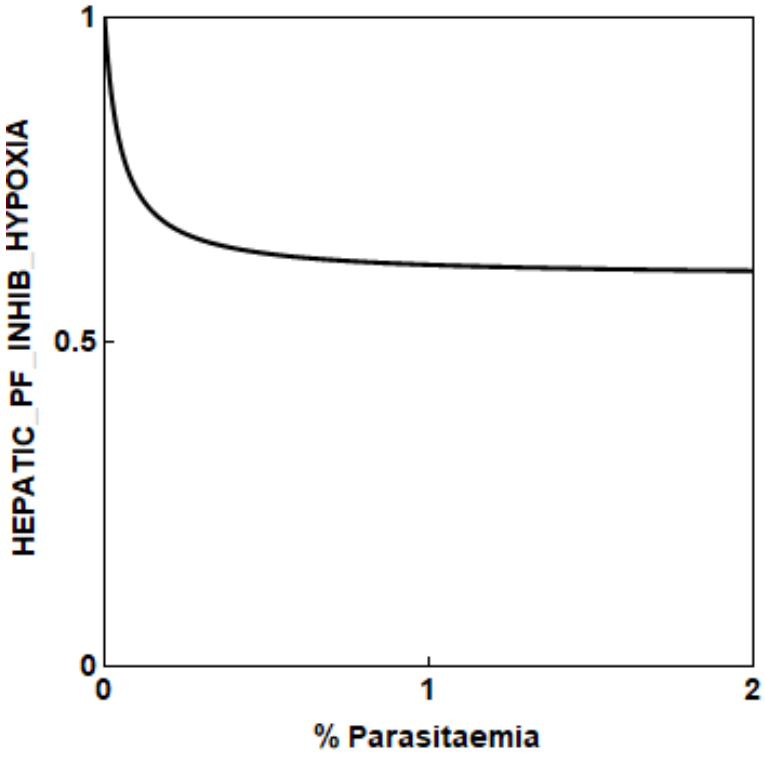

Figure 3.13: Plot of the hypoxia-mediated inhibition coefficient vs percentage parasitaemia.

This inhibition term was then applied as a rate multiplier for fluxes known to either require oxygen, or that have been observed to be inhibited by the presence of parasitaemia. The enzymes in question are v_ENZ_HEPATIC_O2_H2O (oxidative phosphorylation), v_ENZ_HEPATIC_PYRUVATE_CARBOXYLASE, v_ENZ_HEPATIC_PYRUVATE_DEHYDROGENASE and v_ENZ_HEPATIC_TRANSPORTER_MITOCHONDRIAL_PYRUVATE, these enzymes were chosen based on literature reports (108, 152). Given that the literature in question gave only qualitative statements regarding the involvement of the aforementioned enzymes, inhibition of the reactions catalysed by these proteins was parameterised according to how well the resulting outputs matched clinical data in the presence of varying malaria parasite burdens.

3.2.2.3 Cerebral perfusion inhibition

Sequestration of *P. falciparum* within the microvascular beds of the brain causes occlusion of these vessels, reducing blood flow to the brain and causing inhibition of cerebral perfusion (135, 186). To model this process, a phenomenological function was implemented that would reduce the normal, basal blood flow as a function of increasing parasitaemia. This constituted the fourth modulation parameter introduced to the model.

$$BRAIN\_PF\_INHIB\_PERFUSION = 1 - \frac{BRAIN\_PF\_INHIB\_PERFUSION\_MAX \cdot \%\,Parasitaemia}{BRAIN\_PF\_INHIB\_PERFUSION\_KM + \%\,Parasitaemia}$$

The inhibition term was used as a coefficient when calculating the blood flow to the brain (see **Section 3.1.5** for definition of blood flow rate equation).

$$BRAIN\_BLOOD\_FLOW\_Q = BRAIN\_BLOOD\_FLOW\_Q\_BASE \cdot PLASMA\_WEIGHT\_SCALAR \cdot BRAIN\_PF\_INHIB\_PERFUSION$$

Parasite-mediated changes in brain metabolism were limited to inhibition of perfusion, due to the relative dearth of discussion in the literature of aberrations of brain metabolism versus the effect of cerebral microvascular obstruction.

3.2.2.4 Muscle metabolic upregulation

Modulation of muscle metabolism by parasitaemia was implemented based on reasoning that (i) plasma lactate has been observed to rise after generalised convulsions (23), and (ii) basal muscle activity would be raised as part of pyretic thermogenesis (187). Generalized convulsions in particular would likely involve a transient shift towards greater usage of anaerobic glycolysis, owing to the intensity of the muscular contractions and the associated increased demand for rapid ATP supply. Introduction of a component describing this behaviour would thus allow the model to emulate the increased glycolysis that is expected to occur.

This was subsequently modelled using a phenomenological Michaelis-Menten type function that would upregulate the activity of muscle ATPase activity with parasitaemia as input. This term was subsequently implemented as a rate multiplier to muscle ATPase flux as the final modulation parameter incorporated into the model.

$$MUSCLE\_PF\_MOD = 1 + \frac{MUSCLE\_PF\_MOD\_MAX \cdot \%\,Parasitaemia}{MUSCLE\_PF\_MOD\_KM + \%\,Parasitaemia}$$

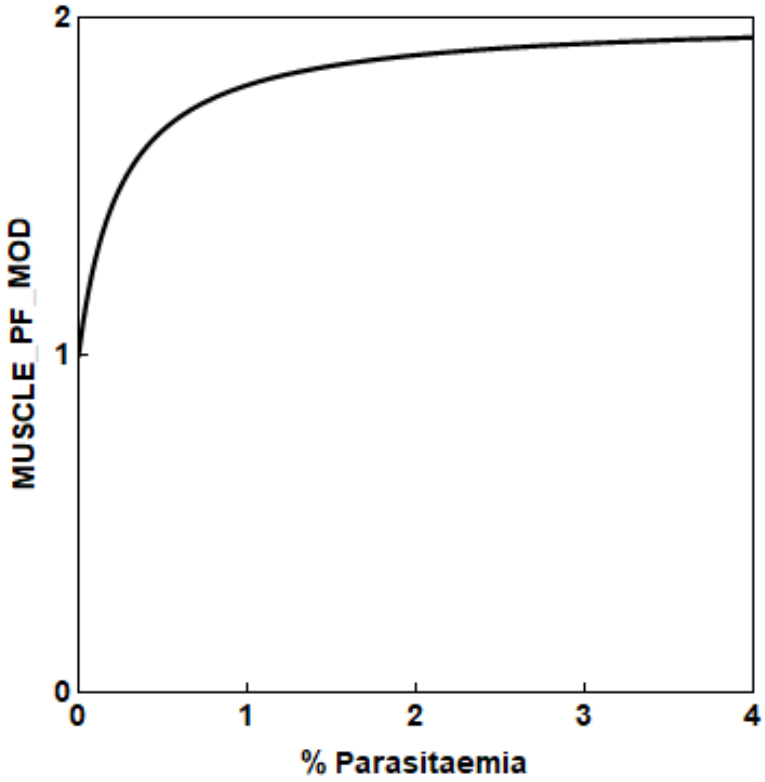

Figure 3.14: Plot of disease-mediated activation coefficient for skeletal muscle ATPase activity

3.2.3 Summary of Changes and Additions

A summary of the changes and additions made to the constituent models during the development of *meyer1* is given in **Table 3.5**. Modifications and extensions are listed by compartment, with each component accompanied with the rationale for its inclusion and the references used to substantiate its implementation, where applicable.

Table 3.5: Compartments and the models they were based on; additions and changes and the rationale thereof

Plasma; green1 (162)		
Glucose feed function	Provision of a constant input of glucose into the plasma compartment; modelled as an average of dietary glucose intake or constant intravenous dextrose infusion	(49, 62, 65, 180)
Glucose utilization function	Accounts for glucose uptake by remaining compartments	(181–184)
Renal lactate excretion	Simulation of renal lactate excretion during hyperlactataemia; indirectly accounts for renal gluconeogenic activity	(88, 106)
Volume scaling	Allowed plasma compartment volume to scale with age; reworked implementation of plasma/erythrocyte compartments to share a finite volume as defined by haematocrit	*
Hepatic; König et al. 2012 (18)		
Unclamped reducing equivalents Transport of reducing equivalents across the mitochondrial membrane Oxidative phosphorylation activity	Extends functionality to include simulation of cellular hypoxia, hypoglycaemia, and hyperlactataemia	(17)
Pyruvate transporter	Provides physiologically realistic means for plasma pyruvate uptake	
Sub-compartment volume scaling	Scaling of enzyme fluxes absolute masses of metabolites by relative volumes of cytosol and mitochondria; allows hepatic function to scale with liver size/volume	
Parasite-mediated inhibition of liver function	Phenomenological additions to simulate effects of parasite sequestration within the hepatic sinusoids, divided into perfusion inhibition (extracellular effects) and hypoxia (intracellular effects)	
Parasite; penkler1 (20)	Redefined how compartment volume was determined; no functional changes were made	
Erythrocyte; dutoit3 (21)		
Modified transport rate coefficients	Unit compatibility with plasma compartment	
Parasite-mediated inhibition of PFK and PK function	Simulation of healthy erythrocyte enzymatic inhibition by bloodborne parasite-derived substances	(185)
Infected erythrocyte; dutoit3 (21)		
Modified transport rate coefficients	Unit compatibility with plasma compartment	
Brain, Heart, Muscle, GIT, Adipose; Kim et al. 2007 (16)		
Parameter adjustment	Adjusted to accommodate clamped fluxes	
Clamping of metabolites	Compatibility with hepatic compartment	
Adaption of hormonal controllers	Compatibility with hepatic compartment and creating a unified global hormonal regulatory system	
Addition of insulin controller to muscle glucose import	Prevented excessive muscle glucose import at low plasma glucose concentrations; improved descriptions of plasma glucose	
Parasite-mediated stimulation of muscle ATPase activity	Phenomenological addition to simulate and account for increased muscle activity during generalised convulsions	
Addition of limiting saturation term to cardiac glycogen synthase activity	Prevented glycogen build-up to physiologically unrealistic levels during extended normo- or hyperglycaemia	
Parasite-mediated inhibition of cerebral perfusion	Phenomenological addition to simulate and account for parasite sequestration within cerebral microvasculature	

* Rows without references are novel additions or changes introduced in the current model

A description of the novel parasite-mediated host modulation terms is shown below in **Table 3.6**. Note that, because each modulation term could be enabled, disabled, and varied independently, the initial parameters for the respective modulation terms were first chosen based on their effect alone, with the final parameters being determined based on their effects on the plasma glucose and lactate vs. parasitaemia curves plotted against clinical data (viz. **Fig. 4.4**, **Appendix C**) with all modulation terms acting in concert.

Table 3.6: Novel host-parasite metabolic interaction terms with descriptions, listed in the order they were introduced

1.	Inhibition of uninfected erythrocyte metabolism	Section 3.2.2.1
	Hyperbolic inhibition of uninfected erythrocyte phosphofructokinase and pyruvate kinase as a function of increasing parasitaemia	
2.	Hepatic perfusion inhibition	Section 3.2.2.2.1
	Hyperbolic increase in the dissociation constant in the rate equations mediating transport of glucose, lactate and pyruvate between the hepatic and plasma compartments, as a function of increasing parasitaemia	
3.	Hepatic hypoxia	Section 3.2.2.2.2
	Decrease in the maximum velocities of the hepatic reactions catalysed by pyruvate carboxylase, pyruvate dehydrogenase, and the mitochondrial pyruvate transporter, as a function of increasing parasitaemia	
4.	Cerebral perfusion inhibition	Sections 3.1.5 (description of blood flow) & 3.2.2.3
	Inhibition of the rate of transport of all metabolites being exchanged between the plasma and brain compartments via a hyperbolic decrease in the common parameter Q, as a function of increasing parasitaemia	
5.	Muscle metabolic upregulation	Section 3.2.2.4
	Hyperbolic increase in a rate multiplier affecting skeletal muscle ATPase reaction velocity, as a function of increasing parasitaemia	

For a visual representation of the effects of varying the parameters mediating each modulation term, the reader is referred to **Appendix C**.

Although many of the effects are currently implemented in a phenomenological way, the model now represents a modular framework for future studies where the different effects can be reparametrized based on clinical data and the parameter values updated, or the modules can be improved if more mechanistic information becomes available.

Chapter 4: Results & Discussion

In Chapter 3 the structure of the model was described, discussing the individual compartments that together form the whole-body model, as well as the modifications and additions that were made to ensure compatibility between the different constituent models and how these compartments were repurposed to specifically address the research question posed in this thesis.

This chapter presents a demonstration of the types of analyses that can be performed on the complete *meyer1* model framework, accompanied by discussion of how these findings could contribute to the research aims and objectives. Due to the fact that the complete model contains a number of phenomenological processes with estimated parameters, no conclusive evidence can be gathered by such analyses at this stage. Although the model goes some way toward a more realistic description of the process involved in whole-body glucose metabolism and its response to malaria infection, model fitting and validation procedures are precluded by the lack of independent, empirical data.

In **Section 4.1**, the results pertinent to research objectives 1 through 3 (identification and merging of independently published models describing separate components of glucose and lactate metabolism, and subsequent validation of this combined whole-body model) are discussed. First, simulation outputs given by *meyer1* in the healthy state are compared with those published for the original constituent models. This was done to ensure that the whole-body *meyer1* model still gave reasonable metabolic descriptions for each individual compartment. This is followed by an examination of how well the *meyer1* model can describe steady-state plasma glucose and lactate concentrations over a range of parasitaemias, when compared with clinical data.

Section 4.2 examines the results obtained from the model pertaining to research objective 4, namely to test whether glycolytic parasite metabolism alone can cause hypoglycaemia and hyperlactataemia in the infected state. Model simulation results indicating the degree to which parasite metabolism contributes to the development of each of these symptoms is discussed in turn.

The results and discussion featured in **Section 4.3** examine the role that hepatic metabolism plays in influencing the appearance of hypoglycaemia and metabolic acidosis in the diseased state, to address research objective 5. Several components of hepatic metabolism as depicted in *meyer1* are discussed, including the dynamics of metabolite transport fluxes into and out of the hepatic compartment, the behaviour of substrate cycles, the overall energy and redox states of the hepatic compartment, and the changes seen

upon implementation and manipulation of the phenomenological host-parasite interactions introduced into the hepatic compartment.

Finally, **Section 4.4** demonstrates how the sixth and final research objective was addressed, by discussing the results of metabolic control analysis and how these can be interpreted to determine which components of parasite and host metabolism can be targeted by novel chemotherapeutics to ameliorate the disease, with particular emphasis on prevention and reversal of malaria-associated hypoglycaemia and hyperlactataemia.

The results accompanying discussion featured in this chapter was limited to those findings judged to be most significant with regards to the research question, aims and objectives. The remainder of the results and discussion can be found in **Appendices B & C**.

4.1 Model Results and Comparisons with Published Data

Before using the combined *meyer1* whole-body model as an investigative tool, we first obtained outputs for healthy and infected states, and compared these results with published data obtained both from the original, unchanged models, as is the case from green1 and K1, and clinical data obtained from literature measuring the plasma glucose and lactate concentrations in malaria patients over a range of parasitaemias. Comparison of the *meyer1*'s results with those of the models it was built upon helps to ascertain the extent to which it resembles the original models, and highlight any differences in outputs, and whether such discrepancies produced anomalous behaviour indicating that the models were merged erroneously or additional effects included incorrectly. Additionally, and perhaps more importantly, comparison of model outputs with clinical data gives an indication of the model's descriptive capacity with regards to the physiological reality of malaria infection. If the model were not able to satisfactorily describe the appearance of hypoglycaemia and hyperlactataemia as a function of increasing parasite burden, then further analysis and conclusions would have little veracity.

4.1.1 Model Reproduction

Comparison of outputs of the reproduced model with those published for the original was carried out repeatedly to confirm both that the independently published models (*dutoit3* (21), *green1* (162), König 2012 (18), Kim 2007 (16)) had been faithfully reproduced, and that the final model was able to give accurate, or at least reasonable descriptions of plasma concentrations of glucose and lactate in both the healthy and diseased state. Note that this section covers reproduction of the constituent models in isolation i.e. prior to incorporation into the merged whole-body model.

Accurate reproduction (construction of reproduced models that produced results closely resembling those published for the original) of the parasite, erythrocyte, and infected erythrocyte models was successful and achieved with minimal effort. This was likely due to the extensive validation that these models had already undergone by the original authors, and that the availability of these models in Mathematica format obviated the need for potentially erroneous re-encoding of the model by hand. Confirmation of the accurate

reproduction of the K1 model was also achieved with relative ease, with simulation outputs in isolation and as part of the combined *meyer1* model remaining approximately similar to those shown in the original publication. However, the process of validating accurate reproduction of the hepatic H1 model proved to be substantially more challenging, both in isolation and after incorporation into the final model.

It is our understanding that the H1 model, originally published in 2012, was still subject to ongoing improvement during the course of the current research. Attempts to reproduce all of the originally published results verbatim were unsuccessful. While smaller components of the model such as the hormonal integral rein controllers were able to be reproduced accurately (**Fig. 4.1**), the remainder of the results shown in the paper proved difficult to reproduce.

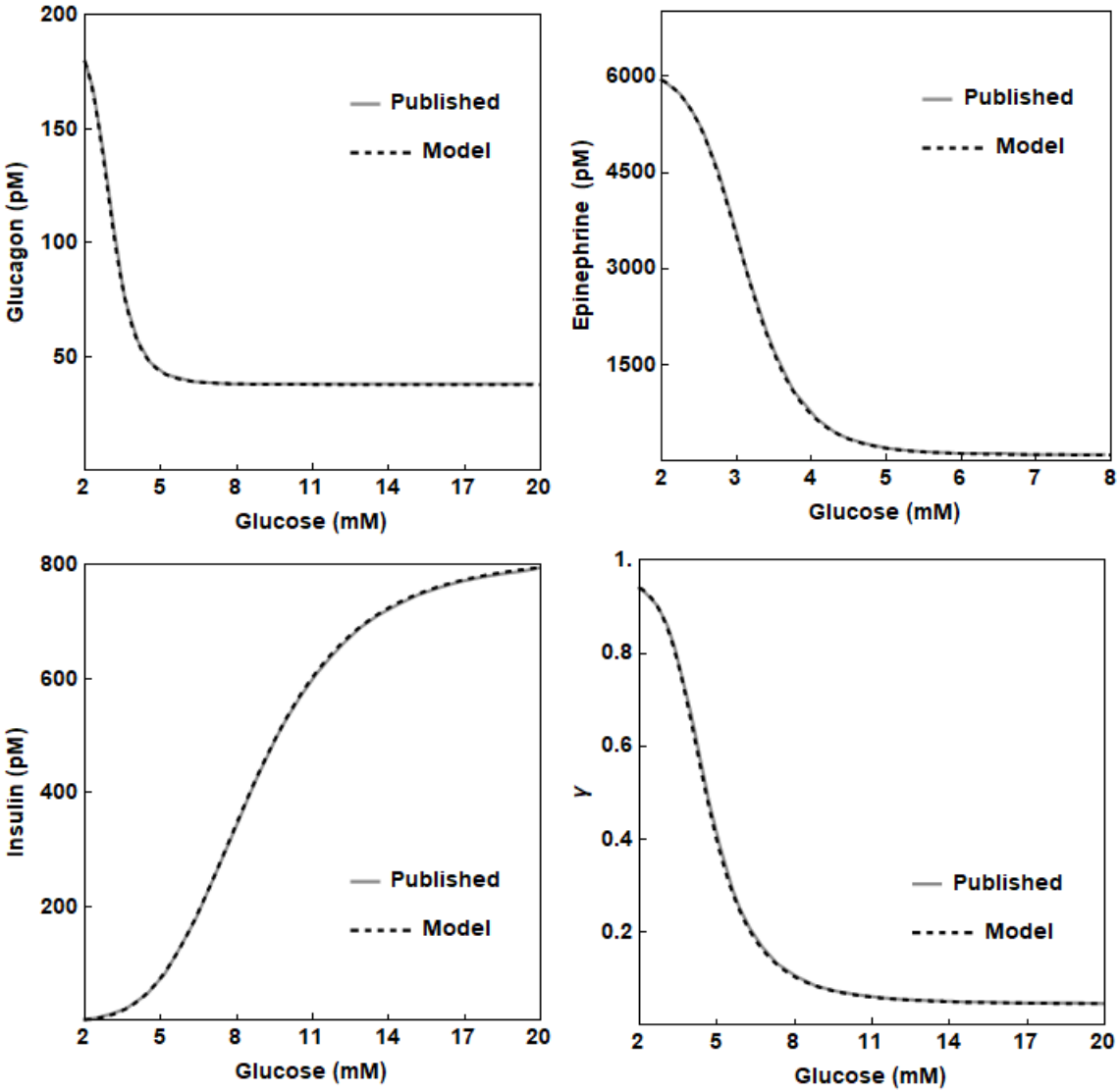

Figure 4.1: Validation plots comparing the reproduced H1's results (dashed lines) with those published by König et al. (Fig. 2 in the original publication, solid lines).

Validation efforts were primarily focused on reproducing the plots depicting the change in enzyme activity over time for several enzymes that represented key junctions of overall flux through hepatic glucose production or utilisation as a function of plasma glucose concentration (**Box 4.1**). Considerable effort was also made to reproduce the published time courses of hepatic glycogen concentration as a function of

differing plasma glucose concentrations (**Fig. 4.2**). While such extensive testing and examination did yield a greater understanding and familiarity with the model, validation was marred by ambiguous parameter specifications in the published appendices and incomplete descriptions present in the SBML version of the model.

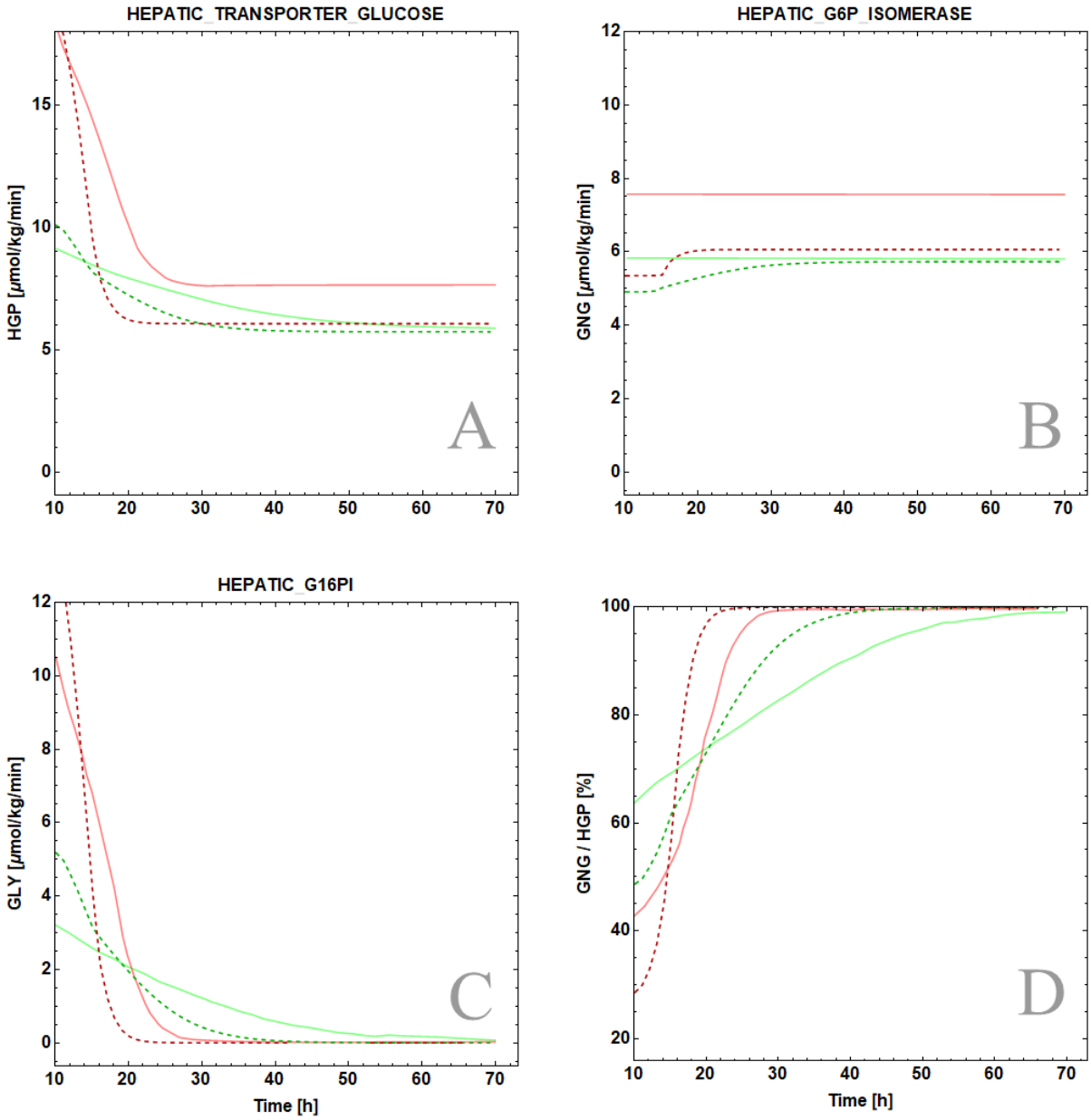

Figure 4.2: Validation plots comparing the modified, extended H1 results (dashed lines) with those published by König et al. (Fig. 3 in the original publication, solid lines). Red lines indicate results obtained with a clamped plasma glucose concentration of 3.6 mM, while green indicates 4.6 mM. Simulations were initiated with the same initial conditions (not shown). (**A**) hepatic glucose production (HGP), represented by flux through the hepatic glucose transporter (**B**) gluconeogenesis (GNG), represented by G6P isomerase flux (**C**) glycogenolysis (GLY), represented by glucose-1-phosphate 1,6-phosphomutase flux, (**D**) relative percentage contribution of gluconeogenesis to HGP

Ultimately, the pursuit of an exact reproduction was discontinued after the realisation that the model would have to undergo substantial changes and extensions in order to provide the function required within the scope of the current research in any case. The results of comparing the simulation results of the modified, extended hepatic compartment with those of the original paper are shown in **Figures 4.2 and 4.3**. All remaining components of H1 that were not modified, including the initial values, remained the same.

While the general shapes of the curves appear to be reasonably similar (**Fig. 4.2 A-C, Fig 4.3**), the values of the graphs differ, with the current model showing substantially smaller variation in outputs when simulated at different plasma glucose concentrations. It can be argued that the initial timecourse discrepancies are inconsequential, since this model is intended to provide results only at steady-state. Even so, some plots still differ even at steady-state (**Fig. 4.2 A & B**).

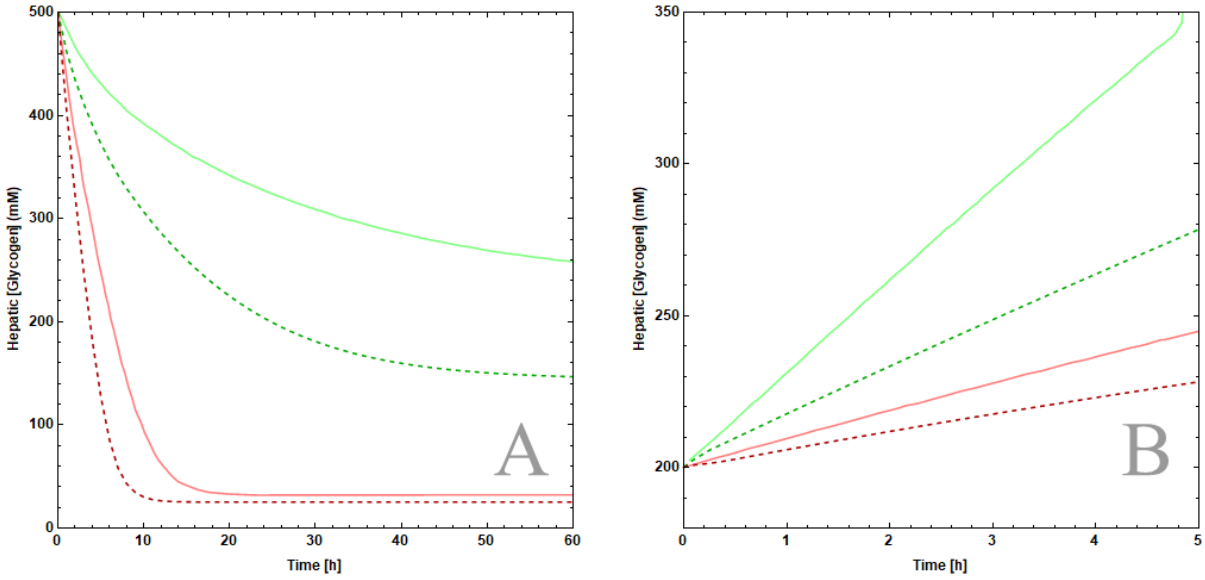

Figure 4.3: Validation plots comparing the modified, extended H1 results (dashed lines) with those published by König et al. (Fig. 4 in the original publication, solid lines). Clamped glucose concentrations are (**A, red**) 3.6 mM; (**A, green**) 5.0 mM; (**B, red**) 5.5 mM; (**B, green**) 8.0 mM

Full resolution of this issue was ultimately prevented by time constraints, and the finding that, despite these discrepancies, the modified hepatic compartment, functioning in tandem with the rest of the model, was able to provide reasonable descriptions of real-world clinical data.

Box 4.1: The Problem of Hepatic Pyruvate Kinase

The extremely low PK flux in both the infected and uninfected states was noticed during the analysis stage of H1 in isolation, and it was thought that this implausibly low level of activity in such an important component of the glycolytic pathway was due to an error during reproduction of the original model. However, upon further investigation it was discovered that the rate expression for pyruvate kinase had indeed been reproduced verbatim, and that it displayed low steady-state concentration of its substrate, phosphoenolpyruvate (PEP). This low PEP concentration is likely due to the absence of PEP provision by gluconeogenic flux through malate. As shown in the original model schema presented below, the authors had possibly intended to include kinetic descriptions of mitochondrial oxaloacetate flux through malate dehydrogenase to form malate, the latter subsequently being able to cross the mitochondrial membrane to form cytosolic oxaloacetate.

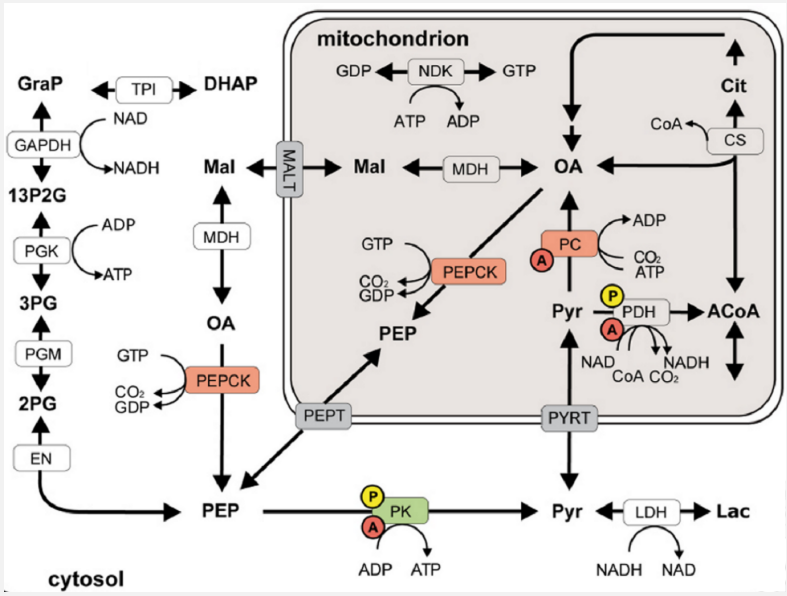

Cytosolic oxaloacetate, in turn, can subsequently be converted to cytosolic PEP, thereby providing an adequate substrate pool for PK activity. But, as with the decision to utilize clamped energy carriers and reducing equivalents, the authors possibly chose to omit such descriptions due to their inclusion being unnecessary in achieving the research objectives the original model was built to achieve. However, while simplified or disabled components such as energy and reducing equivalents or cytosolic PEPCK activity were still present in the model, complete with parameters and rate equations, no mention or description of malate dehydrogenase kinetics were present outside of the published model schema. Since it had already been decided during development of the current model that the *de novo* introduction of pathway components to an established model was ultimately not conducive to producing a reliable model, malate dehydrogenase activity was not included. In the final version of the model, this results in PEP turnover being dominated by its release from the mitochondrion and subsequent utilization by enolase, to the near-complete exclusion of PK activity.

This concludes the section devoted to reproduction of the original models in isolation. The subsequent section examines the results given by simulations of the combined model, *meyer1*.

4.1.2 Comparison of the Combined *meyer1* Model with Previous Models

The results shown here were obtained from simulations using the combined whole-body *meyer1* model, which includes the constituent compartments detailed in the previous section, as well as the modifications and additions summarised in **Table 3.5**. As these are the results of simulations in the healthy state, the modulation terms listed in **Table 3.6** were disabled as a consequence of the lack of parasitaemia.

Simulation outputs for the steady-state transport fluxes of glucose (**Table 4.1**) and lactate (**Table 4.2**) between somatic compartments and the plasma compartment obtained from *meyer1* were compared with those published by previous models, where applicable. These were conducted at 0% parasitaemia, i.e. in the uninfected state.

Differences between model results were noted for the rates of glucose transport mediated by the hepatic and skeletal muscle compartments. While the current model's result for hepatic glucose uptake displays approximate agreement with that shown by *green1*, it differs substantially from that obtained by the original K1 model. The skeletal muscle compartment also shows a much higher rate of glucose uptake than both the K1 and green1 models. No reversal of uptake or release was observed.

Table 4.1: Comparison of steady-state uptake and release rates of glucose between models in the healthy state

Compartment	**Kim 2007** (16)	**green1** (162)	**meyer1**
Brain	-0.380	-	-0.416
Heart	-0.040	-	0.000
Liver	0.731	0.0053	0.041
GIT	-0.076	-	-0.080
Muscle	-0.165	-0.053	-0.283
Adipose	-0.038	-0.053	-0.049
Others	-0.062	-0.077	-0.168

Negative values indicate uptake, positive values indicate release of glucose
All values in mmol/min

Smaller differences were observed when comparing the current model's results with those of K1 and *green1* with regards to lactate transport. The brain displayed a relatively small amount of lactate release in the healthy state, when compared with the reported value of zero in K1. This result is consistent with experimental observations showing a small net lactate release by the brain (188).

Conversely, the current model also displayed negligible lactate transport between the cardiac and plasma compartments, contrasting with a rate of 0.04 mmol/min reported for the K1 model. Negligible lactate transport by the cardiac compartment in the resting, healthy state contradicts experimental studies showing the heart to mediate approximately 5% of whole-body lactate uptake (**Section 2.6.2.4**)(113). This finding could be explained by the clamping of the glycerol, free fatty acid, and glycerol phosphate variables in the cardiac compartment (**Table 3.2**). Keeping these variables constant may have resulted in the need for lactate's use as a supplemental fuel being obviated at steady-state. Clamping of these same variables in the adipose compartment may also account for the reversal in lactate transport shown by the adipose compartment.

Other notable differences include an approximately 50% decrease in lactate release by the skeletal muscle compartment when comparing the values of K1 and the current model, as well as a reversal from lactate release to uptake for the adipose compartment.

Table 4.2: Comparison of steady-state uptake and release rates of lactate between models in the healthy state

Compartment	**Kim 2007** (16)	**green1** (162)	**meyer1**
Brain	0	-	0.030
Heart	-0.040	-	0.000
Liver	-0.270	-0.042	-0.238
GIT	0	-	-0.006
Muscle	0.112	0.0078	0.065
Adipose	0.056	-	-0.020
Others	0.142	-0.0011	0.129

Negative values indicate uptake, positive values indicate release of lactate
All values in mmol/min

The skeletal muscle compartment of *meyer1* exhibiting a higher rate of glucose uptake combined with a lower rate of lactate release may indicate that either more glucose is being stored as glycogen, or that a greater portion of glycolytic intermediates are entering pathways other than anaerobic glycolysis, such as oxidative phosphorylation. In either case, these results indicate that the skeletal muscle compartment in *meyer1* occupies a metabolic state more representative of the resting, anabolic state.

4.1.3 Comparison with Clinical Data

Clinical data specifying both percentage parasitaemia and plasma glucose or lactate concentrations was obtained from literature for both children (14, 123, 189–196) and adults (53, 63, 64). These measurements of plasma concentrations of glucose and lactate were subsequently used as a guide for model calibration. (**Fig. 4.4**). Additionally, simulation outputs were compared with those obtained by the *green1* model (162), the latter being used as a reference point. As one of the penultimate goals of the current research was to

construct a model that could give accurate descriptions of clinical data, the green curves represent data obtained from the final *meyer1* model with all changes and additions (as listed in **Tables 3.5 & 3.6**) active.

The results shown in **Fig. 4.4** are an extension of those published by Green (162), and reflect the research aims and objectives set out at the beginning of this thesis: to construct a model that can be used to explore malaria metabolic abnormalities while still producing results that fall within the bounds of real-world examples. Visual inspection of **Fig. 4.4** shows that the more sophisticated and in-depth descriptions of glucose metabolism in organs external to erythrocytes yielded significantly improved descriptions over a range of parasitaemias.

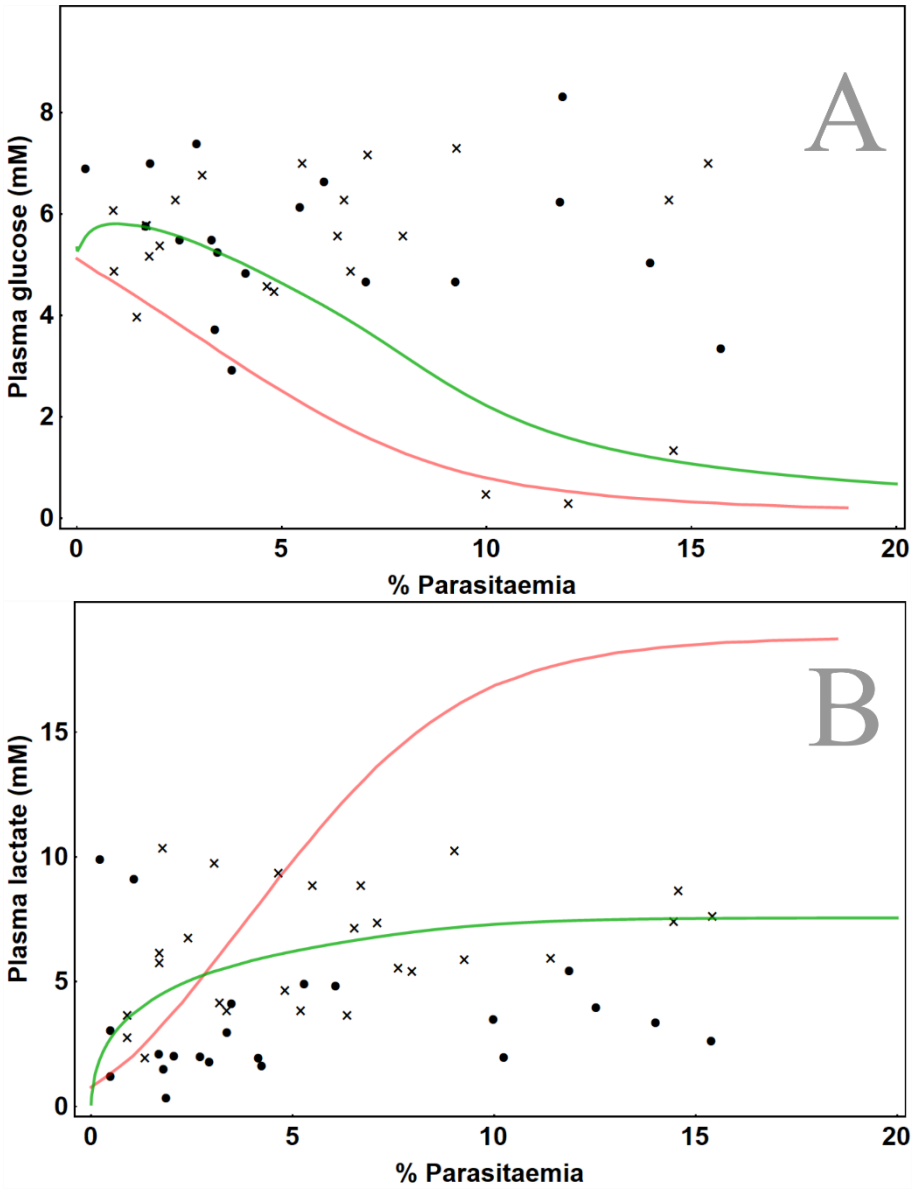

Figure 4.4: Percentage parasitaemia vs simulated steady-state concentrations of plasma glucose (**A**) and plasma lactate (**B**). Red line: simulations obtained from green1 model. Green line: simulations obtained from the current *meyer1* model. Dot symbols: data points obtained from adults (53, 63, 64).. Cross symbols: data points obtained from children (14, 123, 189–196).

The descriptions given by the current model showed good agreement overall with the clinical data, with the exception of plasma glucose concentration at parasitaemias exceeding 5%. The similarity between simulated and measured plasma glucose and lactate concentrations varied according to both the range of percentage parasitaemia, and whether the data was obtained from children or adults. An initial rise in plasma glucose can be seen between 0-1% parasitaemia. Plasma glucose results approximate the data well between 0-5% parasitaemia, but proceed to exhibit a bias towards hypoglycaemia at higher parasitaemias. This bias was tolerated with the rationale that the model was constructed with the purpose of simulating hypoglycaemia in severe malaria, a symptom that, while occurring in a subset of the population, is still indicative of poor clinical outcomes. Furthermore, it could not be ruled out that the apparent bias was due to the lack of data available (N = 37) as well as the specificity of the data itself (e.g. publication of population means versus individual patient measurements).

Results for plasma lactate appear to coincide significantly more closely for data obtained from children, although the initial curve does not describe that hyperlactataemia will occur until approximately 3% parasitaemia, in contrast to the clinical data, which shows multiple data points indicating metabolic acidosis (greater than 5 mM blood lactate (45)) in the 0-3% parasitaemia range. Nevertheless, the curve displays a good general approximation of plasma lactate levels for children with malaria up to the 15% parasitaemia mark.

4.2 The Contribution of Parasite Metabolism to Hypoglycaemia and Hyperlactataemia

To determine the degree to which parasite metabolism is responsible for the appearance of hypoglycaemia in cases of malaria infection, the rate of glucose uptake by infected erythrocytes was examined within the context of whole-body glucose metabolism. This was done by examining the relative contribution of each compartment to the steady-state plasma glucose concentration by calculating the percentage of the absolute flux of each compartment at a given parasitaemia.

$$\%\,\phi_{ss}^{Compartment} = 100 \times \frac{\left|\phi_{ss}^{Compartment}\right|}{\left|\phi_{ss}^{PLASMA\_GLUCOSE\_FEED}\right| + \cdots + \left|\phi_{ss}^{RBCi\_TRNSP\_PLASMA\_GLC}\right|}$$

Since all fluxes affecting a given variable sum to zero at steady state, the total of the absolute value of the fluxes at steady state was used as a denominator instead. Although this precludes the ability to distinguish between positive and negative fluxes during further calculations, it nevertheless gives an indication of the relative ‘share’ that individual fluxes have over a variable at steady state.

The results of these simulations are shown in **Figure 4.5**. Since the PLASMA_GLUCOSE_FEED function was considered as representing glucose absorption from the phenomenological gastrointestinal compartment, it was plotted separately.

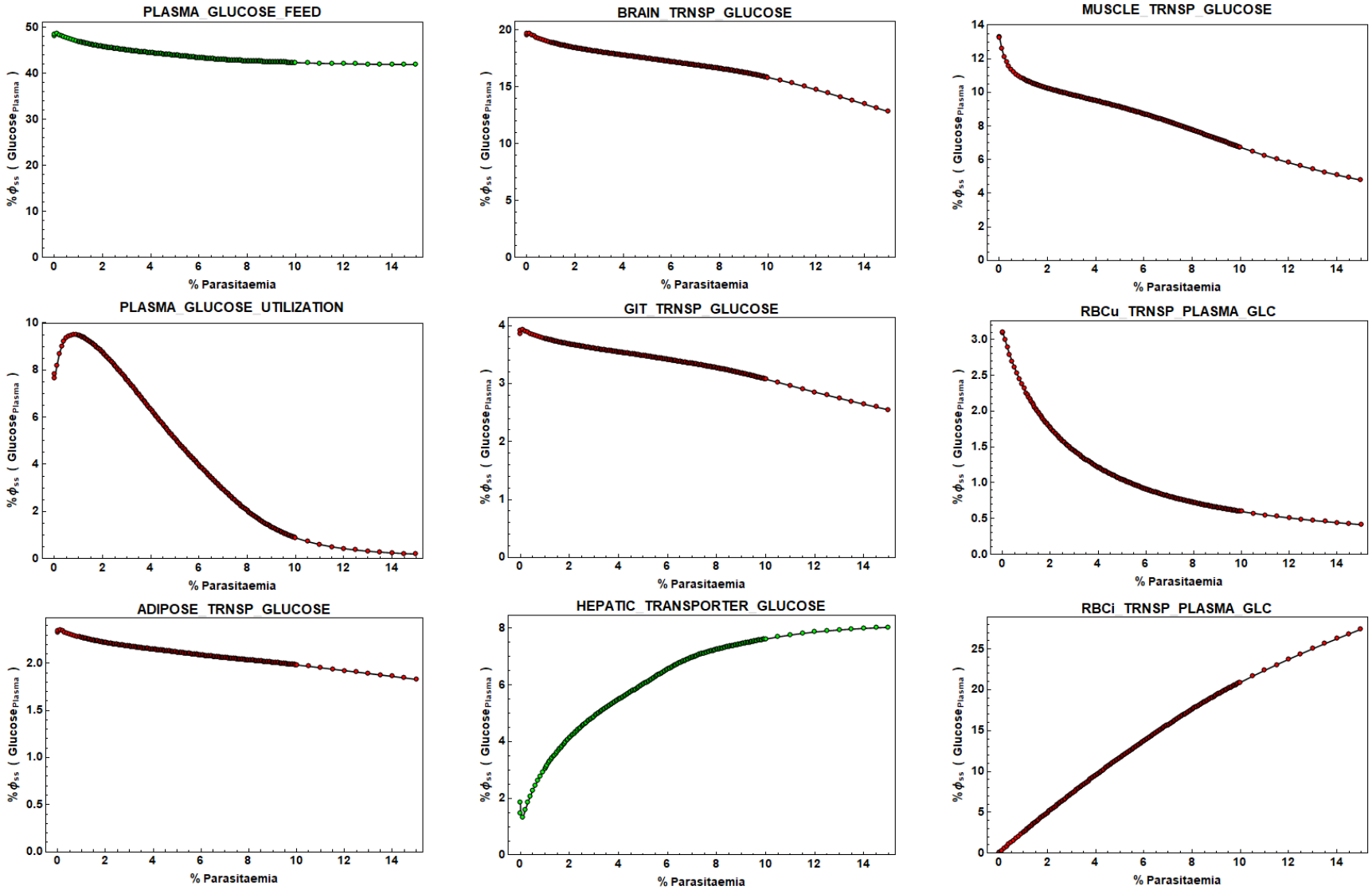

Figure 4.5: Relative contributions of fluxes to plasma glucose flux at steady state in the meyer1 model. Percentages are calculated from a rate's absolute flux over the sum of absolute fluxes at a given percentage parasitaemia. Simulation points for positive (glucose release) and negative (glucose uptake) are shown in green and red, respectively. Cardiac compartment omitted due to negligible contribution.

The glucose feed function appears to account for both the majority of glucose influx into the compartment, and the majority of glucose flux overall, with its values remaining in the range of 40-50%. Glucose export by the liver into the plasma compartment rises in a hyperbolic trend from approximately 2% at zero parasitaemia to around 8% at 14% parasitaemia. Glucose removal from plasma by the remaining compartments consistently decreases with increasing parasitaemia, except for the infected erythrocyte compartment, which shows an almost linear increase from zero percent to over 25% at 14% parasitaemia. Note that, above parasite burdens of approximately 1%, no other negative flux increases in magnitude, while that of infected erythrocytes shows a perpetual climb.

These results support the notion that the appearance of hypoglycaemia is due to plasma glucose uptake by infected erythrocytes overwhelming the host's ability to maintain blood glucose homeostasis. Considering both **Figs. 4.4 & 4.5**, it appears that this relationship holds only at higher percentage parasitaemias in excess of 10%, where the curve for plasma glucose crosses the threshold value of 2.2 mM that marks entry into hypoglycaemia. This threshold also coincides with the percentage parasitaemia where infected erythrocytes account for 20% or more of plasma glucose flux. Below this parasitaemia threshold, the model shows that the body would still be able to compensate for the increased glucose demand through gluconeogenic means. One of the chief gluconeogenic substrates is lactate, a metabolite often found to be at exceedingly high plasma concentrations in cases of malaria infection.

As for **lactate** fluxes: simulation results from this model show that lactate efflux by the infected erythrocyte compartment and, by proxy, the parasite compartment, is insufficient to overcome the host's capacity for lactate clearance. Hepatic lactate uptake is able to exceed infected erythrocyte (RBCi) lactate export until approximately 5% parasitaemia; this has been established under conditions where the liver function is inhibited by the presence of infection (**Fig 4.6**). Furthermore, if the second major organ displaying significant lactate uptake were to be included, which in the case of this model is the brain, then the additive hepatic and cerebral rate of lactate clearance substantially exceeds the rate of RBCi lactate efflux.

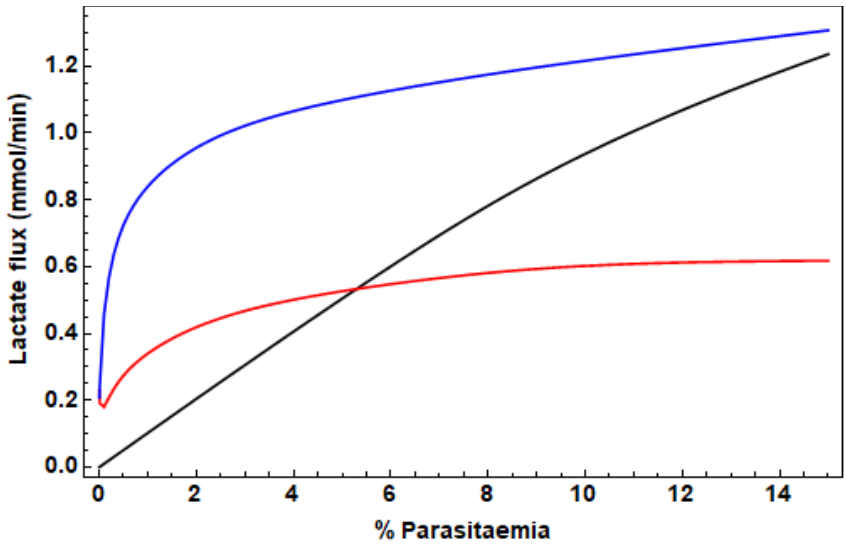

Figure 4.6: Steady-state fluxes at varying parasitaemias for infected erythrocyte lactate release (black), hepatic lactate uptake (red), and the sum of brain and liver lactate uptake (blue) in the *meyer1* model.

4.3 The Role of Hepatic Function in Severe Malaria

As the only compartment within the model equipped with gluconeogenic kinetics, the liver is the only organ capable of directly reversing the concomitant syndromes of hypoglycaemia and lactic acidosis present during severe *P. falciparum* infection. As described in **Section 3.1.3**, the original model published by König et al. (18) did not feature kinetic descriptions of non-carbohydrate metabolism, and it was decided during adaption and incorporation of this model into the current whole-body framework that expansion to include the gluconeogenic contributions of alanine and glycerol would be beyond the scope of the current research. Significant changes were however made to other components of the hepatic compartment, a process that was expedited by an existing, but disabled, framework already being in place. These modifications centred on the implementation of a dynamic system of reducing equivalents that could be exchanged between the cytosol and mitochondria, the addition of a pyruvate transporter, and the incorporation of parasite inhibition terms.

To ascertain the role that liver function plays in the pathogenesis of metabolic syndromes associated with severe *P. falciparum* infection, several facets of the hepatic compartment will be examined. These are (i) the net transport fluxes of glucose, pyruvate and lactate, (ii) the relative fluxes through the glycolytic/gluconeogenic substrate cycles, and (iii) the overall energy and redox state of the hepatic compartment. Together, these three sections encompass the examination of how innate hepatic function changes during the transition from a healthy state through nascent and severe malaria infection, and whether these changes indicate that impaired hepatic gluconeogenic function can be considered a primary cause of HG/HL in severe malaria.

An additional fourth and final section examines in greater detail the effects of phenomenological parasite-liver interactions modelled after literature reports on hepatic function, and the subsequent influence that such interactions have on the pathogenesis of HG/HL in severe malaria infection.

Note that the results presented within this section were obtained from the final *meyer1* model with all modifications and parasite-host modulation terms (listed in **Tables 3.5 & 3.6**) active.

4.3.1 Hepatic Transport Fluxes

The liver appears to export glucose and import pyruvate and lactate at all levels of parasitaemia; for glucose and lactate, a hyperbolic relationship is seen, and for pyruvate, a linear trend appears that slightly decreases at parasitaemia levels above 6% (**Fig 4.7**). The hepatic compartment at steady state generally imports lactate twice as fast as it does pyruvate, although this apparent preference is likely due to pyruvate's comparatively low plasma concentration. An increase in net hepatic gluconeogenic activity can be seen (**Fig. 4.7**, bottom-right), as the ratio of lactate/pyruvate import to glucose export decreases asymptotically with increasing parasitaemia.

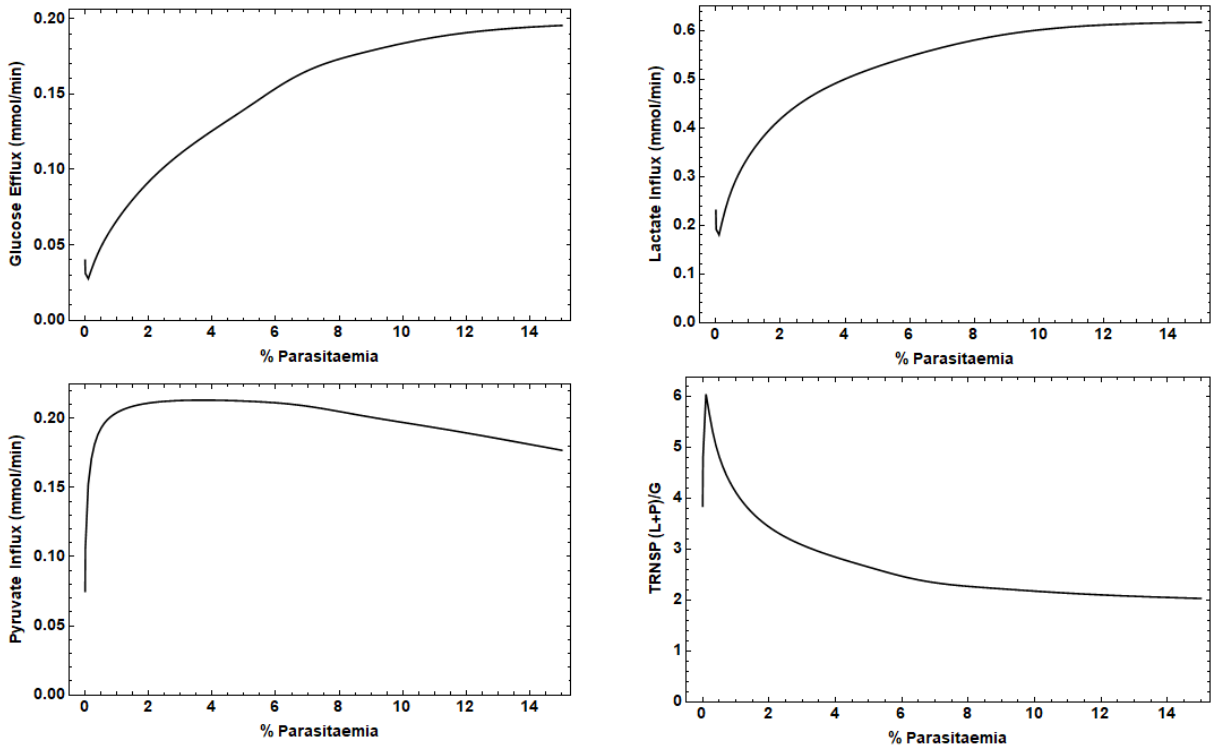

Figure 4.7: Metabolite transport fluxes for the hepatic compartment and the hepatic gluconeogenic ratio in the *meyer1* model. TRNSP (L+P)/G is calculated as [½(Lactate Influx + Pyruvate Influx)/Glucose Efflux]

Here we have demonstrated that, across the entire range of parasitaemias used as input, model simulations show a net import of lactate and pyruvate with a concomitant net release of glucose into the circulation. These results unambiguously indicate that, from a purely input/output perspective, the liver functions as a wholly gluconeogenic organ within the context of the malaria disease state as simulated in this model.

4.3.2 Hepatic Glycolytic/Gluconeogenic Substrate Cycling

Recall that the pathways of hepatic glycolysis and gluconeogenesis are identical, save for three irreversible steps. First, the phosphorylation of glucose to form G6P is catalysed by glucokinase (GK) and reversed by glucose 6-phosphatase. Second, the conversion of fructose 6-phosphate to fructose 1,6-bisphosphate, catalysed in the forward direction by 6-phosphofructo-1-kinase (PFK1) and in the reverse by fructose 1,6-bisphosphatase (F16BP). Finally, pyruvate kinase (PK) catalyses the conversion of phosphoenolpyruvate (PEP) to pyruvate, a reaction reversed by the sequential action of pyruvate carboxylase (PC) and phosphoenolpyruvate carboxykinase (PEPCK). For each substrate cycle, the ratio of the two fluxes will determine the flow of metabolites at that juncture, and the overall ratio of these flux pairs will ultimately determine whether the hepatic compartment is in a glycolytic or gluconeogenic state.

With this in mind, the fluxes of these reactions within the hepatic compartment were determined at steady state over a range of parasitaemias, as well as the flux ratios of these opposing processes to ascertain the degree to which gluconeogenesis is favoured at each respective junction (**Fig. 4.8**).

In accordance with the observations regarding the liver's net glucose export across a range of parasitaemias, the substrate cycles demonstrate ratios decidedly in favour of gluconeogenic glucose synthesis (**Fig 4.8**).

Both the ratios of G6Pase / GK and F16BP / PFK1 increase rapidly above 7% parasitaemia, from an initial ratio of 1.11 and 1.25 to a final value of 5.95 and 36.28, respectively. Pyruvate kinase activity, however, shows only a single symmetrical peak centred on 2% parasitaemia, the value of which is effectively negligible.

Hepatic PC and mitochondrial PEPCK, the gluconeogenic counterparts to PK, parallel one another with hyperbolic trends, increasing from 0.0827 mmol/min and 0.0794 mmol/min to 0.5297 mmol/min and 0.3910 mmol/min, respectively.

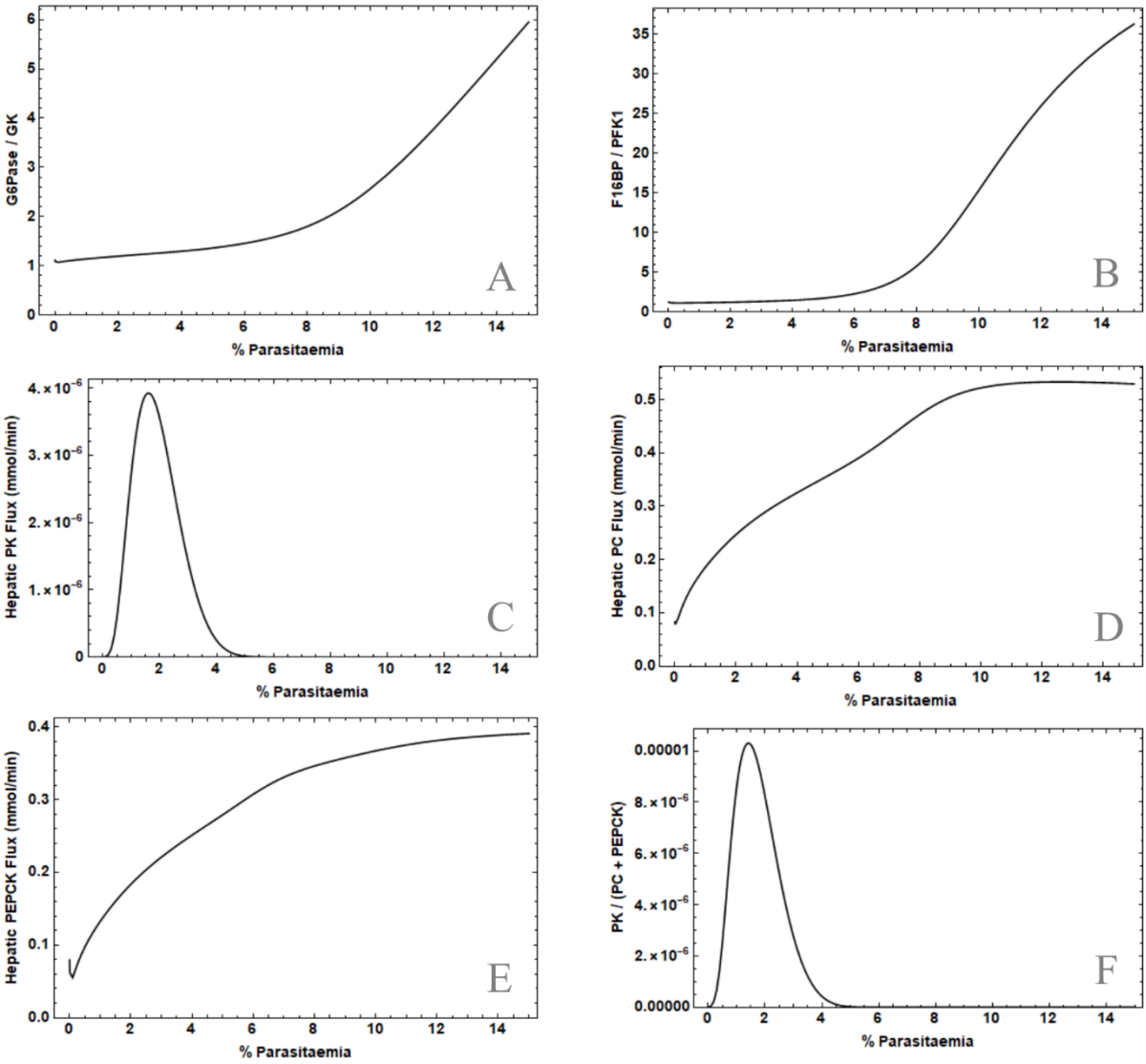

Figure 4.8: Steady-state reaction ratios of hepatic substrate cycle reactions (**A, B, F**) in the *meyer1* model. The steady-state flux values for PK (**C**), PC (**D**) and mitochondrial PEPCK (**E**) are shown for clarity. Abbreviations: G6Pase, glucose 6-phosphatase; GK, glucokinase; F16BP, fructose 1,6-bisphosphatase; PFK1, 6-phosphofructo-1-kinase; PK, pyruvate kinase; PC, pyruvate carboxylase; PEPCK, mitochondrial phosphoenolpyruvate carboxylase

Of note is the observation that, for percentage parasitaemias leading up to approximately 5%, flux ratios of G6Pase/GK and F16BP/PFK1 remain approximately unitary, but increase rapidly thereafter, reaching respective ratios of 6 and 35 at 15% parasitaemia (**Fig. 4.8**). These steep increases parallel plasma lactate concentration's above approximately 5 mM, the threshold generally considered as constituting

hyperlactataemia. Conversely, while flux through the reactions catalysed by PC and PEPCK also increase in proportion to parasitaemia and appear to share the same approximate inflection point, the ratio of their combined flux vs PK activity is difficult to ascertain. Nevertheless, when also considering the transport flux behaviour described in **Section 4.3.1**, these results clearly indicate that the enzymatic machinery of hepatic gluconeogenesis remains functional, and the failure thereof can thus be ruled out as a primary cause of circulatory hyperglycaemia and hyperlactataemia within the scope of this model.

4.3.3 Hepatic Energy and Redox States

As explained in **Section 3.1.3.1**, the clamped set of phosphoryl donors and reducing equivalents was converted to a dynamic system whereby they are consumed and recycled through the cytosolic and mitochondrial compartments. Had the change not been made, the hepatic compartment would effectively possess an infinite supply of energy, and the system as a whole would be completely unresponsive to reductions in substrate supply. However, with the new dynamic implementation in place, the energy and redox state of the hepatic compartment is open to examination.

Within the context of this model's hepatic compartment, the reducing equivalent pair NAD^+/NADH forms part of four enzyme-catalysed reactions, viz. those catalysed by GAPDH and LDH within the cytosolic compartment; PDH within the mitochondrion, and the phenomenological NAD^+/NADH exchanger mediating antiport transport of these species between cytosol and mitochondria.

Since gluconeogenesis depends both directly and indirectly on the activity of these reactions, the presence of appropriate concentrations of reducing equivalents is thus essential for gluconeogenesis to proceed. It was thus investigated whether the presence of malaria infection had any deleterious effects on the rates of these reactions and thereby the magnitude of the flux through gluconeogenesis. Additional consideration is also given to the dynamics of energy carriers, considering their direct (kinase activity) or indirect (oxidative phosphorylation, glycogen turnover) effect on hepatic glucose metabolism.

Within the cytosolic compartment, oxidized NAD^+ constitutes the near entirety of the redox pair across all parasitaemias, including the uninfected state (**Fig. 4.9**). These values parallel those found in both König *et al.*'s (18) and Li *et al.*'s (17) original published models (**Table 4.3**). NAD^+ is abundant in the cytoplasmic compartment regardless of parasitaemia, maintaining the redox degree at near zero. In the mitochondrial compartment, the fraction of NADH increases with growing parasitaemia, reaching a maximum of 0.4 at 4%, which steadily declines to 0.25 at 10%, at which it remains for further increases in parasitaemia.

Table 4.3: Comparison of reducing equivalent concentrations between models in the healthy state

	[$NADH_{cyto}$]	**[NAD^+_{cyto}]**	**[$NADH_{mito}$]**	**[NAD^+_{mito}]**
König 2012 (18)	0.00056	1.22	0.24	0.98
Li 2009 (17)	0.0002778	0.15	0.4975	3.15
meyer1	0.0000370	0.15	0.246	3.40

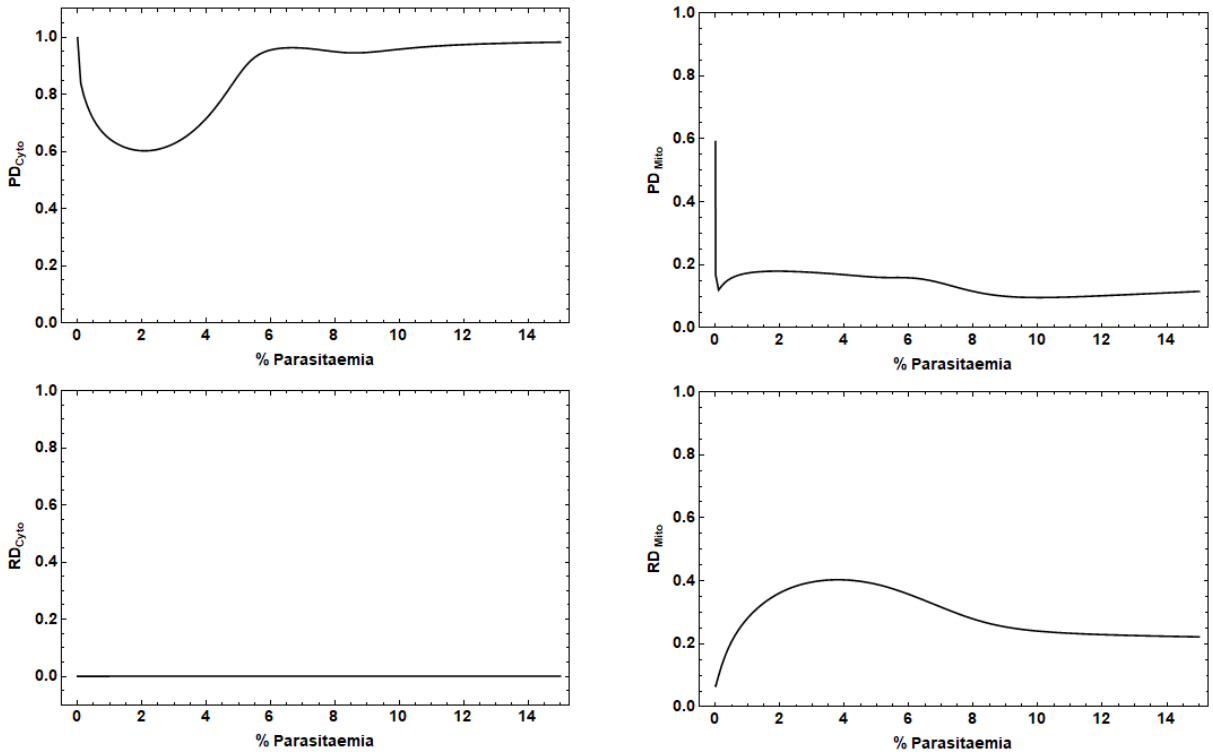

Figure 4.9: Phosphorylation and redox states for the hepatic cytosolic and mitochondrial compartments as simulated in the *meyer1* model. $PD_x = ATP_x / (ATP_x + ADP_x)$; $RD_x = NADH_x / (NADH_x + NAD_x)$

Analysis of percentage flux partitioning shows a trend whereby NADH production in the cytosolic compartment is dominated by LDH activity (**Fig. 4.10**). LDH activity mediates the entirety of positive flux for hepatic cytosolic NADH, and half overall. GAPDH and NADH/NAD^+ exchanger activity both mediate negative cytoplasmic NADH flux, with GAPDH activity overtaking NADH/NAD^+ exchanger flux as parasitaemia rises and hepatic gluconeogenesis increases. The NADH produced by LDH is either consumed by GAPDH, or exchanged for NAD^+ with the mitochondrial compartment. In the mitochondrial compartment, the NADH produced by PDH and imported by the NADH/NAD^+ exchanger is consumed by oxidative phosphorylation activity (**Fig. 4.11**).

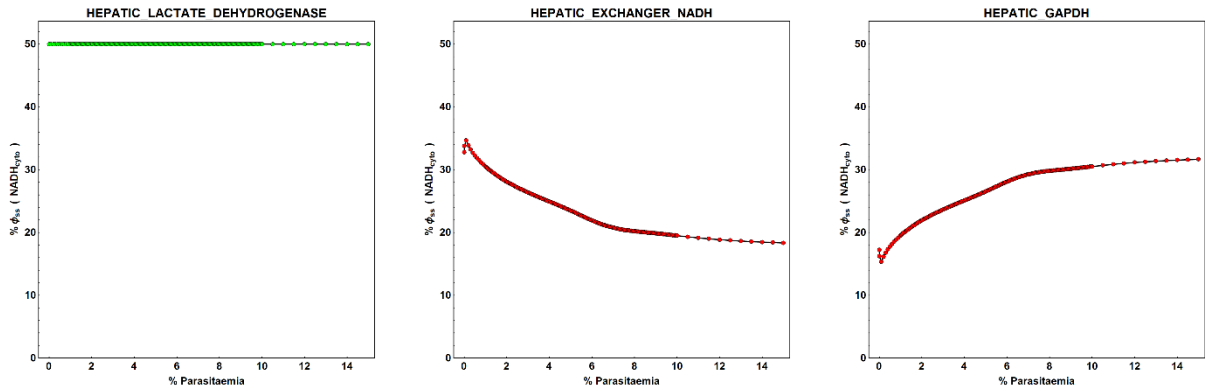

Figure 4.10: Percentage flux contributions to steady-state hepatic cytosolic NADH in the *meyer1* model. Values were calculated according to the individual absolute flux over the absolute flux total. Relative percentage flux contributions were calculated in the same method as described for Figure 4.5. Green and red data points correspond to percentages calculated from positive and negative fluxes, respectively

PDH and NADH/NAD$^+$ activity is responsible for positive NADH flux in the mitochondrial compartment, having approximately equal fractions overall (**Fig 4.11**). Oxidative phosphorylation activity, which consumes NADH, constitutes half of all flux overall.

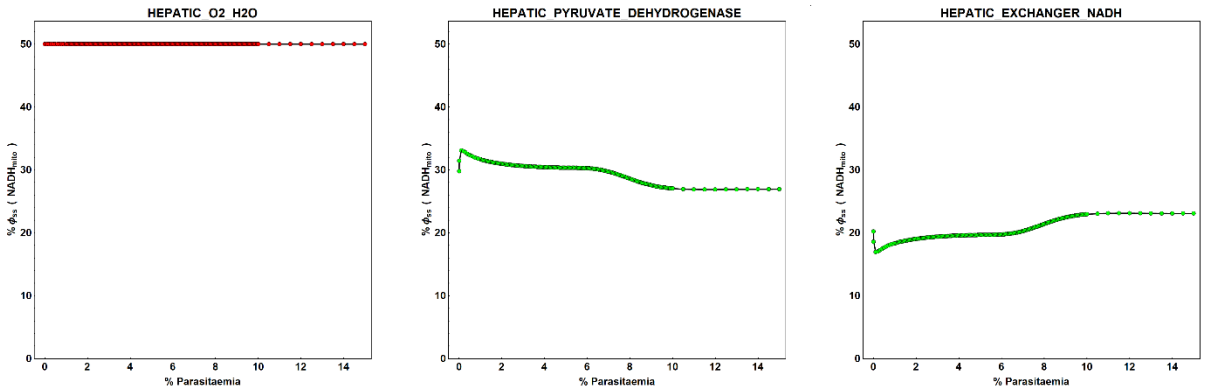

Figure 4.11: Percentage flux contributions to steady-state hepatic mitochondrial NADH in the *meyer1* model. Green and red data points correspond to percentages calculated from positive and negative fluxes, respectively

The mitochondrial NAD$^+$ produced by oxidative phosphorylation is subsequently transported back into the cytosolic compartment, where it provides substrate for lactate oxidation via LDH. Thus, a cycle is established whereby gluconeogenic activity is sustained through constant maintenance of cytosolic NAD$^+$ concentration, which enables continued lactate oxidation and subsequent gluconeogenesis.

The relative fractions of hepatic ATP and ADP show different trends depending on the sub-compartment under consideration (**Fig. 4.9**). ATP makes up almost the entirety of the adenosine phosphate pool within the cytosolic compartment (**Table 4.4**). In the mitochondrial compartment, approximately only 20% of the adenosine phosphate pool consists of ATP in the infected state; this is down from approximately 60% in the uninfected state. In the mitochondrial compartment, ATP synthesized by oxidative phosphorylation is used either by PC, or by NDK-GTP, which provides the GTP required by mitochondrial PEPCK; both of these enzymes constitute essential parts of the mitochondrial gluconeogenic pathway.

Table 4.4: Comparison of adenosine phosphate concentrations between models in the healthy state

	[ATP$_{cyto}$]	**[ADP$_{cyto}$]**	**[ATP$_{mito}$]**	**[ADP$_{mito}$]**
König 2012 (18)	2.8	0.8	2.8	0.8
Li 2009 (17)	5.924	0.0178	8.68	7.84
meyer1	5.983	0.0035	14.02	2.50

The consideration of these observations as a whole give a clear indication that hepatic gluconeogenic function is not obstructed by deficient levels of energy carriers or reducing equivalents. Flux partitioning of these metabolites in the infected state reflects a state of active, continued gluconeogenesis. Thus, these results support the notion of the hepatic compartment being entirely geared towards sustained gluconeogenesis, especially as percentage parasitaemia increases, if additional parasite-liver interaction is not considered.

4.3.4 Parasite-Liver Interaction

One of the chief research objectives of this thesis was to delineate the causes of hypoglycaemia and lactic acidosis in the event that parasite metabolism *per se* was found to not be able to account for these phenomena. Simulations of the *meyer1* model that included effect of parasite metabolism but not parasite-mediated modulation of host metabolism (see **Section 4.2**) supports this notion. Although the metabolic effects mediated by the parasites could cause hypoglycaemia, results suggest that they are insufficient to explain hyperlactatemia. Further investigation was orientated towards examining if and how the possible diminished capacity of hepatic gluconeogenesis through other effects was the causative factor. As shown above, hepatic fluxes and species concentrations are fully in favour of gluconeogenesis (**Fig. 4.8**); thus, the innate capacity of the liver to convert imported lactate (and to a lesser extent, pyruvate) into glucose and export it to the circulation is not saturated. This leaves the aetiology of hypoglycaemia and lactic acidosis to factors external to native hepatic metabolism, specifically those belonging to parasite-mediated modulation of hepatic function, such as impairment of hepatic blood flow and metabolite delivery to the liver parenchyma.

When modelling the putative mechanisms of parasite-liver interactions, two phenomenological functions were implemented: inhibition of oxygen-requiring processes, such as oxidative phosphorylation, and inhibition of perfusion i.e. blood flow through the hepatic circulation (**Section 3.2.2.2**). Perfusion inhibition was included in the model to allow an *in silico* assessment of the possible effect of microvascular occlusion rendered by parasite sequestration, as described in the literature (12, 64, 127). Reduced perfusion was modelled by decreasing the affinity of hepatic transporters for plasma glucose, lactate and pyruvate as a function of increasing parasitaemia. For each of the two parasite-mediated inhibition terms introduced into the hepatic compartment, two parameters specifying the percentage parasitaemia producing half-maximal effect (KM), and the maximum magnitude of effect (MAX) were used.

Of the novel parasite-host interactions introduced as part of the current research, the inhibition of hepatic perfusion by increasing parasite burden appeared to have the most dramatic effect on plasma lactate concentrations (a full description of the effects of parasite-host interactions is given in **Appendix C**). To ascertain the effects of varying degrees of maximum parasite-mediated perfusion inhibition (**Section 3.2.2.2.1**), the value of the *MAX* parameter was varied between 0 (no inhibition) to 50 (its default value) (**Fig 4.12**). The absence of perfusion inhibition prevented the appearance of lactic acidosis entirely, while delaying the onset of hypoglycaemia. In other words, if parasite-mediated inhibition of hepatic lactate uptake was lifted, then plasma lactate concentrations do not rise above the 5 mM threshold considered as constituting lactic acidosis, even at the maximum percentage parasitaemia simulated (due to the capacity of hepatic gluconeogenesis). These results indicate that glycolytic parasite metabolism alone cannot cause hyperlactataemia in cases of severe *P. falciparum* infection, a conclusion that parallels that expressed by previous literature. While still providing evidence for parasite metabolism as a contributory factor, a clear indication is given that the primary aetiology of metabolic acidosis could lie within parasite-mediated disturbances of host metabolism and homeostasis.

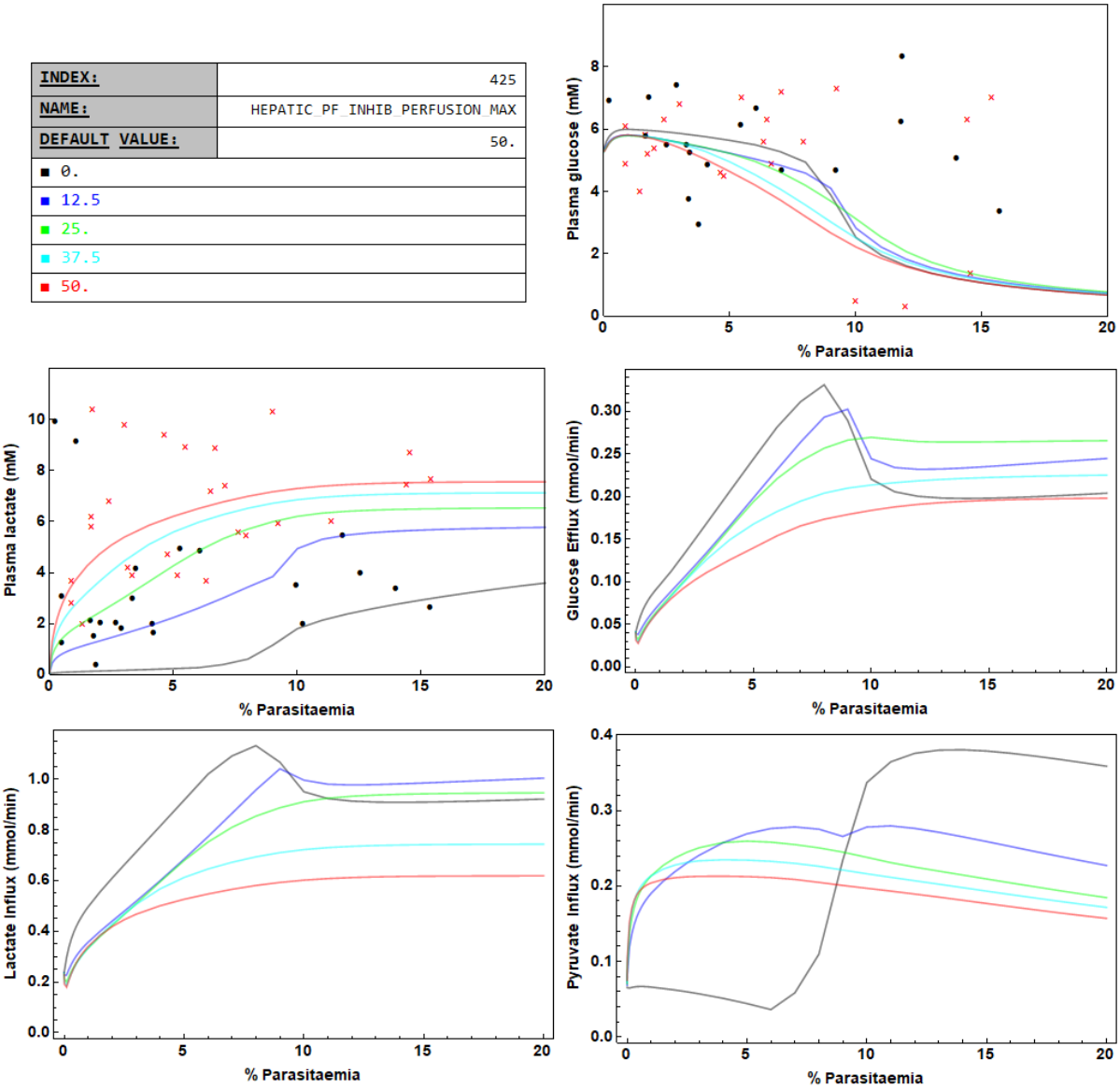

Figure 4.12: Changes in selected *meyer1* model outputs with variation of the maximal perfusion inhibition parasite modulation parameter. Glucose, lactate and pyruvate fluxes refer to influx or efflux into or out of the **hepatic** compartment. Details presented in information box, top-left. The colour of each curve corresponds to simulations conducted with the matching parameter value. Data as presented in Fig 4.4.

In contrast to the dramatic changes seen in steady-state plasma lactate concentrations observed upon variance of the maximal perfusion inhibition parasite modulation parameter, implementation of parasite-mediated hepatic mitochondrial hypoxia yielded minimal improvement in the descriptive capacity of the model. The results of the introduction of this host-parasite interaction, as well as the remainder of those described in **Section 3.2.2**, can be found in **Appendix C**.

4.4 MCA and Potential Drug Targets

One of the advantages of metabolic control analysis is that it allows a large-scale biochemical network to be searched for components that have the strongest influence over a particular outcome, whether this be the concentration of a metabolite, or a particular steady-state flux. One of objectives of the current research was to identify which components of the whole-body model have the most significant role in mediating the appearance of hypoglycaemia and hyperlactataemia as part of malaria infection, and would therefore be expected to yield the greatest improvement in clinical outcome if targeted by specific treatments. To achieve this, metabolic control analysis was conducted on all reactions to identify the rates exhibiting the greatest control over steady-state plasma glucose and lactate concentration.

Since the current model allows us to obtain steady-state data for any given parasitaemia, MCA was conducted over a range of parasitaemias that included both uncomplicated and severe infection. For a range of parasitaemia values, control coefficients with regards to plasma glucose and lactate were calculated for all rates. Thereafter, the integral of each rate's control coefficients versus percentage parasitaemia was determined, to give an indication of which rates had the greatest overall control across the range of parasitaemias simulated. These integrals were subsequently ranked in descending order, the results of which are shown below in **Figs. 4.13 & 4.14**.

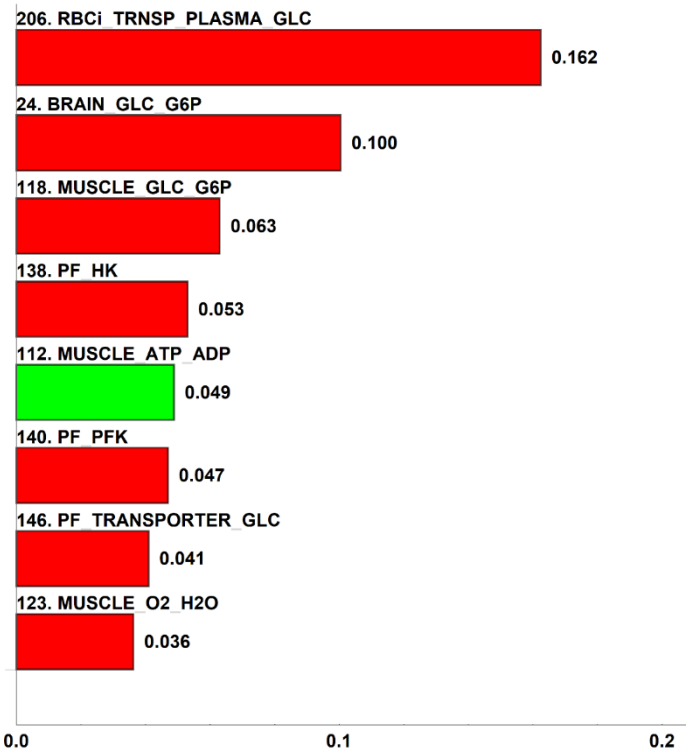

Figure 4.13: Eight rates showing significant control coefficients with regards to plasma glucose, integrated over a range of parasitaemias from ~0% to 15%. Green bars indicate positive values, red bars indicate negative values. Rates for brain and muscle compartments are denoted as COMPARTMENT_SUBSTRATE_PRODUCT.

The significant control coefficients with regards to steady-state plasma glucose concentration are dominated by rates located in the infected erythrocyte and parasite compartments, particularly those mediating the uptake of glucose into the infected erythrocyte and its subsequent catabolism within the parasite. The data presented here indicates three possible junctures where novel chemotherapeutics could have the greatest impact on improving plasma glucose concentrations: entry of glucose into the infected erythrocyte, uptake of glucose into the parasite from the infected erythrocyte cytosol, and glycolytic catabolism within the parasite, as mediated by parasitic hexokinase (HK) and phosphofructokinase (PFK).

Uptake of glucose from the infected erythrocyte cytosol into the parasite itself presents another potential target for chemotherapeutic interventions, an avenue of research that has already undergone exploration (197). Of the possibilities described here, this would likely constitute one of the options least disruptive to host metabolism, since it would theoretically allow the infected erythrocyte's native metabolism and physiological function to continue while simultaneously starving the parasite of glucose. The specific enzymes that would be targeted to prevent uptake of glucose by the parasite would likely either be the non-selective, high-capacity channel mediating transporting of glucose across the parasitophorous vacuolar membrane (197), or parasite hexose transporter 1 (PHT1).

The significant control coefficients with regards to plasma glucose shown by parasitic HK and PFK activity, in addition to that exhibited by parasite glucose uptake, parallel the results obtained from the *green1* model in the author's original thesis (162). The enzymes HK and PFK mediate the first and third reactions of glycolysis within the parasite compartment and are both irreversible (PFK was characterised as irreversible in the original published model)(20). Both exhibit significant negative control over plasma glucose concentration, indicating that targeted inhibition of these enzymes would help slow the appearance of hypoglycaemia in cases of malaria infection. These interventions would, however, need to be specific for only the parasitic forms of these enzymes, so as not to disrupt host metabolism.

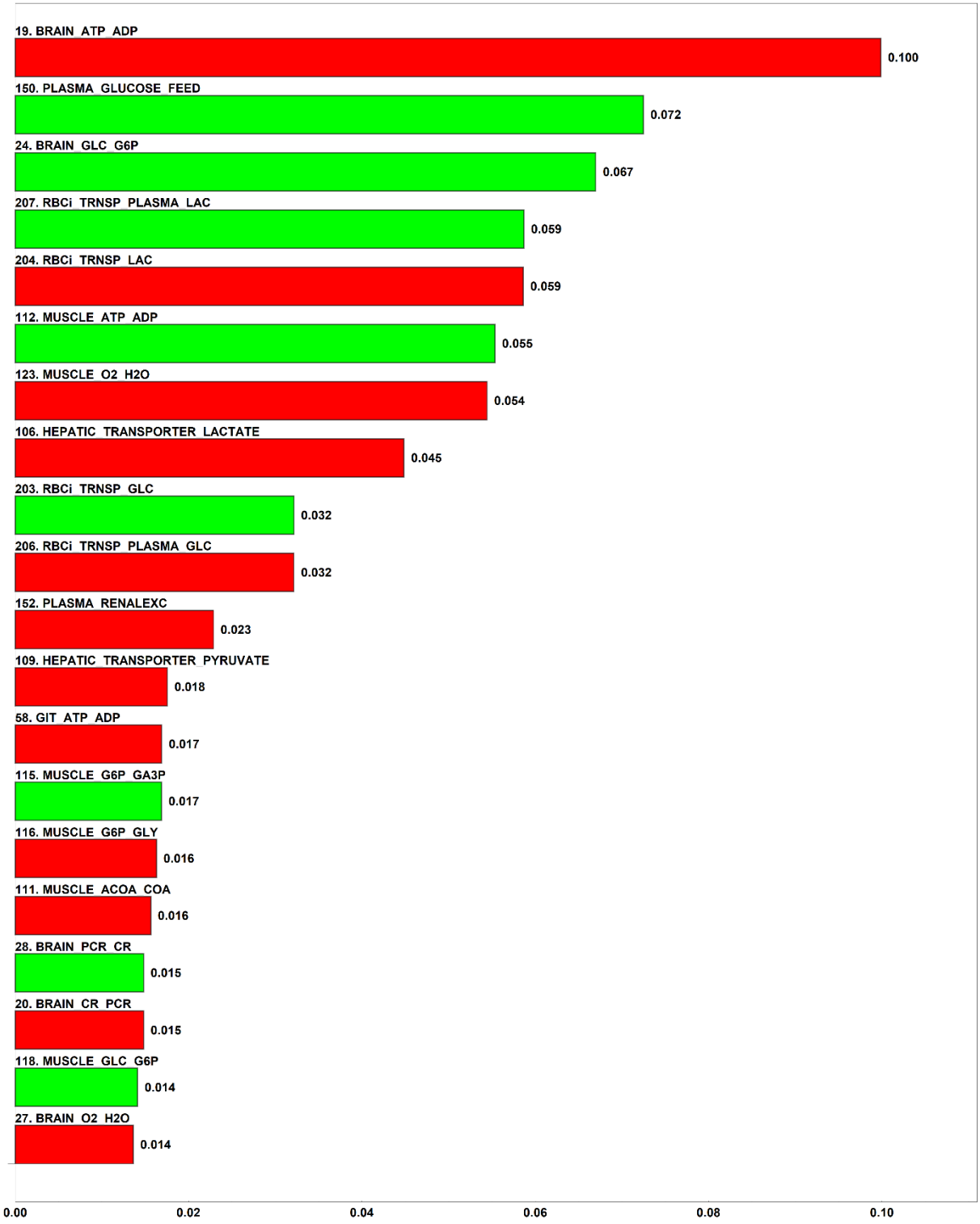

Figure 4.14: Twenty rates showing the most significant control coefficients with regards to plasma lactate, integrated over a range of parasitaemias from ~0% to 15%. Green bars indicate positive values, red bars indicate negative values. Rates for brain and muscle compartments are denoted as COMPARTMENT_SUBSTRATE_PRODUCT.

Interpretation of the control analysis with regards to plasma lactate indicates that the concentration of this metabolite is more strongly influenced by rates external to the infected erythrocyte milieu. While strong control over plasma lactate by the infected erythrocyte lactate transporter is still present, targeting the parasitic monocarboxylate transporters or band 3 anion transport proteins does not seem optimal, since

lactate itself is capable of diffusion of the protonated form across the parasite plasma membrane bilayer (21). Furthermore, such an intervention would likely not ameliorate the development of hypoglycaemia due to parasite glucose uptake. However, two other rates with substantial negative control over plasma lactate are worthy of discussion, especially since one is tied to the phenomenological host-parasite interactions implemented as part of the current research. As described and discussed in **Sections 3.2.2.2.1 & 4.3.4**, phenomenological inhibition of hepatic transporters, including lactate transport, has a profound effect on steady-state lactate concentrations across a range of parasitaemias. The significant negative control displayed by the hepatic lactate transporter can thus be interpreted as supporting the notion that reducing the degree of microvascular obstruction within the hepatic sinusoids would assist the process of lactate uptake by the liver for subsequent gluconeogenic disposal. A possible means whereby this could be accomplished is disruption of *P. falciparum* erythrocyte membrane protein 1 (PfEMP1), the central protein mediating the process of microvascular blockage via adherence, rosetting, and aggregation (11). Considering the contribution of parasite-mediated microvascular obstruction to not only impaired liver function, but also the appearance of multi-organ dysfunction (93), such a targeted intervention would likely yield systemic improvements giving a substantially improved clinical outcome.

As described in **Section 2.3**, uptake of glucose by the infected erythrocyte is mediated not only by existing endogenous mechanisms, but also new permeability pathways (NPPs). These NPPs are non-specific integral membrane proteins that mediate the uptake of glucose as well as other nutrients required by the parasite. NPPs were not modelled explicitly in the current research, and the contribution made to glucose uptake by these pathways would be in addition to the transport mechanisms already mentioned. Considering the substantial negative control exhibited by the transporter activity that was included, it could be speculated that parasite NPPs would exhibit negative similar control, albeit of an unknown degree. Research assessing whether NPPs exert a control high enough to warrant targeted therapy could therefore possibly yield another candidate for novel chemotherapeutics.

Chapter 5: Recommendations, Summary & Conclusion

5.1 Model Shortcomings and Recommendations for Possible Future Research

Severe *P. falciparum* malaria is a complex, multi-organ disease that can present with a range of symptoms, including that of hyperglycaemia and hyperlactataemia. To date, the causes of HG/HL in severe malaria as reported to literature have only been described qualitatively, with a lack of empirical data that can give clear indications as to which causes are most responsible for the appearance of hypoglycaemia and hyperlactataemia. As stated in the research aims and objectives, one of the core goals of the current research was the construction of a whole-body model of glucose and lactate dynamics in both the healthy and infected host. This model would subsequently serve as a framework that could be adapted and extended to describe the host-parasite interactions that have been reported to give rise to HG/HL. While this aspect of the research has been achieved, and has moved us closer towards a means of quantifying the relative contributions of the reported causes of HG/HL, the final model still possesses a significant shortcoming, caused by the same issue that motivated its inception: a lack of quantitative, empirical data.

The final *meyer1* model contains several phenomenological implementations equipped with estimated parameters. These modifications and additions were developed based on how well model outputs of plasma glucose and lactate concentrations, as a function of percentage parasitaemia, matched that of clinical observations. However, these extensions still contain many unknown factors. These unknowns include both the form of the expressions describing host-parasite interactions, as well as the value of the associated parameters. Owing to these limitations, the conclusions that can be drawn from the results given by the *meyer1* model remain relegated to the theoretical realm. However, the model has nevertheless facilitated progress towards a quantitative understanding of the aetiology surrounding HG/HL in severe malaria, since the modular implementation of host-parasite interactions allows each of these aspects to be developed and parameterised independently. The research presented in this thesis is thus best characterised as a pilot study demonstrating the types of analyses that can be conducted on a more complete, empirically parameterised version of the model.

A focal point of the current research was the investigation of the role played by gluconeogenesis in cases of severe *P. falciparum* malaria presenting with hypoglycaemia and hyperlactataemia. However, this investigation was limited to include only the gluconeogenic substrate contribution of pyruvate, the product of

lactate oxidation via lactate dehydrogenase activity. As described in **Section 2.6.1** and shown by **Fig. 2.6**, pyruvate and lactate form the bulk of the gluconeogenic substrate pool, but are far from the only materials utilized by gluconeogenic metabolism to synthesize glucose in response to hypoglycaemia. Other substrates, particularly alanine, glutamine, and to a lesser extent arginine, constitute a sizeable portion of substrates used for gluconeogenesis. The contribution of glycerol is also too significant to be ignored. Extension of the model to include kinetic descriptions of gluconeogenic metabolism drawing from sources other than pyruvate and lactate could thus substantially improve the capacity of the model to describe clinical data. Moreover, metabolic disturbances germane to these metabolites have been observed in malaria patients, namely impaired rates of alanine clearance (64), increased levels of glycerol (63), and decreased levels of arginine (198). Expansion of the model to enable investigation of such metabolic changes associated with malaria infection, and subsequently provide insight regarding their aetiology, thus forms an attractive possible avenue of future research.

The extension of the hepatic compartment to include a dynamic system of energy carriers and reducing equivalents was judged to be a successful addition to the model, but could be further improved. As explained in **Section 3.1.3.1**, the implementation of this system was necessitated due to the integral role that these molecules play in dictating balance of hepatic glycolysis and gluconeogenesis in response to hypoglycaemia and metabolic acidosis. While the addition of dynamic variables was made expedient by the existing, clamped expressions present in the original model, kinetic descriptions of transport of these molecules between the hepatic mitochondria and cytosol, as well as oxidative phosphorylation activity, had to be obtained from a separate model. These ‘foreign’ components were effectively introduced verbatim from their original model, with little modification of parameter values. While this implementation has yielded satisfactory results and plausible model simulation outputs, it remains an attractive candidate for replacement with more suitable kinetic descriptions that have been specifically modelled and validated within the context of reducing equivalent and adenosine phosphate metabolism within the hepatocyte.

Another shortcoming related to the model’s depiction of gluconeogenesis is the description of renal function. After the liver, the kidneys form the second most significant site of gluconeogenesis. Additionally, renal excretion of lactate has been observed under conditions of sufficiently high lactataemia (**Section 2.6.2.3**). Inclusion of a kinetic description of renal function can potentially be implemented in a manner similar to that used for the hepatic compartment, i.e. adaption and incorporation of an independently published model featuring descriptions of glycolysis and gluconeogenesis, with further possible inclusion of renal lactate excretion functionality. A cursory search for such a model was conducted during model development, but the lack of models published that were appropriate to this task, as well as the complexity that another detailed compartment would add to the model, led to the decision to not pursue this venture. Nevertheless, the contribution of renal metabolism to whole-body glucose and lactate metabolism, as well as the marked incidence of kidney injury in cases of severe malaria (106), makes the renal compartment a suitable candidate for inclusion in a future model.

While the extension of the model to include a more comprehensive kinetic description of gluconeogenesis was not included, modulation and scaling of the model as a function of age was implemented (**Section 3.1**). However, due to time constraints, this was not utilized functionally in the current research. The clinical presentations of severe *P. falciparum* malaria, including the relative incidence of metabolic acidosis and hypoglycaemia, vary significantly with age (**Section 2.4**, **Fig. 2.4**, **Fig. 4.4**). This phenomenon lead to the implementation of a model architecture that allows the size and metabolic contribution of the individual compartments to whole-body glucose and lactate metabolism to be scaled independently. The ability to further modulate model structure and properties as a function of age in an enzyme-specific manner was also planned, but was not pursued upon the realization of the amount of time that would be required for data collection, programmatic implementation, testing and validation that such a feature would require. Future allocation of time and resources to the development of this feature could well lead to greater insights and understanding with regards to the differential metabolic abnormalities associated with the age at which an individual suffers from malaria infection.

As stated in the beginning of this section, the host-parasite interactions introduced as part of the current model development were rudimentary, phenomenological functions that were not necessarily accurate mathematical representations of the interactions taking place. A notable example of this is the implementation of decreasing hepatic transporter substrate affinity as a function of increasing parasitaemia (**Section 3.2.2.2.1**). Statements from scientific literature relating the deleterious effect of parasite sequestration within the hepatic microvasculature to lactate clearance by the liver were interpreted mathematically as a hyperbolic increase in the K_M values for the hepatic glucose, lactate and pyruvate transporters, a relatively straightforward implementation. While use of this function substantially improved the descriptive capacity of the model with regards to plasma lactate concentration (**Section 4.2**), the expressions used to relate parasitaemia and transporter affinity were not derived mechanistically, nor parameterised with quantitative data obtained from experimental studies. Without a detailed description of the specific molecular entities and reactions that mediate the development of microvascular obstruction, more in-depth analysis cannot be carried out. For example, as described in **Section 2.6.4**, the process of cytoadherence, sequestration, and microvascular occlusion is mediated by a number of known protein ligands, including ICAM-1, CD36, and PfEMP1. A mechanistic description of the interactions between these ligands, present on the infected erythrocyte membrane and intraluminal capillary surface, would enable methodologies such as metabolic control analysis to identify which ligands, or possibly enzymatic components mediating their expression, would be most vulnerable to novel chemotherapeutic interventions. It is thus specifically recommended that future studies collect, at minimum, the following measurements in patients suffering from severe *P. falciparum* malaria: plasma glucose and lactate concentration, microvascular obstruction (percentage of blocked capillaries, in as many organs as is viable), and parasite burden (parasite count, parasite biomass). Such data would allow the empirical development of expressions describing two crucial relationships: that between the parasite burden, sequestration and microvascular blockage, and that between the degree of microvascular obstruction and plasma glucose and lactate concentrations. The variables and parameters of these empirically derived expressions should ideally

represent known biochemical entities (such as the mediators of cytoadherence mentioned previously) involved in the process of parasite-mediated microvascular occlusion, thereby removing the theoretical, phenomenological limitations present in the current model. Further development and expansion of the model to include such detailed mechanistic descriptions thus presents a promising and exciting avenue for future research.

Should the model undergo further development, the process will be expedited by the custom software routines (as presented in **Appendix A**) that are already in place and specifically suited towards analysis of *meyer1*. The MCA and parameter scanning (assessing the changes in model outputs as a function of iteratively varying the value of a single parameter) functionality is particularly ideal for evaluating the changes in model outputs (of the form of those presented in Chapter 4) as new and existing modules are introduced and improved.

5.2 Summary & Conclusion

Malaria is the most prominent parasitic disease capable of infecting humans. Despite continued advances in science and medicine for over a century, the disease is yet to be fully eradicated, and continues to levy a substantial health burden in countries where the disease is endemic. Malaria caused by *Plasmodium falciparum* is particularly dangerous, and is responsible for a high mortality rate in children where the infection has progressed to severe disease. While effective medicines exist to halt and reverse the progression of severe *P. falciparum* malaria, the need for novel chemotherapeutics is necessitated by the continued threat of drug resistance by the parasite. To this end, novel drug targets must be identified that can be exploited to circumvent resistance while maintaining favourable clinical outcomes. However, the development of new drugs is marred by the complexity of the disease, the variation in clinical presentation, and an incomplete understanding of malaria pathogenesis.

One such aspect of *P. falciparum* malaria that remains unclear is the paradoxical co-presentation of hypoglycaemia and hyperlactataemia (HG/HL) in patients suffering from severe disease, with these symptoms predicting a high risk of mortality. Though the appearance of these symptoms has been qualitatively attributed to a number of factors in the scientific literature, a thorough mechanistic understanding complete with robust quantitative evidence has yet to be established. It is this gap in understanding that the current research aimed to help rectify.

At the outset of this research, we posed the research question of what causes of HG/HL in cases of severe *P. falciparum* malaria can be discovered using a kinetic modelling approach. In order to answer this, we aimed to construct a whole-body model of glucose and lactate metabolism that could describe changes in metabolic behaviour at both the level of organ compartments and individual reactions. Another aim that guided the research was to use this whole-body model as a platform to implement the possible host-parasite interactions contributing to the development of hypoglycaemia and hyperlactataemia, and provide quantitative evidence indicating which of these interactions had the most significant role in the appearance of these symptoms.

These aims were translated into six research objectives, which, once achieved, would provide an answer to the research question, as well as insights into malaria pathophysiology that contribute to the discovery and development of novel chemotherapeutics designed to prevent and reverse the course of the disease.

With these research goals in place, we proceeded to review literature regarding which metabolic aspects of malaria pathophysiology would be most likely to yield insights into the development of HG/HL once described *in silico* using a kinetic modelling approach. These aspects were identified as glucose consumption by the parasite, hepatic gluconeogenesis, and the effects of parasite sequestration within the peripheral microcirculation. We also discussed the applicability of metabolic modelling and control analysis to investigating the relative contribution of these pathophysiological features to the appearance of HG/HL in severe disease.

Chapters 3 and 4 describe the process of how research objectives 2 (model construction), 3 (model validation), 4 (parasite glycolysis alone as a cause of hypoglycaemia) and 5 (introduction of host-parasite interactions to account for hyperlactataemia) were achieved. Once the whole-body model had been constructed, its simulation outputs were compared with both those published for the original constituent models, and clinical data of plasma glucose and lactate concentrations in patients suffering from malaria. These results indicated that the model was capable giving reasonable descriptions in both the healthy and infected state over a range of parasitaemias. To produce these outputs, the model had undergone several modifications and extensions to include the most important pathophysiological features pertinent to HG/HL mentioned previously. Simulation and analysis results obtained from this final version of the model allowed both parts of the research question to be addressed. It was determined that parasite metabolism alone was a likely candidate for the appearance of hypoglycaemia in severe malaria, but could not account for hyperlactataemia. Reasonable descriptions of increasing plasma lactate concentration as a function of rising parasitaemia was achieved only once host-parasite interactions were implemented in the model. Of these interactions, the effect of microcirculatory obstruction within the hepatic compartment emerged as the most significant interaction giving rise to dangerously high plasma lactate concentrations.

Several important conclusions can be drawn from the present work. First, following the completion of the whole-body *meyer1* model, it was demonstrated through a process of reproduction and comparison that independently published models originally constructed to serve distinct research purposes could be adapted and combined into a newer, larger model that could be used to answer novel research questions, while still maintaining the functionality of the original constituent models. Attention was also given as to how these models could be made mutually compatible despite their varying levels of detail through techniques such as the clamping of plasma metabolites (e.g. alanine, FFAs) and the implementation of a uniform description of hormonal control between compartments. Furthermore, it was also shown that components of the substituent models could be extended to allow more biochemically realistic behaviour, as was the case for the dynamic implementation of energy carriers and reducing equivalents in the hepatic compartment. The demonstration of the validity of this approach substantiates the rationale for continued use of this methodology when extending the model to incorporate additional features of host-parasite interaction that may prove useful in

furthering our understanding of the metabolic pathophysiology involved in the appearance of HG/HL in severe *P. falciparum* malaria.

Simulation results allowed conclusions to be drawn regarding which components of infected host glucose and lactate metabolism were most responsible for the appearance of HG/HL. It was shown that parasite glycolysis alone could account for the appearance of hypoglycaemia, albeit only at heavier parasite burdens (**Section 4.2**). Metabolic control analysis results indicated that the degree of hypoglycaemia in severe malaria could be substantially ameliorated with drugs targeted towards inhibiting glucose uptake by the infected erythrocyte (NPPs), transport of glucose into the parasite cytosol (non-selective high capacity channel, PHT1), and the initial enzymes catalysing glycolysis within the parasite (HK & PFK)(**Section 4.4**). These results thus place more emphasis on the parasite's prolific glucose consumption as a primary cause of low blood sugar, as opposed to other causes reported in the literature, such as a global shift in host metabolism towards anaerobic glycolysis. The finding that parasite lactate production would be unable to overwhelm the host's capacity for lactate clearance was, however, in keeping with previous published statements. It was shown that the host's rate of lactate uptake, as mediated by the liver and other organs, would comfortably exceed the rate of lactate production by the parasite, even in severe disease.

Given the liver's central role in the conversion of lactate to glucose, the gluconeogenic function of the hepatic compartment was investigated, and it was readily concluded that hepatic gluconeogenesis was not impaired to any appreciable degree in the presence of the changes in blood glucose and lactate concentrations brought on by *P. falciparum* infection (**Sections 4.3.1-4.3.3**). Hepatic substrate cycle function, redox state and net conversion of lactate to glucose all gave a definitive indication of functional hepatic gluconeogenesis. The results collected up to this point strongly suggested that parasite metabolism alone could not account for the appearance of metabolic acidosis in severe *P. falciparum* malaria.

Consultation of scientific literature indicated that host-parasite interactions, specifically modulation of host metabolism by the parasite, could be an important cause of high plasma lactate in cases of severe infection. Of the interactions mediating a significant influence over the steady-state plasma lactate concentration over a range of parasitaemias, the degree to which hepatic perfusion was phenomenologically inhibited by increasing parasite burden was found to be the most significant (**Section 4.3.4**, **Appendix C**). Thus, with regards to novel chemotherapeutic interventions slowing or reversing the development of hyperlactataemia, MCA results indicate that restoration of hepatic lactate uptake and gluconeogenic utilisation of lactate, via inhibition of parasite sequestration, would likely yield a substantial improvement for this clinical outcome. This finding is supported by numerous references in the scientific literature concerning the importance of hepatic microvascular obstruction in mediating the appearance of hyperlactataemia in severe *P. falciparum* malaria. This strongly encourages further research into targeting of the protein ligands mediating the process of infected erythrocyte cytoadherence and sequestration to prevent hyperlactataemia and improve clinical outcomes.

In addition to the body of work presented here, another product of this research is the software written during model construction, development, and analysis. Wolfram Mathematica, the computational platform used for

this research, does not possess built-in functionality specifically geared towards kinetic modelling of biological systems. Instead, the wide range of existing functionality can be utilised as part of user-defined functions that can be written to accomplish specific tasks. Thus, as the size and the complexity of the model grew, so too did the scope and functionality of the functions written alongside it. This has culminated in a collection of functions that can process large models in order to expedite the process of inspecting model structure, viewing simulation outputs, and efficiently processing large amounts of data during large-scale metabolic control analysis. An overview of this software, as well as example outputs, is shown in **Appendix A**. Given the lack of an existing, continually updated software package geared towards kinetic modelling on the Mathematica platform, and the certainty that the aforementioned custom software would be re-used and further developed as part of possible future research, there exists an attractive prospect of formally combining and packaging the various functions into a coherent suite suitable for use by other researchers in future.

In conclusion, this work presents a multi-compartmental, whole-body model of glucose and lactate metabolism in the *P. falciparum*-infected human host, providing a quantitative means for assessing the relative contributions of pathways, compartments and phenomenological host-parasite interactions to the appearance of hyperglycaemia and hyperlactataemia in severe disease. By combining independently published models relevant to whole-body glucose and lactate metabolism, an *in silico* platform has been constructed that has the potential to reveal which metabolic components of parasite and host metabolism could lead to the greatest improvement in clinical outcome if targeted by novel anti-malarial drugs.

References

1. White NJ, Pukrittayakamee S, Hien TT, Faiz MA, Mokuolu OA, Dondorp AM. 2014. Malaria. Lancet 383:723–735.
2. Barber BE, William T, Grigg MJ, Menon J, Auburn S, Marfurt J, Anstey NM, Yeo TW. 2013. A prospective comparative study of knowlesi, falciparum, and vivax malaria in Sabah, Malaysia: high proportion with severe disease from Plasmodium knowlesi and Plasmodium vivax but no mortality with early referral and artesunate therapy. Clin Infect Dis 56:383–97.
3. Roberts LR, Janovy J. 2008. Foundations of Parasitology, 8th ed. McGraw-Hill.
4. Miller LH, Ackerman HC, Su X, Wellems TE. 2013. Malaria biology and disease pathogenesis: insights for new treatments. Nat Med 19:156–167.
5. Hsu E. 2006. Reflections on the “discovery” of the antimalarial qinghao. Br J Clin Pharmacol 61:666–70.
6. Austin DJ, White NJ, Anderson RM. 1998. The dynamics of drug action on the within-host population growth of infectious agents: Melding pharmacokinetics with pathogen population dynamics. J Theor Biol 194:313–339.
7. Hoshen MB, Stein WD, Ginsburg H. 1998. Modelling the chloroquine chemotherapy of falciparum malaria: the value of spacing a split dose. Parasitology 116:407--416.
8. Hoshen MB, Stein WD, Ginsburg HD. 2001. Pharmacokinetic-pharmacodynamic modelling of the anti-malarial activity of mefloquine. Parasitology 123.
9. Simpson JA, Watkins ER, Price RN, Aarons L, Kyle DE, White NJ. 2000. Mefloquine Pharmacokinetic-Pharmacodynamic Models: Implications for Dosing and Resistance. Antimicrob Agents Chemother 44:3414–3424.
10. Snoep JL, Green K, Eicher J, Palm DC, Penkler G, du Toit F, Walters N, Burger R, Westerhoff H V, van Niekerk DD. 2015. Quantitative analysis of drug effects at the whole-body level: a case study for glucose metabolism in malaria patients. Biochem Soc Trans 43:1157–63.
11. Bernabeu M, Smith JD. 2017. EPCR and Malaria Severity: The Center of a Perfect Storm. Trends Parasitol 33:295–308.
12. Krishna S, Waller DW, Kuile F te., Kwiatkowski D, Crawley J, Craddock CFC, Nosten F, Chapman D, Brewster D, Holloway PA, White NJ. 1994. Lactic acidosis and hypoglycaemia in children with severe malaria: pathophysiological and prognostic significance. Trans R Soc Trop Med Hyg 88:67–73.

13. Sypniewska P, Duda JF, Locatelli I, Althaus CR, Althaus F, Genton B. 2017. Clinical and laboratory predictors of death in African children with features of severe malaria: a systematic review and meta-analysis. BMC Med 15:147.

14. Jarvis JN, Planche T, Bicanic T, Dzeing-Ella A, Kombila M, Issifou S, Borrmann S, Kremsner PG, Krishna S. 2006. Lactic acidosis in Gabonese children with severe malaria is unrelated to dehydration. Clin Infect Dis 42:1719–25.

15. Hanson J, Lam SWK, Mahanta KC, Pattnaik R, Alam S, Mohanty S, Hasan MU, Hossain A, Charunwatthana P, Chotivanich K, Maude RJ, Kingston H, Day NP, Mishra S, White NJ, Dondorp AM. 2012. Relative contributions of macrovascular and microvascular dysfunction to disease severity in falciparum malaria. J Infect Dis 206:571–9.

16. Kim J, Saidel GM, Cabrera ME. 2007. Multi-scale computational model of fuel homeostasis during exercise: effect of hormonal control. Ann Biomed Eng 35:69–90.

17. Li Y, Dash RK, Kim J, Saidel GM, Cabrera ME. 2009. Role of NADH/NAD+ transport activity and glycogen store on skeletal muscle energy metabolism during exercise: in silico studies. Am J Physiol Cell Physiol 296:C25-46.

18. König M, Bulik S, Holzhütter H-G. 2012. Quantifying the contribution of the liver to glucose homeostasis: a detailed kinetic model of human hepatic glucose metabolism. PLoS Comput Biol 8:e1002577.

19. Ashworth WB, Davies NA, Bogle IDL. 2016. A Computational Model of Hepatic Energy Metabolism: Understanding Zonated Damage and Steatosis in NAFLD. PLoS Comput Biol 12:e1005105.

20. Penkler GP. 2013. A Kinetic Model of Glucose Catabolism in Plasmodium falciparum. Stellenbosch University.

21. du Toit F. 2015. Modeling glycolysis in Plasmodium-infected erythrocytes. Stellenbosch University.

22. World Health Organization. 2018. World health statistics 2018: monitoring health for the SDGs, sustainable development goals. Geneva, Switzerland.

23. White NJ. 2014. Malaria, p. 629–698. *In* Manson's Tropical Diseases, 23rd ed. Elsevier.

24. Molina-Cruz A, Zilversmit MM, Neafsey DE, Hartl DL, Barillas-Mury C. 2016. Mosquito Vectors and the Globalization of Plasmodium falciparum Malaria. Annu Rev Genet 50:447–465.

25. Sinka ME, Bangs MJ, Manguin S, Rubio-Palis Y, Chareonviriyaphap T, Coetzee M, Mbogo CM, Hemingway J, Patil AP, Temperley WH, Gething PW, Kabaria CW, Burkot TR, Harbach RE, Hay SI. 2012. A global map of dominant malaria vectors. Parasit Vectors 5:69.

26. Sinka ME, Bangs MJ, Manguin S, Coetzee M, Mbogo CM, Hemingway J, Patil AP, Temperley WH, Gething PW, Kabaria CW, Okara RM, Van Boeckel T, Godfray HCJ, Harbach RE, Hay SI. 2010.

The dominant Anopheles vectors of human malaria in Africa, Europe and the Middle East: occurrence data, distribution maps and bionomic précis. Parasit Vectors 3:117.

27. World Health Organisation. 2017. World malaria report 2017. Geneva, Switzerland.

28. Spielmann T, Montagna GN, Hecht L, Matuschewski K. 2012. Molecular make-up of the Plasmodium parasitophorous vacuolar membrane. Int J Med Microbiol 302:179–86.

29. Kirk K. 2001. Membrane transport in the malaria-infected erythrocyte. Physiol Rev 81:495–537.

30. Sherman IW. 1998. Malaria: Parasite biology, pathogenesis and protection. ASM Press, Washington D.C.

31. Lang-Unnasch N, Murphy AD. 1998. Metabolic changes of the malaria parasite during the transition from the human to the mosquito host. Annu Rev Microbiol 52:561–90.

32. Woodrow CJ, Burchmore RJ, Krishna S. 2000. Hexose permeation pathways in Plasmodium falciparum-infected erythrocytes. Proc Natl Acad Sci U S A 97:9931–6.

33. Krishna S, Woodrow CJ, Burchmore RJ, Saliba KJ, Kirk K. 2000. Hexose transport in asexual stages of Plasmodium falciparum and kinetoplastidae. Parasitol Today 16:516–21.

34. Foth BJ, Stimmler LM, Handman E, Crabb BS, Hodder AN, McFadden GI. 2005. The malaria parasite Plasmodium falciparum has only one pyruvate dehydrogenase complex, which is located in the apicoplast. Mol Microbiol 55:39–53.

35. Jensen MD, Conley M, Helstowski LD. 1983. Culture of Plasmodium falciparum: the role of pH, glucose, and lactate. J Parasitol 69:1060–7.

36. Desai SA, Krogstad DJ, McCleskey EW. 1993. A nutrient-permeable channel on the intraerythrocytic malaria parasite. Nature 362:643–6.

37. Woodrow CJ, Penny JI, Krishna S. 1999. Intraerythrocytic Plasmodium falciparum expresses a high affinity facilitative hexose transporter. J Biol Chem 274:7272–7.

38. Roth E. 1990. Plasmodium falciparum carbohydrate metabolism: a connection between host cell and parasite. Blood Cells 16:453–60; discussion 461-6.

39. Cranmer SL, Conant AR, Gutteridge WE, Halestrap AP. 1995. Characterization of the enhanced transport of L- and D-lactate into human red blood cells infected with Plasmodium falciparum suggests the presence of a novel saturable lactate proton cotransporter. J Biol Chem 270:15045–52.

40. Elliott JL, Saliba KJ, Kirk K. 2001. Transport of lactate and pyruvate in the intraerythrocytic malaria parasite, Plasmodium falciparum. Biochem J 355:733–9.

41. Cordery D V, Urban BC. 2009. Immune recognition of Plasmodium-infected erythrocytes. Adv Exp Med Biol 653:175–84.

42. Stipanuk MH, Caudill MA. 2013. Chapter 12. Carbohydrate Metabolism: Synthesis and Oxidation, p.

209–255. *In* Biochemical, Physiological, and Molecular Aspects of Human Nutrition, 3rd ed. Elsevier Saunders, St. Louis.

43. Frayn KN. 2010. Metabolic Regulation: A Human Perspective, 3rd ed. Wiley-Blackwell.

44. Wasserman DH. 2009. Four grams of glucose. Am J Physiol Endocrinol Metab 296:E11-21.

45. WHO. 2014. Severe malaria. Trop Med Int Health 19 Suppl 1:7–131.

46. Madrid L, Sitoe A, Varo R, Nhampossa T, Lanaspa M, Nhama A, Acácio S, Riaño I, Casellas A, Bassat Q. 2017. Continuous determination of blood glucose in children admitted with malaria in a rural hospital in Mozambique. Malar J 16:184.

47. Davis TME, Binh TQ, Thu LTA, Long TTA, Johnston W, Robertson K, Barrett PHR. 2002. Glucose and lactate turnover in adults with falciparum malaria: effect of complications and antimalarial therapy. Trans R Soc Trop Med Hyg 96:411–417.

48. Robinson T, Mosha F, Grainge M, Madeley R. 2006. Indicators of mortality in African adults with malaria. Trans R Soc Trop Med Hyg 100:719–724.

49. Agbenyega T. 2000. Glucose and Lactate Kinetics in Children with Severe Malaria. J Clin Endocrinol Metab 85:1569–1576.

50. Dekker E. 1997. Glucose Homeostasis in Children with Falciparum Malaria: Precursor Supply Limits Gluconeogenesis and Glucose Production. J Clin Endocrinol Metab 82:2514–2521.

51. Dekker E, Romijn JA, Waruiru C, Ackermans MT, Weverling GJ, Sauerwein RW, Endert E, Peshu N, Marsh K, Sauerwein HP. 1996. The relationship between glucose production and plasma glucose concentration in children with falciparum malaria. Trans R Soc Trop Med Hyg 90:654–657.

52. Singh B, Choo KE, Ibrahim J, Johnston W, Davis TME. 1998. Non-radioisotopic glucose turnover in children with falciparum malaria and enteric fever. Trans R Soc Trop Med Hyg 92:532–537.

53. Davis TME, Looareesuwan S, Pukrittayakamee S, Levy JC, Nagachinta B, White NJ. 1993. Glucose turnover in severe falciparum malaria. Metabolism 42:334–340.

54. World Health Organization. 2000. Severe falciparum malaria. World Health Organization, Communicable Diseases Cluster. Trans R Soc Trop Med Hyg 94 Suppl 1:S1-90.

55. World Health Organization. 2000. Severe falciparum malaria. World Health Organization, Communicable Diseases Cluster. Trans R Soc Trop Med Hyg 94 Suppl 1:S1-90.

56. van Thien H, Ackermans M., Weverling G., Thanh Chien V., Endert E, Kager P., Sauerwein H. 2004. Influence of prolonged starvation on glucose kinetics in pregnant patients infected with Plasmodium falciparum. Clin Nutr 23:59–67.

57. White NJ, Miller KD, Marsh K, Berry CD, Turner RC, Williamson DH, Brown J. 1987. Hypoglycaemia in African children with severe malaria. Lancet (London, England) 1:708–11.

58. White NJ, Warrell DA, Chanthavanich P, Looareesuwan S, Warrell MJ, Krishna S, Williamson DH, Turner RC. 1983. Severe Hypoglycemia and Hyperinsulinemia in Falciparum Malaria. N Engl J Med 309:61–66.

59. Thien H V., Kager PA, Sauerwein HP. 2006. Hypoglycemia in falciparum malaria: is fasting an unrecognized and insufficiently emphasized risk factor? Trends Parasitol 22:410–415.

60. van Thien H, Weverling GJ, Ackermans MT, canh Hung N, Endert E, Kager PA, Sauerwein HP. 2004. FFAs are not involved in regulation of gluconeogenesis and glycogenolysis in adults with uncomplicated P. falciparum malaria. Am J Physiol Metab 287:E609–E615.

61. van Thien H. 2001. Glucose production and gluconeogenesis in adults with cerebral malaria. QJM 94:709–715.

62. English M, Wale S, Binns G, Mwangi I, Sauerwein H, Marsh K. 1998. Hypoglycaemia on and after admission in Kenyan children with severe malaria. QJM 91:191–7.

63. Pukrittayakamee S, White NJ, Davis TME, Supanaranond W, Crawley J, Nagachinta B, Williamson DH. 1994. Glycerol metabolism in severe falciparum malaria. Metabolism 43:887–892.

64. Pukrittayakamee S, Krishna S, ter Kuile F, Wilaiwan O, Williamson DH, White NJ. 2002. Alanine metabolism in acute falciparum malaria. Trop Med Int Heal 7:911–918.

65. World Health Organization. 2013. Pocket book of hospital care for children: Guidelines for the management of common illnesses with limited resources, 2nd ed. WHO.

66. Binh TQ, Davis TME, Johnston W, Thu LTA, Boston R, Danh PT, Anh TK. 1997. Glucose metabolism in severe malaria: Minimal model analysis of the intravenous glucose tolerance test incorporating a stable glucose label. Metabolism 46:1435–1440.

67. Pagliara AS, Karl IE, Haymond M, Kipnis DM. 1973. Hypoglycemia in infancy and childhood. Part I. J Pediatr 82:365–379.

68. Phillips RE. 1989. Hypoglycaemia is an important complication of falciparum malaria. QJM 71:477–483.

69. Zijlmans WCWR, van Kempen AAMW, Serlie MJ, Kager PA, Sauerwein HP. 2014. Adaptation of glucose metabolism to fasting in young children with infectious diseases: a perspective. J Pediatr Endocrinol Metab 27.

70. Sprangers F, Thien H V., Ackermans MT, Endert E, Sauerwein HP. 2004. Glycogenolysis during short-term fasting in malaria and healthy subjects - The potential regulatory role of glycogen content on glycogen breakdown: A hypothesis. Clin Nutr 23:1051–1059.

71. Madrid L, Lanaspa M, Maculuve SA, Bassat Q. 2015. Malaria-associated hypoglycaemia in children. Expert Rev Anti Infect Ther 13:267–277.

72. Ogetii GN, Akech S, Jemutai J, Boga M, Kivaya E, Fegan G, Maitland K. 2010. Hypoglycaemia in

severe malaria, clinical associations and relationship to quinine dosage. BMC Infect Dis 10:334.

73. Philp A. 2005. Lactate - a signal coordinating cell and systemic function. J Exp Biol 208:4561–4575.

74. Huckabee WE. 1958. Relationships of pyruvate and lactate during anaerobic metabolism. I. Effects of infusion of pyruvate or glucose and of hyperventilation. J Clin Invest 37:244–54.

75. Rosenstein PG, Tennent-Brown BS, Hughes D. 2018. Clinical use of plasma lactate concentration. Part 1: Physiology, pathophysiology, and measurement. J Vet Emerg Crit Care (San Antonio) 28:85–105.

76. Kreisberg RA. 1980. Lactate homeostasis and lactic acidosis. Ann Intern Med 92:227–237.

77. Planche T, Krishna S. 2006. Severe Malaria: Metabolic Complications. Curr Mol Med 6:141–153.

78. Bakker J, Nijsten MWN, Jansen TC. 2013. Clinical use of lactate monitoring in critically ill patients. Ann Intensive Care 3:1–8.

79. Van Hall G. 2010. Lactate kinetics in human tissues at rest and during exercise. Acta Physiol (Oxf) 199:499–508.

80. Gutierrez G, Wulf ME. 2005. Lactic acidosis is sepsis: Another commentary lactic. Crit Care Med 33:2420–2422.

81. Robergs RA. 2011. Counterpoint: Muscle lactate and H+ production do not have a 1:1 association in skeletal muscle. J Appl Physiol 110:1489–1491.

82. Adeva-Andany M, López-Ojén M, Funcasta-Calderón R, Ameneiros-Rodríguez E, Donapetry-García C, Vila-Altesor M, Rodríguez-Seijas J. 2014. Comprehensive review on lactate metabolism in human health. Mitochondrion 17:76–100.

83. Glinghammar B, Rafter I, Lindström A-K, Hedberg JJ, Andersson HB, Lindblom P, Berg A-L, Cotgreave I. 2009. Detection of the mitochondrial and catalytically active alanine aminotransferase in human tissues and plasma. Int J Mol Med 23:621–31.

84. Perriello G, Jorde R, Nurjhan N, Stumvoll M, Dailey G, Jenssen T, Bier DM, Gerich JE. 1995. Estimation of glucose-alanine-lactate-glutamine cycles in postabsorptive humans: role of skeletal muscle. Am J Physiol 269:E443-50.

85. Bouzat P, Oddo M. 2014. Lactate and the injured brain: Friend or foe? Curr Opin Crit Care 20:133–140.

86. Liberti M V, Locasale JW. 2016. The Warburg Effect: How Does it Benefit Cancer Cells? Trends Biochem Sci 41:211–218.

87. Voet D, Voet JG, Pratt CW. 2016. Fundamentals of Biochemistry: Life at the Molecular Level, 5th ed. Wiley.

88. Levy B. 2006. Lactate and shock state: the metabolic view. Curr Opin Crit Care 12:315–321.

89. Haji-Michael PG, Ladrière L, Sener A, Vincent J-L, Malaisse WJ. 1999. Leukocyte glycolysis and lactate output in animal sepsis and ex vivo human blood. Metabolism 48:779–785.

90. Kramer PA, Ravi S, Chacko B, Johnson MS, Darley-Usmar VM. 2014. A review of the mitochondrial and glycolytic metabolism in human platelets and leukocytes: Implications for their use as bioenergetic biomarkers. Redox Biol 2:206–210.

91. De Backer D, Creteur J, Silva E, Vincent J-L. 2001. The hepatosplanchnic area is not a common source of lactate in patients with severe sepsis. Crit Care Med 29:256–261.

92. van Genderen PJJ, van der Meer IM, Consten J, Petit PLC, van Gool T, Overbosch D. Evaluation of plasma lactate as a parameter for disease severity on admission in travelers with Plasmodium falciparum malaria. J Travel Med 12:261–4.

93. Day NP, Phu NH, Mai NT, Chau TT, Loc PP, Chuong L V, Sinh DX, Holloway P, Hien TT, White NJ. 2000. The pathophysiologic and prognostic significance of acidosis in severe adult malaria. Crit Care Med 28:1833–40.

94. Bricker DK, Taylor EB, Schell JC, Orsak T, Boutron A, Chen Y-C, Cox JE, Cardon CM, Van Vranken JG, Dephoure N, Redin C, Boudina S, Gygi SP, Brivet M, Thummel CS, Rutter J. 2012. A mitochondrial pyruvate carrier required for pyruvate uptake in yeast, Drosophila, and humans. Science 337:96–100.

95. Madias NE. 1986. Lactic acidosis. Kidney Int 29:752–774.

96. Patel KP, O'Brien TW, Subramony SH, Shuster J, Stacpoole PW. 2012. The spectrum of pyruvate dehydrogenase complex deficiency: clinical, biochemical and genetic features in 371 patients. Mol Genet Metab 106:385–94.

97. Watts JA, Kline JA. 2003. Bench to bedside: the role of mitochondrial medicine in the pathogenesis and treatment of cellular injury. Acad Emerg Med 10:985–97.

98. Ruggieri AJ, Levy RJ, Deutschman CS. 2010. Mitochondrial dysfunction and resuscitation in sepsis. Crit Care Clin 26:567–575.

99. DiMauro S, Schon EA. 2003. Mitochondrial Respiratory-Chain Diseases. N Engl J Med 348:2656–2668.

100. Fisher-Wellman KH, Neufer PD. 2012. Linking mitochondrial bioenergetics to insulin resistance via redox biology. Trends Endocrinol Metab 23:142–53.

101. Battezzati A, Caumo A, Martino F, Sereni LP, Coppa J, Romito R, Ammatuna M, Regalia E, Matthews DE, Mazzaferro V, Luzi L. 2004. Nonhepatic glucose production in humans. Am J Physiol Endocrinol Metab 286:E129-35.

102. Jitrapakdee S, St Maurice M, Rayment I, Cleland WW, Wallace JC, Attwood P V. 2008. Structure, mechanism and regulation of pyruvate carboxylase. Biochem J 413:369–87.

103. Cao H, van der Veer E, Ban MR, Hanley AJG, Zinman B, Harris SB, Young TK, Pickering JG, Hegele RA. 2004. Promoter polymorphism in PCK1 (phosphoenolpyruvate carboxykinase gene) associated with type 2 diabetes mellitus. J Clin Endocrinol Metab 89:898–903.

104. van den Berghe G. 1996. Disorders of gluconeogenesis. J Inherit Metab Dis 19:470–7.

105. Blanco G, Blanco A. 2017. Medical Biochemistry, 1st ed. Elsevier.

106. Sriboonvorakul N, Ghose A, Hassan MMU, Hossain MA, Faiz MA, Pukrittayakamee S, Chotivanich K, Sukthana Y, Leopold SJ, Plewes K, Day NPJ, White NJ, Tarning J, Dondorp AM. 2018. Acidosis and acute kidney injury in severe malaria. Malar J 17:128.

107. Chung ST, Chacko SK, Sunehag AL, Haymond MW. 2015. Measurements of Gluconeogenesis and Glycogenolysis: A Methodological Review. Diabetes 64:3996–4010.

108. Vernon C, LeTourneau JL. 2010. Lactic Acidosis: Recognition, Kinetics, and Associated Prognosis. Crit Care Clin 26:255–283.

109. Levraut J, Ciebiera JP, Chave S, Rabary O, Jambou P, Carles M, Grimaud D. 1998. Mild hyperlactatemia in stable septic patients is due to impaired lactate clearance rather than overproduction. Am J Respir Crit Care Med 157:1021–6.

110. Meyer C, Stumvoll M, Dostou J, Welle S, Haymond M, Gerich J. 2002. Renal substrate exchange and gluconeogenesis in normal postabsorptive humans. Am J Physiol Endocrinol Metab 282:E428-34.

111. Stanley WC. 1991. Myocardial lactate metabolism during exercise. Med Sci Sports Exerc 23:920–924.

112. Stanley WC. 2001. Changes in cardiac metabolism: A critical step from stable angina to ischaemic cardiomyopathy. Eur Hear Journal, Suppl 3:2–7.

113. Bergman BC, Tsvetkova T, Lowes B, Wolfel EE. 2009. Myocardial glucose and lactate metabolism during rest and atrial pacing in humans. J Physiol 587:2087–99.

114. Gertz EW, Wisneski JA, Stanley WC, Neese RA. 1988. Myocardial substrate utilization during exercise in humans. Dual carbon-labeled carbohydrate isotope experiments. J Clin Invest 82:2017–25.

115. Ahlborg G, Felig P. 1982. Lactate and glucose exchange across the forearm, legs, and splanchnic bed during and after prolonged leg exercise. J Clin Invest 69:45–54.

116. Consoli A, Nurjhan N, Reilly JJ, Bier DM, Gerich JE. 1990. Contribution of liver and skeletal muscle to alanine and lactate metabolism in humans. Am J Physiol 259:E677-84.

117. Van Hall G, Jensen-Urstad M, Rosdahl H, Holmberg H-C, Saltin B, Calbet JAL. 2003. Leg and arm lactate and substrate kinetics during exercise. Am J Physiol Endocrinol Metab 284:E193-205.

118. Ferguson BS, Rogatzki MJ, Goodwin ML, Kane DA, Rightmire Z, Gladden LB. 2018. Lactate metabolism: historical context, prior misinterpretations, and current understanding. Eur J Appl

Physiol 118:691–728.

119. Newton PN, Stepniewska K, Dondorp A, Silamut K, Chierakul W, Krishna S, Davis TME, Suputtamongkol Y, Angus B, Pukrittayakamee S, Ruangveerayuth R, Hanson J, Day NPJ, White NJ. 2013. Prognostic indicators in adults hospitalized with falciparum malaria in Western Thailand. Malar J 12:229.

120. von Seidlein L, Olaosebikan R, Hendriksen ICE, Lee SJ, Adedoyin OT, Agbenyega T, Nguah SB, Bojang K, Deen JL, Evans J, Fanello CI, Gomes E, Pedro AJ, Kahabuka C, Karema C, Kivaya E, Maitland K, Mokuolu OA, Mtove G, Mwanga-Amumpaire J, Nadjm B, Nansumba M, Ngum WP, Onyamboko MA, Reyburn H, Sakulthaew T, Silamut K, Tshefu AK, Umulisa N, Gesase S, Day NPJ, White NJ, Dondorp AM. 2012. Predicting the clinical outcome of severe falciparum malaria in african children: findings from a large randomized trial. Clin Infect Dis 54:1080–90.

121. Day NP, Phu NH, Bethell DP, Mai NT, Chau TT, Hien TT, White NJ. 1996. The effects of dopamine and adrenaline infusions on acid-base balance and systemic haemodynamics in severe infection. Lancet (London, England) 348:219–23.

122. Brand NR, Opoka RO, Hamre KES, John CC. 2016. Differing causes of lactic acidosis and deep breathing in cerebral malaria and severe malarial anemia may explain differences in acidosis-related mortality. PLoS One 11:e0163728.

123. Taylor TE, Borgstein A, Molyneux ME. 1993. Acid-base status in paediatric Plasmodium falciparum malaria. Q J Med 86:99–109.

124. Dondorp AM, Lee SJ, Faiz MA, Mishra S, Price R, Tjitra E, Than M, Htut Y, Mohanty S, Yunus E Bin, Rahman R, Nosten F, Anstey NM, Day NPJ, White NJ. 2008. The relationship between age and the manifestations of and mortality associated with severe malaria. Clin Infect Dis 47:151–7.

125. Marsh K, Forster D, Waruiru C, Mwangi I, Winstanley M, Marsh V, Newton C, Winstanley P, Warn P, Peshu N. 1995. Indicators of life-threatening malaria in African children. N Engl J Med 332:1399–404.

126. Njim T, Dondorp A, Mukaka M, Ohuma EO. 2018. Identifying risk factors for the development of sepsis during adult severe malaria. Malar J 17:278.

127. Dondorp AM, Pongponratn E, White NJ. 2004. Reduced microcirculatory flow in severe falciparum malaria: pathophysiology and electron-microscopic pathology. Acta Trop 89:309–17.

128. Dondorp AM, Ince C, Charunwatthana P, Hanson J, van Kuijen A, Faiz MA, Rahman MR, Hasan M, Bin Yunus E, Ghose A, Ruangveerayut R, Limmathurotsakul D, Mathura K, White NJ, Day NPJ. 2008. Direct In Vivo Assessment of Microcirculatory Dysfunction in Severe Falciparum Malaria. J Infect Dis 197:79–84.

129. Hanson J, Lee SJ, Hossain MA, Anstey NM, Charunwatthana P, Maude RJ, Kingston HWF, Mishra SK, Mohanty S, Plewes K, Piera K, Hassan MU, Ghose A, Faiz MA, White NJ, Day NPJ, Dondorp

AM. 2015. Microvascular obstruction and endothelial activation are independently associated with the clinical manifestations of severe falciparum malaria in adults: an observational study. BMC Med 13:122.

130. Ishioka H, Ghose A, Charunwatthana P, Maude R, Plewes K, Kingston H, Intharabut B, Woodrow C, Chotivanich K, Sayeed AA, Hasan MU, Day NP, Faiz A, White NJ, Hossain A, Dondorp AM. 2016. Sequestration and red cell deformability as determinants of hyperlactatemia in falciparum malaria. J Infect Dis 212:788–793.

131. Marchiafava E, Bignami A. 1894. Two monographs on malaria and the parasites of malarial fevers (ed. translated by JH Thompson). New Sydenham Soc 1–232.

132. Silamut K, Phu NH, Whitty C, Turner GDH, Louwrier K, Mai NTH, Simpson JA, Hien TT, White NJ. 1999. A quantitative analysis of the microvascular sequestration of malaria parasites in the human brain. Am J Pathol 155:395–410.

133. Pouvelle B, Buffet PA, Lépolard C, Scherf A, Gysin J. 2000. Cytoadhesion of Plasmodium falciparum ring-stage-infected erythrocytes. Nat Med 6:1264–1268.

134. Tripepi S, Saita A. 1985. Ultrastructural analysis of spermiogenesis in Admetus pomilio (Arachnida, amblypygi). J Morphol 184:111–120.

135. Pongponratn E, Turner GDH, Day NPJ, Phu NH, Simpson JA, Stepniewska K, Mai NTH, Viriyavejakul P, Looareesuwan S, Hien TT, Ferguson DJP, White NJ. 2003. An ultrastructural study of the brain in fatal Plasmodium falciparum malaria. Am J Trop Med Hyg 69:345–59.

136. Ho M, White NJ. 1999. Molecular mechanisms of cytoadherence in malaria. Am J Physiol 276:C1231–C1242.

137. Nguansangiam S, Day NPJ, Hien TT, Mai NTH, Chaisri U, Riganti M, Dondorp AM, Lee SJ, Phu NH, Turner GDH, White NJ, Ferguson DJP, Pongponratn E. 2007. A quantitative ultrastructural study of renal pathology in fatal Plasmodium falciparum malaria. Trop Med Int Heal 12:1037–1050.

138. Cunnington AJ, Riley EM, Walther M. 2013. Microvascular dysfunction in severe Plasmodium falciparum Malaria. J Infect Dis 207:369–70.

139. Hanson J, Dondorp AM, Day NP, White NJ. 2013. Reply to Cunnington et al. J Infect Dis 207:370–371.

140. Tan J, Bull PC. 2015. Agglutination Assays of the Plasmodium falciparum-Infected Erythrocyte. Methods Mol Biol 1325:115–129.

141. Dondorp AM, Chotivanich KT, Fucharoen S, Silamut K, Vreeken J, Kager PA, White NJ. 1999. Red cell deformability, splenic function and anaemia in thalassaemia. Br J Haematol 105:505–508.

142. Dessy C, Feron O. 2004. Pathophysiological roles of nitric oxide: In the heart and the coronary vasculature. Curr Med Chem Anti-inflamm Anti-Allergy Agents 3:207–216.

143. White NJ, Turner GDH, Day NPJ, Dondorp AM. 2013. Lethal Malaria: Marchiafava and Bignami Were Right. J Infect Dis 208:192–198.

144. Li X, Fang P, Li Y, Kuo Y-M, Andrews AJ, Nanayakkara G, Johnson C, Fu H, Shan H, Du F, Hoffman NE, Yu D, Eguchi S, Madesh M, Koch WJ, Sun J, Jiang X, Wang H, Yang X. 2016. Mitochondrial Reactive Oxygen Species Mediate Lysophosphatidylcholine-Induced Endothelial Cell ActivationHighlights. Arterioscler Thromb Vasc Biol 36:1090–1100.

145. Alom-Ruiz SP, Anilkumar N, Shah AM. 2008. Reactive Oxygen Species and Endothelial Activation. Antioxid Redox Signal 10:1089–1100.

146. Kim H, Higgins S, Liles WC, Kain KC. 2011. Endothelial activation and dysregulation in malaria: A potential target for novel therapeutics. Curr Opin Hematol 18:177–185.

147. Yeo TW, Lampah DA, Gitawati R, Tjitra E, Kenangalem E, Piera K, Price RN, Duffull SB, Celermajer DS, Anstey NM. 2008. Angiopoietin-2 is associated with decreased endothelial nitric oxide and poor clinical outcome in severe falciparum malaria. Proc Natl Acad Sci 105:17097–17102.

148. Lopansri BK, Anstey NM, Weinberg JB, Stoddard GJ, Hobbs MR, Levesque MC, Mwaikambo ED, Granger DL. 2003. Low plasma arginine concentrations in children with cerebral malaria and decreased nitric oxide production. Lancet 361:676–678.

149. Anstey NM. 1996. Nitric oxide in Tanzanian children with malaria: inverse relationship between malaria severity and nitric oxide production/nitric oxide synthase type 2 expression. J Exp Med 184:557–567.

150. Yeo TW, Lampah DA, Gitawati R, Tjitra E, Kenangalem E, McNeil YR, Darcy CJ, Granger DL, Weinberg JB, Lopansri BK, Price RN, Duffull SB, Celermajer DS, Anstey NM. 2007. Impaired nitric oxide bioavailability and l-arginine–reversible endothelial dysfunction in adults with falciparum malaria. J Exp Med 204:2693–2704.

151. Liles WC, Kain KC. 2014. Endothelial activation and dysfunction in the pathogenesis of microvascular obstruction in severe malaria - A viable target for therapeutic adjunctive intervention. J Infect Dis 210:163–164.

152. Vary TC. 1996. Sepsis-induced alterations in pyruvate dehydrogenase complex activity in rat skeletal muscle: Effects on plasma lactate. Shock 6:89–94.

153. Taylor WRJ, Hanson J, Turner GDH, White NJ, Dondorp AM. 2012. Respiratory manifestations of malaria. Chest 142:492–505.

154. Buffet PA, Safeukui I, Deplaine G, Brousse V, Prendki V, Thellier M, Turner GD, Mercereau-Puijalon O. 2011. The pathogenesis of Plasmodium falciparum malaria in humans: insights from splenic physiology. Blood 117:381–92.

155. Price RN, Simpson JA, Nosten F, Luxemburger C, Hkirjaroen L, ter Kuile F, Chongsuphajaisiddhi T,

White NJ. 2001. Factors contributing to anemia after uncomplicated falciparum malaria. Am J Trop Med Hyg 65:614–22.

156. Klipp E, Liebermeister W, Wierling C. 2016. Systems Biology: A Textbook, 2nd ed. Wiley-Blackwell, Weinheim.

157. Rissanen J. 1986. Stochastic Complexity and Modeling. Ann Stat 14:1080–1100.

158. Gershenfeld N. 1998. The Nature of Mathematical Modeling. Cambridge University Press.

159. Klipp E, Liebermeister W, Wierling C, Kowald A. 2016. 4.2 Metabolic Control Analysis, p. 50–60. *In* Systems Biology: A Textbook, 2nd ed. Wiley-Blackwell, Weinheim.

160. Bruggeman FJ, Snoep JL, Teusink B. 2012. Molecular Systems Biology. VU Universiteit, Amsterdam, The Netherlands.

161. Xu K, Morgan KT, Todd Gehris A, Elston TC, Gomez SM. 2011. A whole-body model for glycogen regulation reveals a critical role for substrate cycling in maintaining blood glucose homeostasis. PLoS Comput Biol 7:e1002272.

162. Green K. 2017. Whole body modelling of glucose metabolism in malaria patients. Stellenbosch University.

163. Mulquiney PJ, Bubb WA, Kuchel PW. 1999. Model of 2,3-bisphosphoglycerate metabolism in the human erythrocyte based on detailed enzyme kinetic equations: in vivo kinetic characterization of 2,3-bisphosphoglycerate synthase/phosphatase using 13C and 31P NMR. Biochem J 342 Pt 3:567–80.

164. Mulquiney PJ, Kuchel PW. 1999. Model of 2,3-bisphosphoglycerate metabolism in the human erythrocyte based on detailed enzyme kinetic equations: equations and parameter refinement. Biochem J 342 Pt 3:581–96.

165. Mulquiney PJ, Kuchel PW. 1999. Model of 2,3-bisphosphoglycerate metabolism in the human erythrocyte based on detailed enzyme kinetic equations: computer simulation and metabolic control analysis. Biochem J 342 Pt 3:597–604.

166. Berndt N, Bulik S, Wallach I, Wünsch T, König M, Stockmann M, Meierhofer D, Holzhütter H-G. 2018. HEPATOKIN1 is a biochemistry-based model of liver metabolism for applications in medicine and pharmacology. Nat Commun 9:2386.

167. Dash RK, Yanjun Li, Jaeyeon Kim, Saidel GM, Cabrera ME. 2008. Modeling Cellular Metabolism and Energetics in Skeletal Muscle: Large-Scale Parameter Estimation and Sensitivity Analysis. IEEE Trans Biomed Eng 55:1298–1318.

168. Halestrap AP. 2013. Monocarboxylic acid transport. Compr Physiol 3:1611–43.

169. Lin RY, Vera JC, Chaganti RS, Golde DW. 1998. Human monocarboxylate transporter 2 (MCT2) is a high affinity pyruvate transporter. J Biol Chem 273:28959–65.

170. Halestrap AP, Price NT. 1999. The proton-linked monocarboxylate transporter (MCT) family: structure, function and regulation. Biochem J 343 Pt 2:281–99.

171. Halestrap AP, Wilson MC. 2012. The monocarboxylate transporter family-Role and regulation. IUBMB Life 64:109–119.

172. Overmoyer BA, McLaren CE, Brittenham GM. 1987. Uniformity of liver density and nonheme (storage) iron distribution. Arch Pathol Lab Med 111:549–54.

173. Saunders PT, Koeslag JH, Wessels JA. 1998. Integral rein control in physiology. J Theor Biol 194:163–73.

174. Saunders PT, Koeslag JH, Wessels JA. 2000. Integral rein control in physiology II: a general model. J Theor Biol 206:211–20.

175. Chianura L, Errante IC, Travi G, Rossotti R, Puoti M. 2012. Hyperglycemia in severe falciparum malaria: a case report. Case reports Crit care 2012:312458.

176. Pukrittayakamee S, White NJ, Looareesuwan S, Supanaranond W, Desakorn V, Chaivisuth B, Williamson DH. 1992. Hepatic blood flow and metabolism in severe falciparum malaria: clearance of intravenously administered galactose. Clin Sci 82:63–70.

177. Tinning K, Acworth J. 2007. Make your Best Guess: an updated method for paediatric weight estimation in emergencies. Emerg Med Australas 19:528–34.

178. Ali K, Sammy I, Nunes P. 2012. Is the APLS formula used to calculate weight-for-age applicable to a Trinidadian population? BMC Emerg Med 12:9.

179. Morgan G, Mikhail M, Murray M. 2006. Morgan's Clinical Anesthesiology, 4th ed. McGraw-Hill Education.

180. Krishna S, Nagaraja N V, Planche T, Agbenyega T, Bedo-Addo G, Ansong D, Owusu-Ofori A, Shroads AL, Henderson G, Hutson A, Derendorf H, Stacpoole PW. 2001. Population pharmacokinetics of intramuscular quinine in children with severe malaria. Antimicrob Agents Chemother 45:1803–9.

181. Dinneen S, Gerich J, Rizza R. 1992. Carbohydrate metabolism in non-insulin-dependent diabetes mellitus. N Engl J Med 327:707–13.

182. Gerich JE. 1993. Control of glycaemia. Baillieres Clin Endocrinol Metab 7:551–86.

183. Gerich JE. 2000. Physiology of glucose homeostasis. Diabetes Obes Metab 2:345–50.

184. Woerle HJ, Meyer C, Dostou JM, Gosmanov NR, Islam N, Popa E, Wittlin SD, Welle SL, Gerich JE. 2003. Pathways for glucose disposal after meal ingestion in humans. Am J Physiol Endocrinol Metab 284:E716-25.

185. Mehta M, Sonawat HM, Sharma S. 2006. Glycolysis in Plasmodium falciparum results in modulation

of host enzyme activities. J Vector Borne Dis 43:95–103.

186. Idro R, Jenkins NE, Newton CRJC. 2005. Pathogenesis, clinical features, and neurological outcome of cerebral malaria. Lancet Neurol 4:827–40.

187. Evans SS, Repasky EA, Fisher DT. 2015. Fever and the thermal regulation of immunity: the immune system feels the heat. Nat Rev Immunol 15:335–49.

188. van Hall G, Strømstad M, Rasmussen P, Jans O, Zaar M, Gam C, Quistorff B, Secher NH, Nielsen HB. 2009. Blood lactate is an important energy source for the human brain. J Cereb Blood Flow Metab 29:1121–9.

189. White NJJ, Marsh K, Turner RCC, Miller KDD, Berry CDD, Williamson DHH, Brown J, Marsh K, Berry CDD, Turner RCC, Williamson DHH, Brown J. 1987. Hypoglycaemia in African children with severe malaria. Lancet (London, England) 1:708–11.

190. Taylor TE, Molyneux ME, Wirima JJ, Fletcher KA, Morris K. 1988. Blood glucose levels in Malawian children before and during the administration of intravenous quinine for severe falciparum malaria. N Engl J Med 319:1040–7.

191. Waller D, Krishna S, Crawley J, Miller K, Nosten F, Chapman D, ter Kuile FO, Craddock C, Berry C, Holloway PA. 1995. Clinical features and outcome of severe malaria in Gambian children. Clin Infect Dis 21:577–87.

192. Allen SJ, O'Donnell A, Alexander ND, Clegg JB. 1996. Severe malaria in children in Papua New Guinea. QJM 89:779–88.

193. Planche T, Agbenyega T, Bedu-Addo G, Ansong D, Owusu-Ofori A, Micah F, Anakwa C, Asafo-Agyei E, Hutson A, Stacpoole PW, Krishna S. 2003. A prospective comparison of malaria with other severe diseases in African children: prognosis and optimization of management. Clin Infect Dis 37:890–7.

194. Dzeing-Ella A, Nze Obiang PC, Tchoua R, Planche T, Mboza B, Mbounja M, Muller-Roemer U, Jarvis J, Kendjo E, Ngou-Milama E, Kremsner PG, Krishna S, Kombila M. 2005. Severe falciparum malaria in Gabonese children: clinical and laboratory features. Malar J 4:1.

195. Issifou S, Kendjo E, Missinou MA, Matsiegui PB, Dzeing-Ella A, Dissanami FA, Kombila M, Krishna S, Kremsner PG. 2007. Differences in presentation of severe malaria in urban and rural Gabon. Am J Trop Med Hyg 77:1015–9.

196. Seydel KB, Kampondeni SD, Valim C, Potchen MJ, Milner DA, Muwalo FW, Birbeck GL, Bradley WG, Fox LL, Glover SJ, Hammond CA, Heyderman RS, Chilingulo CA, Molyneux ME, Taylor TE. 2015. Brain swelling and death in children with cerebral malaria. N Engl J Med 372:1126–37.

197. van Niekerk DD, Penkler GP, du Toit F, Snoep JL. 2016. Targeting glycolysis in the malaria parasite Plasmodium falciparum. FEBS J 283:634–46.

198. Lopansri BK, Anstey NM, Weinberg JB, Stoddard GJ, Hobbs MR, Levesque MC, Mwaikambo ED, Granger DL. 2003. Low plasma arginine concentrations in children with cerebral malaria and decreased nitric oxide production. Lancet (London, England) 361:676–8.

199. Aveseh M, Nikooie R, Sheibani V, Esmaeili-Mahani S. 2014. Endurance training increases brain lactate uptake during hypoglycemia by up regulation of brain lactate transporters. Mol Cell Endocrinol 394:29–36.

200. Dienel GA. 2012. Brain lactate metabolism: the discoveries and the controversies. J Cereb Blood Flow Metab 32:1107–38.

201. Dienel GA. 2019. Brain Glucose Metabolism: Integration of Energetics with Function. Physiol Rev 99:949–1045.

202. Garcia-Alvarez M, Marik P, Bellomo R. 2014. Sepsis-associated hyperlactatemia. Crit Care 18:503.

Appendices

Appendix A: Software Used

Wolfram Mathematica 11.3 was used as the software platform to construct and analyse all iterations of the model. COPASI 4.25 was used to view the original specifications of XML-based models prior to import into Mathematica, and for viewing the original, unedited versions of models for validation purposes. These models were obtained in SBML-XML format through personal correspondence, or reproduced manually in Mathematica using published supplemental material and appendices.

A.1 PARVIO: The Common Structure of a Model

During the course of this thesis, a pattern was observed with regards to model structure that could be applied to any models that were to be incorporated into the final mathematical framework. This common pattern was termed ‘PARVIO’, an abbreviation of a series of components that consisted of parameters, assignments, rates (rate equations), variables, initial values, and ODEs.

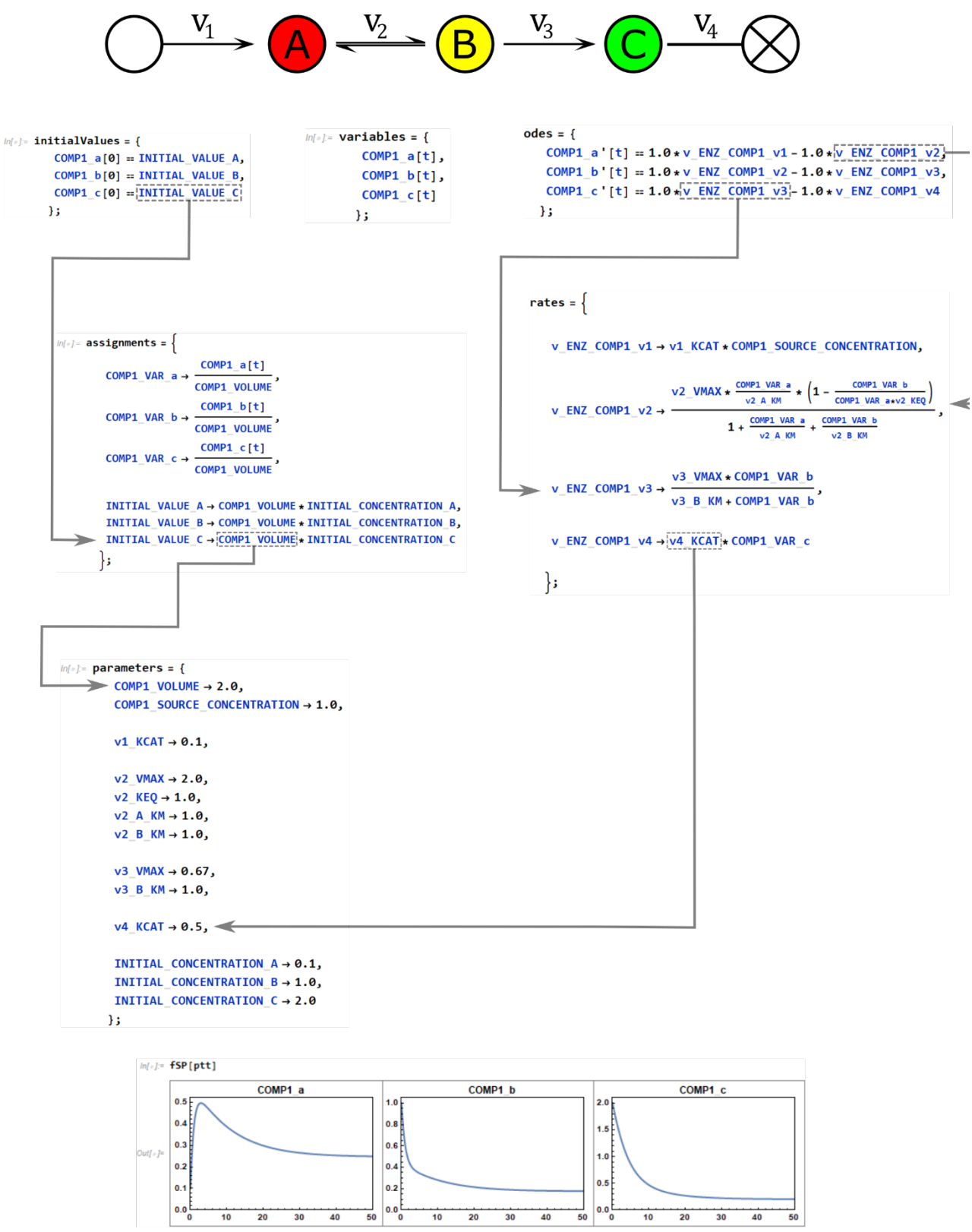

Figure A.1: Diagrammatical flowchart illustrating PARVIO structure. A simple model pathway (top) is described mathematically (middle), with the output plots shown (bottom). The components of PARVIO are all shown in list (curly bracketed) format: parameters, assignments, rates, initial values, and ODEs. Arrows indicate the order of substitution, whereby the components of complex expressions are replaced by their respective assignments or values as defined in the rates, assignments, and parameters (see text). The PARVIO is combined and passed as input to the NDSolve function (not shown), which finds a numerical solution to the equations specified in the ODEs. Finally, the output of this function is used to plot the timecourses of the metabolites A, B, and C.

This format was based on the template given as output by JWS Online's Mathematica notebook output feature, which gives the same components, albeit in a different order. The PARVIO format is mentioned and described here due to its ubiquity in the custom software written during model development, with all functions dealing with the model as a whole being programmed to recognise this specific, logical ordering of components.

Below, a brief explanation will be allotted to each PARVIO component.

A.1.1 Parameters

A *parameter* can be defined as a rule the replacement value of which is purely numeric, consists of a single entity, and does not require further substitution to achieve a numerical value.

The vast majority of parameters are used to provide the basic constants inherent in rate equations, particularly those describing enzyme kinetics. Common examples include values for parameters such as V_{max}, K_m, K_{eq}, K_i, K_a and the Hill coefficient n. Parameter rules can also be used to specify the initial concentration of a particular metabolite within a given compartment, from which its initial mass can be derived. Finally, parameters can also be used to specify important quantities that have substantial effects on the entire model, such as the percentage parasitaemia present in the blood, or the age or weight of an individual being simulated.

A.1.2 Assignments

An *assignment* falls in the grey area between parameters and rates. An arbitrary guideline used in the current research is that the right-hand side of an assignment expression can neither express a purely numerical quantity, nor a rate equation, enzymatic or otherwise. However, assignments fulfil an essential role by acting as aliases for frequently repeated, often complex expressions, or providing a logical chain of substitution rules that can make the structure of an otherwise complicated expression much easier to discern. The example below will be used to illustrate the utility of assignments.

First, let us consider the expression used to denote the molar concentration of glyceraldehyde 3-phosphate (GAP) in the cytosol of the infected red blood cell:

$$RBCi\_VAR\_gap \rightarrow \frac{RBCi\_gap[t]}{RBCi\_VOLUME}$$

At first glance, this appears to be a simple expression describing the concentration of a metabolite as its molar mass (*RBCi_gap[t]*) divided by the volume of its enclosing compartment (*RBCi_VOLUME)*. However, while the variable *RBCi_gap[t]* requires no further substitution, the value of *RBCi_VOLUME* is dependent on a number of subexpressions and parameters.

The volume of the infected red blood cell compartment *RBCi_VOLUME* denotes the total cytosolic volume of infected erythrocytes that is not taken up by the volume of the parasite. It is expressed as the product of two terms:

$$RBCi\_VOLUME \rightarrow RBCi\_CELL\_VOLUME\_FRACTION \cdot RBCi\_VOLUME\_FRACTION$$

Where *RBCi_CELL_VOLUME_FRACTION* denotes the volumetric fraction of an infected red blood cell that is not taken up by the trophozoite

$$RBCi\_CELL\_VOLUME\_FRACTION \rightarrow 1 - \frac{PF\_MISC\_volPFTroph}{RBCu\_MISC\_volRBCDefault}$$

And *RBCi_VOLUME_FRACTION* denotes the infected fraction of the total erythrocyte cytosolic volume

$$RBCi\_VOLUME\_FRACTION \rightarrow PF\_AUX\_PS \cdot RBC\_CYTOSOL$$

Where PF_AUX_PS indicates percentage parasitaemia. In turn, the total erythrocyte cytosolic volume *RBC_CYTOSOL* is derived from the subfraction of the blood plasma volume

$$RBC\_CYTOSOL \rightarrow RBCu\_MISC\_AlphaCellWaterFraction \cdot PLASMA\_HAEMATOCRIT \cdot PLASMA\_TotVolmL$$

Finally, the term *PLASMA_TotVolmL* is itself an assignment determined by a chain of assignment rules which ultimately depend on the age of the individual being simulated:

$$PLASMA\_TotVolmL \rightarrow 1000 \cdot PLASMA\_COMPARTMENT\_VOLUME\_LITERS$$

$$PLASMA\_COMPARTMENT\_VOLUME\_LITERS \rightarrow fAgeWeightBV[PLASMA\_AUX\_AGE]$$

This description is intended to show how the use of assignments can be used to delineate complex compound expressions into concise, logical, and easy-to-follow chains of components. Furthermore, while the list of assignments laid out above may seem exceedingly verbose, their necessity is perhaps best illustrated by how *RBCi_VAR_gap* would be expressed had only parameters been used:

$$\frac{RBCi\_gap[t]}{\left(1 - \frac{PF\_MISC\_volPFTroph}{RBCu\_MISC\_volRBCDefault}\right) \cdot (PF\_AUX\_PS \cdot [RBCu\_MISC\_AlphaCellWaterFraction \cdot PLASMA\_HAEMATOCRIT \cdot (1000 \cdot [fAgeWeightBV[PLASMA\_AUX\_AGE]])])}$$

In effort to preserve a modicum of brevity and legibility, the body of the function *fAgeWeightBV* is not included here.

Thus, the use of assignments to organise complex rate equations facilitates comprehension, expedites troubleshooting, and improves the ease of editing or modification.

A.1.3 Rates

The initial intuitive definition of a rate equation is an equation describing the kinetics of a single enzyme, as shown above. The left-hand side of the rate equation will subsequently be used to denote the derivative governing the turnover of the relevant metabolites as part of their respective ODE, for example:

```
{
 RBCu_sed7p'[t] == -v_ENZ_RBCu_TA + v_ENZ_RBCu_TK4,

 RBCu_gap'[t] == v_ENZ_RBCu_ALD - v_ENZ_RBCu_GAPDH - v_ENZ_RBCu_TA - v_ENZ_RBCu_TIM + v_ENZ_RBCu_TK2,

 RBCu_ery4p'[t] == v_ENZ_RBCu_TA - v_ENZ_RBCu_TK5,

 RBCu_f6p'[t] == -v_ENZ_RBCu_PFK + v_ENZ_RBCu_PGI + v_ENZ_RBCu_TA + v_ENZ_RBCu_TK6
}
```

(Note that transaldolase catalyzes the reaction *sedoheptulose 7-phosphate + glyceraldehyde 3-phosphate ↔ erythrose 4-phosphate + fructose 6-phosphate*)

A 'rate' can therefore be defined as any expression that appears on the right-hand side of an ODE equation, usually with a stoichiometric coefficient attached. Consider the following ODE equation for plasma glucose:

```
PLASMA_glucose'[t] == Total[{
   1.0*v_ENZ_PLASMA_GLUCOSE_FEED,
   -1.0*v_ENZ_PLASMA_GLUCOSE_UTILIZATION,
   -1.0*v_ENZ_HEPATIC_TRANSPORTER_GLUCOSE,
   -1.0*v_ENZ_PLASMA_TRNSP_GLC_PLASMA_FAT,
   -1.0*v_ENZ_PLASMA_TRNSP_GLC_PLASMA_MUSCLE,
   -1.0*v_ENZ_RBCu_TRNSP_PLASMA_GLC,
   -1.0*v_ENZ_RBCi_TRNSP_PLASMA_GLC
  }]
```

While most of the rate names refer to the activities of the transport proteins of their separate compartments, the terms *v_ENZ_PLASMA_GLUCOSE_FEED* and *v_ENZ_PLASMA_GLUCOSE_UTILIZATION* refer to broader processes which may not necessarily involve enzymatic activity, such as the rate of an intravenous glucose infusion or the combined activity of several organs which, while not under study, still have an important role in mediating plasma glucose turnover.

Each rate name will have a corresponding rule providing its matching rate equation, the latter of which is composed of a combination of assignments and parameters, as outlined above.

A.1.4 Variables

Variables constitute the least complex component of PARVIO. From a biochemical perspective, their utility is limited to simply listing the metabolites or species in the model that are subject to change. However, they form a compulsory argument of NDSolve, as the variables are the 'functions' that NDSolve computes a numerical solution for e.g. *x[t]* being a function of time.

A.1.5 Initial Values

As the name suggests, the initial values specify the numerical quantity that a variable assumes at the start of the computation when $t = t_{start}$ (more often when $t = 0$). While this may at first seem straightforward, the utility that can be extracted from different forms of the right-hand side of initial value equations should not be underestimated.

In simpler models where the values of variable are expressed in terms of concentration, the initial value of a metabolite can simply be equated to a number.

```
PLASMA_glucose[0] == 5.0
```

For ease of use, or when the procedural variation of the initial value is desired, a parameter value can be used instead.

```
PLASMA_glucose[0] == PLASMA_INITIAL_VALUE_glucose
```

Consider a multi-compartmental model whereby the numeric value of variables is expressed in millimoles, initial concentrations are specified in millimolar, and the volumes of the respective compartments are subject to change.

These changes can be easily accommodated via the use of assignment rules, which scale the initial mass of the metabolite as a function of the volume of its enclosing compartment, e.g.

```
PLASMA_INITIAL_VALUE_glucose → PLASMA_INITIAL_CONCENTRATION_glucose * PLASMA_COMPARTMENT_VOLUME
```

A.1.6 ODEs

The final part of the PARVIO is composed of ordinary differential equations, or ODEs. This involves one or more equations each of which specifies the time derivative of variable on the left-hand side, and one or more terms on the right. Within the context of PARVIO, each right-hand side term represents a rate, usually with a stoichiometric coefficient attached. While the stoichiometric coefficient can be safely omitted when its value is one, it is usually helpful to add a coefficient of 1.0 for the sake of consistency and readability.

A.2 Software Tools

A.2.1 Rate Visualisation

Models used in systems biology are written in code, whether this be in the form of standardised XML (e.g. Systems Biology Markup Language) that requires interpretation prior to simlation, or code that can be directly simulated in languages such as Python, MATLAB or Mathematica. Unfortunately, the programmatic depiction of mathematical expressions does not lend itself well to legibility, as the combination of forward slashes, asterisks, and nested parentheses can quickly accumulate to render previously elegant expressions almost indecipherable to the human eye. This problem is most often encountered when dealing with rate equations, which will typically contain the bulk of mathematical expressions used in a model.

A Graphical User Interface (GUI) based approach to viewing the structure of a model's rate equations becomes increasingly desirable as the size and complexity of the model grows. This is due to several reasons.

i. **Comprehension and legibility.** As described above, the programmatic implementation of mathematical expressions, especially intricate and complex expressions, can produce illegible lines of code that lend themselves more to misinterpretation and confusion than insight and understanding. Furthermore, attempting to edit and modify such code can quickly and easily lead to a frustrating experience attempting to find an obscure variable or a missing parenthesis. Fortunately, Mathematica has some built-in features that facilitate the neat expression of mathematical code, such as use of a division bar or superscript notation for exponents. With more lengthy expressions, however, these formatting measures are automatically abandoned by the program as it attempts to fit the entire expression within the limits of the display window.

ii. **Accessibility.** Model source code, especially that which has been recently imported from an online database or converted from another format, is usually not formatted or organised in such a way that particular parts of the model can be found in an easy or intuitive manner. For example, a new model may appear as one long, contiguous wall of text, lacking any line breaks or tab stops that delineate

separate components. Another difficulty is the lack of sorting or organisation, whereby lists of variables, rates and parameters are not sorted alphabetically (or according to any other ordering schema), making the identification of a particular variable a frustrating exercise in chance as one hopes that it lies close to wherever one chooses to start reading.

iii. **Troubleshooting.** The occurrence of human error becomes virtually unavoidable as the size and complexity of a model grows. This becomes especially problematic when the error is relatively minor and difficult to spot, such as accidentally entering a stoichiometric coefficient as negative instead of positive. Additionally, such missteps may not be readily apparent upon simulation, and can produce apparently sane outputs that are only identified as erroneous upon later, more detailed analysis. Unless the structure and composition of the model is presented in a clear, unambiguous manner, finding the error can become an intensely frustrating and laborious exercise.

With this rationale in mind, and considering the standardised PARVIO model structure described above, a GUI-based interface for viewing model rate equations should ideally have the following features:

i. **Standard mathematical format**. The mathematical expressions of the model should be parsed in such a way that the output resembles the notation used in scientific publications as closely as possible. This includes the use of fraction bars, superscript notation for exponents, and appropriate use of parenthesis. Additionally, redundant information should be omitted for brevity and conciseness. For example, should all of the variables and terms of a given rate equation begin with the same prefix, the prefix should be truncated to minimise the use of space.

ii. **Display of substrate, product and modifier stoichiometry.** Each rate equation will have at least one substrate or product with its associated stoichiometric coefficient. Most rate equations will have at least one substrate and one product, each with its own corresponding stoichiometric coefficient. However, some rate equations may have several substrates, several products, as well as modifiers mediating inhibition or activation. Thus, all of these variables should be presented in a way that clearly states their stoichiometric relationship with the rate in question.

iii. **Display of relevant assignments.** Owing to the essential and ubiquitous use of assignment expressions in the construction of rate equations, any assignment rules that form part of a rate equation should be presented alongside the information listed above. The right-hand side of the assignment rules should also be expressed in the same clear mathematical notation as that used for the rate equation. Additionally, since these assignments could be composed of their own sub-assignments, any and all relevant sub-assignments should also be included.

iv. **Display of relevant parameters.** Apart from stoichiometric coefficients, the quantitative properties and behaviour of every rate equation is ultimately dictated by the value of its associated parameters.

Thus, the name and value of every relevant parameter should be displayed. This includes any parameters that form part of the rate equation's assignments.

v. **Display of indexes.** Every non-numeric entity that forms part of a rate equation can be identified by its index, i.e. its sequential position in the model's source code once that latter has been sorted alphabetically. For example, the index of B in the sequence A, B, C will be 2.

vi. **Ease of navigation.** Navigating between different rate equations and/or compartments should be facilitated by use of a drop-down menu, a tab-based interface, or a combination thereof.

vii. **Efficient parsing and rendering.** As the model may contain hundreds of rate equations and assignments, each of which has to be processed individually, the process can become computationally expensive and slow. Thus, code should be optimised to minimise the time and resources spent.

Instead of showing the several hundred lines of code used to produce the GUI output shown in **Fig. A.3**, a terse, conceptual explanation will be given here, using **Fig. A.2** as an aid. First, since model development often involves small, iterative changes to a larger model, it is more expedient to check an existing, previously parsed array for changes, than to process an entirely new object from the beginning. Thus, the program first checks to see if any changes that would affect the final output are present. If an array already exists, and no changes are present, the program immediately provides the existing output. If changes are present, the program parses the input PARVIO into its irreducible components, and compares each of these with the existing array to detect any modifications, additions, or removals. These changes are recorded, and used as input for another function that makes the necessary changes to the existing array to produce an updated array that is subsequently submitted for rendering and output. In the case where no previous array is present, the program defaults to a routine involving the parsing and rendering of the relevant assignment and rate expressions, which can then be submitted for rendering and output.

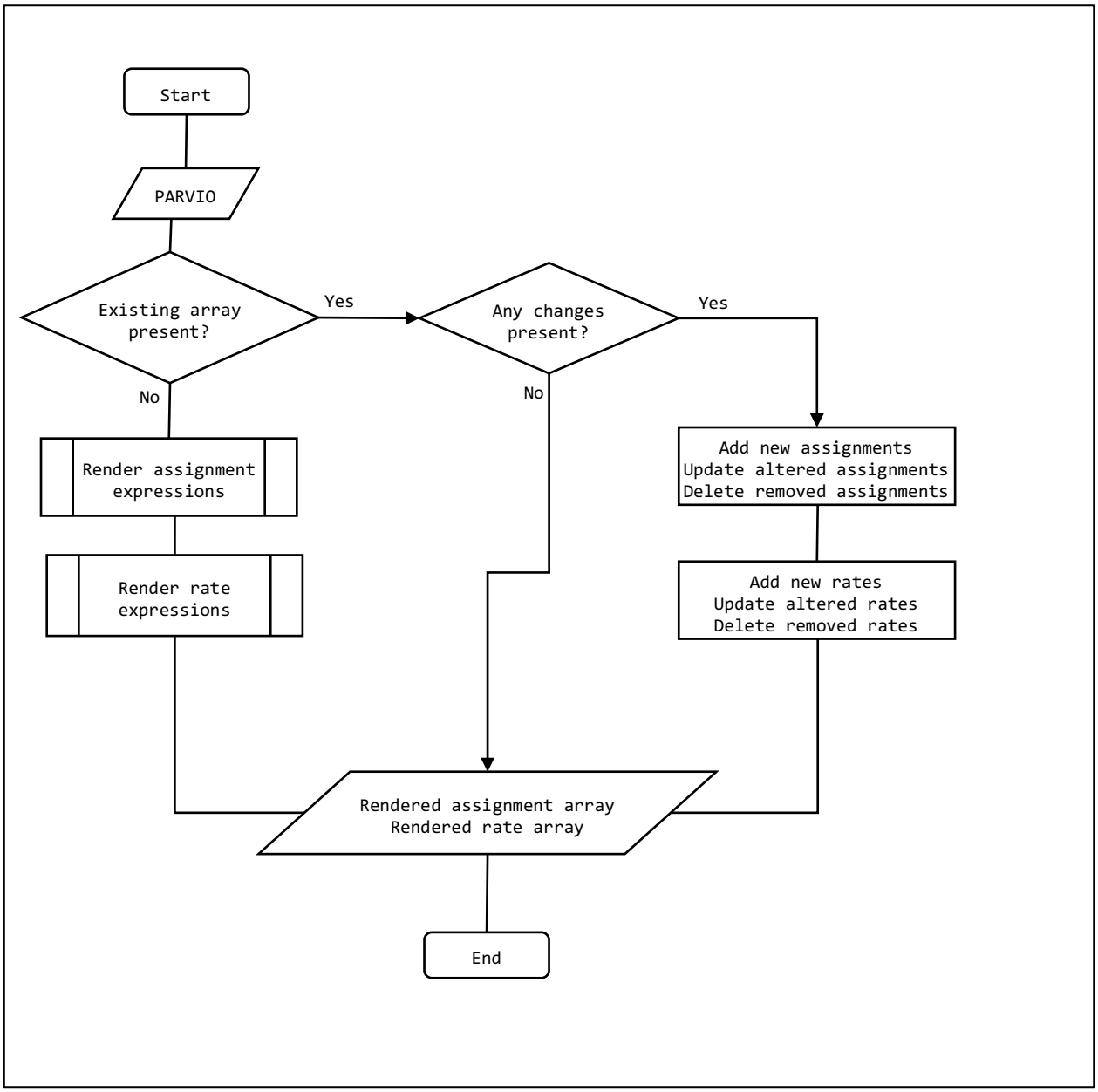

Figure A.2: Program flowchart for rate visualisation functions

The process of parsing and rendering individual assignment and rate expression involves converting the clear, legible mathematical format of the expression to an image file, which is subsequently viewed in the GUI interface. Furthermore, the parameters that form part of each expression, as well as their respective values, are parsed and displayed alongside the appropriate expression. Finally, the program also checks for any and all sub-assignments, in the case of nested, multi-level expressions that undergo several rounds of substitution.

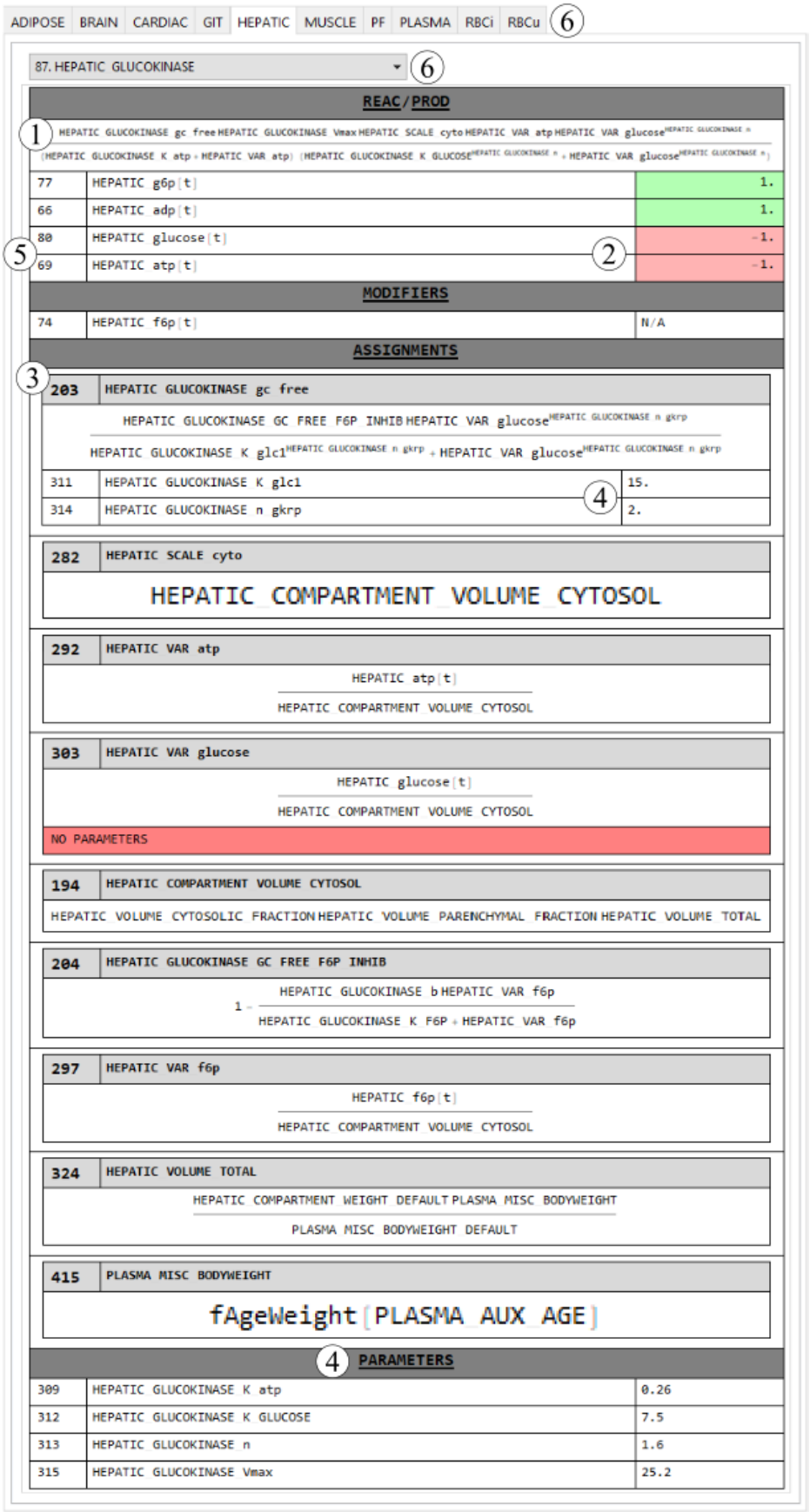

Figure A.3: Example output of the rate visualisation GUI. Label numbers are according to features listed above for a GUI-based interface for viewing model rate equations

A.2.2 Timecourse Visualisation

An integral part of computational systems biology is being able to view how variables change over time, whether these variables be concentrations of metabolites, the relative rates of fluxes, or the state of terms controlling rates dynamically as a function of other rate components. Practical examples would include examining how the concentration of glycogen within a system decreases over time in response to fasting; how the flux of a bidirectional transporter could change between positive and negative as the relative compartmental concentrations of its substrate change, and how plasma insulin levels rise as a result of increasing blood glucose concentrations.

The most common approach with regards to timecourse visualisation is the use of a variable vs time plot, a line graph depicting how the value of a given variable changes as a function of time. While this sounds straightforward, and is indeed relatively simple to implement in Mathematica, it comes with multiple caveats and nuances that, unless considered and addressed, will quickly frustrate the process of examining the model visually, especially once it starts to grow in size and complexity.

These issues became apparent early in the modelling process. As the number of metabolites, fluxes, and other dynamic entities grew, it was decided that the best course of action would be to code a rudimentary set of functions that could automatically discern the best way to present model components, while still being configurable by user input via a GUI. These functions have been modified and developed over time to form a suite of utilities that can effectively address the needs of routine model simulation.

It was found that the most suitable method for plotting simulation outputs was to do this on a per-species basis. In other words, for every dynamic variable, the corresponding output would include information regarding its identity, initial values, and plots of its change in magnitude over time, after which other elements would be parsed and displayed, specifically the fluxes responsible for dictating the turnover of that particular entity.

During the course of this thesis, several features were identified that would be useful in viewing the outputs of model simulations as part of a GUI-based approach. They are listed below:

i. **Easy identification of plotted variables**. Unless less than a handful of variables are being plotted, either on the same or separate graphs, it will be extremely difficult to discern which plot corresponds to which entity. While this concern may sound obvious, it can nevertheless quickly and unexpectedly emerge when visualising multiple entities, such as the concentrations of metabolites in a pathway. Thus, each plot should be accompanied by at least the name of the dependent variable, preferably accompanied by further information such as its index and compartment (if applicable). Furthermore, the minimum value of the y-axis should be defined as zero, since the magnitude of a given chemical species becoming negative indicates a fault or error in the model, and can be quickly discerned by the lack of a line within the plot region.

ii. **Concise display of relevant fluxes**. Similar to the utility of having the relevant substrates, products and modifiers shown as part of rate display, the ability to view the names, indexes and stoichiometry of the set of rates governing the turnover of a particular metabolite at a glance is similarly useful. The value of stoichiometric coefficients is particularly important, since this is not readily apparent as part of a plot.

iii. **Plotting species mass and concentration**. In cases where chemical species are not defined exclusively in terms of concentration, it is useful to be able to view plots of both the change in mass and concentration of a variable over time.

iv. **Plots of relevant fluxes**. The magnitude of each variable over time is a function of its associated inputs or outputs, or, in the case of biochemical models, the rates at which it is produced and consumed. Thus, the activity of the associated rates should be shown, complete with their indexes, names, and a means by which their relationship with the variable (i.e. positive or negative stoichiometric coefficients) can be discerned. Furthermore, since reversable reactions can freely change between positive and negative values, the range of the y-axis should be automatically configured to accommodate this, while still showing the position of the x-axis to discern the relative degree to which the rate becomes positive or negative.

v. **Ease of navigation**. Models can involve dozens, and sometimes hundreds of variables, some of which can be the same chemical species present in different compartments. Thus, the ability to quickly and easily navigate to a desired variable is essential.

vi. **Efficient computation and rendering**. Since multiple variables can depend on the same rate with the same stoichiometry, identical rate plots can potentially be produced repeatedly if outputs are generated on a per-variable basis. Therefore, when processing a list of variables, the code should render each unique rate plot only once, and then produce copies for each relevant variable. This optimisation becomes especially important with large, complex models, and can significantly reduce computation time.

As in **Section A.2.1**, a conceptual explanation of the programmatic implementation of timecourse visualisation will be given here, using **Fig. A.5** as a visual aid and **Fig. A.6** as an example output. Computation begins with the submission of a multi-level, nested array with three major components: the PARVIO, the numeric solutions for the ODEs specified in the PARVIO, and the upper bound of the time for which the solutions were obtained. Thereafter, the ODEs are parsed to identify all unique pairs of stoichiometric coefficients with their accompanying rates, since each of these pairs will be plotted at least once as part of the final output. This identification of unique pairs is part of the optimisation process described in feature 6, above.

To illustrate, let us consider the case of v_2 in **Fig. A.1**. This rate affects the amount of metabolites A **and** B, thus the respective GUI output for each of these variables will both contain a plot of v_2. In the case of metabolite A, v_2 has a negative stoichiometric coefficient, and a positive one in the case of metabolite B. This will thus produce two different plots of the same rate each with the appropriate stoichiometric coefficient. However, let us consider a situation with a hypothetical metabolite D, that is also formed by v_2, uses metabolite A as substrate, and has the same set of stoichiometric coefficients (**Fig. A.4**). A practical example of this would be the reaction catalysed by aldolase (shown in **Fig. 3.3**). In this case, the same coefficient and rate pair would appear in the ODE equations for both metabolites B and D. If optimisation were not implemented, v_2 would be parsed and plotted twice, producing two plot objects, one each for the GUI outputs of metabolites B and D. However, if this duplication were detected beforehand, as has been implemented in code, then the coefficient-rate pair would only need to be parsed and rendered once, thus saving on computational burden and time. A similar process is also applied when parsing the numerical values of the rates themselves before multiplication with the stoichiometric coefficient, but this will not be discussed here. Thus, when working with large, complex models with many branch points, such optimisation can significantly reduce the time taken to render simulation results and expedite analysis.

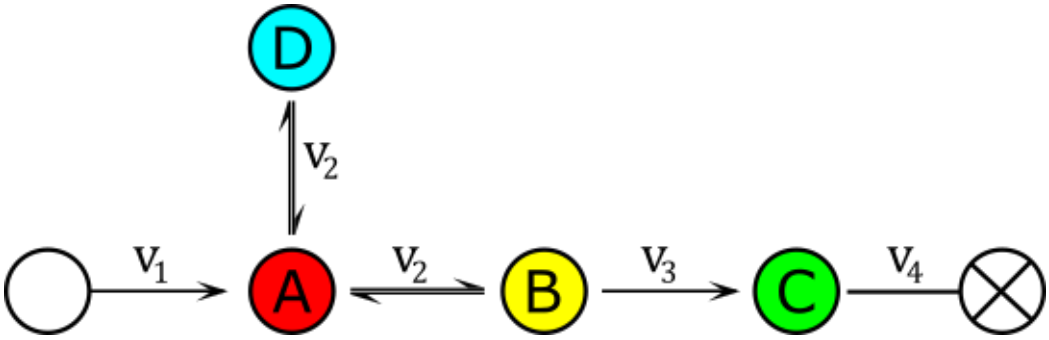

Figure A.4: Example schema of a branched pathway with rate duplication.

Once all unique coefficient-rate pairs have been identified, they are each parsed, rendered and plotted once, and allocated to an array. Thereafter, the plotting process is repeated for the mass and concentration timecourses of all dynamic variables, which are allocated to their own, separate array. With these two arrays in place, the GUI output can be constructed for each dynamic variable, with the relevant rate plots being accessed from the previously constructed array. These GUI outputs are grouped by the compartment the variable belongs to, and the final result is displayed, as shown in **Fig A.6**.

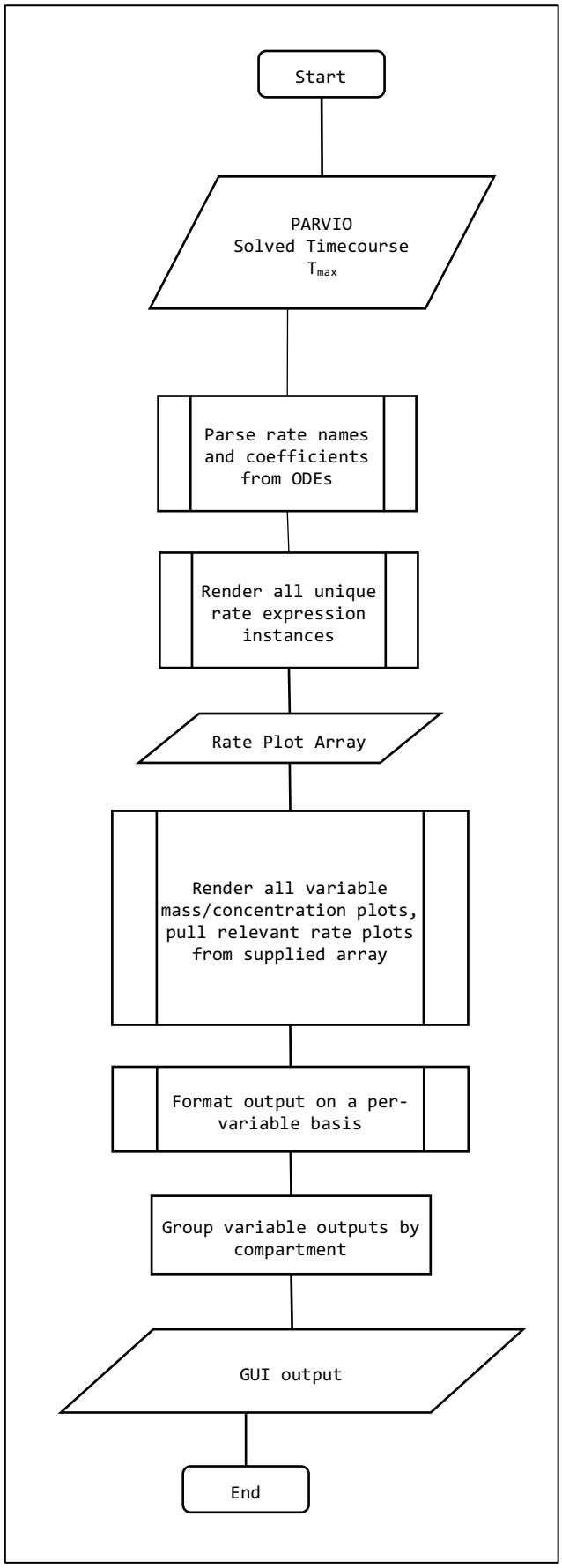

Figure A.5: Program flowchart for timecourse visualisation functions

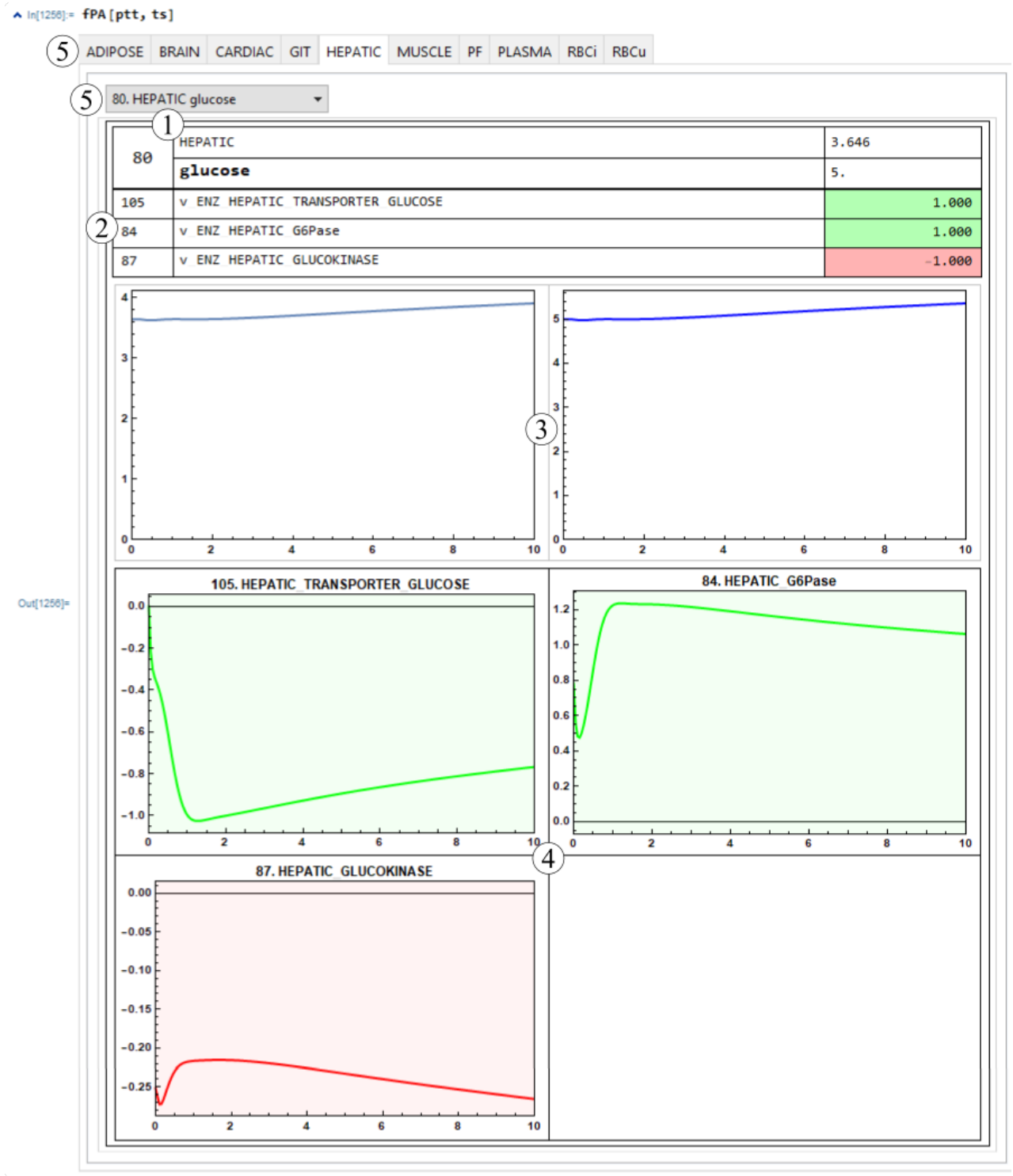

Figure A.6: Example output of the timecourse visualisation GUI. Label numbers are according to features listed.

A.2.3 MCA

The process of carrying out large scale metabolic control analysis (MCA) was a challenging one, and it is fortunate that this undertaking occurred towards the end of thesis development, when the level of

programming proficiency was at its highest. The primary source of difficulty was not necessarily the calculation of the sensitivity coefficients themselves, indeed, this could be accomplished with a simple, terse function:

```
Clear[fMCACRDU];
fMCACRDU[xWT_?NumericQ, xD_?NumericQ, xU_?NumericQ, pertFactor_Real:0.01] := If[
  PossibleZeroQ[xWT],
  Return[0],
      (xU - xD)
  ----------------
  2 * pertFactor * xWT
];
```

This function first checks to see if the wild-type denominator is zero, in which case it returns zero as output. Otherwise, it returns a sensitivity coefficient as described in Section 2.7.2

For analysing the control coefficient of a single rate expression, or the response coefficient of a single parameter, the process is fairly straightforward:

i. Provide a wild-type PARVIO, solved timecourse, and t_{end} as input. This will usually already be present during the course of routine model simulations.

ii. Determine the wild-type steady-state values for all rate expressions and chemical species. This is usually a quick and easy task, accomplished by simply substituting the relevant expressions with the variable masses obtained at $t = t_{end}$.

iii. Construction of a base argument containing all components that are not subject to perturbation. Since only a single model entity is to be perturbed, the set of ODEs and initial conditions can be substituted with the remainder of the replacement rules, thereby leaving only a single entity to be replaced prior to each analysis.

iv. Pre-allocation of steady-state flux and variable arrays. For each dependent entity (for example, a flux or variable concentration), an array is allocated with the following elements:

$$\{ \quad \{ \textit{index, name} \} \quad y_{wt}^{ss} \quad y_{\downarrow}^{ss} \quad y_{\uparrow}^{ss} \quad c_x^y \quad \}$$

The index, name, and steady-state wild type value will already be supplied from step 2, the remainder of the array elements will be set to 0 by default. This sub-array forms the elements of two larger arrays, one for all rate expressions, and one for all variables.

v. Computation of numerical solutions of steady-state values for variables following perturbation. Using the double perturbation method, two arguments are created from the base argument, each supplied with a fractionally increased and decreased model entity, respectively. These arguments are subsequently solved at steady-state.

vi. Retrieval of steady-state flux and variable values. The third and fourth array elements of the sub-array shown in step 4 are stored in memory, their values derived from substitution of the relevant entities by the steady-state variable masses obtained in step 5.

vii. Computation of sensitivity coefficients. With all of the requisite elements present, the final element of the sub-array, the control or response coefficient, can be calculated for each flux or variable.

However, this is only the computation required for a *single* perturbed rate or parameter. Should one wish, for example, to carry out MCA on all the rates or parameters of a model, the computational burden becomes substantially heavier. To illustrate, the current model at the time of writing has the following dimensions:

```
In[1208]:= fReportPRV[prvF]
          PARVIO dimensions
          ------------------
          Parameters      : 1422
          Assignments     : 1003
          Rates           : 266
Out[1208]= Variables      : 251
          Initial Values  : 251
          ODEs            : 251
```

Obtaining a numerical solution for the wild-type model takes approximately 1.5 seconds to complete:

```
In[ ]:= NDSolve[arg, varF, {t, 0, tmaxSS}][[1]]; // AbsoluteTiming
Out[ ]= {1.47059, Null}
```

Note that this does not include any other processes, such as argument substitution or determination of steady-state values of model entities.

Since computation of a numerical solution usually takes up the bulk of computation time, let us assume a conservative estimate of 2.5 seconds for completion of steps 1-7 described above, doubling this value to 5 seconds to account for the double perturbation. Therefore, using these values, we can calculate the length of time required to sequentially conduct MCA by perturbing all 266 rates of the model, which comes out to 22 minutes and 10 seconds.

```
In[ ]:= QuotientRemainder[(266 * 5.0), 60]
Out[ ]= {22, 10.}
```

Furthermore, assuming that the list of parameters selected for response analysis was reduced to a more reasonable length of 900, computation would be of the order of 75 minutes.

```
In[ ]:= QuotientRemainder[(900 * 5.0), 60]
Out[ ]= {75, 0.}
```

While such computation times may seem acceptable, and even reasonable when compared to the amount of time effort required by some laboratory processes, they nevertheless remain very undesirable, for two important reasons. First, Mathematica does not permit more than one evaluation on the same kernel, meaning that one could not proceed with other work while the computation is running. Secondly, and perhaps most importantly, these computations are done at a single percentage parasitaemia. Since this thesis is interested in the metabolic dynamics across a range of parasitaemias, the multiplicative total time required would be prohibitively lengthy.

Fortunately, however, this issue can be mostly overcome using parallel computation. Mathematica possesses built-in functionality for use of multi-core central processing units, whereby computations can be evaluated in parallel across multiple CPUs. The combination of CPUs can provide a platform of multiple kernels, with each kernel being able to process one evaluation at a time. On the machine used to conduct most of the analysis, 16 kernels were available. Thus, using parallel computation, the time required for obtaining numerical solutions could be reduced by a factor of 16.

To implement this, during computation the program was instructed to pre-allocate a *m* by *n* array, with *m* being the number of entities perturbed and *n* representing the number of perturbations per entity, usually two (one increase, one decrease). This array, as well as the base argument, list of perturbations, and other data required for computation, was distributed across all kernels. Each kernel was then instructed to obtain a numeric solution for a perturbed model with perturbed entity *i* and perturbation (up or down) *j*, independently of the other kernels, and store this solution at array address (*i, j*). The possibility of two different kernels parsing the same element was eliminated by the distribution (sharing) of the array across all kernels simultaneously. Additional code was also written to be able to monitor the progress of the computation on each kernel and as a whole, in case any errors occurred during computation (**Fig. A.7**).

```
controlArray = fMCAcontrol[pttSS, {}];
PARVIO dimensions
Parameters      : 1423
Assignments     : 1003
Rates           : 266
Variables       : 251
Initial Values  : 251
ODEs            : 251
PF AUX PS       : 1.×10^7
PLASMA AUX AGE  : 18
00:02:42 [DONE] Determining wild-type steady-state values.
00:26:57 Parsing 532 timecourses.

11% [ 60 / 532 ]

Kernel  Rate
1       v ENZ HEPATIC NDK UTP
2       v ENZ HEPATIC GAPDH
3       v ENZ HEPATIC F16BP
4       v ENZ HEPATIC ALDOLASE
5       v ENZ GIT TRNSP CARBON DIOXIDE
6       v ENZ GIT GRP TG
7       v ENZ GIT ACOA COA
8       v ENZ CARDIAC PYR ACOA
9       v ENZ CARDIAC GLR GRP
10      v ENZ CARDIAC FA ACOA
11      v ENZ BRAIN TRNSP LACTATE
12      v ENZ BRAIN O2 H2O
13      v ENZ BRAIN G6P GA3P
14      v ENZ ADIPOSE TRNSP LACTATE
15      v ENZ ADIPOSE GRP TG
16      v ENZ ADIPOSE FA ACOA
```

Figure A.7: Example dynamic output monitoring the progress of control coefficient calculation

Once the numerical solutions had been obtained, the program proceeded to obtain the perturbed, steady-state values of fluxes and chemical species concentrations, perform the relevant sensitivity calculations, and return these as a structured array ready for formatting and visual display (**Fig. A.8**).

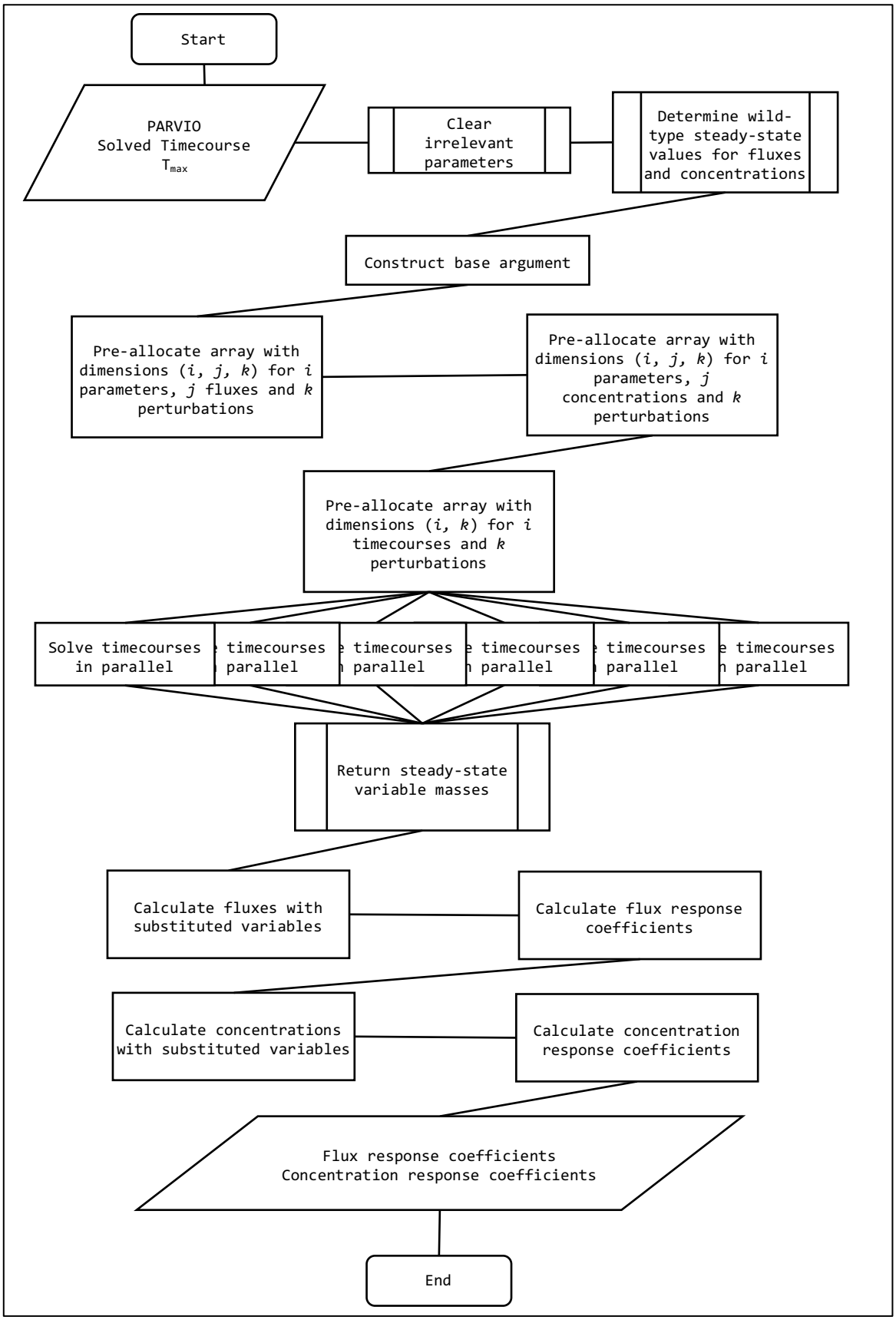

Figure A.8: Program flowchart MCA functions obtaining response coefficients

Appendix B

B.1 Rank-based Metabolic Control Analysis

Considering the size of the model, in particular the large number of rates and parameters, a rank-based approach was implemented when identifying the most significant sensitivity coefficients with regards to steady-state concentrations of plasma glucose and lactate. This involved calculation of both control and response coefficients for all rates and parameters at regular percentage parasitaemia intervals. For each percentage parasitaemia, the control and response coefficients were ranked in descending order according to their absolute value. Thereafter, coefficients were selected with the criteria that they each appeared at least once in the top ten highest ranked coefficients for any of the percentage parasitaemias simulated. Using this method, 19 and 24 rates were selected as having significant control over steady-state glucose and lactate concentrations, respectively. For response coefficients, 32 parameters were found as having significant response coefficients with regards to the steady-state concentration of plasma glucose, and 34 for the steady-state concentration of plasma lactate.

Each set of control or response coefficients for plasma glucose or lactate were then ranked again, based on the area under the curve when plotting the coefficient against the percentage parasitaemia at which it is obtained; plots of the hepatic rates exhibiting significant control on plasma glucose and lactate concentration are shown below. For each plot, the alphabetical position of the rate is shown in the title on the left, with its ranking in parenthesis on the right. The plot markers themselves indicate whether the coefficient obtained at the relevant percentage parasitaemia is positive (green) or negative (red). This visual representation shows how the magnitude of a particular coefficient changes as a function of parasite burden.

B.1.1 MCA of the Hepatic Compartment

As shown by the results presented below, the hepatic lactate transporter displayed strong positive and negative control over steady-state plasma glucose and lactate concentrations, respectively. The hepatic compartment yielded two rates with significant control coefficients across all data sets: the lactate transporter, ranked 13th, and glucokinase, ranked 19th (**Fig B.1**). Lactate transport exerted generally increasing positive control over plasma glucose as parasitaemia increased. Glucokinase activity showed a trough at approximately 2% parasitaemia, followed by a maximum at roughly 7% parasitaemia.

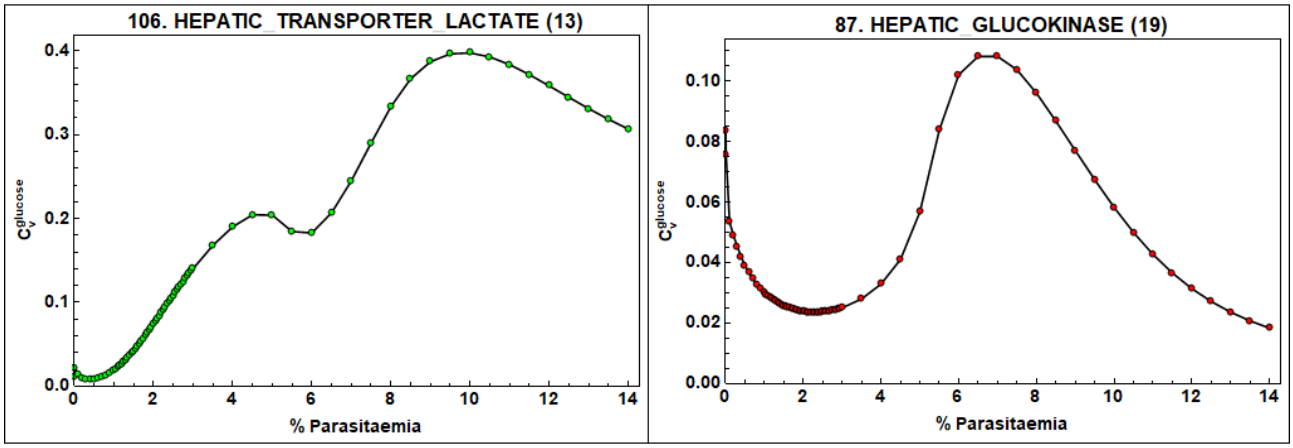

Figure B.1: Significant plasma glucose control coefficients obtained from rate expressions in the hepatic compartment. Green markers indicate positive control, red markers indicate negative control

The hepatic compartment yielded a single significant control coefficient on plasma lactate, specifically that relating to the rate of transport of lactate into and out of the hepatic compartment (**Fig. B.2**). The control exhibited by this rate has an initial maximum in the uninfected state, which declines and reaches a second, lower peak at approximately 1% parasitaemia, thereafter decreasing rapidly.

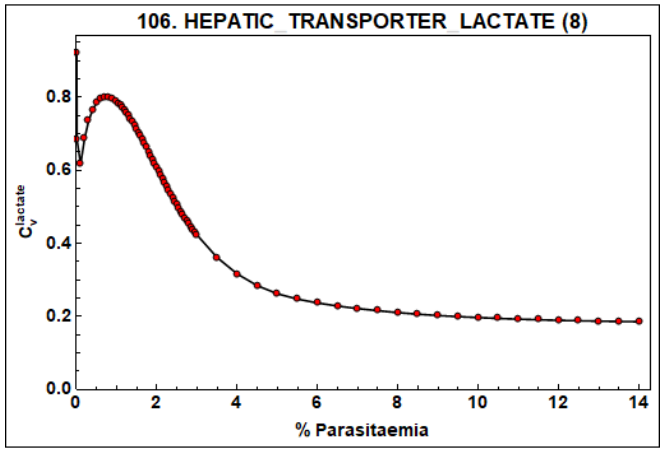

Figure B.2: Significant plasma lactate control coefficients obtained from rate expressions in the hepatic compartment. Red markers indicate negative control

B.2 Metabolic Contribution of Other Organs

The concomitant presence of both hypoglycaemia and hyperlactataemia in patients with severe *P. falciparum* malaria appears paradoxical at first. Considering the fact that lactate usually accounts for over half of all gluconeogenic substrates in the healthy individual (43), the occurrence of low blood sugar despite the overabundance of this precursor points to a fault in the host's gluconeogenic capacity. Indeed, the most intuitive and elegant situation in this regard would be to rectify the host's limited capacity to convert lactate to glucose, thereby solving both problems at once. Since the liver is known to carry out the majority of gluconeogenesis under normal circumstances, it was initially hypothesized that both the cause of, and solution to, simultaneous hypoglycaemia and lactic acidosis would be explained by aberrations of hepatic function. Having examined and investigated the hepatic compartment in detail, and showing that, even with

the presence of phenomenological parasite inhibition mechanisms, it is still capable of maintaining considerable levels of gluconeogenesis, we now turn to examination of the remaining compartments.

B.2.1 Brain Metabolism

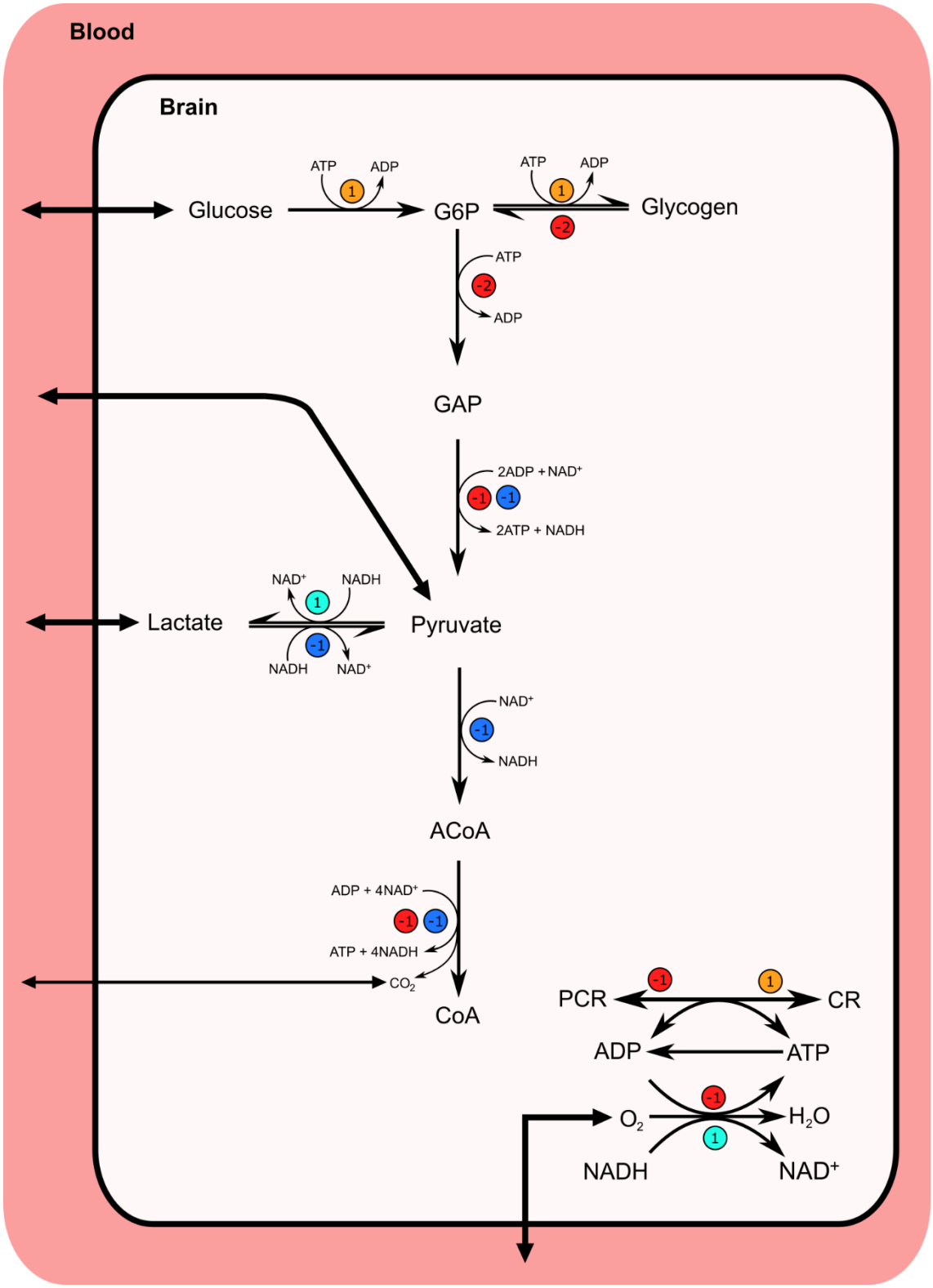

Figure B.3: Pathway diagram of brain carbohydrate metabolism as described in the model.

The relative contributions of the various compartments to plasma lactate turnover are shown in **Figure B.4**. The graph for infected erythrocyte lactate flux appears similar to that of glucose, with export of lactate into plasma increasing as what would appear to be a slightly hyperbolic function of percentage parasitaemia. Removal of lactate from plasma by the liver appears to remain almost static at 20% across all significant parasitaemia values. Renal excretion of lactate shows a sigmoid relationship with increasing parasitaemia, reaching a plateau of approximately 13% at around 10% parasitaemia. The respective graphs for lactate export and import by the muscle and brain compartments appear roughly equal and opposite, with initial values of 30-35% declining to around 20% at maximal parasitaemia. At lower levels of parasitaemia, these results place the brain ahead of the liver in terms of the contribution to plasma lactate uptake.

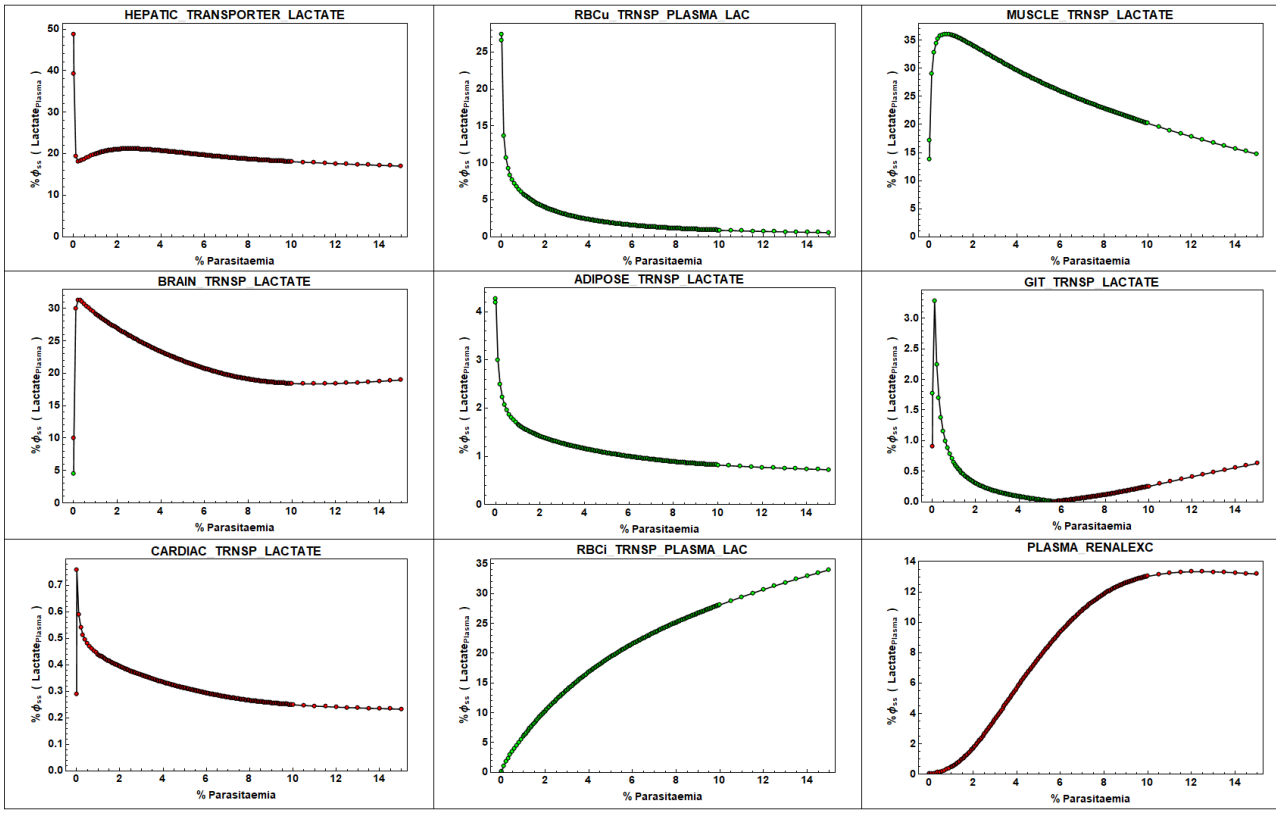

Figure B.4: Relative contributions of fluxes to plasma lactate concentration at steady state. Calculations and colour schemes are identical to Fig. 4.5.

The discovery that the brain was not only a net importer of lactate, but accounted for the majority of lactate clearance upon infection (**Fig. B.4**), was very unexpected. As stated in the literature review, the contemporary consensus surrounding whole-body lactate clearance attributes the overwhelming majority thereof to the two major gluconeogenic organs, the liver and kidney, with the heart a distant third. However, while this is generally the case under typical, resting conditions, the brain is capable of importing lactate when its plasma concentration becomes substantially elevated; this influx of lactate can provide up to 30% of cerebral energy requirements via eventual oxidation through the TCA cycle (199–202). The dearth of discussion regarding cerebral lactate uptake is likely due to both its characterization as an organ that exclusively prefers oxidative carbohydrate catabolism, and the uncertainty and debate surrounding the exact mechanisms of neuronal lactate metabolism (200, 201).

To further investigate the influence of brain metabolism on plasma glucose and lactate concentrations, we can consider the results obtained from metabolic control analysis.

Four rates from the brain compartment produced control coefficients that were deemed significant with regards to plasma glucose. Three rates exerted negative control over plasma glucose, namely hexokinase, phosphocreatine hydrolysis and ATPase activity, ranking 4th, 11th, and 14th, respectively (**Fig. B.5**). The remaining rate, denoting phosphocreatine synthesis, exhibited positive control, and was ranked 12th.

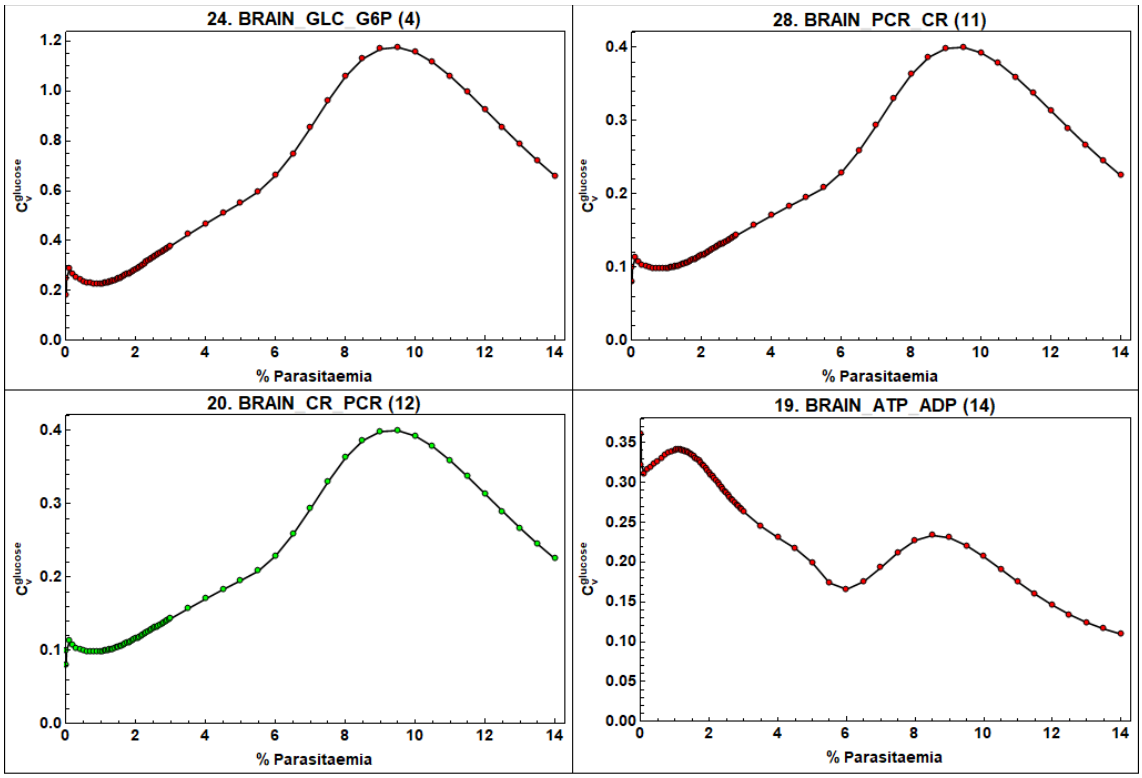

Figure B.5: Significant plasma glucose control coefficients obtained from rate expressions in the brain compartment

Six rates from the brain compartment were identified as having significant control over plasma lactate, with brain ATP hydrolysis and hexokinase ranking first and third for highest control overall (**Fig B.6**). Furthermore, all six rates featured ATP as either substrate or product; whether ATP was produced or consumed as part of the reaction did not appear to predict whether the resultant control would be positive or negative. A notable feature of these trends is the 6-8% percentage parasitaemia at which a minimal plateau is reached; the control coefficients obtained for plasma glucose for the corresponding rates initiate a steep upwards slope at this approximately this same interval. Of interest is the change in sign of response at approximately 11% parasitaemia for the two reactions mediating phosphocreatine turnover.

In addition to the flux observations, the significance of brain metabolism in mediating plasma glucose and lactate levels can be inferred from MCA results. Brain hexokinase activity displayed significant negative and positive control over steady-state plasma glucose and lactate levels, respectively (**Figs. B.6 & B7**). These findings underscore the brain's continued reliance on glucose as a metabolic fuel, despite the metabolic aberrations wrought by increasing parasitaemia.

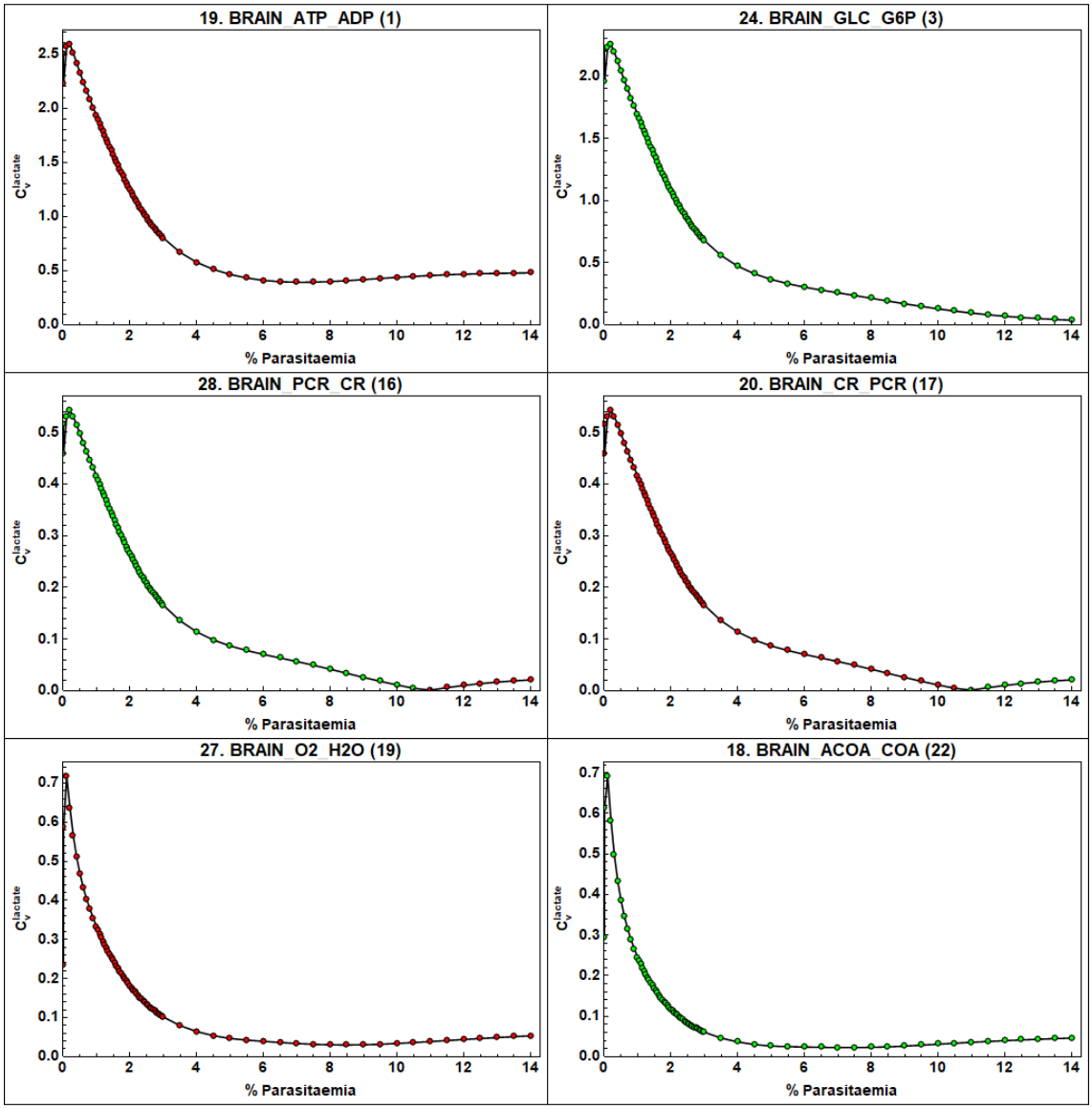

Figure B.6: Significant plasma lactate control coefficients obtained from rate expressions in the brain compartment. Note the switch from positive to negative response at approximately 11% parasitaemia for phosphocreatine flux.

When examining the sensitivity of plasma lactate to model components in the brain compartment, a pattern emerges that points towards the importance of the brain's use of lactate as a supplemental fuel. Oxidative phosphorylation exerts negative control over plasma lactate, while TCA cycle activity shows positive control (**Fig. B.6**). Additionally, substrate affinity parameter responses for plasma lactate are positive in the case of phosphate in oxidative phosphorylation, and negative for phosphate and acetyl-CoA in TCA cycle activity (**Fig. B.7**).

Response coefficients obtained from brain parameters with regards to lactate share an early peak at low levels of parasitaemia (**Fig. B.7**). The substrate affinity constant for ATP in cerebral ATPase activity ranks particularly high, showing positive response. The remainder of the positive response coefficients are relegated to phosphate's Michaelis-Menten constants of ATP for oxidative phosphorylation and creatine for phosphocreatine synthesis. Negative response coefficients all rank lower in comparison, particularly with regards to the affinity constants of phosphate and acetyl-CoA in the cerebral TCA cycle.

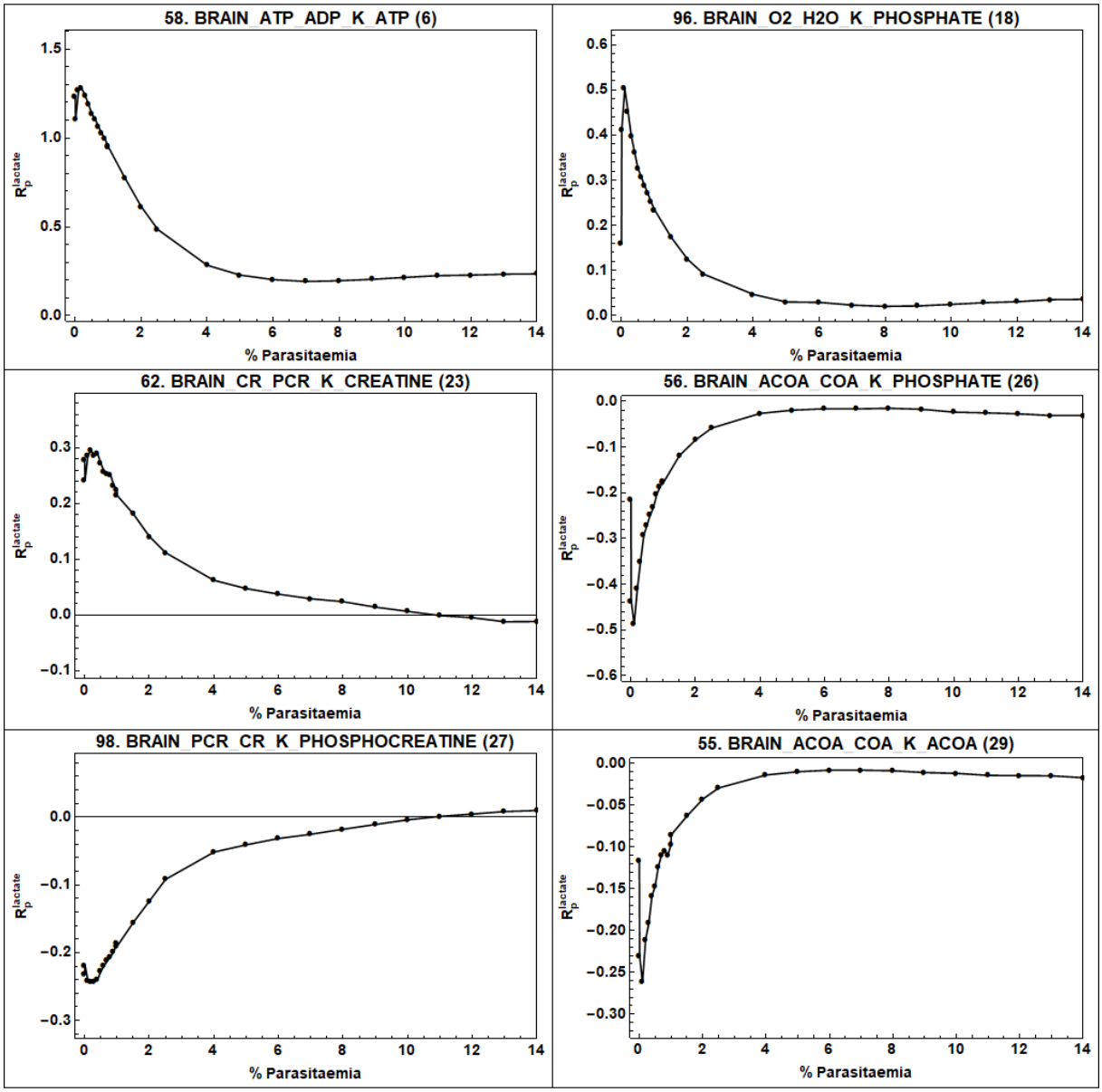

Figure B.7: Significant plasma lactate response coefficients with regards to parameters comprising kinetic expressions located in the brain compartment.

Affinity constants, in this case the K_M values for phosphate and acetyl-CoA, having a negative response coefficient with respect to plasma lactate indicate that the brain TCA cycle activity is proportional to steady-state plasma lactate concentrations. These findings agree with the positive control coefficient of TCA cycle activity, since an increased K_M translates to reduced substrate affinity, which results in decreased reaction velocity. How do these results translate to an increased steady-concentration of plasma lactate as TCA cycle activity increases? For an irreversible reaction at steady state, the substrate concentration is inversely proportional to the maximal rate velocity, since as V_{MAX} increases, the amount of substrate required to produce a flux equal to adjacent reactions decreases. Thus, as the steady-state concentration of acetyl-CoA decreases with increasing steady-state TCA cycle flux, so, too, does the amount of pyruvate. Therefore, the dependence of TCA cycle activity on pyruvate decreases, and the system becomes less reliant on the import and oxidation of lactate.

The negative control coefficients of the ATP hydrolysis and oxidative phosphorylation reactions for both glucose and lactate support this line of evidence. ATP hydrolysis activity produces ADP and phosphate, two substrates required for TCA cycle activity. Thus, as the activity of these two processes increases, the demand for acetyl-CoA, pyruvate, and lactate increases, resulting in increased lactate uptake from the plasma compartment. Oxidative phosphorylation activity's negative control coefficient could likely be due to its provision of ATP for subsequent hydrolysis; its lower rank (19^{th} vs 1^{st} for ATP hydrolysis) supports the notion of its indirect negative control.

Besides net lactate import, another unexpected behaviour was observed during model simulations: net pyruvate export by the brain. Simulations show that, in the infected state, pyruvate export from the brain into the plasma compartment accounts for approximately 30% of negative pyruvate flux at steady state. This behaviour could perhaps be explained by the system attempting to favour the oxidative component of LDH activity by mass action, thereby providing additional NAD^+ that can be used as part of TCA cycle activity.

The results obtained from this model therefore indicate that the brain plays a significant function in limiting the rise of plasma lactate to pathologically high levels, through its use of lactate as a supplemental fuel during hypoglycaemia. This result was unexpected, and could possibly be a result of how the model was structured, rather than a physiological reality. Nevertheless, further investigation determining the significance and validity of these results is certainly warranted.

B.2.2 The Involvement of Skeletal Muscle

Skeletal muscle proved to be a difficult compartment to model within the context of this thesis. Even within the generalized, simplified framework of Kim et al.'s (16) description, carbohydrate, protein, and lipid metabolism are included (**Fig. B.8**). As explained in the methods section, only pathways directly involving glucose catabolism could be included, thereby precluding the model from analysing the dynamic behaviour and effect of noncarbohydrate metabolism in skeletal muscle. The possible dynamic interactions of muscular protein and lipid metabolism with the altered levels of plasma glucose and lactate would have been interesting to determine. However, having recognized these limitations, several conclusions can still be drawn from the data available.

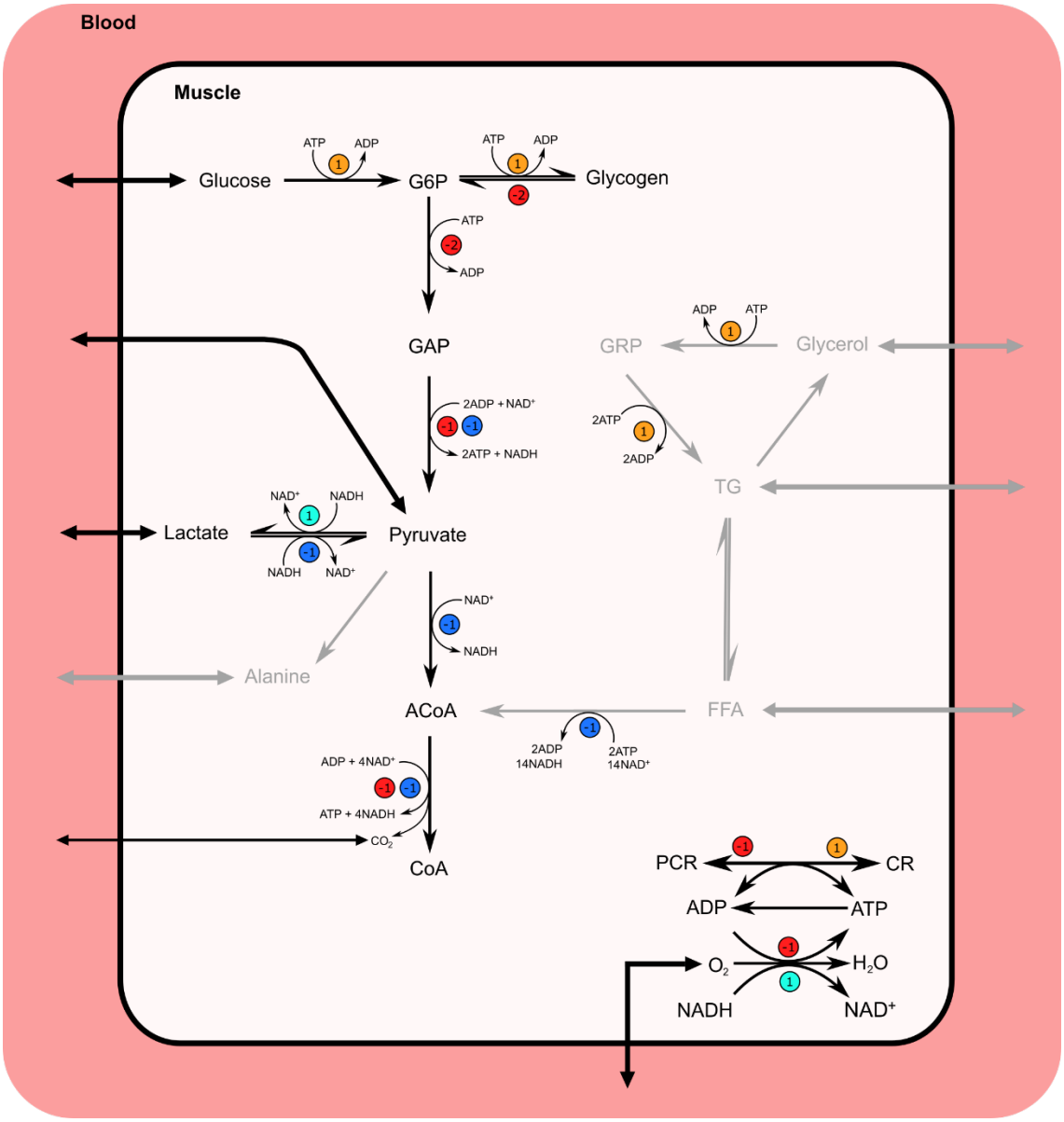

Figure B.8: Pathway diagram of muscle carbohydrate metabolism as described in the model. Grey species and rates denote clamped variables and processes.

Skeletal muscle is a metabolically complex organ capable of utilizing numerous pathways for free energy production under different physiological states. A comprehensive review of the endpoints of muscular glucose metabolism can unfortunately not be included here, and therefore it was considered reasonable to assume here the reductionist view that, in both healthy and diseased states, skeletal muscle is generally a net exporter of lactate, exhibiting a preference for anaerobic glycolysis over oxidative catabolism.

Use of such a simplified view is indeed propitious when considering the observations showing skeletal muscle's substantial contribution to plasma lactate levels, particularly in response to increasing parasitaemia. Simulations show an approximate 15% increase in skeletal muscle's contribution to plasma lactate flux from the healthy state to nascent infection (**Fig. B.4**, 0.1% parasitaemia).

As a whole, the simulation results for the skeletal muscle compartment indicate a strong preference for anaerobic glycolysis over the alternative processes of glycogen synthesis or oxidative catabolism. Skeletal

muscle exhibits net import of glucose and pyruvate, and net lactate export, demonstrating lactate to be the favoured metabolic terminus. Hexokinase activity, the process responsible for committing glucose to muscle compartment metabolism, shows strong negative and positive control over plasma glucose and lactate, respectively (**Figs. B.9 & B.10**).

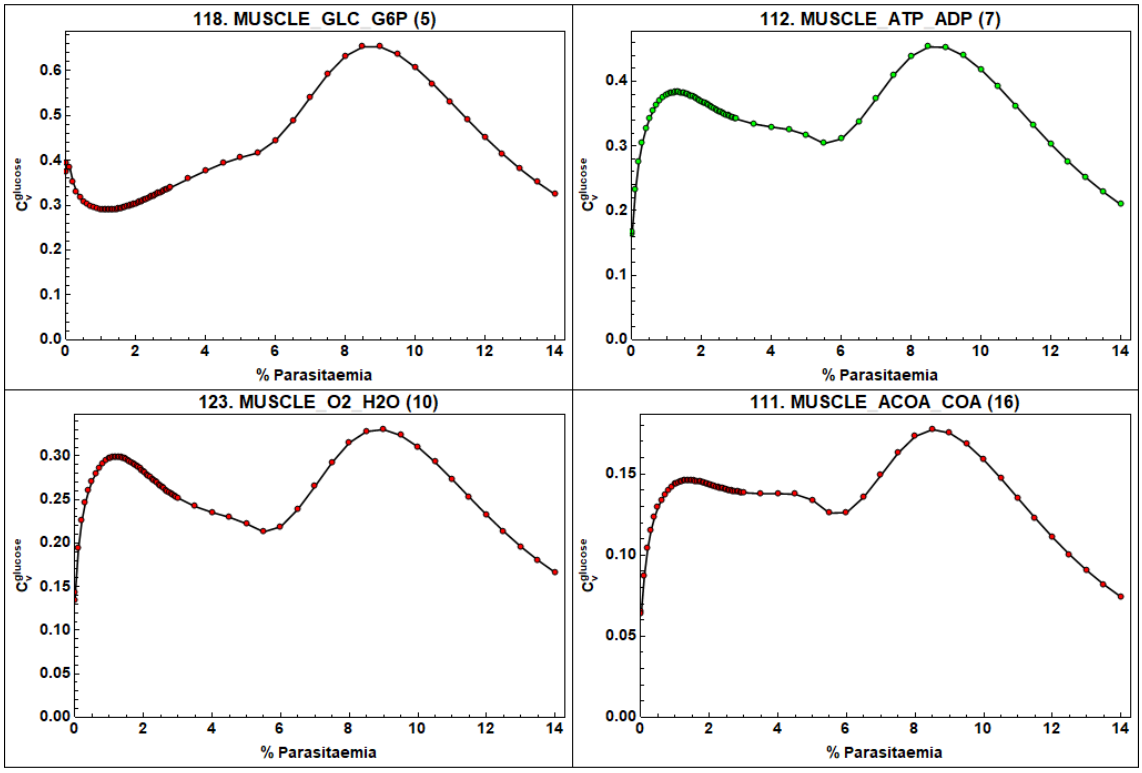

Figure B.9: Significant plasma glucose control coefficients obtained from rate expressions in the skeletal muscle compartment

The collection of rates in skeletal muscle exerting significant control over plasma glucose appeared to cover the entirety of oxidative glucose catabolism, and showed particularly similar trends, with the shapes of the graphs becoming near identical above 6% parasitaemia (**Fig B.9**). Negative control was observed for initial glucose phosphorylation and the lumped oxidative phosphorylation and TCA cycle pathways; ATPase activity showed positive control over steady-state plasma glucose concentration, with a shallow trough centred at approximately 6% parasitaemia.

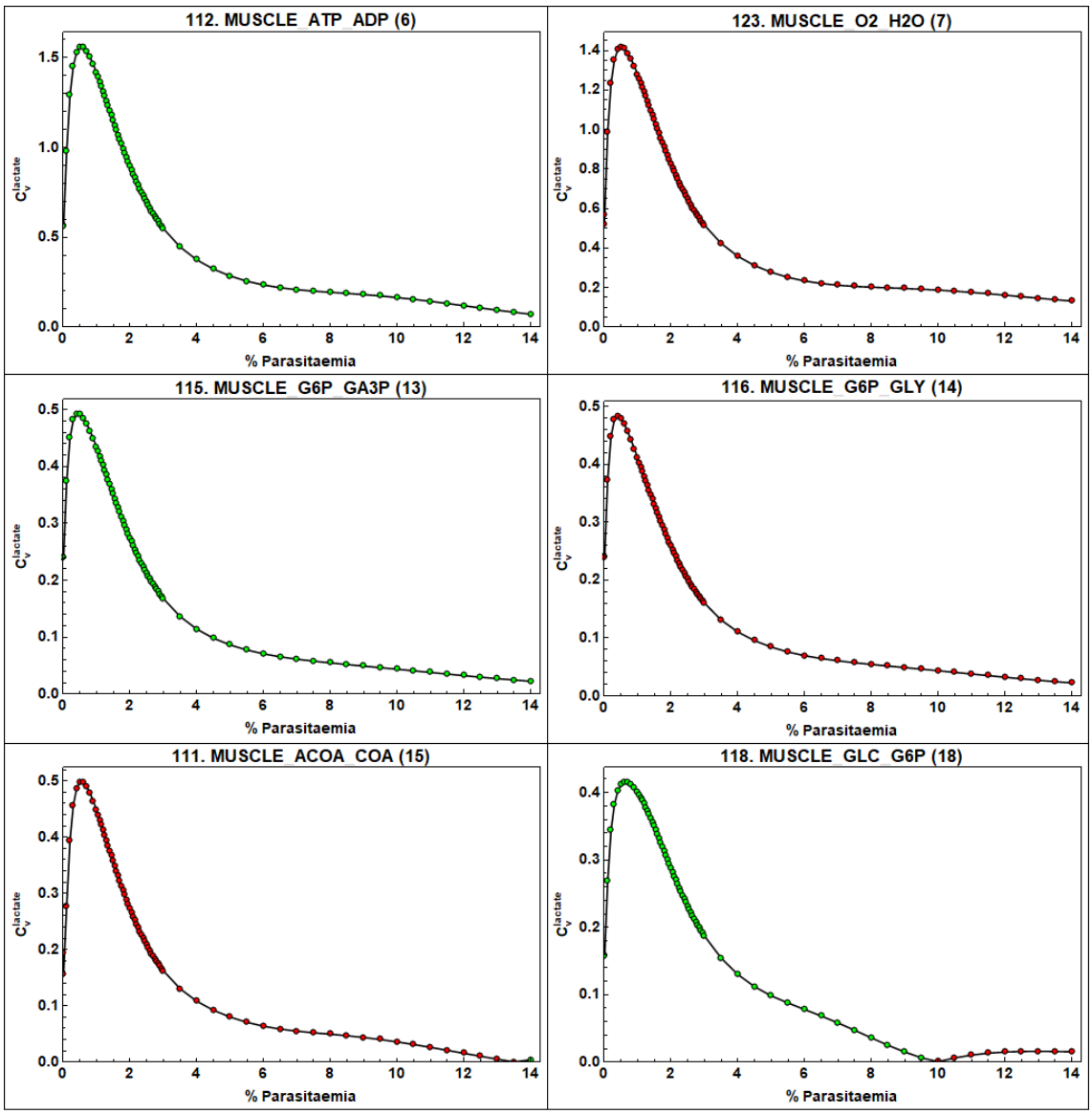

Figure B.10: Significant plasma lactate control coefficients obtained from rate expressions in the skeletal muscle compartment

Six rates from the skeletal muscle compartment showed significant control over steady-state lactate concentration. Four of these six rates comprised the entirety of fluxes mediating significant control over plasma glucose, namely ATPase activity, phenomenological hexokinase activity, and the lumped oxidative phosphorylation and TCA cycle pathways (**Fig B.10**). Of these, only one has changed sign; ATP hydrolysis, oxidative phosphorylation, and the lumped TCA cycle appear to exert negative control on the steady-state plasma concentrations of both glucose and lactate, albeit with differing magnitudes and distributions across the parasitaemia datasets. Similar to the graphs obtained for plasma glucose, plots of plasma lactate control coefficients appear remarkably similar in shape across the differing rates, regardless of sign. A peak in absolute magnitude is reached at approximately 1% parasitaemia, which then declines hyperbolically with an inflection point situated at approximately 3.5%. A change in sign is observed for the lumped TCA cycle and hexokinase activity, occurring at relatively high parasitaemias.

Furthermore, a greater portion of G6P, the product of hexokinase activity, undergoes glycolysis instead of storage as glycogen as parasitaemia increases and the need for free energy production takes precedence over

glycogen storage (**Fig. B.11**). Muscle glycogen content decreases rapidly from an initial 1534 mM to 400 mM at approximately 1.5% parasitaemia, after the graph assumes a less steep slope, which proceeds roughly linearly to a final minimum of 103 mM. The ratio of glycogenolysis to glycogenesis exhibits an inverted trend with regards to muscle glycogen concentration, rapidly increasing from 0.233 to 0.800 at approximately 1.5%, after which it gradually increases to a final maximum of 0.973.

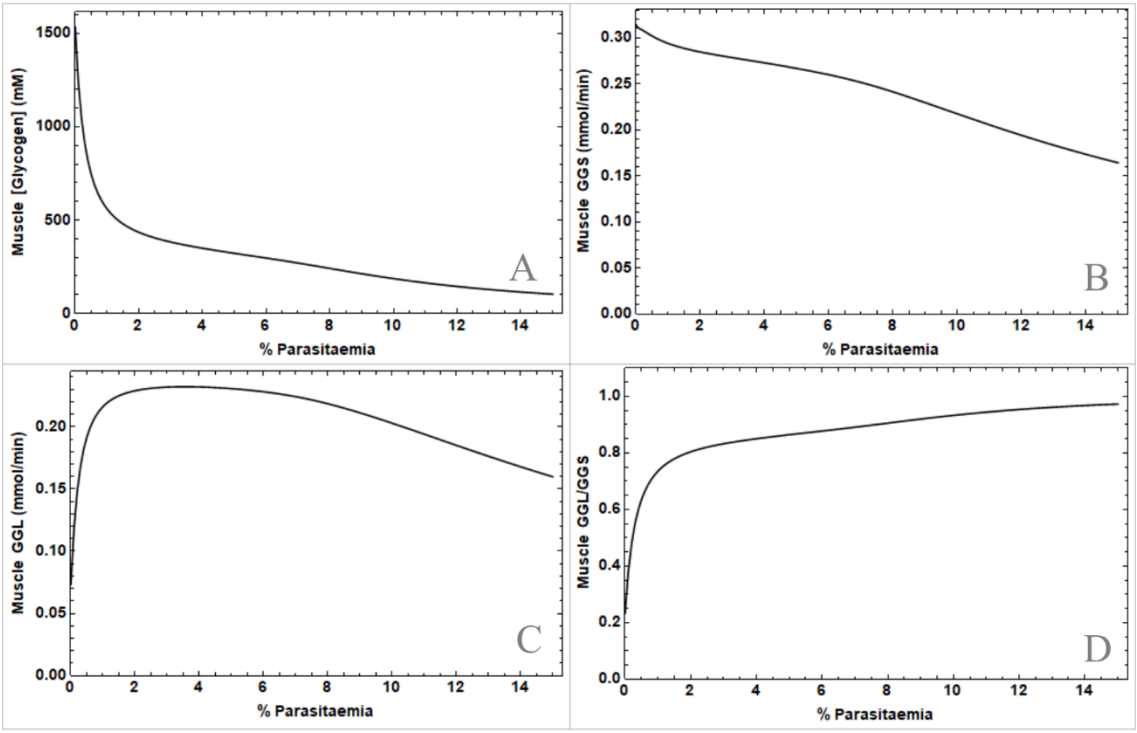

Figure B.11: Components of skeletal muscle glycogen metabolism simulated at varying parasitaemias, measured at steady-state. (**A**) Muscle glycogen concentration (**B**) The rate of glycogenesis (GGS) (**C**) The rate of glycogenolysis (GGL) (**D**) Ratio of glycogenolysis to glycogenesis

Increased partitioning of glucose utilization to glycolysis rather than gluconeogenesis is thus illustrated by the steady-state muscle glycogen concentration declining rapidly with increasing parasitaemia, particularly at parasitaemias leading up to 1.5%; and the negative control that glycogenesis exerts over plasma lactate. Further indirect evidence for increased catabolism vs storage is the positive control displayed by the irreversible conversion of G6P to GAP over plasma lactate, which irrevocably removes G6P from the potential glycogenic substrate pool.

Besides glucose, another important metabolic node representing a crossroads between anaerobic glycolysis and other forms of oxidation is pyruvate. The steady-state concentration of pyruvate within the skeletal muscle compartment is determined by the activity of several fluxes, both direct and indirect (**Fig. B.8**). Positive fluxes consist of synthesis from GAP, oxidation of lactate, or import from the circulation. Oxidation to acetyl-CoA, reduction to form lactate, or transamination to alanine form the negative fluxes. Simulations show pyruvate reduction to lactate making up the majority of all negative pyruvate flux across the complete range of parasitaemia values (**Fig. B.12**). Consumption of pyruvate increases rapidly upon initial infection, reaching near-maximal levels at approximately 1% parasitaemia with a plateau thereafter. Pyruvate consumption is dominated by LDH activity, whereby the reduction of pyruvate to lactate accounts for about

90% of all pyruvate catabolism across all parasitaemias. Additionally, the conversion of pyruvate to acetyl-CoA is also upregulated, increasing the relative contribution that it makes to cellular acetyl-CoA when compared with production of acetyl-CoA from free fatty acids.

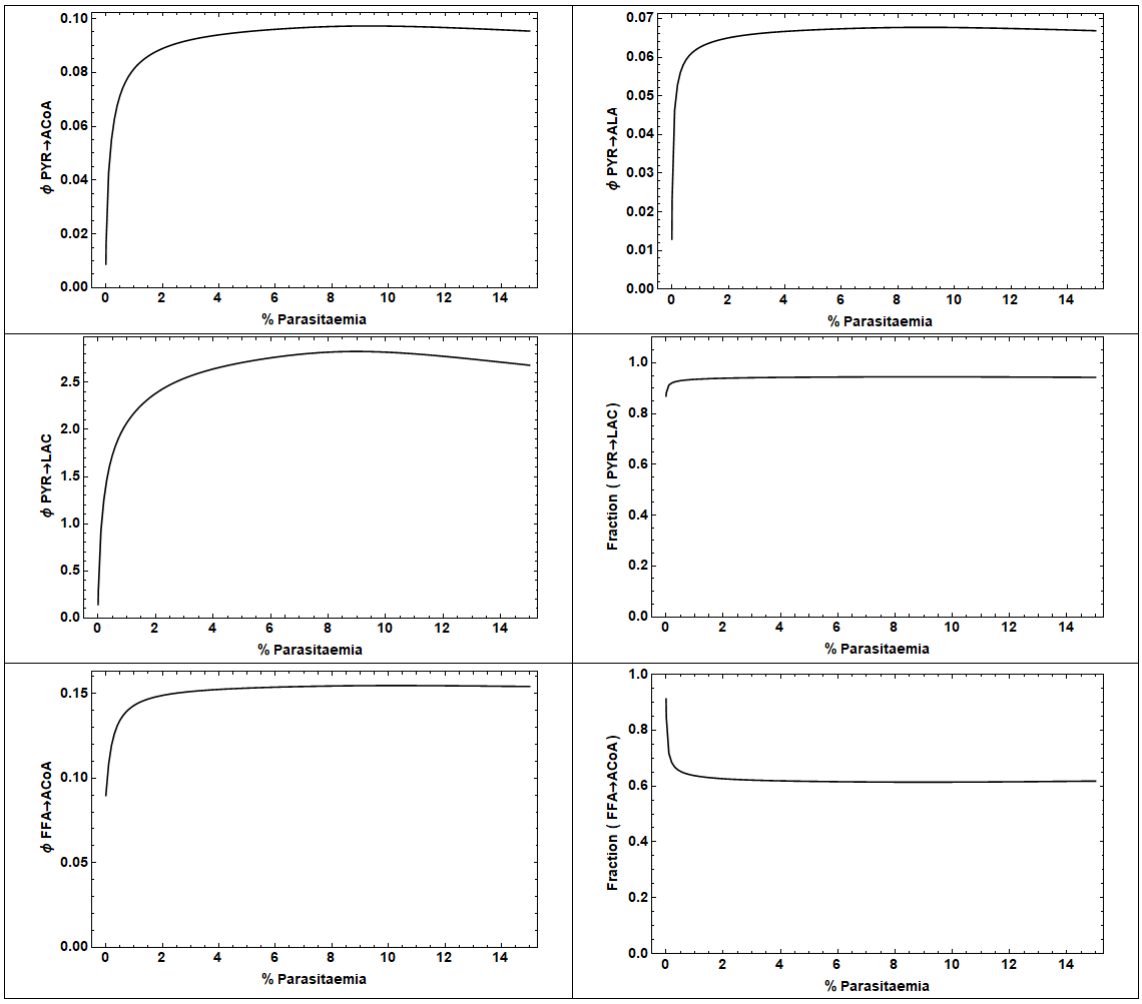

Figure B.12: Relative contributions and fractions of fluxes mediating a decrease in muscle pyruvate; the flux of fatty acid oxidation (FFA→ACoA) together with its fraction with regards to PYR→ACoA is also shown

Four parameters from the muscle compartment were identified as having significant response coefficients (**Fig B.13**). Two are constants mediating the control of the cellular redox state on reactions utilising NAD^+/NADH (the separate value of ν for the oxidative phosphorylation reaction is due to a distinct specification by the original authors), with the constant for ATP synthesis having positive response, and the constant governing the remainder of the reactions displaying negative response coefficients. The parameter specifying the maximum degree of skeletal ATP hydrolysis upregulation by the parasite displayed a positive response coefficient across all parasitaemias, sharply increasing between 0% and 1.5% parasitaemia. The Michaelis-Menten constant for ATP in the ATP hydrolysis reaction yielded negative response coefficients across all parasitaemias. The significant response with regards to plasma glucose displayed by the parameter ν (NU) reflects the dominant role that pyruvate/lactate interconversion plays in muscle metabolism.

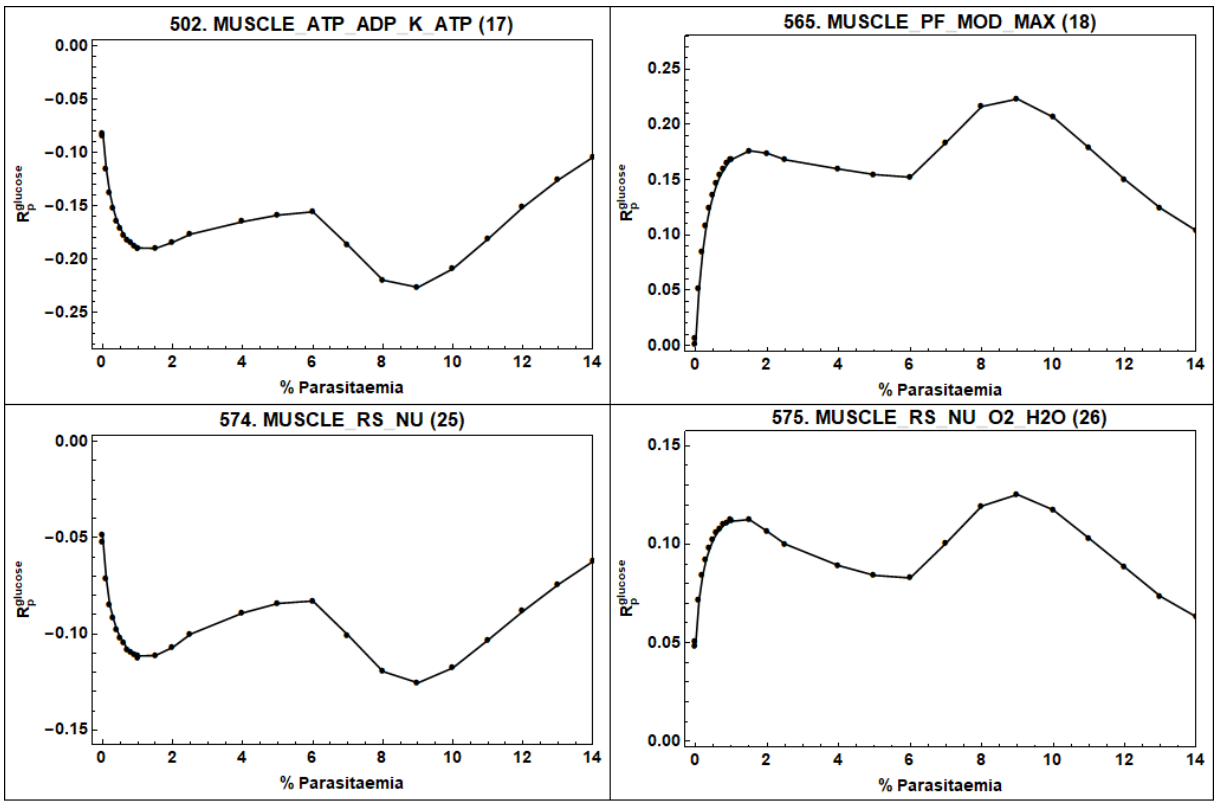

Figure B.13: Significant plasma glucose response coefficients with regards to parameters comprising kinetic expressions belonging to the skeletal muscle compartment.

Recall that this parameter is a phenomenological affinity constant for the redox state controller, denoting the ratio of NADH/NAD^+ required for a controller value of half. Thus, an increase in this parameter will drive the system towards an increased NADH/NAD^+ ratio, which in this case would translate to increased lactate oxidation vs pyruvate reduction. This parameter shows a negative response with regards to steady-state plasma concentrations of both glucose and lactate (**Figs. B.13 & B.14**).

The significant response coefficients for plasma lactate in the skeletal muscle compartment primarily involve energy- and reducing-equivalent metabolism (**Fig B.14**). The affinity constant of ATP for the ATP hydrolysis reaction shows strong negative response at early parasitaemias. The redox state controller constants show early peaks, with positive and negative values for the oxidative phosphorylation-specific and general constants, respectively. Similar to its effect on plasma glucose, the parameter determining the maximal degree of parasite-mediated ATP hydrolysis stimulation also shows positive responses across all datasets, also peaking at approximately 1.5%. However, it does not maintain this behaviour, and decreases relatively rapidly thereafter.

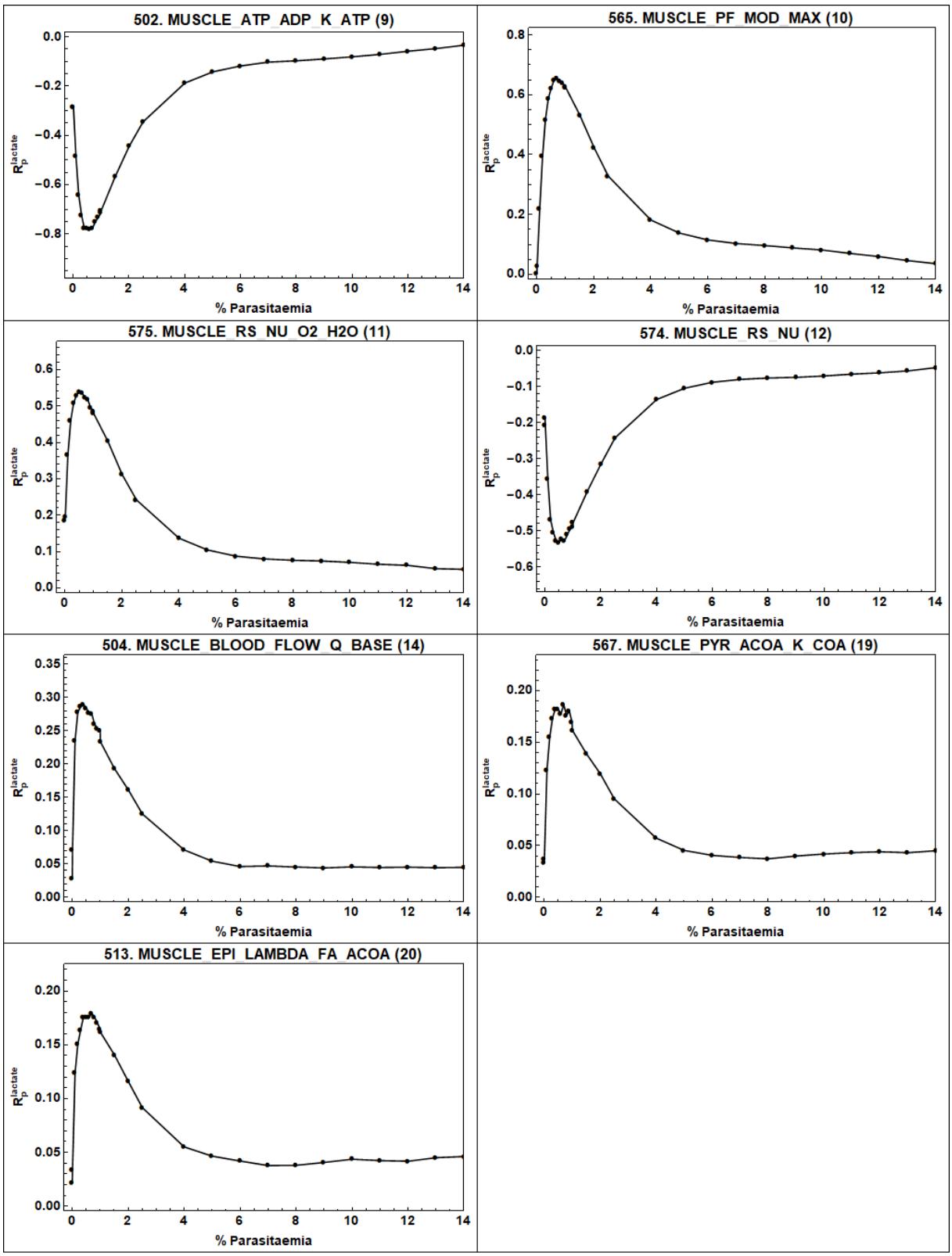

Figure B.14: Significant plasma lactate response coefficients with regards to parameters comprising kinetic expressions belonging to the skeletal muscle compartment.

The negative response with regards to lactate can be readily explained by diminished lactate oxidation activity; negative response concerning plasma glucose is likely due to the system upregulating glucose uptake to drive pyruvate reduction via mass action through the anaerobic glycolytic pathway.

The remainder of the results obtained from MCA lend further credence to the notion of anaerobic glycolysis being the dominant pathway in skeletal muscle in the presence of severe malarial infection. The negative control exerted by TCA cycle and oxidative phosphorylation activity over both steady-state plasma glucose and lactate concentrations, together with the associated response coefficients, indicate that the muscle compartment responds to a decreased flux of pyruvate to lactate by increasing its uptake of glucose as a mass-action compensatory mechanism, to sustain pyruvate oxidation through LDH and offset the subsequent decreased release of lactate.

By contrast, the positive control displayed by ATP hydrolysis activity over plasma glucose and lactate could demonstrate an inversion of the processes described above. The increased production of ADP provides additional substrate for TCA cycle and oxidative phosphorylation activity, thereby upregulating these processes through mass action. Furthermore, the lumped TCA cycle reaction produces NADH, which can subsequently be utilized by oxidative phosphorylation for synthesis of ATP and NAD^+. Therefore, the concomitant upregulation of these processes will result in a greater flux of pyruvate through the aerobic pathway, thereby lessening the need for glucose uptake, and reducing the fraction of pyruvate reduced to lactate. The positive response exhibited by the parameter denoting maximum parasite-mediated ATPase stimulation (MUSCLE_PF_MOD_MAX) further supports this explanation.

It should be noted that, in contrast to the brain compartment, the skeletal muscle includes a description of fatty acid oxidation, which provides acetyl-CoA, ADP, and NADH. The relatively large amount of acetyl-CoA provided by this reaction in comparison to that produced by pyruvate oxidation (**Fig. B.12**) was noted early in the analysis stage. It stands to reason that this reaction frees up a considerable amount of pyruvate that can instead be oxidized to lactate, and is likely a major contributor to the preference for anaerobic glycolysis exhibited by the skeletal muscle compartment in this model. As mentioned previously, the clamped free fatty acid concentration provides an effectively constant, unlimited supply of substrate for this reaction, thereby precluding the useful observations that could be made with a dynamic pool of free fatty acids and distal metabolites. It therefore feels appropriate to reiterate the utility of unclamping these variables as part of possible future research.

The findings and assertions discussed above should, however, be considered together with the limitations of this particular compartment as portrayed in the current model. As noted by the authors of K1 in their original paper, the lack of distinction between cytosolic and mitochondrial compartments substantially limits the predictive capacity of the model (16). This is particularly important when considering the separate subcellular compartments in which the reactions catalysed by lactate dehydrogenase (cytosol) and oxidative phosphorylation (mitochondria) take place. The absence of such a distinction also precludes the model from being able to accommodate separate compartments for the different skeletal muscle fibre types, each having their own capacity for aerobic versus anaerobic glycolytic metabolism. While the resolution of these limitations was judged to lie well beyond the scope of the current research, they should nonetheless be considered in the case of future model development.

In summary, skeletal muscle is not capable of appreciable net glucose export or complete gluconeogenesis, but it has been consistently described as an important organ with regards to maintaining blood glucose homeostasis. This has been due to its ability to switch between net lactate export and import, and its contribution of alanine, a major gluconeogenic precursor, during times of catabolic stress. However, its role within this model has been limited to that of a major lactate exporter, theoretically exacerbated by the increase in anaerobic glycolysis during convulsions. Furthermore, the absence of a dynamic system of alanine exchange with the circulation likely hampers the descriptive power of the model, especially given the observations from clinical data noting disturbed amino acid metabolism (64, 198).

B.2.3 The Role of the Kidney

The kidney has two possible means of plasma lactate disposal: uptake for use as a gluconeogenic substrate (88), or excretion into the urine (106). Though this model does not feature a detailed renal compartment with kinetic descriptions for gluconeogenesis, a phenomenological function for renal lactate excretion was included. This function was implemented in such a way that renal lactate excretion only became significant once plasma lactate exceeded a certain threshold. This threshold was set to 6.8 mM, slightly higher than 5-6 mM reported in literature (88). This approach appeared to work as intended (**Fig. B.15**), with renal lactate excretion remaining largely inactive below the threshold, but constituting a maximum of approximately 13% of plasma lactate flux once the threshold had been exceeded (**Fig. B.4**).

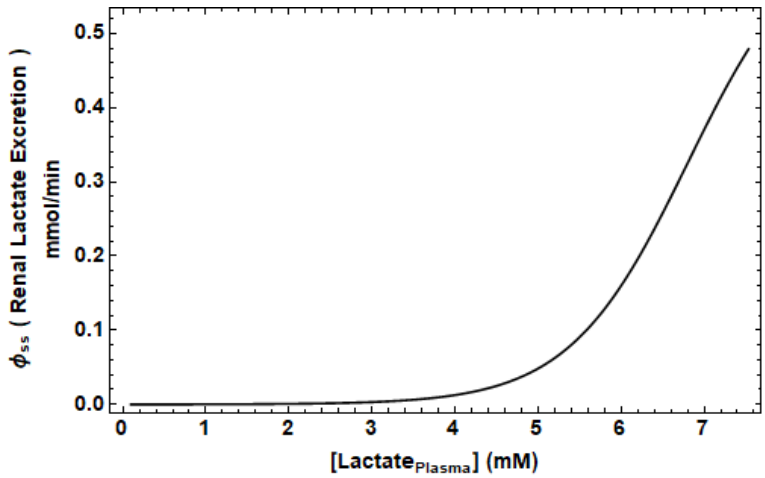

Figure B.15: Renal lactate excretion flux vs steady-state plasma lactate concentration in the *meyer1* model.

Due to the lack of clinical data, this phenomenologically modelled renal lactate excretion was parameterized to fit the data, and not based on quantitative measurements of renal lactate excretion kinetics, as would ideally be the case. Furthermore, a committed renal compartment complete with kinetic descriptions of gluconeogenesis was not included. However, the single function that was implemented, though approximate, could be regarded as a stand-in for the combined activity of renal excretion and gluconeogenesis.

Parasitized erythrocytes have a particular propensity to sequester within the renal microvasculature (106), and the development of renal pathology, particularly malaria-associated acute renal failure, contributes to kidney failure as one of the three most common causes of death in severe malaria (137). Since it has been successfully demonstrated in the current work that the effects of microvascular obstruction can be integrated into existing models of organ-specific function and metabolism, the kidney is an ideal candidate for incorporation as part of possible future development of the model.

In summary, within the context of metabolic acidosis, contemporary literature has often cited the kidney's significant ability to carry out gluconeogenesis; the capacity of the kidney to excrete lactate during severe metabolic acidosis has only rarely been mentioned. Therefore, while the inclusion of a simple first-order renal lactate excretion function has comparatively little support in literature, within the scope of this model it can be thought as a stand-in for a more comprehensive model of renal glucose metabolism.

Appendix C

C.1 Parasite-Mediated Changes in Host Metabolism

In order to model the effects that *P. falciparum* might have on host metabolism, several terms were introduced into the model to inhibit or accelerate specific metabolic processes in certain compartments. These terms generally took on the form of Michaelis-Menten type functions, with associated values dictating the maximum degree of effect and the 'affinity' that these effects had for percentage parasitaemia. However, due to the lack of quantitative data with which to parameterise these functions, values were chosen arbitrarily, and subsequently adjusted based on visual inspection and comparison with the clinical data described in **Section 4.1.3**. Each parasite modulation parameter was varied across a range of values the boundaries of which were chosen based on their plausibility. Numerical solutions were obtained for each of these values across a range of parasitaemias encompassing the percentages described in the collated clinical data. Since plasma glucose and lactate concentrations comprise the only dependent variables against which the model outputs could be validated, plots of the steady-state values of these metabolites were produced for each parasite modulation parameter value and superimposed on scatter plots of clinical data. Each parameter value was assigned a different colour to facilitate comparison.
The 'default value' specifies the parameter value used in the final model.

C.1.1 Brain

The percentage parasitaemia at which half-maximal cerebral perfusion would be present appeared to have little effect on model outputs, showing virtually no change as the parameter was varied from its default value of 0.005 (corresponding to 0.5% parasitaemia) to 0.05 (5% parasitaemia).

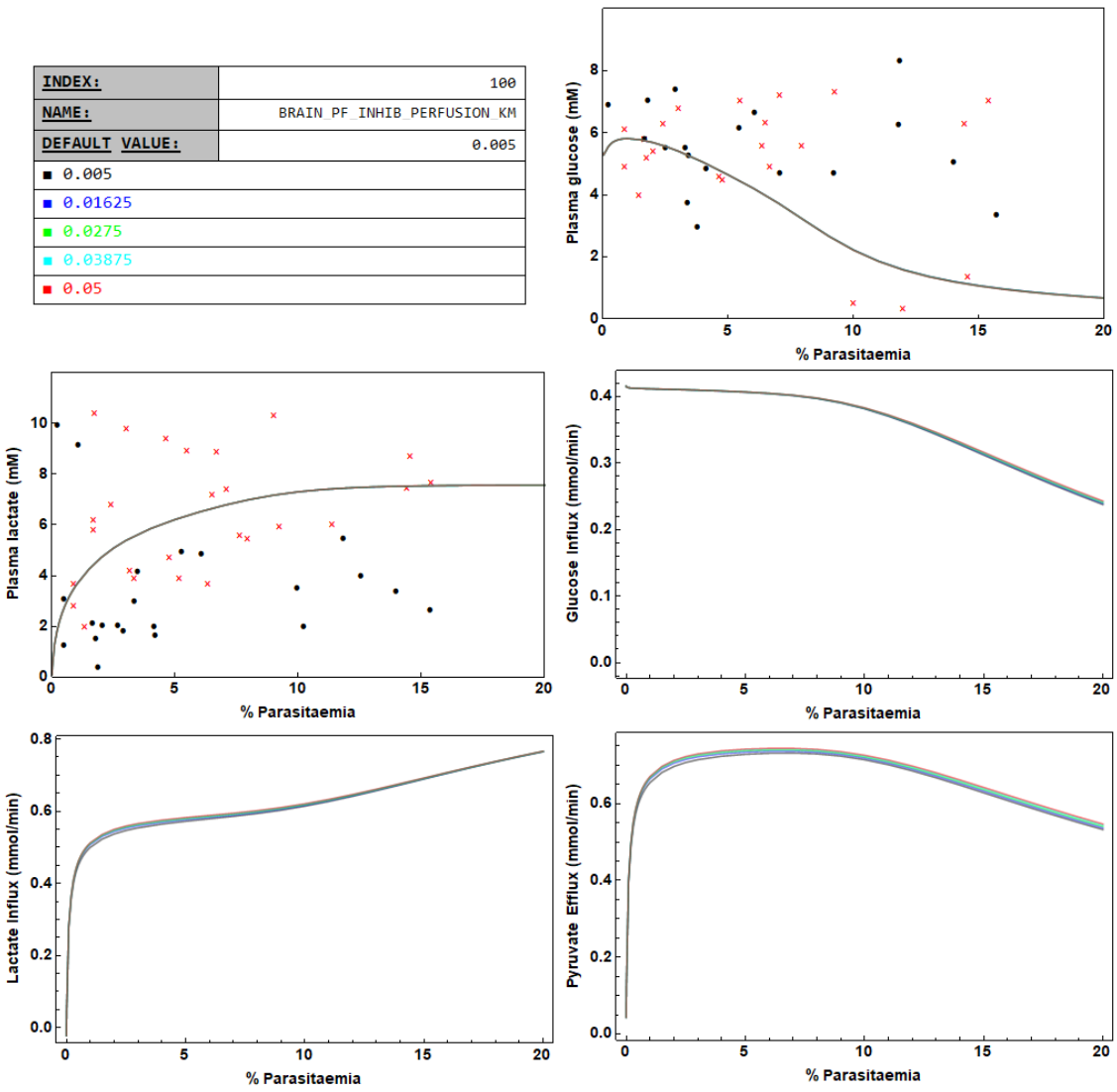

Figure C.1: Changes in selected model outputs with variation of parasite-mediated perfusion affinity modulation parameter in the brain compartment, details presented in information box, top-left. The colour of each curve corresponds to simulations conducted with the matching parameter value. From top-right panel, left-to-right, top-to-bottom: plasma glucose concentration, plasma lactate concentration, glucose influx into the brain compartment, lactate influx into the brain compartment and pyruvate efflux out of the brain compartment

By contrast, the parameter denoting the maximum degree of perfusion inhibition showed substantial changes in model outputs once the default value of 0.3 was increased above 0.6. Values of 0.75 and 0.9 showed particularly drastic alterations, though their inclusion here is mostly for the sake of interest, since it seems implausible that parasite sequestration could cause a 75% or more reduction in cerebral blood flow.

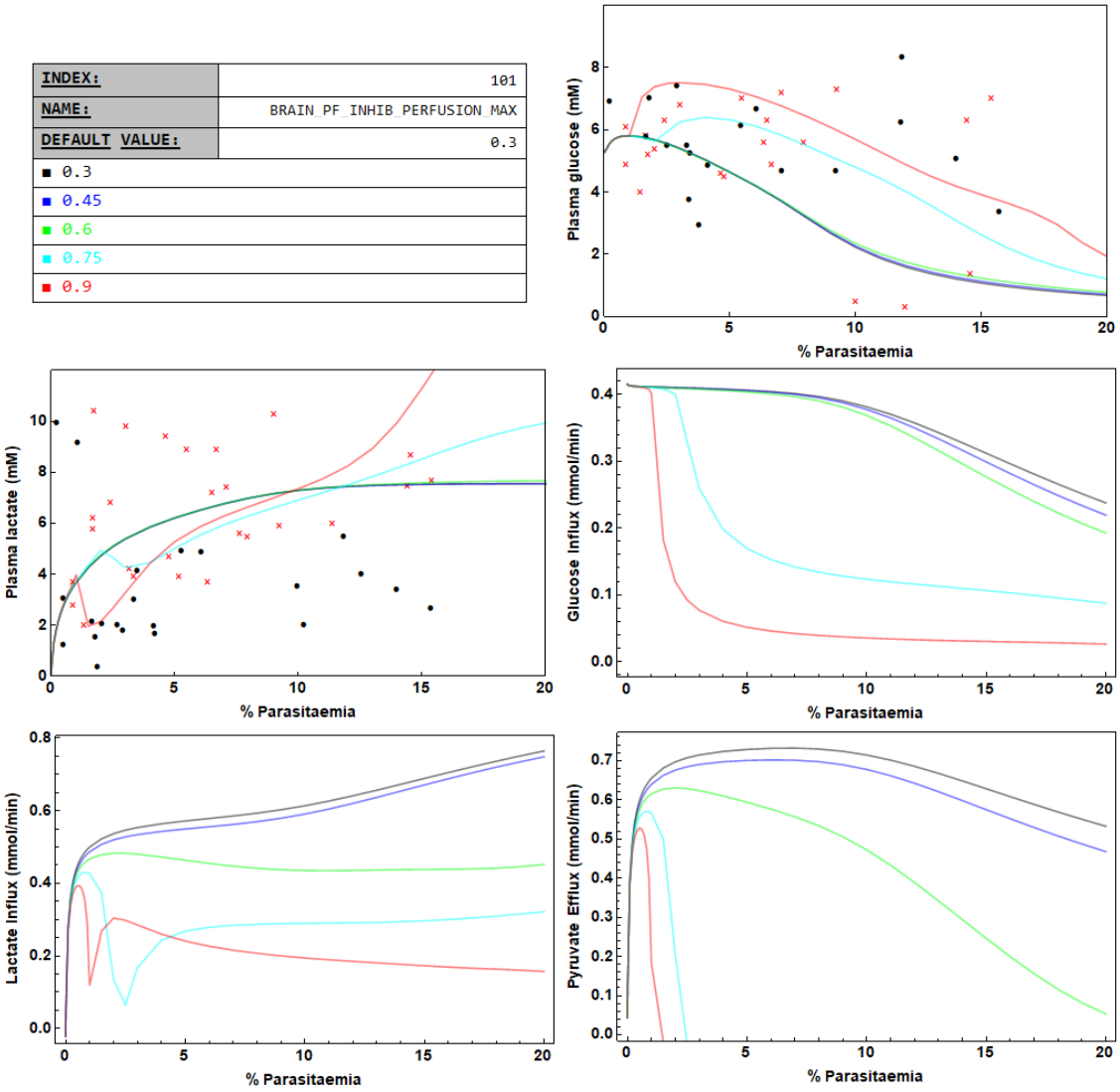

Figure C.2: Changes in selected model outputs with variation of parasite-mediated perfusion velocity modulation parameter. From top-right panel, left-to-right, top-to-bottom: plasma glucose concentration, plasma lactate concentration, glucose influx into the brain compartment, lactate influx into the brain compartment and pyruvate efflux out of the brain compartment

C.1.2 Liver

Two parasite-mediated inhibition terms were introduced into the hepatic compartment, each having two parameters specifying the percentage parasitaemia producing half-maximal effect (K_M), and the maximum magnitude of effect (*MAX*). As described in the Methods section, these terms were applied to rate expressions mediating aspects of mitochondrial metabolism and transport between the hepatic and plasma compartments.

A 100-fold increase in the phenomenological K_M value of parasite-mediated inhibition of selected fluxes in the hepatic mitochondrial compartment showed virtually no effect on the steady-state plasma concentrations of glucose and lactate. However, some minor shifts were seen for the plots showing the steady-state flux of the affected reactions.

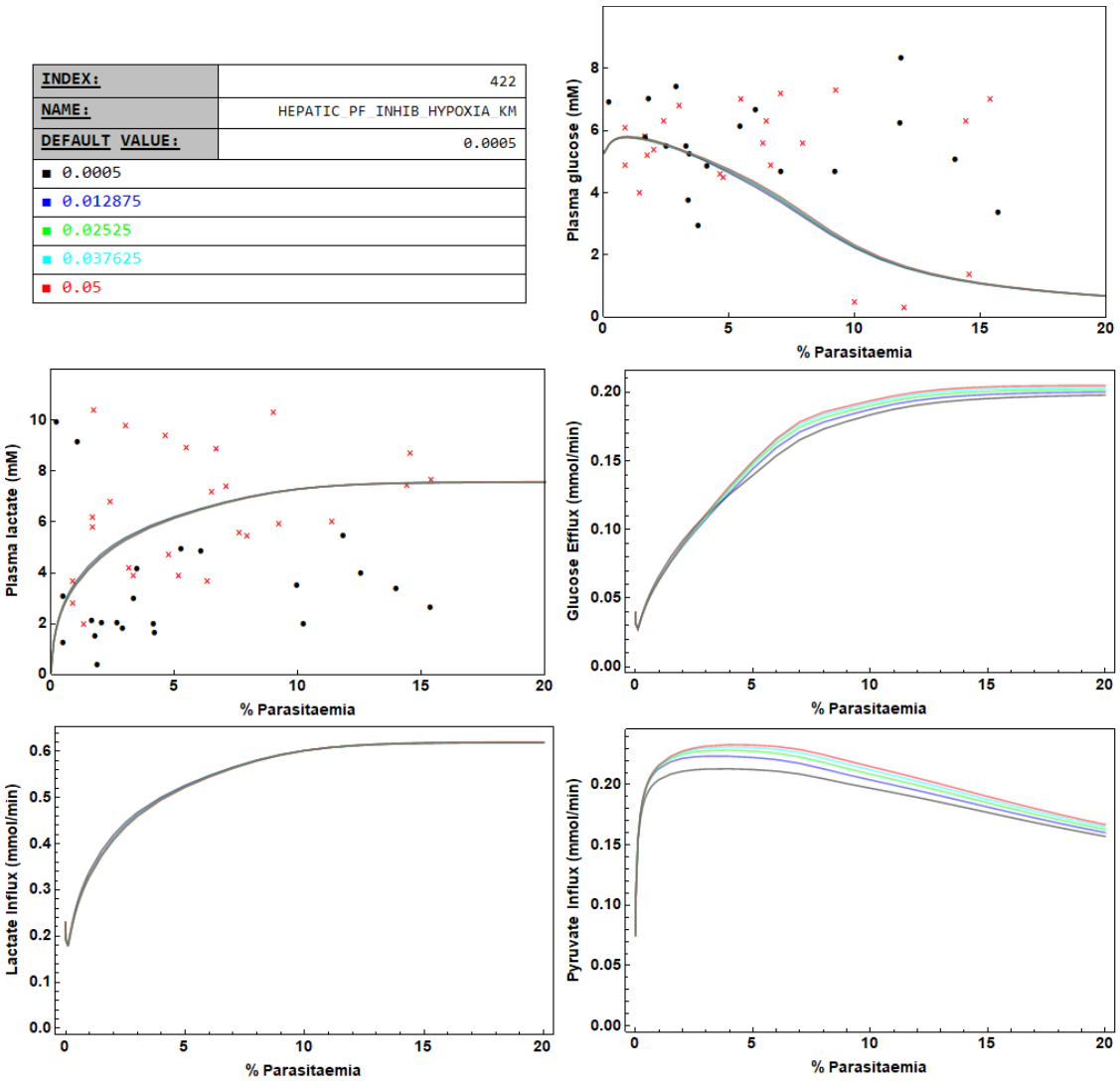

Figure C.3: Changes in selected model outputs with variation of parasite-mediated hypoxia 'affinity' modulation parameter, details presented in information box, top-left. Abbreviations: Trnsp Pyr Mito, mitochondrial pyruvate transporter; PDH, pyruvate dehydrogenase; PC, pyruvate carboxylase; O2→H2O, oxidative phosphorylation activity. All rates are of the hepatic compartment, influx/efflux denotes transport into/out of hepatic compartment for indicated metabolite

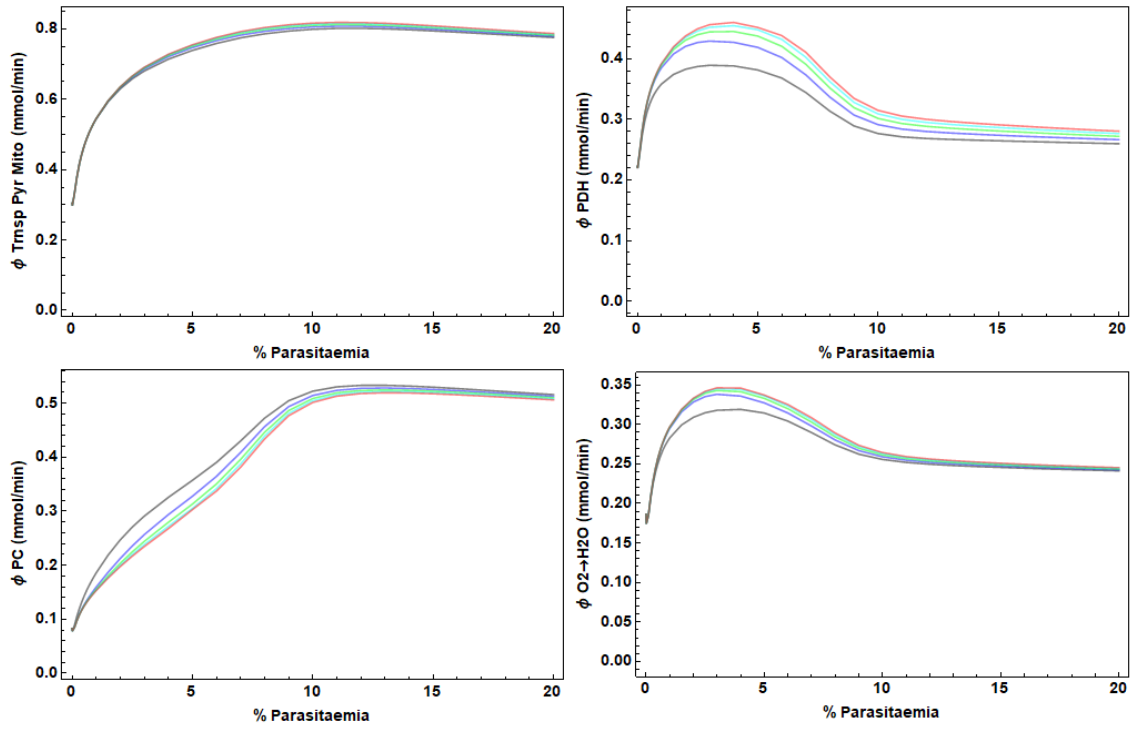

Figure C.3 (contd.): Changes in selected model outputs with variation of parasite-mediated hypoxia 'affinity' modulation parameter. Abbreviations as in above.

Variation of the maximal degree of inhibition showed more pronounced changes, although these were only noticeable for plasma glucose and lactate at values above 0.6. More drastic shifts were however observed for the affected reactions, as well as the fluxes of glucose export and pyruvate import. PDH flux, in particular, displayed almost complete abrogation with a parameter value of 0.8.

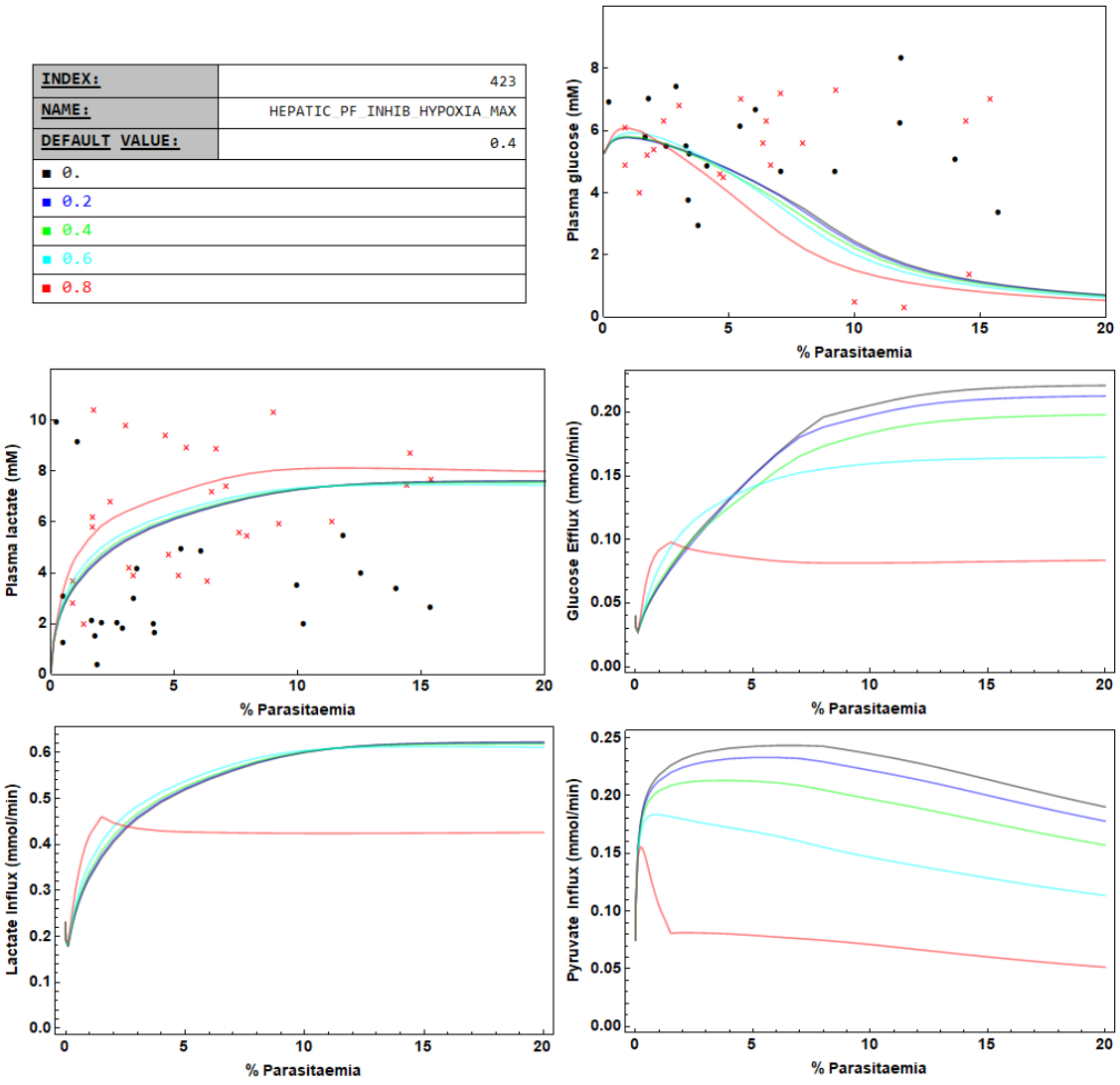

Figure C.4: Changes in selected model outputs with variation of parasite-mediated hypoxia maximum degree modulation parameter. Rates are as in Fig. C.3

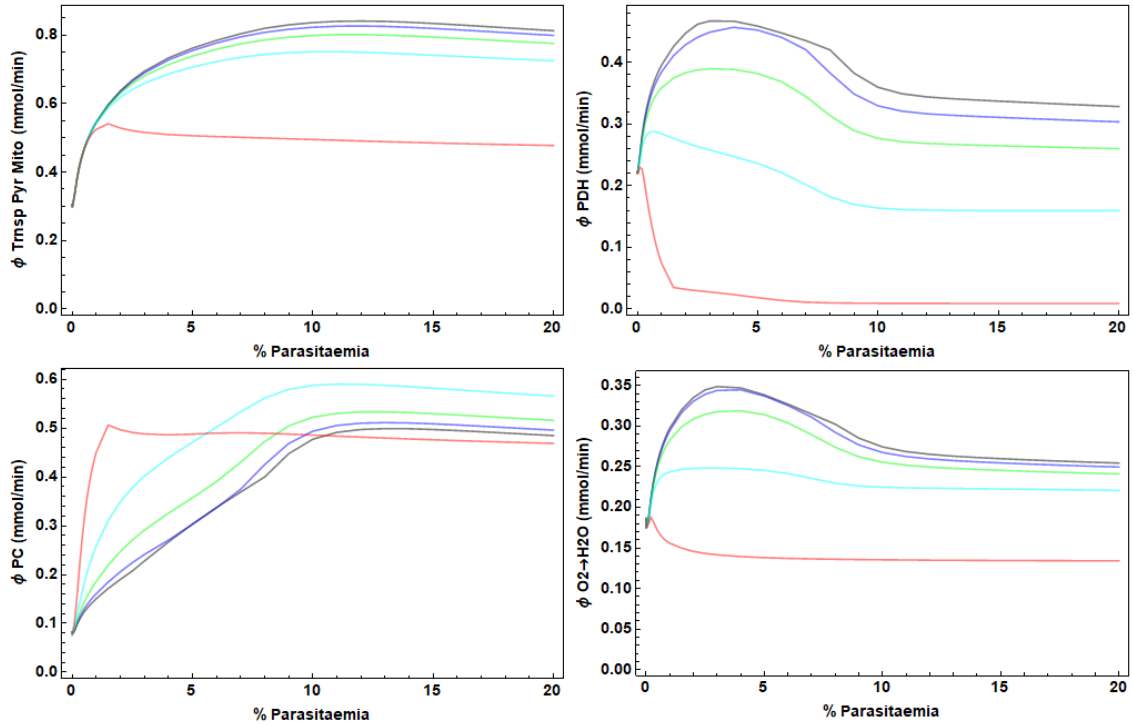

Figure C.4 (contd.): Changes in selected model outputs with variation of parasite-mediated hypoxia maximum degree modulation parameter. Abbreviations as in Fig C.3.

Increasing the K_M value for parasite-mediated hepatic perfusion inhibition by a factor of 100 over several increments yielded a shift towards in the right for the plots of steady-state plasma concentrations of glucose and lactate, with the emergence of lactic acidosis in particular being delayed substantially until higher parasitaemias had been reached. Furthermore, the maximum fluxes of glucose, lactate and pyruvate transport appeared to be proportional to this parameter.

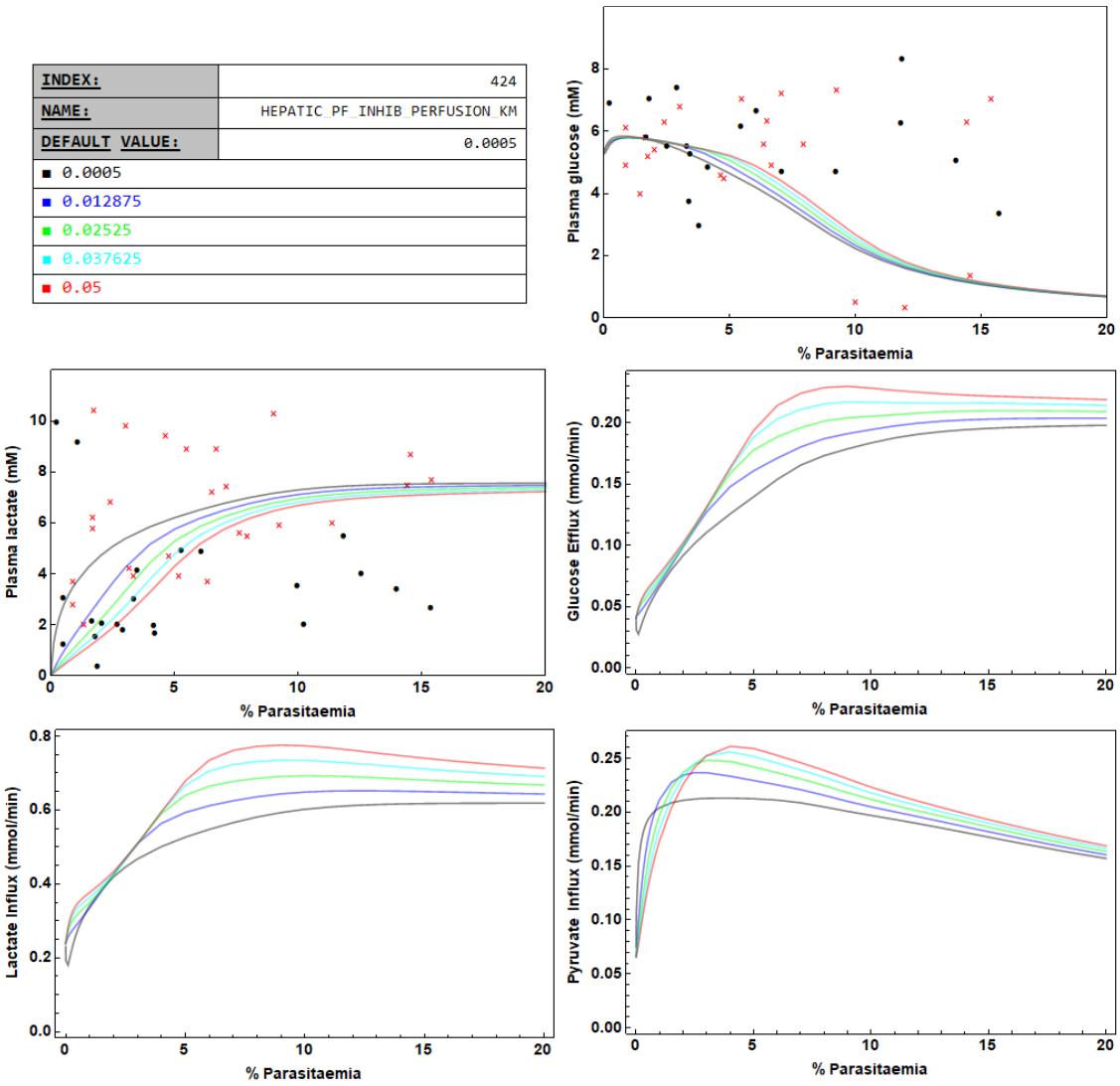

Figure C.5: Changes in selected model outputs with variation of parasite-mediated perfusion affinity modulation parameter in the liver compartment. Rates are as Fig C.3.

To ascertain the effects of varying degrees of maximum parasite-mediated perfusion inhibition, the value of the *MAX* parameter was varied between 0 (no inhibition) to 50 (its default value). The absence of perfusion inhibition prevented the appearance of lactic acidosis entirely, while delaying the onset of hypoglycaemia. Furthermore, metabolite fluxes were seen to be proportional to the magnitude of this parameter.

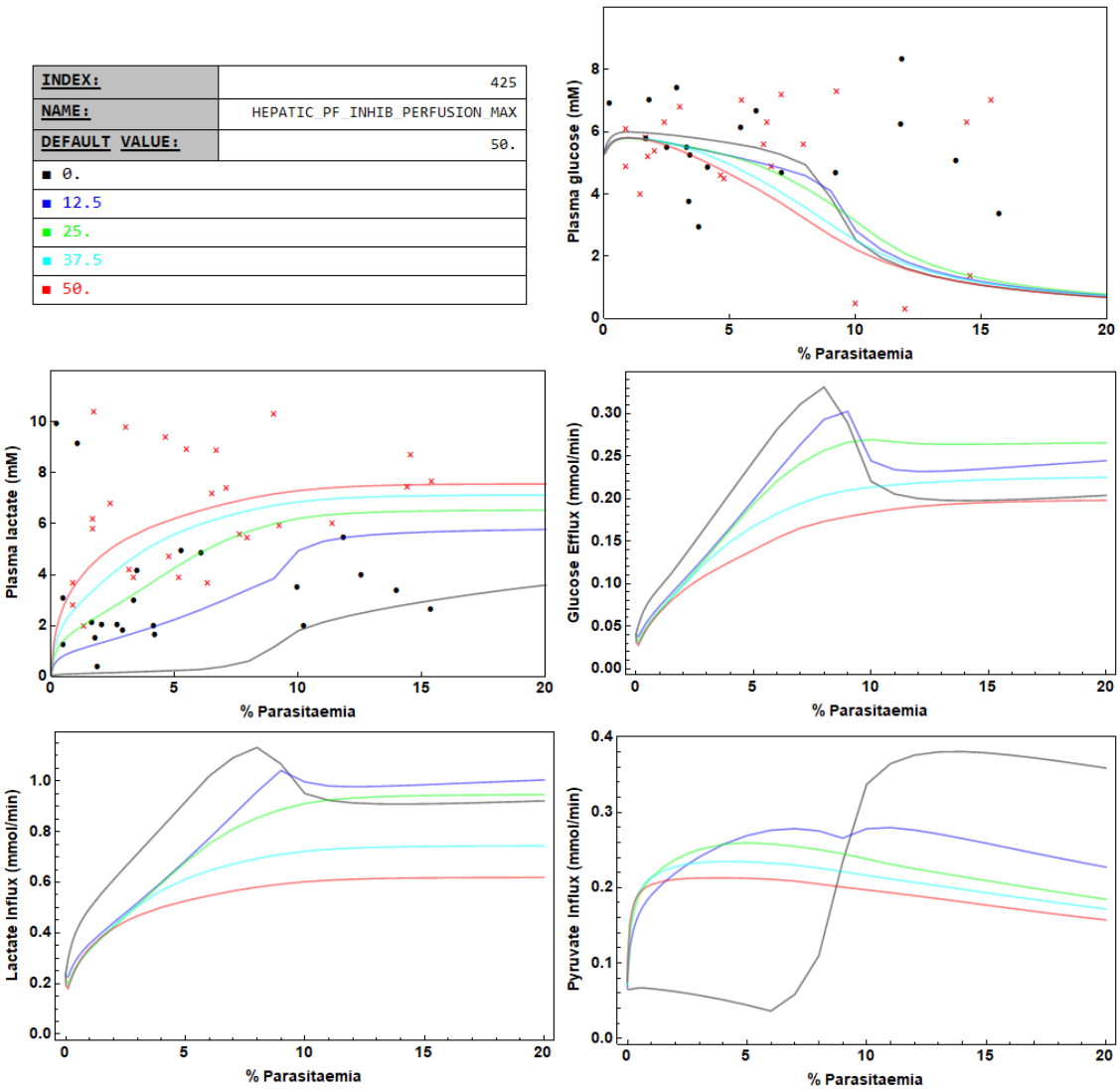

Figure C.6: Changes in selected model outputs with variation of parasite-mediated perfusion velocity modulation parameter in the liver compartment. Rates are as in Fig. C.3.

C.1.3 Muscle

In contrast to the other compartments, modulation of skeletal muscle metabolism was implemented in such a way that the activity of a single rate expression, that describing the rate of ATP hydrolysis, would be accelerated in response to increasing percentage parasitaemias.

A 25-fold increase in the phenomenological K_M value of parasite-mediated upregulation of ATPase activity showed small, albeit noticeable, changes in the curves for plasma glucose and lactate. A value of 0.05 (corresponding to 5% parasitaemia) appeared to eliminate the initial rise in plasma glucose concentrations at early parasitaemias, while simultaneously delaying the onset of hyperlactataemia. ATPase activity declined in response to increases in this parameter. Furthermore, a slight upwards shift was observed for glucose influx, with a more pronounced downward shift seen for lactate efflux.

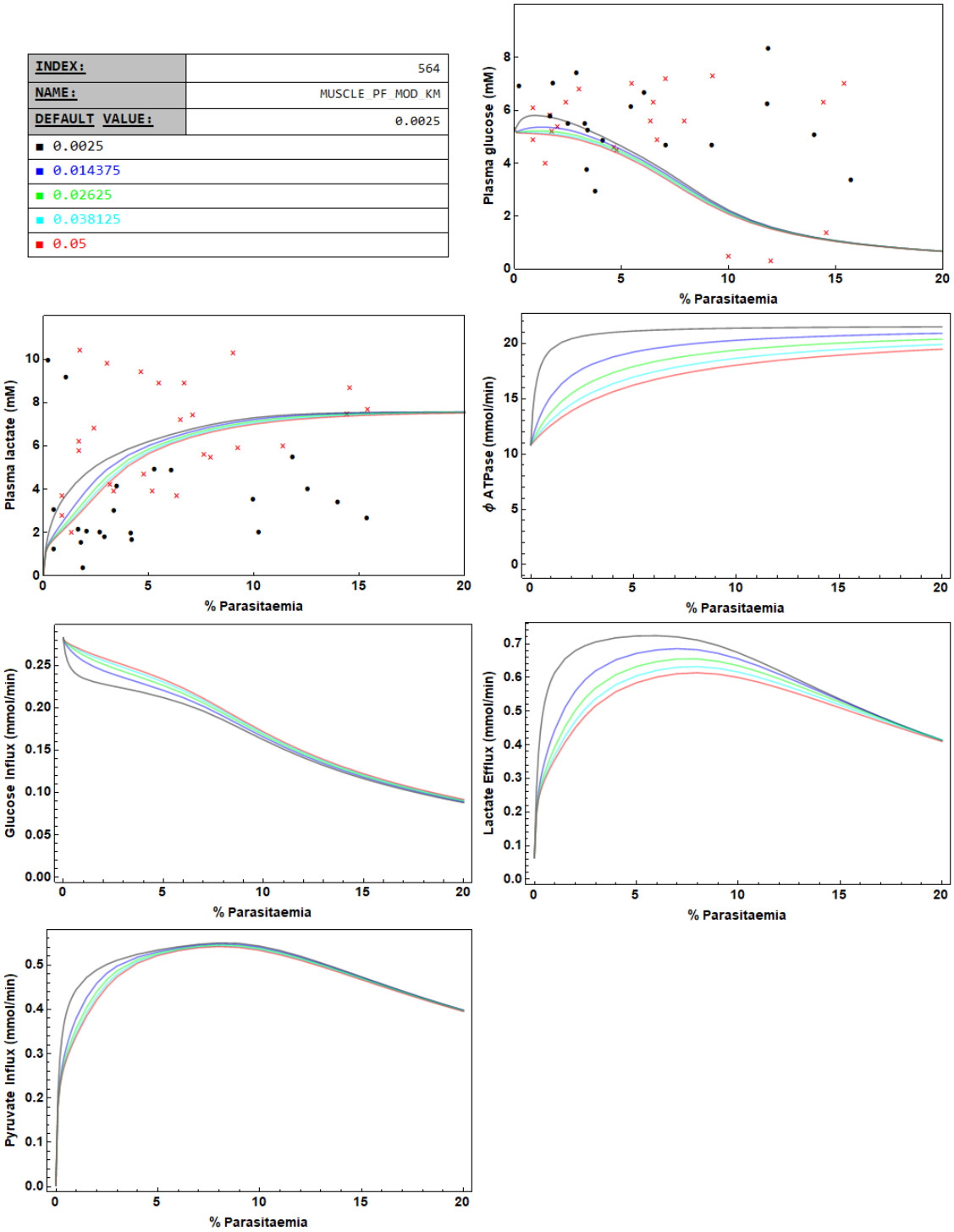

Figure C.7: Changes in selected model outputs with variation of parasite-modulation parameter. From top-right panel, left-to-right, top-to-bottom: plasma glucose concentration, plasma lactate concentration, skeletal muscle ATPase flux, glucose influx into the skeletal muscle compartment, lactate efflux out of the skeletal muscle compartment and pyruvate influx into the skeletal muscle compartment

The maximum degree of parasite-mediated ATPase acceleration was varied between values of 0 (no upregulation) and 2 (twice the default value). With no upregulation, a downward shift is observed for both plasma glucose and lactate, indicating hastened onset of hypoglycaemia with a marginal decrease in the emergence of lactic acidosis at lower percentage parasitaemias. ATPase flux shows direct proportionality to

this parameter, with an increase of 0.5 yielding a concomitant 5 mmol/min increase in flux. Steady-state fluxes of glucose uptake and lactate release show approximately negative and positive proportionality with regards to this parameter, respectively.

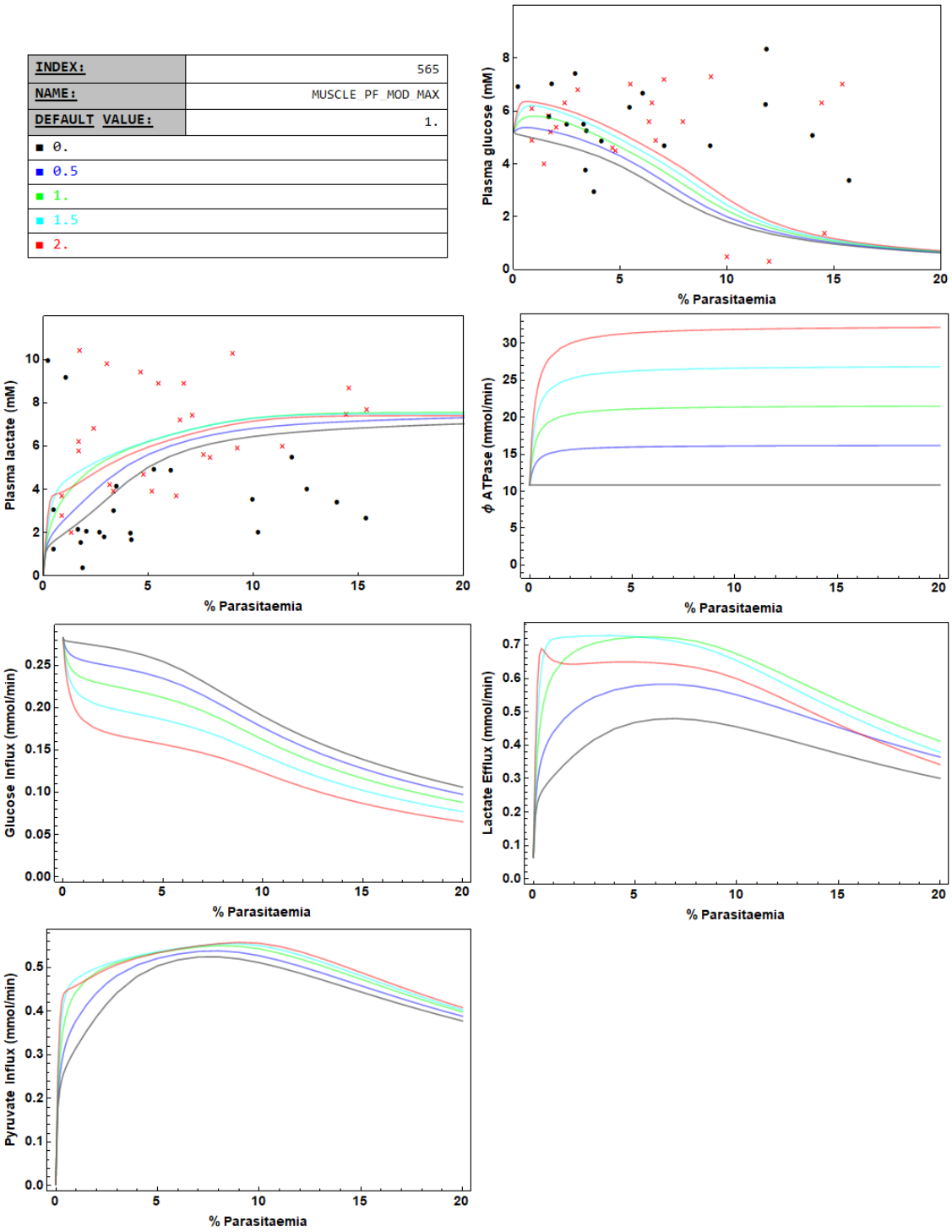

Figure C.8: Changes in selected model outputs with variation of parasite-mediated 'affinity' modulation parameter for ATPase activity in the muscle compartment. Rates are as in Fig. C.7.

C.1.4 Uninfected Erythrocytes

Variation of the K_M parameter of parasite-mediated inhibition of uninfected erythrocyte phosphofructokinase and pyruvate kinase activity showed little appreciable effect on plasma glucose and lactate concentrations. However, as the value of this parameter was increased, the slopes of the flux vs. percentage parasitaemia graphs could be seen to increase for not only PFK and PK, but also the rate of glucose import.

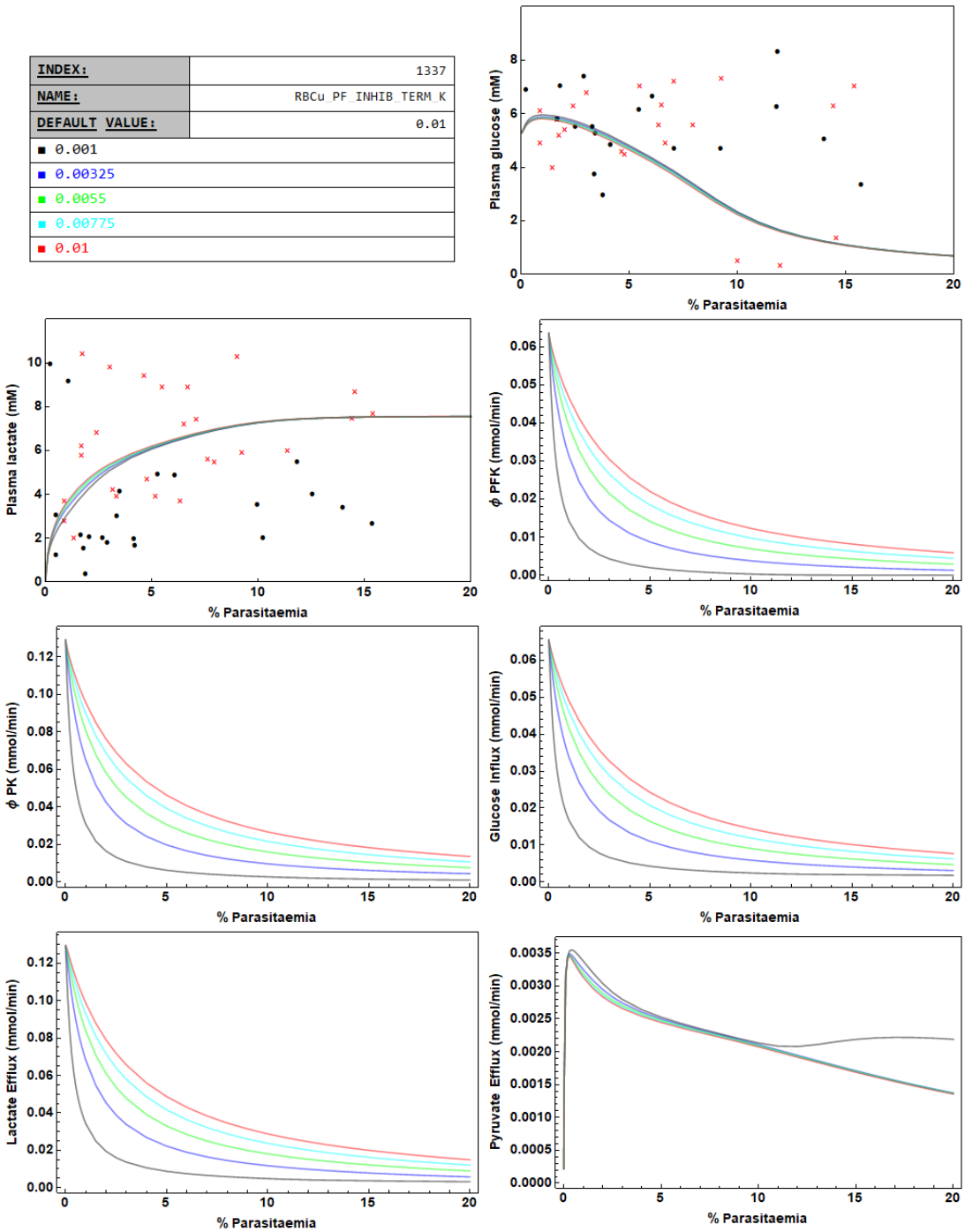

Figure C.9: Changes in selected model outputs with variation of parasite-modulation term parameter, details presented in information box, top-left. Abbreviations: PFK, phosphofructokinase; PK, pyruvate kinase. From top, left-to-right, top-to-bottom: plasma glucose concentration, plasma lactate concentration, PFK flux, PK flux, glucose influx into the uninfected erythrocyte compartment, lactate efflux out of uninfected erythrocyte compartment and pyruvate efflux out of the uninfected erythrocyte compartment